RADSYNCH 2009

5th International Workshop on Radiation Safety at Synchrotron Radiation Sources

May 21-23, 2009 Trieste, Italy

Organized by:

elettra

FERMI @elettra

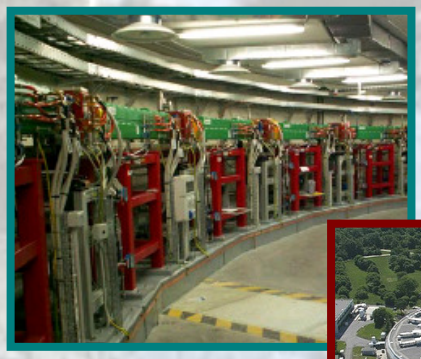

Main topics:

- Shielding design and commissioning of new synchrotron facilities.
- Radiation protection issues in synchrotron light source operation.
- Synchrotron light sources upgrades, with particular interest in top-up mode operation.
- Personnel safety systems for accelerators and beamlines.
- Induced radioactivity and radiation damage.
- Dosimetry and radiological aspects in medical beamlines development.
- Shielding design, commissioning and operation of FELs.

In collaboration with:

ESRF

nsls IR UV X

SPring-8

Sponsored by:

ELSE

Scientific Program Committee

- Yoshihiro Asano, Spring-8, Japan
- Paul Berkvens, ESRF, France
- Panakkal Job, NSLS, USA
- Giuliana Tromba, Elettra, Italy

Local Organizing Committee

- Giuliana Tromba, Elettra, Italy
- Alessandro Vascotto, Elettra, Italy
- Katia Casarin, Elettra, Italy
- Elisabetta La Torre, Elettra, Italy
- Elisa Quai, Elettra, Italy
- Ilde Weffort, Elettra, Italy
- Stefano Deiuri, Elettra, Italy

5th International Workshop on Radiation Safety at Synchrotron Radiation Sources

May 21-23, 2009
Trieste, Italy

Previous editions

RADSYNCH 2001 - APS (USA)
RADSYNCH 2002 - ESRF (France)
RADSYNCH 2004 - Spring-8 (Japan)
RADSYNCH 2007 - CLS (Canada)

List of participants

Abrami	Alessandro	Elettra, Italy
Asai	Juhachi	Canadian Light Source University of Saskatchewan, Canada
Asano	Yoshihiro	Spring-8, Japan
Ballerini	Marcello	El.Se. s.r.l., Italy
Bauer	Johannes	SLAC, USA
Benmerrouche	Mo	Canadian Light Source Inc., Canada
Berkvens	Paul	ESRF, France
Birkel	Ingrid	ANKA-ISS, Germany
Bonner	Paul	Diamond Light Source, UK
Burge	Frances	Diamond Light Source Ltd, UK
Casarin	Katia	Elettra, Italy
Casey	Robert	NSLS-II Brookhaven National Laboratory, USA
Chen	Huang Lung	Feynman Tech. Co. Ltd, Taiwan
Day	Lorraine	LSU/CAMD, USA
Dooling	Jeffrey	Argonne National Laboratory, USA
El Ashmawy	Mostafa	Elettra, Italy
Emery	Louis	Argonne National Laboratory, USA
Esposito	Adolfo	INFN Frascati National Laboratories, Italy
Fernandez	Ferran	CELLS-ALBA, Spain
Guallini	Ferdinando	El.Se. s.r.l., Italy
Hulber	Erik	Radosys Ltd. Company, Hungary
Jheeta	Kuldeep	S M S Medical College and Attached Hospitals, India
Job	Panakkal	Brookhaven National Laboratory, USA
Klett	Alfred	Berthold Technologies GmbH & Co. KG, Germany
La Torre	Elisabetta	Elettra, Italy
Leuschner	Albrecht	DESY, Germany
Lundin	Magnus	Maxlab, Sweden
Longo	Francesco	INFN Trieste & Elettra, Italy
Madacki	Roberto	LNLS, Brazil
Mage	Corinne	SOLEIL, France
Merlino	Giuseppe	El.Se. s.r.l., Italy
Nakamura	Hajime	PF-AR in KEK, Japan
Ott	Klaus	Helmholtz Zentrum Berlin Bessy II, Germany
Prezado	Yolanda	ESRF, France
Pruvost	Jean-Baptiste	SOLEIL, France
Quai	Elisa	Elettra, Italy
Queralt	Xavier	CELLS-ALBA, Spain
Schmidt	Jonathan	Canadian Nuclear Safety Commission, Canada
Sheu	Rong-Jiun	NSRRC, Taiwan
Tromba	Giuliana	Elettra, Italy
Vascotto	Alessandro	Elettra, Italy
Wroblewski	Thomas	HASYLAB DESY, Germany
Wysokinski	Tomasz	Canadian Light Source Inc., Canada
Xia	Xiaobin	Shanghai Institute of Applied Physics Chinese Academy of Sciences (SINAPCAS), China

Program

21/05/2009, Thursday	
08:30 - 09:15	REGISTRATION
09:15 - 09:30	WELCOME
SESSION 1:	**Synchrotron Radiation Sources Upgrades (Chair: R.J.Sheu)**
09:30 - 10:00	*R.Madacki,* LNLS radiological safety improvements
10:00 - 10:30	*M.L.Marceau-Day,* Upgrade Challenges at a 2nd Generation Ring
10:30 - 11:00	*coffee break*
SESSION 2:	**Commissioning of new Facilities (Chair: W.R.Casey)**
11:00 - 11:30	*M.Benmerrouche,* Commissioning of CLS Phase II beamlines
11:30 - 12:00	*X. Queralt,* Radiological studies during the ALBA Linac commissioning
12:00 - 12:30	*F.Fernandez,* Radiological studies during the conditioning of the RF cavity for the ALBA Storage Ring
12:30 - 14:00	*lunch*
SESSION 3:	**Medical Beamlines Issues (Chair: G.Tromba)**
14.00 - 14:30	*P.Berkvens,* Dosimetry issues related to the SSRT project at the ESRF
14:30 - 15:00	*J.Asai,* Dose rate considerations for the BMIT POE3 at the Canadian Light Source
15:00 - 15:30	*A. Abrami,* The SYRMA project for clinical mammography @ Elettra: Safety, Control and Supervision Systems
15.30 - 16:00	*P.Berkvens,* Shielding Design for the Imaging and Medical Beamline at the Australian Synchrotron
16:00 - 16:30	*coffee break*
SESSION 4:	**New Facilities Design - I part (Chair: L.Day)**
16:30 - 17:00	*A.Leuschner,* Radiation Protection Concept and Commissioning of the PETRA III Storage Ring
17.00 - 17:30	*T.Wroblewski,* Radiation Protection at the PETRA III Photon Beam Lines
17:30 - 18:00	*W.R.Casey,* ALARA Review of NSLS-II Design
18:00 - 18:30	*G.Tromba,* The FERMI project @ Elettra: radiation protection and safety issues

22/05/2009, Friday	
SESSION 5:	**Radiation monitoring systems (Chair: P.K.Job)**
09:00 - 09:30	*K.Ott,* Accuracy of Dose Measurements at BESSYII and MLS
09:30 - 10:00	*A.Leuschner,* The Radiation Monitor PANDORA (LB 6419) at PETRA III
10:00 - 10:30	*M.Ballerini,* Development and Experimental Performance Evaluation of a Dose-Rate meter for Pulsed Beam
10:30 - 11:00	*coffee break*
SESSION 6:	**Radiation Measurements - I part (Chair: K.Ott)**
11:00 - 11:30	*A.Esposito,* On the unfolding problem in neutron spectrometry around high-energy electron facilities

11:30 - 12:00	*H.Nakamura,* Radiation Safety issues for the PF-AR in KEK
12:00 - 12:30	*P.K.Job,* Activation Analysis of Soil, Air and Water near the NSLS II Accelerator Enclosures
12:30 - 14:00	*lunch*
SESSION 7:	**Simulation Studies (Chair: Y.Asano)**
14.00 - 14:30	*J.Dooling,* Simulation of Gas Bremsstrahlung Radiation from APS Undulator Straight Sections using MARS
14:30 - 15:00	*P.K.Job,* The Effectiveness of Thin Low-Z Scrapers in Electron Storage Rings
SESSION 8:	**Radiological Aspects in Top-Up Operation (Chair: Y.Asano)**
15:00 - 15:30	*J.Bauer,* Experiences From First Top-Off Injection At The Stanford Synchrotron Radiation Lightsource
15.30 - 16:00	*P. Bonner and F. Burge,* Top-Up at Diamond Light Source: preparation and initial practical experience
16:00 - 16:30	*coffee break*
16:30 - 17:00	*transfer to Elettra*
17:00 - 18:30	*visit at Elettra*
18:30 - 19:00	*transfer to restaurant ("FURLAN" restaurant, Zolla 19, Monrupino, TS)*
19:00 - 22:00	*social dinner*
22:00 - 22:30	*transfer to Adriatic Guest House*

23/05/2009, Saturday	
SESSION 9:	**New Facilities Design - II part (Chair: P.Berkvens)**
08:30 - 09:00	*X.Xia,* Radiation Safety System of Shanghai Synchrotron Radiation Facility
09:00 - 09:30	*R.J.Sheu,* Radiation Safety Considerations for the TPS Accelerators
09:30 - 10:00	*Y.Asano,* Shielding Design of the SPring-8 XFEL Facility
10:00 - 10:30	*M.Lundin,* Bulk shielding design for the MAX IV facility
10:30 - 11:00	*coffee break*
SESSION 10:	**Radiation Measurements - II part (Chair: M.Benmerrouche)**
11:00 - 11:30	*J-B.Pruvost,* In vacuum ID beam line shielding commissioning and direct gas-bremsstrahlung measurements at Synchrotron SOLEIL
11:30 - 12:00	*Closing session (Y.Asano, P.Berkvens, P.K.Job, G.Tromba)*

Contents

LNLS radiological safety improvements

Roberto Madacki[1]

[1]*Brazilian Synchrotron Light Laboratory, LNLS, Campinas city, State of Sao Paulo, Brazil*

Abstract

It will be presented some radiological safety improvements that were done in the LNLS machine since 1997, when the synchrotron source was opened to the users.
At that time the synchrotron source didn't have a Booster, nor shielding roof over the ring, nor totally metallic hutches. Personnel were not allowed to stay in the ring building during injections (except in the rooms of the 1st and 2nd floors of the south side, including the control room). That was our first type of machine operation. One of the most important upgrade on the machine performance was achieved by the construction of a 500 MeV Booster synchrotron, which brought a significant improvement for safety, on the dose distribution profile around the ring. After the installation of concrete roof and inner wall, additional localized lead inside the ring, and new gamma shutters, personnel now are allowed to stay at the experimental hall during injections. We also improved the safety at beamlines.

1. The LNLS machine parameters

The Brazilian Synchrotron Light Laboratory is operated by the Brazilian Association for Synchrotron Light Technology (ABTLuS) under a contract with the National Research Council of the Ministry of Science and Technology (CNPq) and the Brazilian Ministry of Science and Technology (MCT). The equipment was designed, built and is completely operated by Brazilians.

1.1. Initial parameters of the LNLS equipment

The first synchrotron light source in the Southern Hemisphere and the only one of this kind in Latin America has been in operation at LNLS since July 1997. The LNLS synchrotron light source was opened to external users with the following composition [1]:

- 1.37 GeV storage ring, 93 m perimeter (initially, with no roof) (Fig.1)
- Transport line
- 120 MeV electron LINAC injector
- 7 Beamlines

The LINAC is underground. The ring building has 3 floors:

- 1st floor, where are the experimental hall with the beamlines and several rooms for users support
- 2nd floor, where are the control room on the south side and several office rooms
- 3rd floor, for air conditioning machinery and maintenance

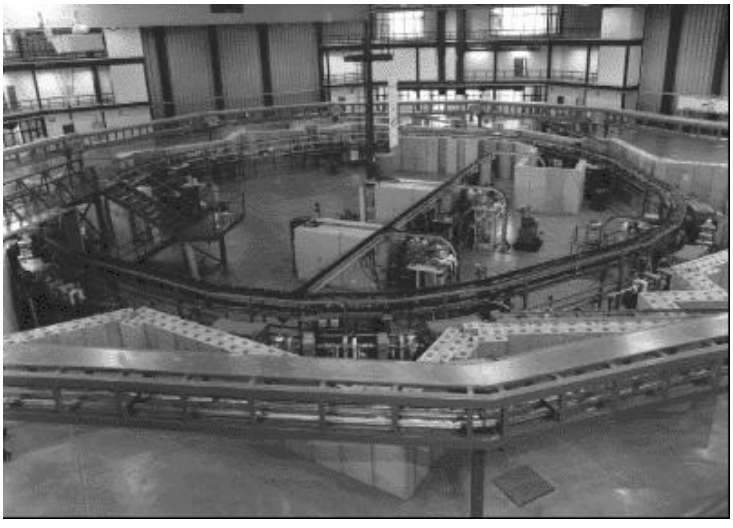

Fig.1 - General view of the LNLS ring in December, 1996.

Originally the storage ring was designed for 1.15 GeV/100 mA but the good performance of the magnets permitted to increase the energy to 1.37 GeV for routine operation (Table 1).

Operation energy	1.37	GeV
Injector	linear accelerator	
Injection energy	120	MeV
Nominal electron current	100	mA
Circumference	93.21	m
Mean diameter	30	m
Magnetic structure	double bend achromat	
Lattice symmetry	6-fold	
Revolution frequency	3.2	MHz
Harmonic number	148	
RF frequency	476	Mhz
Natural emittance	100	nm.rad.
Horizontal betatron tune	5.27	
Vertical betatron tune	2.17	
Synchrotron tune (at 500 kV rf gap voltage)	9.19×10^{-3}	
Natural horizontal chromaticity	-7.8	
Natural vertical chromaticity	-9.5	
Momentum compaction factor	8.3 x 10-3	
Natural energy spread	6.0 x 10-4	
Horizontal betatron damping time	13	ms
Vertical betatron damping time	13	ms
Synchrotron damping time	6	ms
Dipole bending radius	2.735	m
Bending field	1.67	T
Number of dipoles	12	
Number of straight sections for insertion devices	4	
Length available for insertion devices	2.95	m
Energy loss per turn from bending magnets	114	keV
Total radiated power from bending magnets	11.4	kW
Critical photon energy from bending magnets	2.08	keV
Electron lifetime	10	hours

Table 1 - Main parameters of the LNLS electron storage ring

Initially, the LNLS injection system consisted of a 120 MeV LINAC, without a Booster (Fig.2), basically due to financial and time constraints during the construction period, although the addition of a Booster synchrotron was kept as a possible future upgrade of the facility. In order to minimize any dose possibility, the injection region was set diametrically opposite to the south side, where is located the control room, shaded by the concrete and lead shielding covering the transport line.

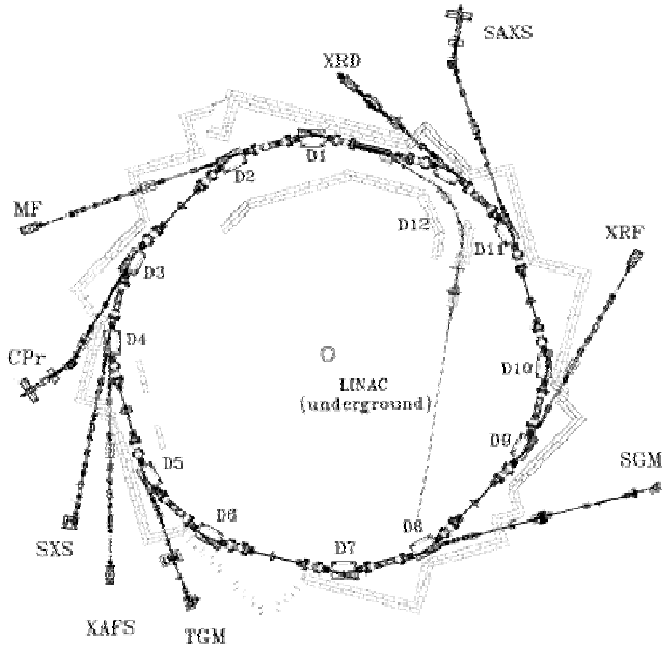

Fig.2 - Plan view of the LNLS storage ring in 1998.

Low injection energy like that can make injection difficult, with relatively high electron losses, and consequently, considering the fact that the ring had no roof, the dose profile around machine was at a higher level than that one aimed for unrestricted access to experimental hall. Because of this, personnel were not allowed to stay at the experimental hall (nor in other places of the ring building, except the 1st and 2nd floors of the south side) during injections. However, the individual doses, if the occupancy of the experimental hall was free all the time with normal injections, would be within the national and international limits for radiation workers, according to our estimates based on calculations and area dosimetry.

1.2. The LNLS machine parameters at the present days

Aiming to improve the injection efficiency and the performance of the stored beam (smaller stored beam transverse dimensions, a higher lifetime, greater total stored beam current, etc.), in particular for the small-gap insertion devices[1], it was constructed a Booster synchrotron, operating at 500 MeV [2]. The new basic composition of the light source consists of:

- 1.37 GeV storage ring, (Fig.3)
- Transport line
- 120 MeV electron LINAC pre-injector (underground)
- 500 MeV Booster synchrotron injector, 34 m perimeter
- 14 beamlines in full time operation for users, 1 under commissioning, 1 under design, 2 beamlines dedicated to beam diagnostics for the exclusive use of the LNLS staff.

The storage ring, transport line and Booster are encased at a 30 cm thick concrete roof with an additional 30 cm thick inner concrete wall. The new beam intensity is more than twice as large as the typical stored beam current before the installation of the Booster synchrotron. The more notable radiological consequence of the new injection system was the decreasing of values in mSv/month in the dose profile around machine, such as in the experimental hall, and in the second and third floor.

2. The improved LNLS shielding

The 1st operation of the 500 MeV Booster was in May of 2001, with no roof. On June 2003 was installed the last concrete block over the Booster. At the end of 2004 the Booster and storage ring were housed into a concrete tunnel (Fig.3), with additional lead shielding. This new machine configuration settled the present type of operation, resulting in the occupancy permit of the experimental hall during injections.

Fig.3 - Current operation type of the LNLS light source: it was constructed a Booster and installed concrete roof and inner wall. After that and other improvements people were allowed to stay at experimental hall during injections.

[1] We have already installed 1 undulator, and 1 normal wiggler. We are going to install 1 sc wiggler at the end of 2009.

3. The old and new dose profile around machine

More than one hundred TLD gamma dosimeters are placed in the ring building, in walls, columns, glass windows, suspended in the air, etc., covering all the neighboring of the machine, after the concrete shielding, including the experimental hall. They are read monthly. The dose profiles are followed with LiF dosimeters and CaSO4 dosimeters, from two different companies, as a comparative procedure. We also have albedo monitors for neutrons mounted on belts which are placed around containers of water, as human body simulators (our "phantoms"), and active monitoring stations for gammas and neutrons.

The Fig.4 shows the light source in the ring building, with the north (N), south (S), east (E) and west (W) orientation. The X marks on the drawing of the Fig.4 give an idea of the positioning of the dosimeters considered in this document (one for each floor, at the N, S, E and W sides, 15-30 m distant from the ring, depending on the location.

The Fig.5, Fig.6 and Fig.7 show the gamma dose distribution, in mSv/month, on the N, S, E and W sides of the 1st, 2nd and 3rd floor, respectively. Some dosimeters in the 3rd floor were placed only after January 1998. The readings from a dosimeter placed inside machine (from January 1999 until March 2007), before any shielding, in the second (horizontal) deflecting dipole at the transport line, is also shown as a reference for the machine operation intensity. Note that the dose profile follows the machine operation profile. It can be noted that the doses related to the 1st floor occurred at lower levels compared to the doses from the 2nd and 3rd floor. The dosimeter on the 2nd floor of the south side is more exposed to the machine than the control room itself.

In the new injection system, the transfer of electrons from the LINAC to Booster and from the Booster to the Ring occur on the N and W side of the ring building, respectively.

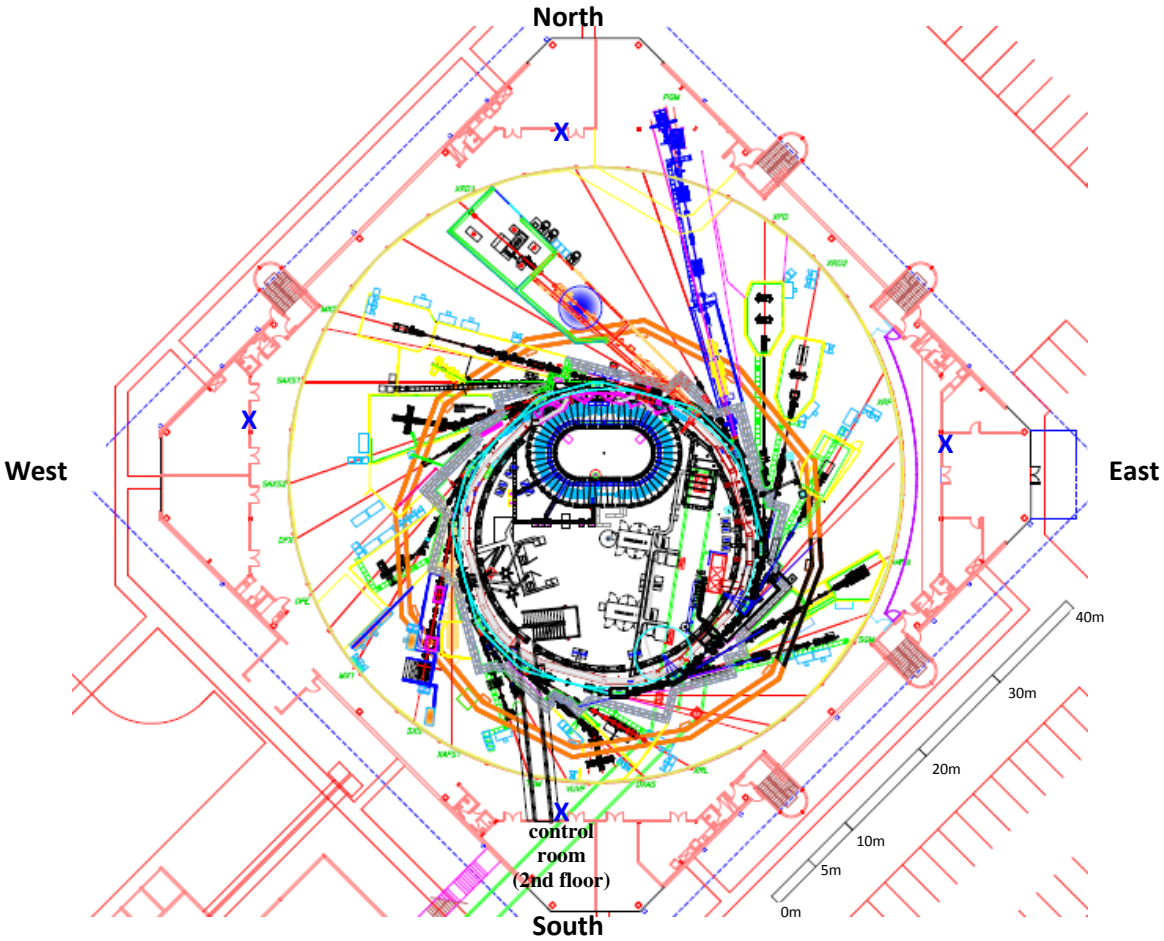

Fig.4 - The light source layout and the ring building. The considered dosimeters are placed in the positions marked X.

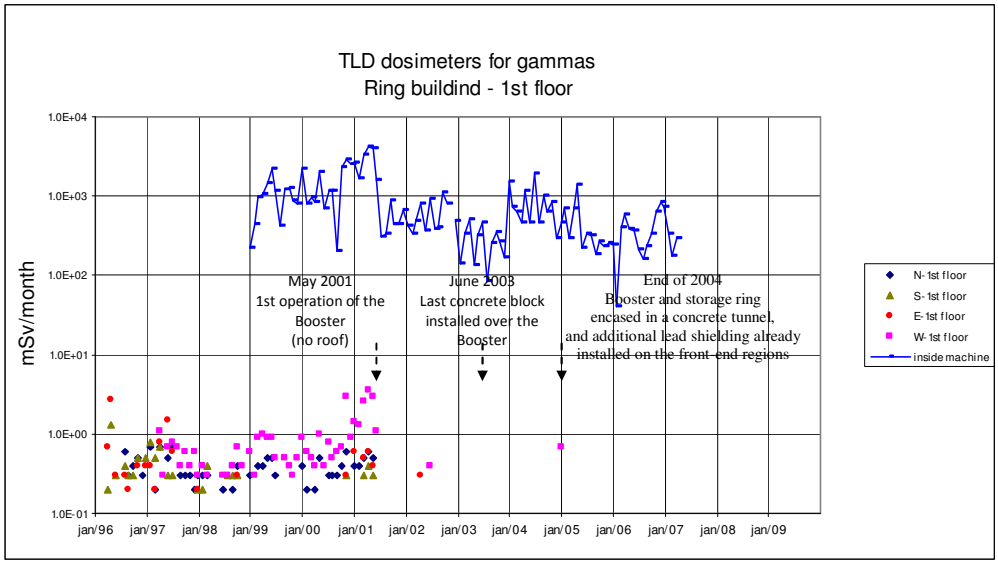

Fig.5 - Monthly doses from TLD dosimeters placed at N, S, E and W sides, in the 1st floor of the ring building.

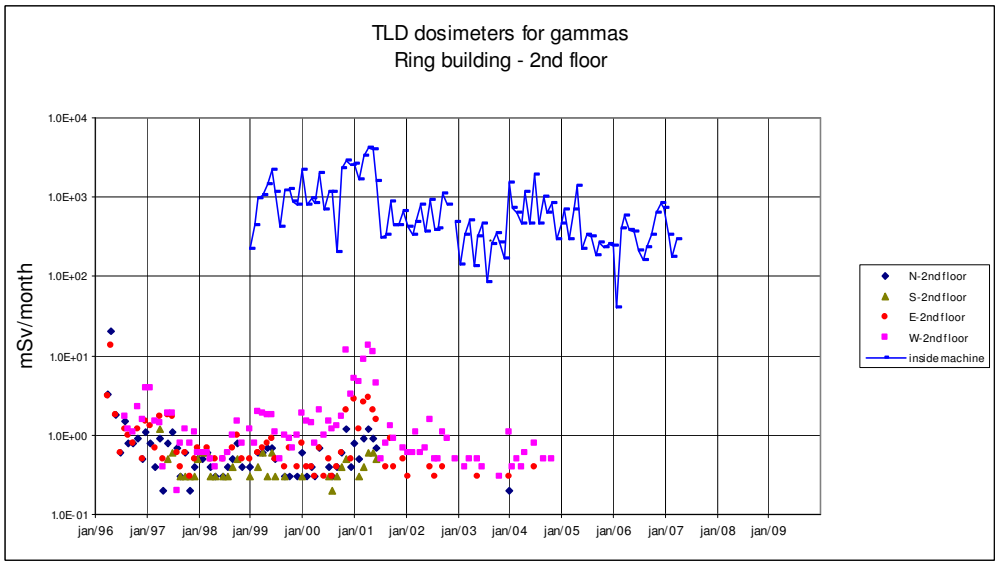

Fig.6 - Monthly doses from TLD dosimeters placed at N, S, E and W sides, in the 2nd floor of the ring building.

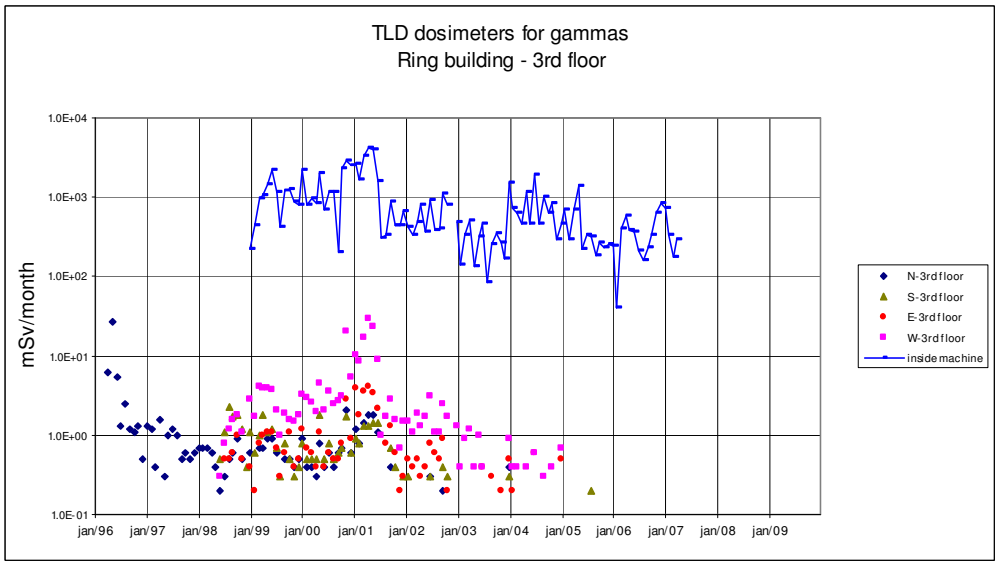

Fig.7 - Monthly doses from TLD dosimeters placed at N, S, E and W sides, in the 3rd floor of the ring building.

The neutron doses, not shown here, were always not greater than the gamma doses. As said above, several dosimeters, not shown, are placed at other positions around machine, covering different distances to the ring.

After the implementation of the current type of machine operation, all readings from all these dosimeters do not have presented values above the natural background levels. If the dose value is smaller than 0.2 mSv in a month, it is considered equivalent to the natural background radiation level (BG), and is plotted numerically zero for the purposes of this text. Note that after December 2004, after completion of the concrete shielding, no dose value was greater than 0.2 mSv in a month.
On the other hand, from the opening to users until now, the individual doses of monitored people at LNLS, given by TLD dosimeters for gammas, are BG. The same is always registered by the albedo monitors for neutrons, "worn" by the phantoms parked at strategic places in the ring building.

4. Beamline safety improvements

The beamlines received all-metal (steel) hutches. Before that, specific metal shielding was installed according to specific radiation monitoring. Now, the lead for gas-Bremsstrahlung in beamlines is designed according to ray-tracing method. Conservatively, we changed the experimental station shutters by ones with the same dimensions and material (Pb) of the gamma shutters.
We also improved our beamlines interlock system, which is now based on AS-i (actuator sensor interface) and programmable logic controllers. It is fail safe, comply redundancy, and has emergency buttons and safety keys.

References

[1] Aldo F. Craievich and A. Ricardo Rodrigues, "LNLS Synchrotron Source and Beamlines: Status, First Experiments and User Access", Brazilian Journal of Physics, vol. 27, Nº 4, December 1997.
[2] P. R. Tavares and Liu Lin, "The 500 MeV Booster Synchrotron for the LNLS Light Source", LNLS News Letter, Nº 2, page 3 (2000).
[3] http://www.lightsources.org/
[4] http://www.lnls.br

Upgrade Challenges at a 2nd Generation Ring

M.L. Marceau-Day[1]

[1]*Center for Advanced Microstructures and Devices, CAMD, Louisiana State University, 6980 Jefferson Highway, Baton Rouge, Louisiana, 70806, United States*

Abstract

Recently, the CAMD facility, a 1.3 GeV, 2nd generation synchrotron source, has been planning some major upgrades. Though funding has not been completely secured, several steps have already been initiated.
It is clear that each CAMD machine upgrade carries with it the potential for increased radiation as a consequence of enhanced energy or flux. Amongst the completed or proposed upgrades are the installation of a 2nd RF cavity in preparation for some new insertion devices. In tandem with this upgrade, the Linac energy will be increased from 200 to 300 MeV and the timing structure increased from 1 to 5 Hz.
Due to space limitations, the addition of a 3rd, 100MeV accelerating section to achieve the desired energy will require the movement of the Linac tunnel chicane, and its associated Radiation Interlock System (RIS), as well as necessitate the removal of the Klystron gallery from the Linac tunnel to the experimental hall floor. This task will require new wave guide structures, another potential radiation source. Knowledge of how and where losses occur remains an important feedback parameter for machine optimization in addition to radiation safety.
This paper will also discuss a novel method for evaluating beam losses in a synchrotron ring.

1. Introduction

The Center for Advanced Microstructures and Devices at Louisiana State University is a 2nd generation synchrotron source optimized for soft X-ray production (Fig.1). The first upgrade, the attachment of a He cryostat to a 7T wiggler, began in January, 2009. Removal of the wiggler (Fig.2) created new radiation patterns and elevated radiation readings during injection but not during the ramp file. The injection process in the CAMD facility takes only about 1 minute. Thus, it is difficult to attempt to pin-point a radiation source that dramatically disappears during the ramp file.
A novel method for the isolation and the characterization of this source point was developed. Knowledge of how and where losses occur remains an important feedback parameter for machine optimization in addition to radiation safety.

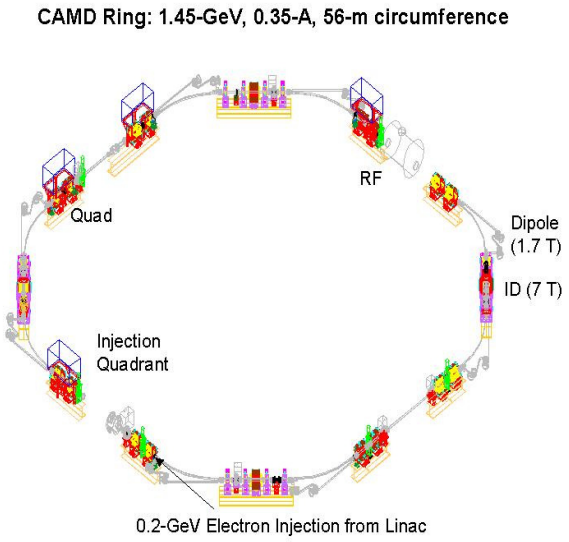

Fig.1 - Layout of the CAMD Storage ring.

Additional shielding had to be implemented. There is a proposal to replace the 7T wave-length shifter with a new super-conducting wiggler of 7.5 T. Two additional undulators are also proposed. Since the operating energy of the ring is severely constrained by the low energy injection, the Linac will be upgraded from 200 to 300 MeV.
Further, the injection rate is scheduled to increase from 1 Hz to 5 Hz. Each of these changes brings to light a myriad of Health Physics problems, each of which must be addressed [1,3]. These include the increased energy of these radiation sources that requires upgraded shielding, as well as a change in the timing structure. These changes can be calculated directly from the power equation (*Eq.1*). There is also a requirement for a new radiation interlock system for the Linac, as well as the movement of the chicane in the tunnel, wave-guide penetrations from the Linac tunnel to the experimental hall floor and relocation of the Klystron gallery to the experimental hall floor which must be assessed and considered for final approval of the new operational parameters. The change in power density is calculated using *Equation 1*.

Watts [Power] = [eV] x [Hz] x [sec] x [Amperes] (1)

2. Materials and Methods

The first phase of the upgrade involved the installation of a 2nd RF cavity, as a precursor to all other upgrades. Following the completion of this task, preparations were made to receive the components for the Linac upgrade as well as for the removal of the 7T super-conducting wiggler.
The wiggler was to be re-furnished with a He cryostat to reuse and to conserve Helium losses. Shielding (20cm) was placed upstream of the wiggler in preparation for this task. Since vacuum had been broken, a period of time was set aside for ring-re-conditioning. However, new radiation patterns emerged and persisted during the injection cycle but not during the ramp file.

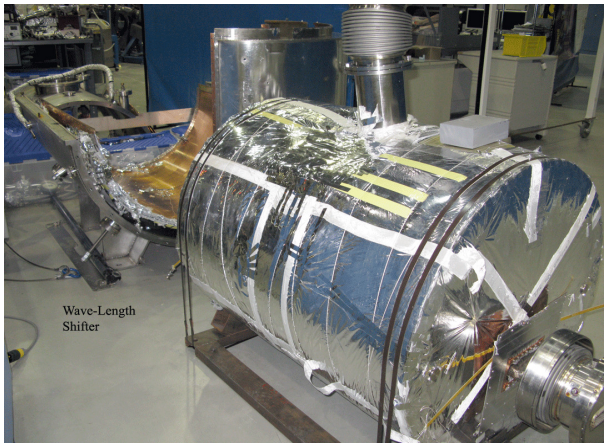

Fig.2 - 7T Wiggler removed from the CAMD storage ring.

To assess this new problem, normal ASA 400 exposed film was calibrated at 1 cm intervals. This film "ruler" was then placed over the suspected area of loss with the leading edge of the film marked on the beam pipe being assessed. This was so that the film could be placed back in the precise position after being surveyed for activation of the AgCl in the exposed film gel. Injection was turned on for 5 minutes without ramping. The film was retrieved from the beampipe and laid on a flat table.
Then, a survey meter (*Ludlum Model 12 equipped with a pancake probe*) was passed over the exposed film. When a section of film was found to be radioactive, it indicated that the Silver Halide had been activated from ^{107}Ag to ^{108}Ag [$T^{1/2}$ = 2.39 minutes]. A pin hole was cut into a 1.58mm plate of lead. This lead shield was placed between the pancake probe and the exposed film, making it possible to isolate the highest radiation reading on the film.
The area with the highest activation was marked on the film and the film placed back in its original exposure position on the beampipe. The hot spot was transferred to the precise location on the accelerator, indicating the source point [3]. The complete assembly is shown below (Fig.3). Due to the extremely short half-life of ^{108}Ag, the film could be re-used within 20 minutes.

Fig.3 - Exposed film with sheet of lead containing a pin-hole (not visible) and the Ludlum Model 12 survey meter equipped with a pancake probe to ascertain the area on the film with the maximum activation. Once maximum activation had been located, the film was transferred back to its original exposure placement and the loss point transferred from the film to the beam pipe to determine where beam was being lost.

3. Results

3.1. Planning and Evaluation of Health Physics Challenges

Several iterations of the Linac upgrade were considered. Due to lack of space to accommodate both the 3rd 100 MeV accelerating section and its associated klystron assembly, it was decided that the optimal solution required the movement of the klystron gallery with its associated modulators up to the experimental hall floor. Both the klystrons and their associated modulators will be moved up to the experimental hall floor (Fig.4).

Some of the other considerations include the movement of the shielding chicane to accommodate the third 100 MeV accelerating section, new wave guides from the Linac tunnel to the klystron-modulator assemblies, a new radiation monitoring system as well as additional shielding to account for the higher energy and timing structure. The output from the power density alone could conceivably increase radiation 6.9 times from current operational modes (Table 1).

P (W) = [eV] x [Hz] x [sec] x [Amperes]	**Watts**
Current	0.4
Approved	1.1
Upgrade	6.9

Table 1 - Increase in power density from current and approved operational modes to "Upgrade" mode as a consequence of proposed energy and frequency changes.

A summary of the various contributions to overall predicted radiation from each proposed change is given in Table 2. Although the maximum current achieved is slightly lower and the damping time (Tau) is decreased, significant radiation increases have been calculated with this upgrade.

Upgrade Component	Predicted Radiation over Current Ops
Energy Increase [from 200 to 300 MeV]	5 to 7.78 times
Frequency Increase [from 1Hz to 5Hz]	5
Pulse length [from 150 to 184nsec]	1.23
Tau	-3.38
Current Decrease [from 30mA to 25mA]	-0.2

Table 2 - Calculations of predicted radiation doses as a consequence of proposed Linac upgrade parameters at the CAMD facility. Not shown are the contributions from the klystrons and their associated modulators which will be moved from the Linac tunnel to the experimental hall floor.

The Linac upgrade will also require additional shielding [5.1cm] in the vertical transport line. The two 45 degree bending magnets in both the upper and lower portions of the vertical transport line may require the gap between the magnets to be narrowed to reach the proposed energy of the upgrade.
In their current configuration, some 5 cm of lead is placed in the band gap of these magnets to limit radiation.

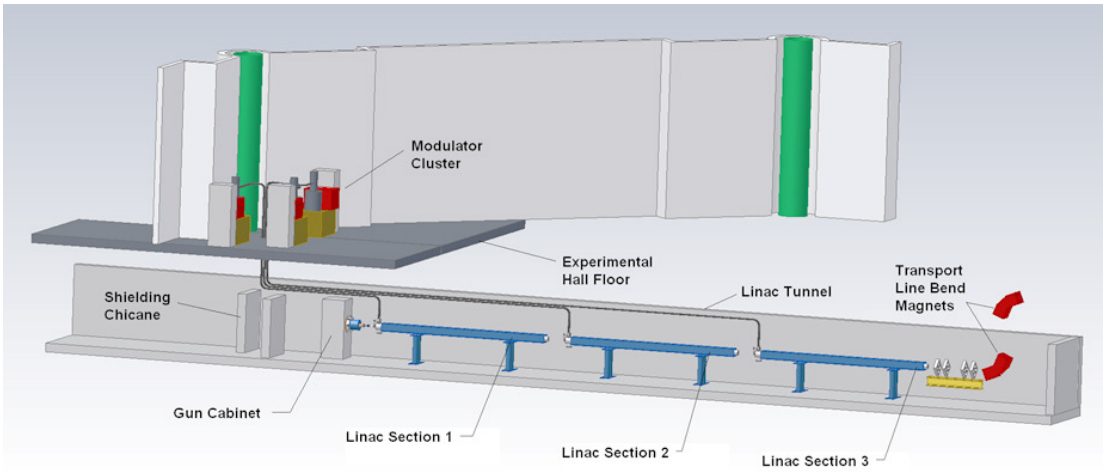

Fig.4 - Proposed new layout of the CAMD Linac upgrade, showing the Klystron galleries moved to the 2nd floor [indicated as modulator cluster], the new waveguide arrangement [shown in black]and the movement of the gun cabinet and the chicane wall [both shown in light grey]to accommodate the 3rd accelerating section (100 MeV) [shown in blue]. One of the Radiation Interlock interfaces occurs at the chicane, necessitating a complete electrical re-run of the Linac portion of the interlock system.

This shielding would have to be reconfigured to fit within the narrower gap and the shielding increased by 2 cm in thickness. Made-to-order shielding will have to be applied to the new klystron unit. Each of the klystron modulators operates at 280 KV, an electrical hazard. Klystrons, as well as, the Linac may be significant sources of dark current, a quantity not easily modeled.
Since the 3rd accelerating section must be tested in the experimental hall, test protocols must be developed for the safe commissioning of this unit within the constraints of a user-occupied facility. It is proposed to conduct these tests with remote radiation monitoring and a locked experimental hall during non-user beam dedicated machine studies time. Nevertheless, care must be taken to limit any activation potential of such activities so as not to create any restricted access places once user-beam is again available.

3.2. Measurements

Radiation monitoring was conducted during the installation and commissioning of the 2nd RF cavity. No radiation excursions were observed. An interesting radiation profile however, developed when the 7T Wiggler was removed. In preparation for this task, 20cm of shielding had been placed upstream of the wiggler.
During re-commissioning of the ring, a unique radiation pattern was found associated only with the injection and not the ramp portion of the ring fill. This persisted even after good operating vacuum had once again

been achieved. Since the injection portion of the fill only takes about one minute, it was difficult to track. However OSL [optically-stimulated luminescent dosimeters] monitoring throughout the facility, showed a higher than anticipated dose in direct line of sight from the former Wiggler position.

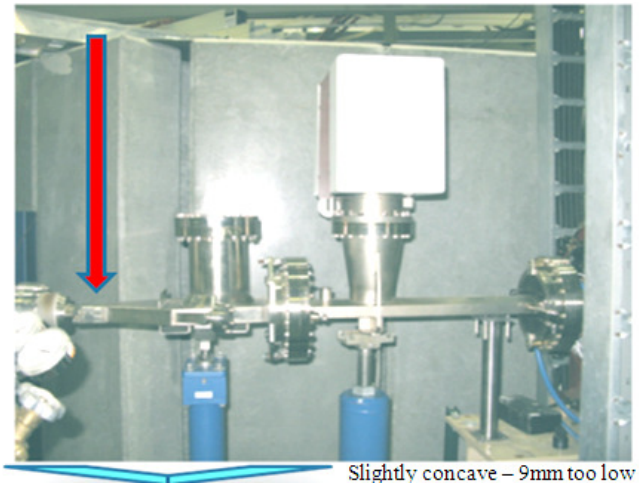

Fig.5 - Location of radiation source as a conse-quence of the beam-pipe being 9 mm too low. Point was identified by unique method of using exposed photographic film and looking for activation of ^{107}Ag to ^{108}Ag in the film emulsion. This isotope has aTt½ of 2.39 minutes. BMP's had been unable to detect this anomaly. With the beam pipe in the correct position, radiation dose was reduced from 72mSv to 32μSv.

This forward directed peak was assumed to be Gas Bremsstrahlung [2], so the shielding in place was increased in both size and breath. This failed to mitigate the injection associated dose pattern.
Radiation Safety suspected that a pair of knife edges where responsible such that the beam was hitting the knife edges. Of course, a 200 MeV beam is larger than the beam during ramp at 1.3GeV. However, beam position monitors [BMP's] indicated the beam was in the correct position. It was possible to verify the loss point through the use of exposed film with a built-in ruler[see under Materials and Methods], then to focus the maximum activation point of the AgCl in the film a pinhole was cut through a 1.6mm sheet of lead.to isolate the maximum activation point. When the maximum loss point was identified the film was placed back in the original exposure position and the source point identified by transferring the maximum loss point on the film to the pipe beam section directly below the film. Even though the BMP's showed the beam to be in the correct position, the beam pipe was 9 mm too low (Fig.5). The realignment of the beam-pipe reduced the overall radiation levels inside the ring from 72 mSv to 32 μSv.

Shortly after the re-positioning of the beam pipe, a bad coil was discovered in dipole magnet 5. This coiled displayed an intermittent short. The fault required beam position optimization two to three times per day.
No "*Golden Orbit*" could be maintained and continual adjustments were required. Since much of this optimization passed through the area that had been mis-aligned (Fig. 5), 20 cm of shielding was added to the area to protect from beam losses during the search for an optimal "Golden Orbit" during each injection cycle. No further radiation excursions were observed following this implementation of this safety precaution as evidenced by radiation surveys and from readings from optically stimulated luminescent dosimeters [OSL] routinely used as passive radiation integrating devices.
Thus, the new placement of Pb shielding continues to offer adequate shielding despite multiple orbits. Recently CAMD achieved a new injection maximum of 412MeV. However, for the moment, shielding appears to be adequate.

Several new insertions devices are also planned for the CAMD facility. This includes a 7.5T multipole wiggler with 18kW beam power, a 3.5T Multipole undulator (2kW) and a 35 period undulator. To accommodate this 3rd insertion device some sextupoles will be removed and the RF cavities split into these shorter straight sections.

4. Conclusions

It is clear that every upgrade requires careful and thorough planning. Despite the best planning scenarios, there are always unanticipated problems. Often, it is necessary to think "out of the box" to achieve the desired results. Health Physicists must rely on intuition in addition to technology. This was exemplified in the problem with the beam pipe in the synchrotron ring. The accelerator group maintained that the beam was in the correct position given the readouts of their BPM's. Through the application of a novel method to ascertain beam losses in the synchrotron ring, it was possible to reduce or eliminate both the parallel and forward directed radiation peaks on the experimental hall floor that were apparent during injection following the removal of the 7T Wiggler to attach a He cryostat. Dose rate measurements inside the ring fell from 72mSv to 32μSv when the beam-pipe was re-positioned. Planning, measurements and simulations [4] will continue through each phase of the proposed upgrades.

5. References

[1] B. Schleien, Editor: "The Health Physics and Radiological Health Handbook", 21-53; 127-218; (1989)

[2] R.H. Thomas, Editor."Radiation Protection for Particle Accelerator Facilities" NCRP Report No. 144, 39-70, (2003).

[3] M.L. Marceau-Day; R. Teague and W.H. Wang "A Novel Method to Assess Beam Losses", Operational Health Physics; *in press* (2009).

[4] J.D. Scott. "Shielding Program for the CAMD facility", unpublished (1993).

Radiological studies during the ALBA Linac commissioning

F.Fernández and X.Queralt

ALBA Synchrotron-CELLS, Carretera BP-1413, km 3, 08290 Cerdanyola del Vallès, Barcelona, Spain

Abstract

The commissioning of the ALBA Linac started in June'08 and finalized in October'08. During this period the klystrons, the accelerating cavities, and the Diagnostic line were set up reaching a maximum electron energy of 108 MeV with a pulse charge of 4 nC and a pulse length of 112 ns at a repetition rate of 3 Hz. Outside the Linac bunker the radiation dose levels were measured by means of online gamma and neutron monitoring, passive dosimetry and portable detectors surveying. Accumulated doses inside the bunker were measured in fixed places also with passive dosimetry. After every Linac operation the activation was measured with portable detectors to control the dose rates inside the bunker. Additional lead shielding was installed next to the electron loss points. Also in order to guarantee that the 0.5 μSv/h limit was not reached, outside the bunker some zones where delimited.

1. Introduction

The ALBA pre-injector is a 100 MeV Linac supplied by THALES Communications as a turn key system. It is located in the Linac bunker with part of the Linac-to-Booster Transfer Line (LTB). A Diagnostic line is mounted next to the first bending magnet of the LTB. During the Linac commissioning, the beam was guided to the diagnostic line to study its characteristics.

1.1. The ALBA Linac and Diagnostic line

The ALBA Linac consists of a 90 kV DC thermoionic gun, followed by the buncher, designed to reduce the energy spread and the electron losses. Two travelling wave constant gradient accelerating sections increase the energy up to >100 MeV [1]. The bunching system and the two accelerating sections are feed by two klystrons located outside the Linac bunker (see Fig.1). The ALBA Linac can work in Single bunch or in Multibunch mode. The Multibunch mode can deliver 4 nC shoots at a maximum repetition rate of 3 Hz.

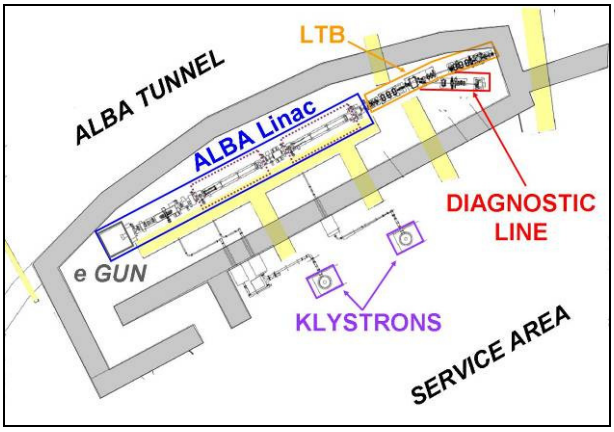

Fig.1 - Top view of the ALBA Linac bunker. The trenches used to pass signal and power cables are indicated in yellow. The heavy concrete (3.2 g/cm^3) walls are indicated in grey. The Booster, not plotted in this figure, is placed at the inner wall of the ALBA Tunnel.

After the ALBA Linac, the Linac-to-Booster transfer line (LTB) drives the electrons to the Booster synchrotron. Two dipole magnets, one inside the bunker and another outside, bend the electron trajectory to the Booster injection septum. The Diagnostic line is installed next to the first LTB bending magnet. This consists of one quadrupole, a fluorescent screen, a scraper with horizontal slits and finally, the Faraday Cup; where the beam current is measured (see Fig.2). Varying the current of the bending magnet coils and the position of the scraper slits, the profile and energy of the beam delivered by the Linac can be measured. In Fig.3 a picture of the LTB and Diagnostic line is shown during its installation period.

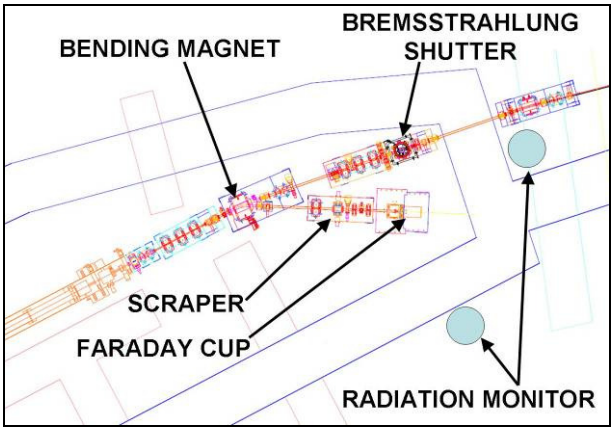

Fig.2 - Top view detail of the LTB and Diagnostic line in the Linac bunker.

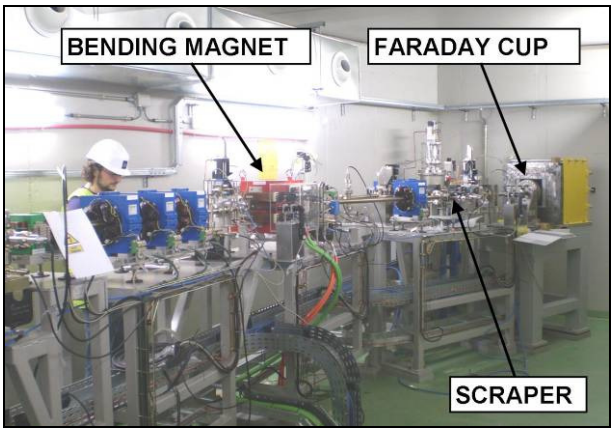

Fig.3 - Picture of the LTB and Diagnostic line in the Linac bunker.

The ALBA Linac commissioning started on June '08 with the startup of the Klystrons and the conditioning of the buncher and the accelerating cavities. After the 12 hours test at the maximum power, on October 16th, the Linac commissioning stopped to replace the provisional water cooling and power supply to the permanent one. In Table.1 the Linac specification values for the Multibunch mode are compared with the final commissioning results.

Parameter	**Specification**	**Measured**
Pulse length	0.3 to 1 μs	112 ns
Charge	≥ 3 nC (in 1 μs)	4 nC
Energy	≥ 100MeV	108 MeV
Pulse to pulse energy variation	≤ 0.25 % (rms)	0.06 % (rms)
Relative energy spread	≤ 0.5 % (rms)	0.23 % (rms)
Norm. Emittance (1σ)	≤ 30 π mm mrad (both planes)	< 25 π mm mrad (both planes)
Pulse to pulse time jitter	≤ 100 ps (rms)	25 ps (rms)
Repetition rate	3 to 5 Hz	1-3 Hz

Table.1 - Comparison between the specifications and the measured values for the Multibunch mode Linac characteristics.

1.2. The safety systems

The Linac bunker concrete walls and the Personal Safety System (PSS) allow the operation of the ALBA Linac at maximum power keeping the personnel radiation doses below the public limit; 1 mSv/y. This zones includes the ALBA Tunnel, which can be accessed while the Linac is operating with the Diagnostic line (Linac Only mode). This goal has been verified by the radiation detection means during the commissioning process.

The Linac bunker consist on 1 m heavy concrete (3.2 g·cm^{-3}) walls and a 1 m normal concrete (2.4 g·cm^{-3}) roof. The roof is formed by two layers of prefabricated blocks that can be removed. These blocks are placed in a way that there is not direct line of sight from inside to outside the bunker. The bunker has floor apertures and wall apertures. The first ones are the trenches through which the power and signal cables enter into the bunker. The second ones are the RF labyrinths used for introducing the RF power into the bunker, the alignment windows, the LTB hole, and the labyrinth entrance door.

The PSS avoid that anyone is irradiated while the Linac is on. This implies that there is no permit of operation if there are personnel inside the bunker, neither if the radiation dose rate levels are higher than 0.5 μSv/h outside the bunker. This system, based on PLC technology, is composed by certified SIL3 components: search and emergency buttons, a door locker and switch, light panels, beepers, access cards, relays and a safety PLC [2]. Also, it is connected to two radiation monitors, one installed in the Service Area and another in the ALBA Tunnel (see Fig.2). Both are placed at the downstream area of the bunker, where the electron energy is larger and most part of the electron losses is expected. The monitor in the ALBA Tunnel has a gamma detector and the one in the Service Area has a gamma and a neutron detectors. When the required conditions are fulfilled, the Linac PSS allow the operation of the electron gun and the klystrons (HVPS and RF signal). The Bremsstrahlung shutter permit is also controlled by the PSS.

In order to verify that the public dose limit is not exceeded, the following types of radiation measurements tools are used: portable detectors, radiation monitors and Termoluminsicent dosimeters (TLDs). The dose rates are controlled with portable detectors during operation in the ALBA Tunnel, the Service Area and the roof, including all the apertures mentioned before. In addition, the dose rates are measured online with the radiation monitors: the two mentioned above plus six monitors mounted on six trolleys, distributed around the Linac bunker. Finally, TLDs provided by an external certified service are placed outside the bunker and read monthly.

Inside the bunker, the activation of the accelerator components is measured with portable detectors after every Linac shift. Also TLDs are placed at the walls inside the bunker to measure the accumulated monthly dose.

2. Radiation measurements

2.1. Passive dosimetry

TLDs are placed outside and inside the bunker attached to the walls at beam height (140 cm). During June ’08 the startup of the electron gun and conditioning of the accelerating cavities and the buncher took place. In Fig.4 the TLDs data of this month is shown. The TLDs that presented higher doses are the closest to the buncher and to the accelerating structures. This is because during the conditioning, X-rays are produced in the cavities [3].

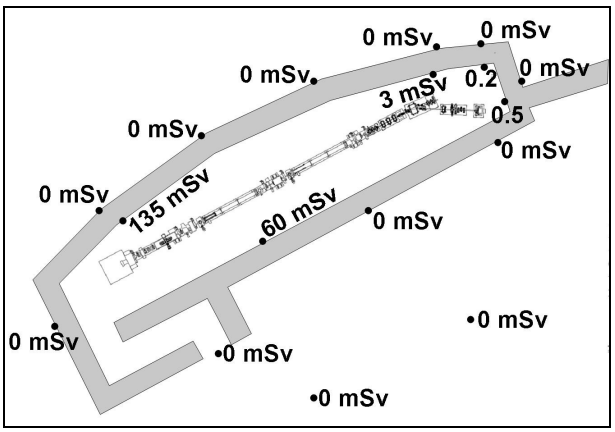

Fig.4 - TLDs data from June ’08. All TLDs are placed at the beam height. The data is shown in mSv.

During October ’08, Linac commissioning at average conditions of 107 MeV, 3 nC and 2 Hz was done. In this case, the TLDs that present higher doses are the ones that are close to the LTB bending magnet and to

the Diagnostic line (see Fig.5). This is because the commissioning tests produce larger electron losses at these Linac components.

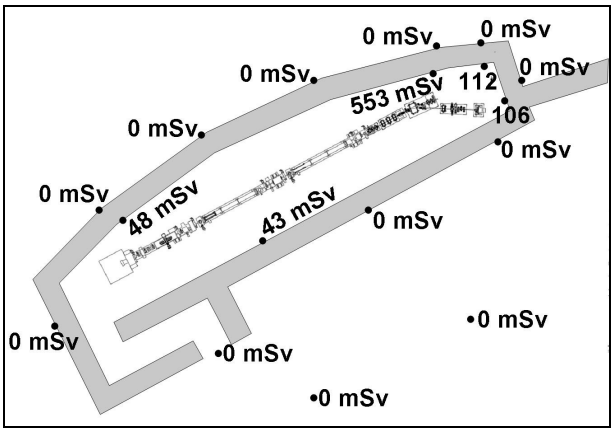

Fig.5 - TLDs data from October '08. All TLDs are placed at the beam height. The data is shown in mSv.

All the TLDs placed outside the bunker at beam height measured 0 mSv from June '08 to October '08. Additionally, twelve dosimeters were placed at the apertures of the bunker mentioned before. They also measured 0 mSv from June '08 to October '08. Only the one placed inside the ALBA Tunnel trench measured 0.5 mSv during October.

2.2. Radiation surveys

During every operation of the Linac, surveys with portable radiation detectors were done outside the bunker. The measurements showed that the dose rates levels are below 0.5 μSv/h except in three places: the klystrons surface opposite to the Linac, the bunker downstream wall and the roof concrete blocks gaps. In the first case, two iron plates 1 cm thick were installed at the klystrons to reduce the dose rate below 0.5 μSv/h. In the second scenario, lead blocks were placed near the LTB bending magnet and the scraper in order to reduce the dose rates near the downstream wall (shadow shielding). Additionally, the area where the dose rate could exceed the 0.5 μSv/h limit, 2m from the downstream wall, was labeled and restricted. Finally, for the third case, the roof access was fenced, even though the access is not permitted. These radioprotection actions guarantee that the radiation dose rate levels are below the public limit at the accessible zones.

2.3. Radiation monitoring

Eight radiation monitors, the two fixed and the six on trolleys, measure the dose rate every two seconds. The two fixed monitors are connected to the PSS. The one in the ALBA Tunnel is a gamma detector that has a dose rate alarm level at 0.5 μSv/h. During the Linac commissioning scans with the LTB bending magnet were done to determine the energy and energy dispersion of the beam. During these scans, part of the beam was not lost in the Faraday Cup but in the scraper and other elements of the diagnostic line. For this reason the mentioned alarm level was increased to 1.2 μSv/h. However, the accumulated dose never exceeded 2 μSv in 4 hours (0.5 μSv/h in average).

The changes in the Linac operation characteristics (increasing the pulse charge or closeing the scraper) can be related with the dose rate; which is proportional to the electron losses. In the Linac Only mode, the magnetic field is reduced when starting a bending magnet scan. Then, the electron beam is directed between the LTB and the Diagnostic line; in the direction of the zone where the detector at the ALBA Tunnel is placed. In Fig.6 a plot of the measured dose rate by the monitor placed at the ALBA Tunnel is shown. During this day the shadow shielding was still not installed and thus, the PSS tripped the Linac operation due to a dose rate alarm level when starting a bending magnet scan.

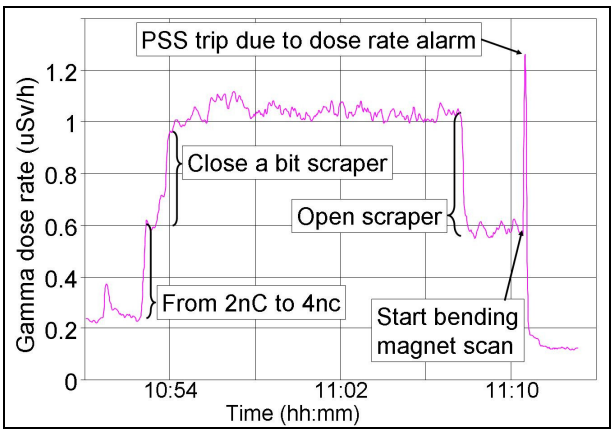

Fig.6 - Measured dose rate at the ALBA Tunnel near the downstream wall on September 26th. The shadow shielding near the bending magnet and the scraper was not installed.

2.4. Activation

The loss of electrons of energies higher than 7-20 MeV produces neutron radiation and activation [4]. The activated material usually generates electromagnetic radiation when the unstable isotope decays. The amount of radiation depends on the amount of electrons lost in that element and the lifetimes of the generated isotopes. The electromagnetic radiation can exit the elements generating a radiation dose rate in the Linac bunker after the Linac operation. The dose rate due to activation was measured along the ALBA Linac, LTB and Diagnostic line after every operation of the Linac by means of portable detectors. These measurements showed also the electron loss points.

In Fig.7 the measurements (in μSv/h) of the radiation due to activation on October 16th are shown. This day, the Linac was operated during 13 hours at 108 MeV, 4 nC and 1 Hz. The Linac most activated components were the Bending magnet and the scraper. This is because these are the components that present largest electron losses. The dose rate due to activation at the bending magnet surface during 12 days is presented in Fig.8 as a function of the time between the Linac operation and the activation measurement.

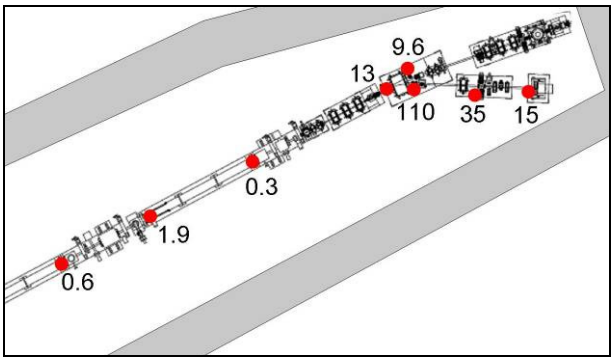

Fig.7 - Radiation measurements due to activation at the surface of the Linac and Diagnostic line elements on October 16th; just after13 hours of operation at 108 MeV, 4 nC and 1 Hz (all data in μSv/h).

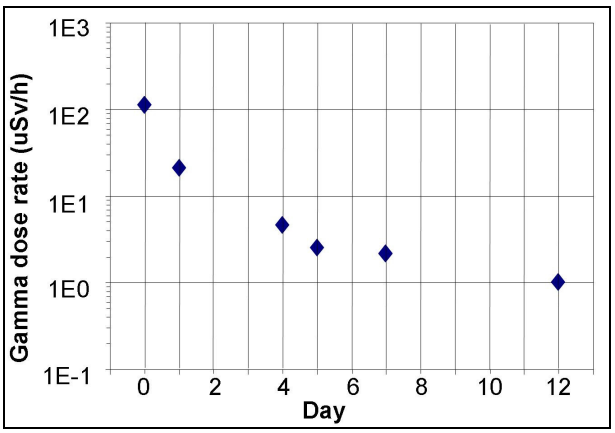

Fig.8 - Radiation measurements due to activation at the bending magnet surface for 12 days starting on October 16th.

The activation measurements were done just after every Linac operation to control the radiation levels and limit the zones that requires it. This protocol verifies that the radiation dose received by the workers do not exceed the public limit. For that reason, the Linac bunker access is controlled by administrative procedures.

3. Conclusions

The radiation dose measurements during the Linac commissioning have been presented as well as the radioprotection actions. The experimental data has shown that the Linac bunker maintains the dose rates outside the shielding below the public limit of 0.5 μSv/h. During Linac commissioning, the beam can be intercepted by the scraper when scanning the beam with the bending magnet. In this scenario extra radiation is produced and then, extra shielding is required. In this case, the use of local lead bricks shielding showed good results. Permanent lead screens are going to be installed.

The dose rate monitoring has been also presented. This equipment allows a precise and instantaneous follow up of the radiation levels due to the electron losses in the Linac bunker. The fast response of the PSS when exceeding a dose rate alarm has also been verified.

Finally, the activation measurements of Linac components have shown the need of an access control procedure after the Linac operation. This will be implemented through an administrative procedure and through the PSS; that will not allow the access into the Linac bunker during a given period of time after the Linac use.

Acknowledgments

We want to thank the Thales team and the ALBA Linac team for the fruitful discussions and help given.

References

[1] M. Pont, D. Einfeld, A. Falone, A. Setty, D. Jousse, J-L. Pastre, F. Rodriguez, A. Sacharidis, “Status of the 100 MeV preinjector for the ABLA synchrotron” Proceedings of the European Particle Accelerator Conference, (2008).

[2] D. Fernández, “Contract specification for the design, supply, programming, installation and acceptance demonstration of the Personnel Safety System for the Linac, booster synchrotron and the storage ring”, Technical Specifications (2006).

[3] F. Fernández, X. Queralt, J. Sentkerestiova, “Radiological studies during the conditioning of the RF cavity for the ALBA Storage Ring” Proceedings of the 5th International Workshop on Radiation Safety at Synchrotron Radiation Sources (2009).

[4] J. S. Levinger, “Theories of photonuclear reactions”, Annual Review of Nuclear Science, vol 4, 13-32 (1954).

Radiological studies during the conditioning of the RF cavity for the ALBA Storage Ring

F.Fernández[1], X.Queralt[1] and J.Sentkerestiova[2]

[1]*ALBA Synchrotron-CELLS, Carretera BP-1413, km 3, 08290 Cerdanyola del Vallès, Barcelona, Spain*

[2]*Institute of Biophysics ASCR, v.v.i., Královopolská 135, 612 65 Brno, Czech Republic*

Abstract

ALBA is a 3 GeV, 400 mA, 3rd generation Synchrotron Light Source that is in the construction phase in Cerdanyola, Spain. The Storage Ring (SR) will have 6 RF single cell cavities to maintain the beam energy at 3 GeV. The first cavity was delivered in 2007 and it was conditioned during 2008. The conditioning was done inside a bunker aiming to guarantee the dose rate level below 0.5 µSv/h at any work place outside this bunker. We present the radiation measurements performed during this conditioning stage. The measurements were done using TLD dosimetry, online gamma monitor, portable detector and gamma spectrometer.

1. Introduction

This paper describes the first radiation measurements performed during the conditioning stage of one of the six ALBA SR cavities. Radiation measurements outside the shielding have been done to verify that the shielding reduces the dose rate below 0.5 µSv/h. Dose rate and spectrum measurements inside the shielded area have been done to study the production of radiation as a function of the RF power.

1.1. ALBA RF system

The ALBA SR RF System provides 3.6 MV of accelerating voltage and restore up to 540 kW of power to the electron beam [1]. This will be done by 6 High Order Mode damped cavities tuned at 500 MHz, designed at BESSY and known as the EU cavity (see Figure 1). Each cavity will be feed by two RF amplifiers based on an Inductive Output Tube (IOT) that delivers up to 80 kW each one. The six cavities are grouped in three pairs along the SR. In Fig.2 a picture of one of the three RF plants partially installed at the ALBA Service Area is shown.

Fig.1 - ALBA SR cavity inside the bunker.

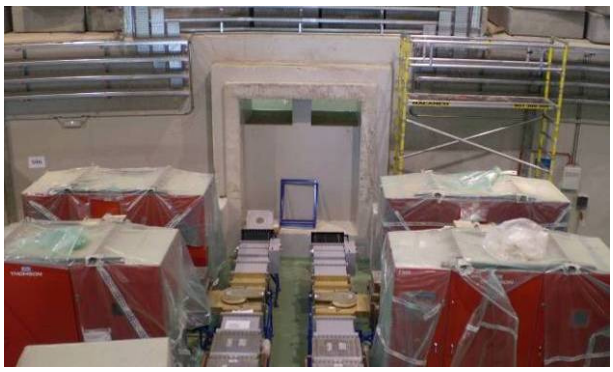

Fig.2 - ALBA SR RF plant. The four IOTs are in the four red cabinets. The two apertures of the tunnel wall can be observed because the RF labyrinth cover is removed for the installation of the waveguides (not finished yet).

1.2. The RF bunker

For the conditioning of the RF cavities, the six of the SR and the one of the Booster, a dedicated bunker was built aiming to guarantee a free access outside it (0.5 μSv/h). Like in the RF system at the ALBA synchrotron, the IOT is placed outside the bunker, and the cavity inside. A waveguide drives the power from the IOT to the cavity entering the bunker through the upper part (see Fig.3). The bunker has no roof. The cavity is oriented in a way that the beam axis crosses the measurement point A and the wall of measurement point C perpendicularly.

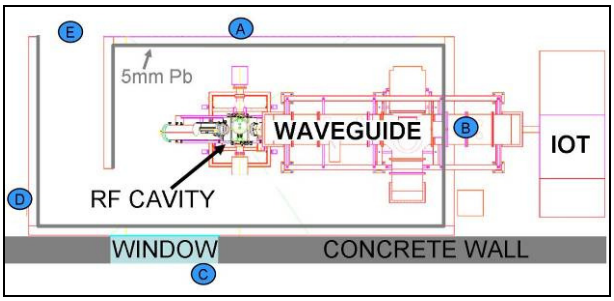

Fig.3 - Top view of the RF bunker. The measurement points outside the bunker are indicated in the blue circles.

In order to absorb the radiation generated in the cavities, the brick walls are covered with a lead foil of 5 mm. The calculations to determine this thickness are based on experimental results of dose rates outside the cavity as a function of the power [2]. In this study, the cavity has the same design as the ALBA Booster RF cavity, also commissioned in this bunker.

The first radiation measurements with the SR cavities (see later), revealed the need of a RF bunker shielding reinforcement. As a result, the wall side of measurement point A was reinforced with 30 cm thickness heavy concrete blocks of 3.8 g/cm^3 (see Fig.4). In the opposite side, a lead screen of 5 cm was installed inside the bunker between the cavity and the wall of measurement point C (see Fig.4).

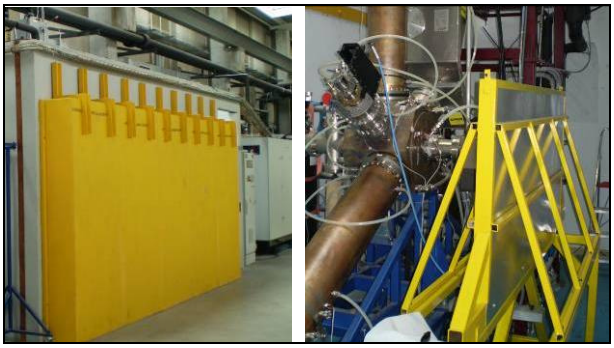

Fig.4 - Heavy concrete shielding reinforcement at measurement point A (left) and lead shielding reinforcement between the cavity and measurement point C (right).

A Personal Safety System (PSS) is installed in the RF bunker. It prevents anyone to be in the bunker while the cavity is receiving power. This system, based in PLC technology, is composed by search and emergency buttons, a door locker and switch, light panels, beepers, access cards and a safety PLC. The PSS components are certified as SIL3 security level [3].

2. Measurements

During the conditioning phase of the SR cavity, measurements were done using TLD dosimetry, portable detectors, an online gamma monitor and a gamma spectrometer. The measurements are divided in two categories: measurements outside the bunker and measurements inside the bunker.

2.1. Dose rates outside the bunker

The measurements outside the bunker aim to verify that the dose rates at public zones are below 0.5 μSv/h. The commissioning of the RF system started with the IOT startup. The dose rate measured with portable detectors outside the IOT cabinet with the door closed was 0 μSv/h. Inside the cabinet, the dose rate on surface of the IOT raised up to 100 μSv/h at 80 kW; the maximum power. Thus, the access to the cabinet is restricted and controlled with a key. The portable detectors used for the measurements are gas chambers suitable for X-ray energies higher than 25 keV.

During the first tests of the SR cavity the maximum power (80 kW) could be achieved with a duty cycle of 20 ms at 10 Hz (20% of average power). The dose and dose rates were measured by means of TLDs and portable detectors. In Table-1 the survey measurements with portable detectors are shown. The dose rates were much higher in the beam axis direction; the direction where the electric field is expected to be maximum. In order to guarantee that the dose rate outside the bunker is below 0.5 μSv/h, at a duty cycle of 100% a shielding reinforcement was required at the walls that intercept the beam axis; the ones of measurement point A and C.

	Dose rate (μSv/h) @ point				
	A	B	C	D	E
Without shielding reinforcement	14-25	0.3	3.5	0.0	0.5
With shielding reinforcement	0.07	0.3	0.08	0.0	0.5

Table 1 - Measured dose rates outside the RF cavity bunker with and without shielding reinforcement with portable detectors. The measurements were done at 80kW RF power, 20% duty cycle, at beam height.

The required extra shielding was determined measuring the dose rates with a detector shielded with different materials and thicknesses. These measurements were done at a duty cycle of 20%. The results were extrapolated to guarantee dose rates outside the bunker below 0.5 μSv/h at a 100% duty cycle. The wall of measurement point A was reinforced with 30 cm thickness heavy concrete blocks of 3.8 g/cm^3. In the other direction, a lead screen of 5 cm was installed between the cavity and the measurement point C. The measurements were repeated with 20% duty cycle after the installation of the shielding reinforcement (see Table-1). The dose rates of points A and C decreased below the 0.1 μSv/h limit; what corresponds to 0.5 μSv/h for a 100% duty cycle.

The bunker has no roof. The radiation doses were measured at a RF power of 80 kW with a duty cycle of 20%. The dose rate above point A on top of the wall (3 m height) was 70 μSv/h. At 3 m height the dose rates were 0.8 μSv/h, 0.6 μSv/h and 0.4 μSv/h at one, two and four meters away the bunker wall. Thus, a special permission is required to work at height near the bunker while the RF is on.

2.2. Dose rates inside the bunker

Three types of measurements were done inside the bunker, TLD dosimetry, online dose rate monitoring and X-ray spectroscopy. These measurements aim to study the generation of radiation by the cavity and relate it with the RF power. The production of dark currents by field emission in radiofrequency (RF) cavities is well known [4]. These electrons are accelerated in the cavities and can impact the inner walls generating Bremsstrahlung radiation. These X-rays can leave the cavity generating a radiation environment around it

[5]. The production of the dark currents, and therefore the X-rays, is much more important throughout the first runs of the cavity, the conditioning period.

The accumulated dose at the outer surface of the cavity was measured with TLDs at 80 kW and 20% duty cycle during one hour of operation. The dose rate at the RF surfaces that intercepts the beam axis (facing the measurement points A and C) was ~14 mSv/h. The dose rate at the RF surfaces perpendicular to the beam axis (facing the measurement points B and D) was ~3 mSv/h. Also at 80 kW and 20% duty cycle, the dose rates were measured at the inner surfaces of the bunker walls with TLDs. Next to points A, B, C and D, the dose rates inside the bunker were 227 µSv/h, 6 µSv/h, 174 µSv/h and 26 µSv/h, in that order. The dose rates were much higher in the direction of the beam axis. This direction is the one that maximizes the electric field and therefore the direction which more electrons can be extracted through field emission and the dark current electrons can be more accelerated. These dose rates were calculated from the TLDs accumulated dose and the RF cavity operation hours.

A radiation monitor was installed inside the bunker next to measurement point A to acquire the photon dose rate online (see Fig.1). This let us correlate the radiation dose with the RF power in the cavity; also measured online. In Fig.5 the dose rate and the RF power are shown during one cycle; increase the RF power from 0 kW up to 80 kW and decrease it again to 0 kW. The radiation generated by the RF cavity is measured for RF powers lager than 25 kW.

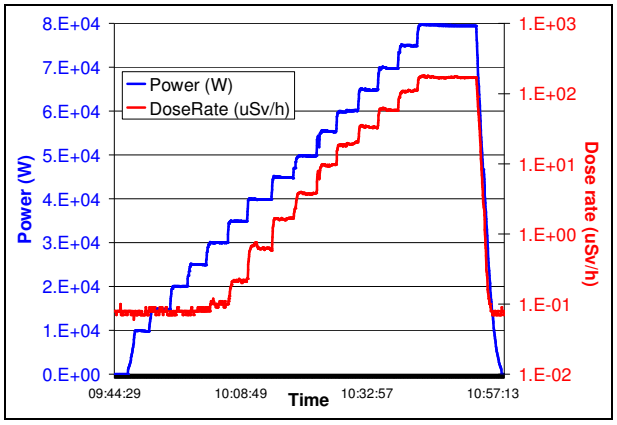

Fig.5 - RF power and photons dose rate inside the bunker during one cycle.

In Fig.6, the dose rate is plotted as a function of the RF power for different cycles for different days. The dose rate decreased as the cavity was more conditioned. The dose rate corresponding to April 29th was higher when decreasing the RF power. The explanation of this effect is still under discussion.

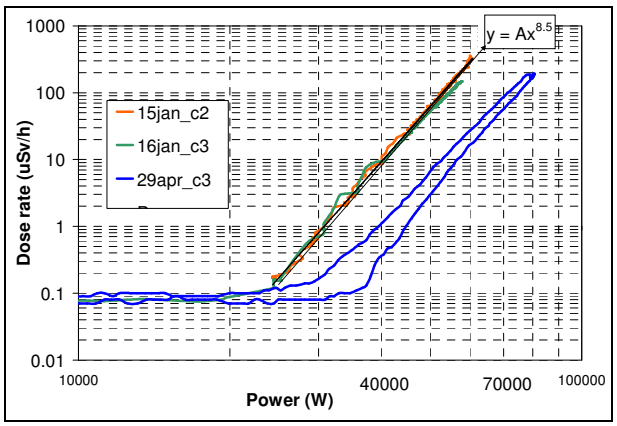

Fig.6 - Photons dose rate as a function of the RF power during three cycles of different days. The April 29th cycle dose rate is higher during the RF decrease.

The January 15th data is fitted to a power function (see Fig.6). This dependence is described in other works, where the power constant is 10.5 [5] or 9.6 [4]; while in our case is 8.5. The difference in the exponent could be probably attributable to the characteristics of the different cavities.

The X-ray spectrum was measured inside the bunker. The spectrum was measured during two minutes for different RF powers from 45 kW to 80 kW in steps of 5 kW (see Fig.7). The maximum energy detected by the spectrometer increased when increasing the RF power. This is because the electric field inside the cavity increases when increasing the RF power. The maximum energy of the Bremsstrahlung radiation that can be generated in the cavity is the maximum energy of the dark current electrons; which is proportional to the electric field in the cavity. As the RF power is proportional to the square of the electric field in the cavity, the maximum X-ray energy that can be generated in the cavity is proportional to the square root of the RF power. In Fig.8, the maximum energy of the X-rays spectrum is plotted as a function of the square root of the RF power. The data is fitted to a linear function showing a good agreement (R^2=0.990). During the whole conditioning period, the maximum X-ray energy measured with the spectrometer was 800 keV; at the beginning of the conditioning period.

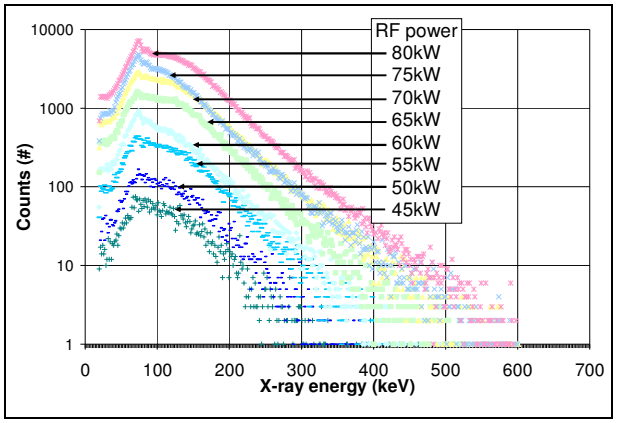

Fig.7 - X-ray spectrums at a different RF power from 45kW to 80kW in steps of 5kW. The spectrums were measured at 1m from the cavity surface inside the bunker (near measurement point A).

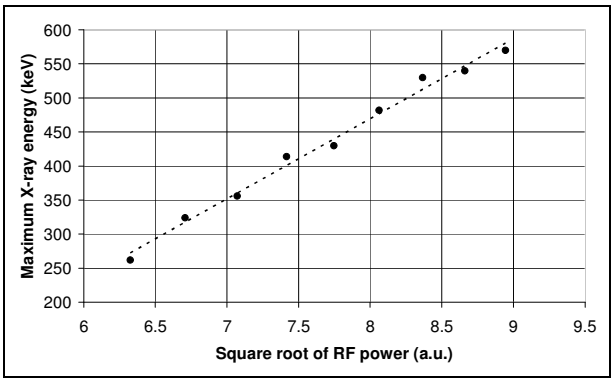

Fig.8 - Maximum energy of the x-ray spectrum as a function of the square root of RF power.

3. Simulations

A Monte-Carlo simulation of the cavity is done with the FLUKA code [6]. This simulation aims to estimate the current of electrons extracted from field emission and accelerated inside the cavity. The gamma dose per primary electron hitting the inner part of the cavity is simulated inside and outside the bunker. For this simulation two simplifications are taken: consider the cavity as a 15 mm thick walls copper cylinder and consider a 800 keV monoenergetic dark current electron beam (see Fig.9). The first assumption is taken because it is not known where the electrons hit the cavity. Fifteen millimeters is the average surface thickness of the face where the electrons can impact. Secondly, 800 keV is the maximum X-ray energy measured with this cavity.

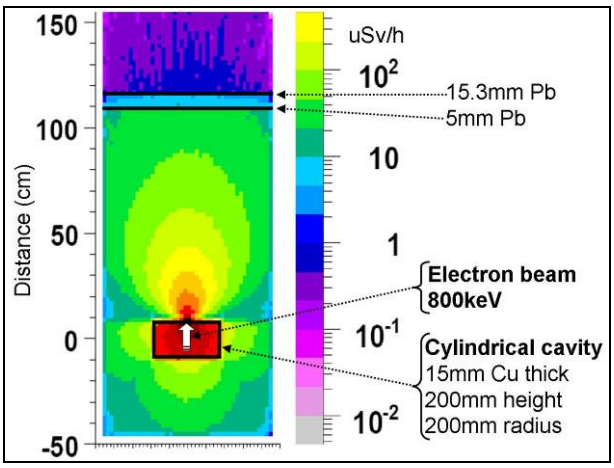

Fig.9 - RF cavity simulation layout and dose rates. The electron current has been scaled to fit the measured dose rates.

The electron current in the cavity is estimated matching the simulated pSv per primary electron after two lead foils ($2.5 \cdot 10^{-13}$ pSv/e and $3.4 \cdot 10^{-14}$ pSv/e) with the measured dose rate (14.3 μSv/h and 1.9 μSv/h). The first lead foil corresponds to the bunker wall shielding and the second one was added for the measurement. The heavy concrete reinforcement was not installed yet during this measurement. The obtained dark current is 2.5nA; what is in the range of the currents measured in other published works [4].

4. Conclusions

The radiation dose rate levels have been studied inside and outside the RF bunker during the conditioning period. The need of a shielding near these elements has been shown. Subsequent measurements have confirmed that the shielding reinforcement guarantees dose rate levels below 0.5 μSv/h outside the bunker. The power dependence of the radiation as a function of the RF power is studied monitoring the radiation inside the bunker. The measured dependence is in agreement with published studies. Also inside the bunker, the X-ray spectrum has been measured at different RF powers. A linear dependence between the maximum X-ray energy and the square root of RF power has been shown. This could be explained relating the maximum energy of the dark current electrons with the electric field in the cavity; which is proportional to the square root of RF power. Finally, Monte-Carlo simulation of the generated dose rate has been carried out. From this simulation, the dark current has been estimated.

Acknowledgements

We are especially indebted to the ALBA RF group, Michel Langlois, Francis Pérez, Ángela Salom and Francisco Sánchez, for many fruitful discussions and help given.

References

[1] M.Langlois, P. Sanchez, M.Cornelis, F.Perez "Measurements on the RF cavity for the ALBA Storage Ring", Proceedings of the European Particle Accelerator Conference, (2008).
[2] K. Amsink, K.P. Klimek, H.P. Scholz, "Die Dosisleistung durch Róntgentstrahlung beim Betrieb von Hochfrequenz-Resonatoren" DESY D3/MHF-51, (1984).
[3] International Standard 61508-7, "Functional safety of electrical/electronic/programmable electronic safety-related systems", (2003).
[4] J. Norem, V. Wu, A. Moretti, M. Popovic, Z. Qian, L. Ducas, Y. Torun, N.Solomey, "Dark current, breakdown, and magnetic field effects in a multicells, 805 MHz cavity" Physical Review Special Topics – Accelerators and Beams, V6, 072001 (2003).
[5] J. Norem, A. Moretti, M. Popovic, "The radiation environment in and near high gradient rf cavities", Nuclear Instruments & Methods in Physics Research, A 472, 600-605, (2001).
[6] G. Battistoni, S. Muraro, P.R. Sala, F. Cerutti, A. Ferrari, S. Roesler, A. Fasso`, J. Ranft, "The FLUKA code: Description and benchmarking" Proceedings of the Hadronic Shower Simulation Workshop 2006, Fermilab 6--8 September 2006, M. Albrow, R. Raja eds., AIP Conference Proceeding 896, 31-49, (2007).

Dosimetry issues related to the SSRT project at the ESRF

P. Berkvens[1], J. F. Adam[2], E. Brauer[1], A. Bravin[1], F. Esteve[2], C. Nemoz[1], Y. Prezado[1], M. Renier[1], H. Requardt[1] and M. Vautrin[2]

[1]*European Synchrotron Radiation Facility – BP220 Grenoble Cedex 09 France*

[2]*INSERM-U647/ESRF, Grenoble, France; MRI Unit, Grenoble University Hospital, Grenoble, France*

Abstract

The present paper describes the Stereotactic Synchrotron Radiotherapy (SSRT) project at the ESRF, emphasizing on the particular radiation safety issues related to this novel technique. The dosimetric characterization of the monochromatic X-ray beams used for therapy and for both 2D and tomography imaging is described. The dosimetry protocol is based on the IAEA 398 protocol, with the special provision to simulate uniform radiation fields by scanning an ionization chamber and a water phantom through the beam. The duality between the scanning ionization chamber geometry and the standard broad beam geometry is mathematically derived. It is shown that the use of a transmission ionization chamber scanned through the beam allows the on-line measurement of the integrated dose during patient treatment.

1. Introduction

The ID17 beamline at the European Synchrotron Radiation Facility in Grenoble, France is dedicated to medical applications. In the past a medical research protocol in the field of synchrotron radiation angiography has been conducted. Presently two radiation therapy programs, the Stereotactic Synchrotron Radiotherapy program (SSRT) and the Mircobeam Radiation Therapy program are being investigated and are progressing towards the clinical phase.
The SSRT technique consists in the stereotactic irradiation of a (brain) tumour using a monochromatic beam, with a dose enhancement effect due to the injection of a contrast agent in the tumour.
Synchrotron radiation beams are characterized by their reduced height (typically of the order of 1 mm). This particular aspect requires special attention concerning the dosimetric characterization of these beams.
International dosimetry protocols recommend the use of ionisation chambers to characterize and to calibrate X-ray beams used for radiotherapy purposes. The most widely used protocol for conventional radiotherapy in hospitals is the IAEA 398 protocol [1] and is based on absorbed dose in water. However, other protocols [2], using ionisation chambers calibrated in air in terms of air kerma, are used in reference dosimetry protocols for low- and medium-energy x-rays for radiotherapy and radiobiology.
These protocols assume broad beam irradiation geometries, which imply that the transverse dimensions of the X-ray beam are larger than the transverse dimensions of the ionisation chamber. In the case of radiotherapy techniques using synchrotron radiation X-ray beams the broad beam irradiation condition can not be fulfilled, since the X-ray beams will always have at least one transverse dimension which is smaller that the corresponding dimension of any commercially available ionisation chamber. The standard dosimetry protocols therefore need to be adopted to take into account this particular aspect. This is the purpose of the dosimetry protocol based on scanning the ionisation chamber through the X-ray beam, described hereafter.

2. The use of a thimble ionisation chamber in a flat beam

Ionisation chambers used for absolute dosimetry in radiation therapy must be calibrated in uniform broad radiation fields, whose transverse dimensions are much larger than the corresponding dimensions of the ionisation chamber. When using the ionisation chamber in a flat beam, the geometry is completely different from the standard calibration conditions. We must therefore proof that we can nevertheless use the broad beam calibration factors of the ionisation chamber.
When exposing an ionisation chamber to a uniform field, the different parts of the active volume of the chamber respond in a highly non-uniform way, depending on the chamber's geometry and due to the presence of the central electrode. Figure 1 shows the response of a PTW 31002 ionisation chamber to a flat beam, as a function of the transverse position of the beam relative to the ionisation chamber [3].

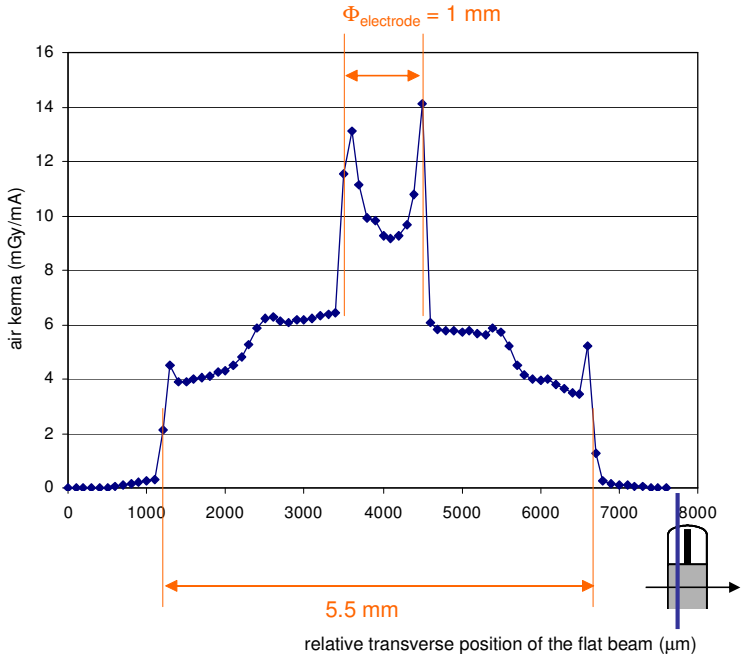

Fig.1 - Response of a PTW 31002 ionisation chamber to a flat beam.

If we denote by S(z) the relative sensitivity of the ionisation chamber as a function of one of its transverse dimensions, the measured dose rate $\dot{D}_{calibration}$ when exposing the ionisation chamber to a uniform calibration radiation field with an absolute dose rate $\dot{D}_{beam}$ can be expressed as:

$$\dot{D}_{calibration} = C \times \dot{D}_{beam} \times \int_{active\ volume} S(z) \cdot dz \,, \tag{1}$$

with C a calibration factor.

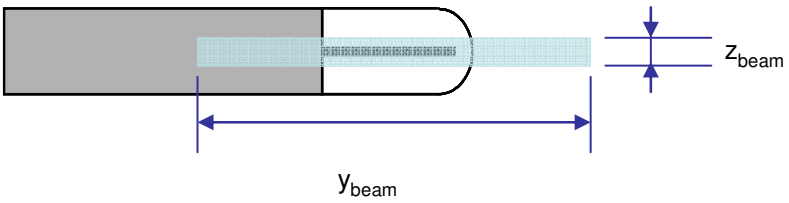

Fig.2 - Typical geometry encountered in synchrotron radiation X-ray dosimetry.

Consider the geometry of figure 2. An ionisation chamber is exposed to an X-ray beam that has one transverse dimension (y_{beam}) larger than the corresponding dimension of the ionisation chamber, while the second transverse beam dimension (z_{beam}) is smaller than the corresponding dimension of the ionisation chamber. Assuming that the beam is uniform over its entire surface, and is characterized by a dose rate $\dot{D}_{beam}$ (absorbed dose in water or air kerma), the dose rate $\dot{D}_{measured}$ (absorbed dose in water or air kerma) measured with the ionisation chamber will be given by

$$\dot{D}_{measured} = C \times \dot{D}_{beam} \times \int_{\Delta z = z_{beam}} S(z) \cdot dz \,. \tag{2}$$

Expression (2) shows that the accurate measurement of the ionisation chamber's transverse response S(z) allows the use of a standard ionisation chamber to carry out absolute dosimetry measurements in typical synchrotron radiation X-ray beams. The real difficulty of this method results from the fact that the transverse response function S(z) of the ionisation chamber depends on the energy spectrum of the X-ray beam at the point of measurement and from the fact that the measured dose rate will be very sensitive to the exact

position of the ionisation chamber. These two complications are avoided by scanning the ionisation chamber through the beam along the z direction, at a constant speed v_z and measuring the integrated dose, instead of doing a static dose rate measurement (see figure 3).

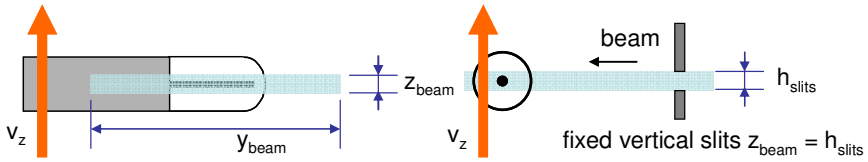

Fig.3 - Principle of scanning ionisation chamber.

Every plane cutting the ionisation chamber at a given position z will be exposed to a beam with a dose rate $\dot{D}_{beam}$ (absorbed dose in water or air kerma) during a constant time interval z_{beam}/v_z. The measured integrated dose $D_{measured}$ (absorbed dose in water or air kerma) will therefore given by.

$$D_{measured} = C \times \int_{active\ volume} \left(S(z) \times \int_{\Delta t = z_{beam}/v_z} \dot{D}_{beam} \cdot dt \right) \cdot dz = C \times \dot{D}_{beam} \times \frac{z_{beam}}{v_z} \times \int_{active\ volume} S(z) \cdot dz \qquad (3)$$

or:

$$\dot{D}_{calibration} = D_{measured} \times \frac{v_z}{z_{beam}} \qquad (4)$$

Expression (4) shows that from the measured integrated dose during the ionisation chamber scan a value for the dose rate can be obtained by multiplying the measured integrated dose, using the broad beam calibration factors, by the factor v_z/z_{beam}. Expression (4) is theoretically only valid if the intensity of the radiation field is such that the ionisation chamber is used in a regime where ion recombination is negligible. Indeed, the space charge distributions inside the ionisation chamber are obviously different when irradiating the chamber at once in a broad beam or when irradiating its different parts one after the other and the effects of ion recombination are expected to be different. Measurements using a PTW 31002 semiflex ionisation chamber seem to indicate that expression (4) would still be valid for ion recombination effect as large as 8% [3].

3. Relationship between a static uniform beam and a scanned synchrotron radiation beam

Consider a pencil-type beam, with transverse dimensions dy and dz and with a uniform distribution, e.g. characterised by its fluence F_0 (at x = 0). The dose rate in the point $(x_0,y_0,0)$ due to the pencil beam parallel to the x-axis, at the transverse position (y,z), for a given static geometry (infinite water phantom or irradiation on air) can be written as (see figure 4):

$$\dot{D}(x_0, y_0, 0) = F_0 \times T_{pencil}(x_0, y_0; y, z) \cdot dy \cdot dz \qquad (5)$$

with $T_{pencil}(x_0,y_0;y,z)$ the geometry dependent conversion factor between fluence and dose rate ($Gy \cdot cm^2$).

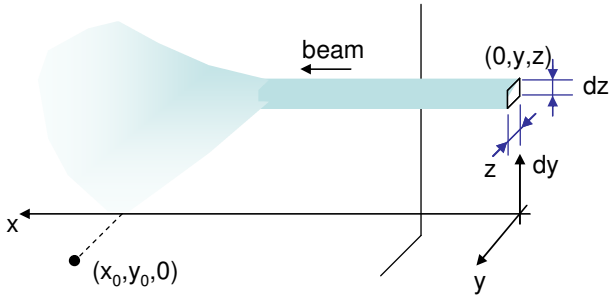

Fig.4 - Irradiation by a pencil-type beam.

The dose rate in the point $(x_0,y_0,0)$ due to a uniform broad beam, with field size Δy, Δz, centred around the x-axis is then given by:

$$\dot{D}_{broad}(x_0, y_0, 0) = F_0 \times \iint_{\Delta y, \Delta z} T_{pencil}(x_0, y_0; y, z) \cdot dy \cdot dz = F_0 \times \int_{\Delta z} T_{flat\ \Delta y}(x_0, y_0, z) \cdot dy$$
$$\left(T_{flat\ \Delta y}(x_0, y_0, z) \cdot dz = dz \times \int_{\Delta y} T_{pencil}(x_0, y_0; y, z) \cdot dy \right) \quad (6)$$

$T_{flat\ \Delta y}(x_0,y_0,z)\cdot dz$ is the dose rate in the point $(x_0,y_0,0)$ due to a flat horizontal beam with width Δy, centred around the x-axis, and with a height dz, located at a vertical position z (see figure 5, left part).

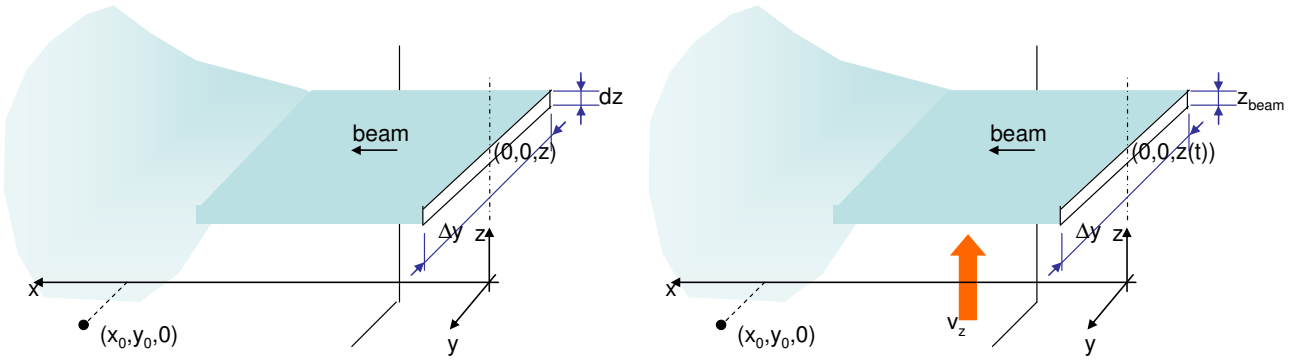

Fig.5 - Irradiation by a flat beam (left: static; right: scanning through flat beam).

We consider next the configuration used for SSRT, where we scan the object to be irradiated through the flat synchrotron radiation beam. If z_{beam} denotes the height of the beam, and Δy its width, the dose rate in the point $(x_0,y_0,0)$ is given by (see figure 5, right part):

$$\dot{D}(x_0, y_0, 0, t) = F_0 \times T_{flat\ \Delta y}(x_0, y_0, z(t)) \times z_{beam}. \quad (7)$$

The object is scanned at a constant speed v_z through the beam. The dose in the given point, integrated during the scan over a height Δz, centred on the beam, is given by:

$$D(x_0, y_0, 0) = \int_{\Delta t} \dot{D}(x_0, y_0, 0, t) \cdot dt = \frac{z_{beam}}{v_z} \times F_0 \times \int_{\Delta z} T_{flat\ \Delta y}(x_0, y_0, z) \cdot dz = \frac{z_{beam}}{v_z} \times \dot{D}_{broad}(x_0, y_0, 0). \quad (8)$$

Expression (8) is the theoretical basis for defining the dosimetric characterisation of the flat X-ray beam and to define the link with the treatment planning software.

4. Comparison between the scanning ionisation chamber protocol and the IAEA 398 protocol

The IAEA 398 protocol defines the determination, on the central axis, of the absorbed dose under reference conditions, the determination of the central axis depth dose distributions and the determination of dose profiles at different depths. Expression (8) showed that a broad beam irradiation is perfectly simulated by scanning the phantom vertically through the flat X-ray beam, at constant speed. The standard dosimetric quantities can be measured by scanning a thimble ionisation chamber vertically through the beam, at constant speed. Expression (4) showed that the standard, broad beam, calibration factors for the ionisation chamber can be used. The broad beam field size is obtained horizontally by setting the slits to the required width Δy and vertically by the height of the scan Δz (symmetrically around the beam axis). The measurement of the absorbed dose under reference conditions is obtained from expression (8) by using the appropriate value for x_0 and for $y_0 = 0$. The central axis depth dose is obtained by measuring the dose, using expression (8), for different values of x_0, always for $y_0 = 0$. An example of measured percentage depth dose profiles is given in figure 6. These measurements were carried out using a PTW 31002 semiflex ionisation chamber in a

30 cm_x × 20 cm_y × 20 cm_z water phantom, for a quasi-monochromatic beam of 80 keV [4]. Finally by measuring the dose, using expression (8) for a given value of x_0 and for different values of y_0, horizontal dose profiles are obtained. Figure 6 shows an example of measured horizontal dose profiles.

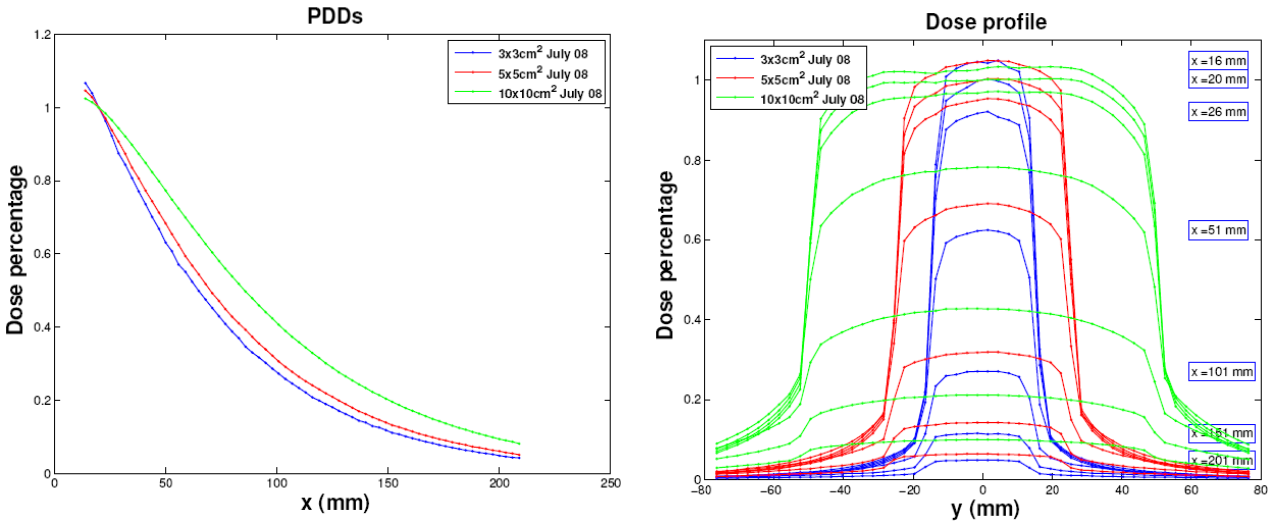

Fig.6 - Measured percentage depth dose profiles (left) and horizontal dose profiles (right).

5. Dose measurements during the patient treatment

Contrary to a conventional radiation treatment, where the integrated dose can be measured online using a calibrated transmission ionisation chamber, expression (8) shows that the use of a fixed, calibrated transmission ionisation chamber will not allow an online measurement of the integrated dose, because of the dependence of the integrated dose on the vertical scanning speed v_z. This would make the implementation of a reliable integrated dose interlock in the patient safety system too complicated. A different dose measurement must therefore be implemented. The solution will consist in the installation of a transmission ionisation chamber moving with the medical chair (see figure 7). As shown hereafter, the insertion of a transmission ionisation chamber, behind the 2D mask, moving together with the mask (and the medical chair) vertically through the beam, will provide a measurement for the integrated dose delivered to the patient for a given orientation.

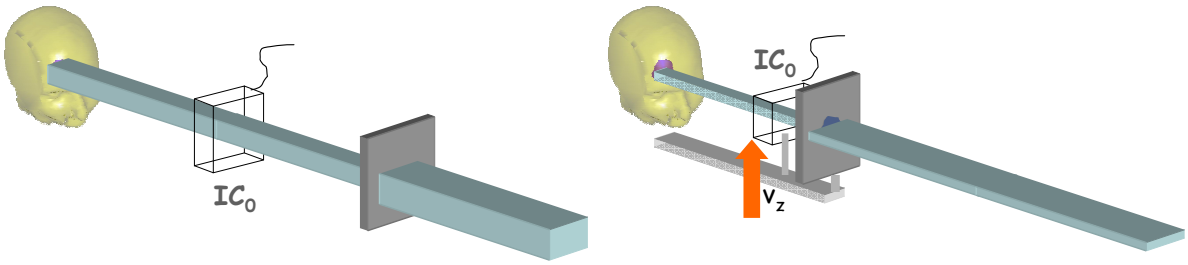

Fig.7 - Left: fixed ionisation chamber IC_0 in standard radiation therapy; right: scanned ionisation chamber IC_0 behind 2D mask in SSRT configuration.

The treatment planning software defines, for each individual irradiation orientation, the optimum two-dimensional shape of the uniform beam and the corresponding dose to the tumour. Using the same beam the treatment planning software gives a value for the corresponding on-axis dose at the reference depth in the standard water phantom (see figure 8). The initial (x = 0) transverse beam shape can be described by z_{min} and z_{max}, the minimum and maximum beam height respectively and by $(y_{max} - y_{min})(z)$ the z-dependent beam width. The dose rate in the reference point $(x_0,0,0)$ is then given by:

$$\dot{D}_{2D\ beam}(x_0,0,0) = F_0 \times \int_{z_{min}}^{z_{max}} \left(\int_{y_{min}(z)}^{y_{max}(z)} T_{pencil}(x_0,0;y,z) \cdot dy \right) \cdot dz \ . \qquad (9)$$

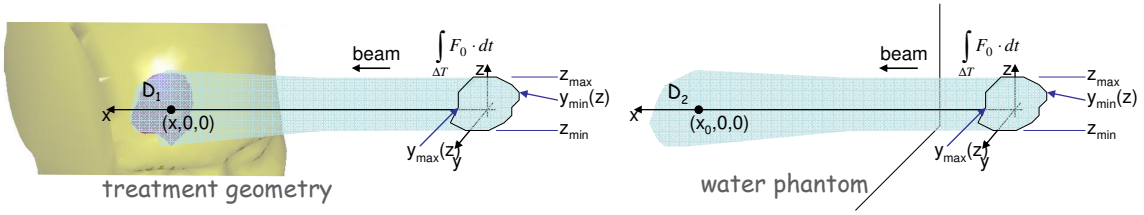

Fig.8 - Correspondence between dose D_1 delivered to the tumour and the absorbed dose to water D_2 at the reference depth in the water phantom.

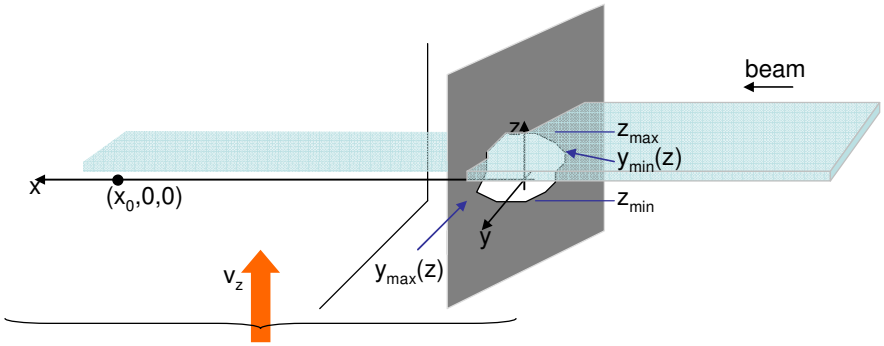

Fig.9 - Geometry for dosimetry measurement with moving 2D collimator.

The geometry of figure 8 is reproduced by inserting a 2D collimator, with a shape identical to the 2D beam defined by the treatment planning software, centred on the x-axis, fixed to the medical chair (therefore moving at the same speed during the vertical scan). If the 2D collimator is sufficiently thick to attenuate completely the beam, the dose rate in the reference point $(x_0,0,0)$ for the geometry in figure 9 is given by:

$$\dot{D}(x_0,0,0,t) = F_0 \times z_{beam} \times \int_{y_{max}(z)}^{y_{max}(z)} T_{pencil}(x_0,0;y,z(t)) \cdot dy \qquad (10)$$

The integrated dose over the vertical scan (scan interval covers at least the interval $z_{min} - z_{max}$) is given by:

$$D(x_0,0,0) = F_0 \times \frac{z_{beam}}{v_z} \times \int_{z_{min}}^{z_{max}} \left(\int_{y_{max}(z)}^{y_{max}(z)} T_{pencil}(x_0,0;y,z(t)) \cdot dy \right) \cdot dz = \frac{z_{beam}}{v_z} \times \dot{D}_{2D\ beam}(x_0,0,0). \qquad (11)$$

Expression (11) shows that the correspondence between the integrated dose during a vertical scan and the on-axis absorbed dose rate in water obtained from the treatment planning software still holds. The integrated dose $D(x_0,0,0)$ can now again be measured using a thimble ionisation chamber, at the condition that the opening of the 2D collimator covers completely the active volume of the ionisation chamber (the minimum size of the tumours to be treated will be such that this condition will be fulfilled).
The measurement of the integrated dose with the ionisation chamber not only allows obtaining the dose rate in the 2D beam, using expression (11), but actually provides a direct measurement of the integrated absorbed dose to water in the reference point (the dose D_2 in figure 8), and which can therefore be related, via the treatment planning software, to the integrated dose delivered to the tumour, scanned with the same speed v_z through the beam with the same beam height z_{beam} (the dose D_1 in figure 8).
The integrated dose measured with a transmission chamber, inserted behind the 2D collimator, covering the entire collimator hole and moving together with the collimator during the scan, will be proportional to the integrated absorbed dose to water at the reference depth. It is therefore possible to calibrate this transmission ionisation chamber relative to the thimble ionisation chamber placed at the reference depth in the water phantom. In this way the transmission ionisation chamber will provide a direct measurement of the integrated absorbed dose in water in the reference point, the latter being directly related to the dose delivered to the tumour under the same scanning conditions.
It is important to note that the dose, measured with the thimble ionisation chamber, and the dose, measured with the transmission ionisation chamber, vary in the same way with the scanning speed v_z and the beam height z_{beam}. The calibration factor thus obtained for the transmission ionisation chamber will be independent

of v_z and z_{beam}. The online dose measurement with the transmission ionisation chamber, during the patient treatment, and the associated dose interlock will therefore be independent of the scanning speed v_z and the beam height z_{beam}. This is a fundamental advantage of the proposed dosimetry system.
Although the calibration factor of the transmission ionisation chamber is, as mentioned above, independent of the absolute value of the vertical speed of the chair v_z, it is important to keep this speed constant during the calibration of the transmission ionisation chamber, because of the z-dependence of the response function of the thimble ionisation chamber (or more precisely, because of the difference between the z-dependence of the response functions of the thimble ionisation chamber and of the transmission ionisation chamber).
In the same way, although the value for the dose delivered to the tumour, derived from the integrated dose measured with transmission ionisation chamber, is independent of the absolute value of the vertical chair speed v_z, , it is again important to keep this speed constant during the patient treatment, because a non constant speed will result in a vertically inhomogeneous dose delivery.
It should be noted that the duality between the dose D_2 obtained from the treatment planning software and the dose measured when scanning the ionisation chamber is mathematically only exact if the geometry used by the software treatment planning to obtain the dose D_2 is at all times identical to the geometry during the scan. This requires that the transmission chamber moves together with the collimator and the water phantom. Indeed, a transmission ionisation chamber, placed behind the 2D collimator, but remaining at the fixed beam height, would create a variable geometry during the scan, which cannot correspond to the static geometry used by the software.

6. Conclusions

We have shown that a commercially available thimble ionisation chamber can be used to characterise flat X-ray beams, by scanning it at constant speed through the beam, using the standard broad beam calibration factors of the ionisation chamber.
The Monte Carlo based treatment planning software relates the dose delivered to the tumour to the dose at the reference depth in a water phantom. The latter can be measured online by inserting a transmission ionisation chamber behind the 2D collimator, fixed to the medical chair.

References

[1] IAEA Technical Reports no. 398, Absorbed dose determination in external beam radiotherapy, Vienna, 2000.
[2] C. M. Ma et al., AAPM protocol for 40-300 kV x-ray beam dosimetry in radiotherapy and radiobiology, *Med. Phys*. 28(6), 868-893, 2001.
[3] Feasibility of a dosimetry protocol using a thimble ionisation chamber for MRT experiments on ID17, internal report, P. Berkvens, 26 April 2005.
[4] Mathias Vautrin, SSRT Dosimetry – Internal experiment Report, 6 March 2009.

Dose rate considerations for the BMIT POE3 at the Canadian Light Source

Juhachi Asai[1*], Tomasz W. Wysokinski[1], Dean Chapman[2] and Curtis Mullin[1]

[1]*Canadian Light Source Inc., 101 Perimeter Road, University of Saskatchewan, Saskatoon, SK, Canada S7N 0X4*

[2]*Department of Anatomy and Cell Biology, 107 Wiggins Road, University of Saskatchewan, Saskatoon, SK, Canada S7N 5E5*

Abstract

A dose rate study is undertaken when gas bremsstrahlung strikes a monochromator, a copper absorber and a tungsten beam stop in the third primary optical enclosure (POE3) of the BioMedical Imaging and Therapy (BMIT) insertion device (ID) beamline. In the POE3, computed tomography, diffraction enhanced imaging and K-Edge subtraction monochromators are housed to conduct various diagnostic and therapeutic studies. The safety features of this beamline must be examined with great care, as this multipurpose beamline is intended for use on animals and humans.

In the POE3 a tungsten beam stop, two safety shutters, and a lead movable wall are placed for the safe operation of the BMIT beamline. However, for one particular usage of the monochromator, bremsstrahlung and X-rays propagate closely together until the former is stopped by the tungsten beam stop while the safety shutters remain open to allow the passage of the latter to the experimental area. It is thus imperative to know the anticipated dose rate around the POE3, especially behind the back wall. The dose rate estimates are presented based on a realistic model of the POE3 with its safety features.

1. Introduction

The Canadian Light Source (CLS) is a 2.9 GeV, 500 mA, third-generation synchrotron facility. High-energy electrons interacting with residual molecules in the vacuum chamber generate the gas bremsstrahlung. When produced in the ID straight section, highly forward-peaked bremsstrahlung may travel with synchrotron radiation to the experimental area. The purpose of this report is to assess the radiation levels when bremsstrahlung strikes a beam stop placed in the POE3 of the BMIT ID beamline.

The BMIT-ID beamline [1] is one of the Phase II beamlines being built at present. The POE3 houses three monochromators, listed in order of the location from upstream: the computed tomography (CT) monochromator, the diffraction enhanced imaging (DEI) monochromator and the K-Edge subtraction (KES) monochromator. The bremsstrahlung beam stop is placed outside the KES monochromator. This beam stop must be small enough vertically for the KES beam to be deflected above or below and for the CT and DEI beam to pass over the top of the beam stop. However, the beam stop must be thick enough to stop the bremsstrahlung. At present the vertical distance between the CT and the bremsstrahlung is 1.5 cm.

The beam from the monochromator propagates toward the 13 cm-thick lead movable wall to which two safety shutters are attached. There are two holes on the movable wall for the higher and the lower energy X rays of the KES. When the DEI or CT is in operation, the movable wall is shifted upward or downward so that the KES X-rays are prohibited from entering the experimental hall as shown in Fig.1. It is noted that in this situation two safety shutters are open.

* Corresponding author. Tel.: +1 306 657 3511; fax: +1 306 657 3535.
E-mail address: juhachi.asai@lightsource.ca (J. Asai)

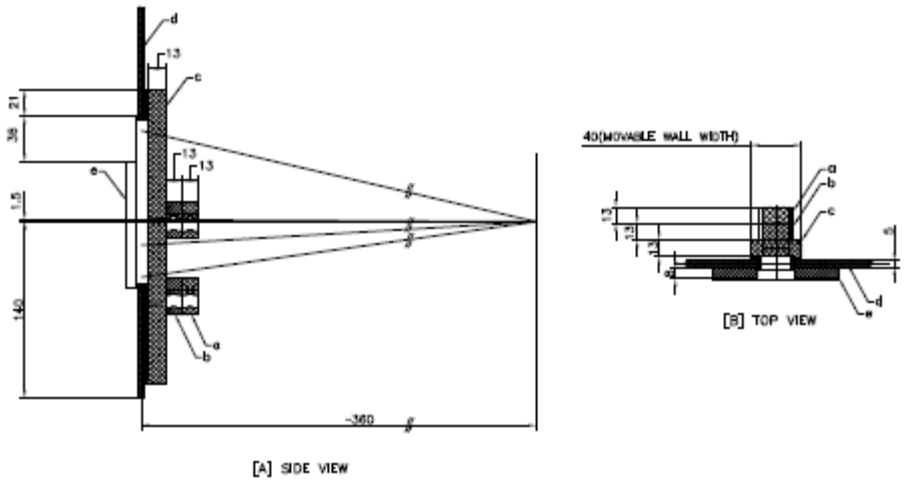

Fig.1 - Shielding setting for the CT operation. Safety shutters are in open position. a) safety shutter SS1, b) safety shutter SS2, c) lead movable wall, d) lead back wall and e) lead centre reinforcement. Note the small opening on the lead movable wall. The length is in units of cm.

If various possible settings are considered, the worst case scenario might be that the CT rays are passing over the bremsstrahlung stop which is only 1.5 cm above the top surface. These X-rays propagate through the movable wall to the experimental area, whereas the bremsstrahlung is stopped by the beam stop. This bremsstrahlung stop consists of a copper absorber followed by a tungsten beam stop. The dimension of the tungsten stop is (X(width), Y(height), Z(thickness))=(21.4, 1.8, 18.0) in units of cm. The hole of the movable wall has a dimension (X, Y)=(21.4, 3.0). Hence there exists an open area (X, Y)=(21.4, 0.6) over the top surface of the beam stop when the CT rays are in use. The radiation originates from the copper absorber tungsten unit and could travel through the opening to the experimental floor.

Although the optical elements and the movable lead wall in the POE3 are yet to be installed, the aim of this paper is to estimate the expected dose rates behind the back wall of the POE3. These assessments will allow for safe operation of the BMIT beamline, as this multipurpose beamline is intended for use on animals and humans.

In Section 2, the model of the POE3 structure and the beam stops are constructed as close as possible to the planned construction of the POE3. Section 3 gives the dose rates estimate behind the back wall. Section 4 gives the conclusion.

2. Model and parameters used for dose rate estimates

The inside width, height and length of the POE3 are taken as 224 cm, 360 cm and 360 cm, respectively. The elements considered from upstream in the POE3 include a silicon crystal, a copper absorber followed by a tungsten stop. There are two lead safety shutters (SS1 and SS2) which are attached to the lead movable wall. The back wall is a 5 cm-thick lead wall reinforced by an 8 cm-thick lead centre piece. The side is a 3 cm-thick lead wall and the roof is constructed by lead 1 cm-thick. The lead wall thicknesses have been determined by our previous investigations [2, 3]. A schematic view of the POE3 and elements considered in it are given in Fig.2.The bremsstrahlung direction defines the Z axis which is 140 cm up from the floor. The bremsstrahlung entrance to the POE3 is taken as the coordinate origin (X, Y, Z)=(0, 0, 0) where the silicon crystal is placed. The number of photons (NOFPs) produced is found to be 3.71×10^9 /h. A more detailed account is found in our previous report [2].

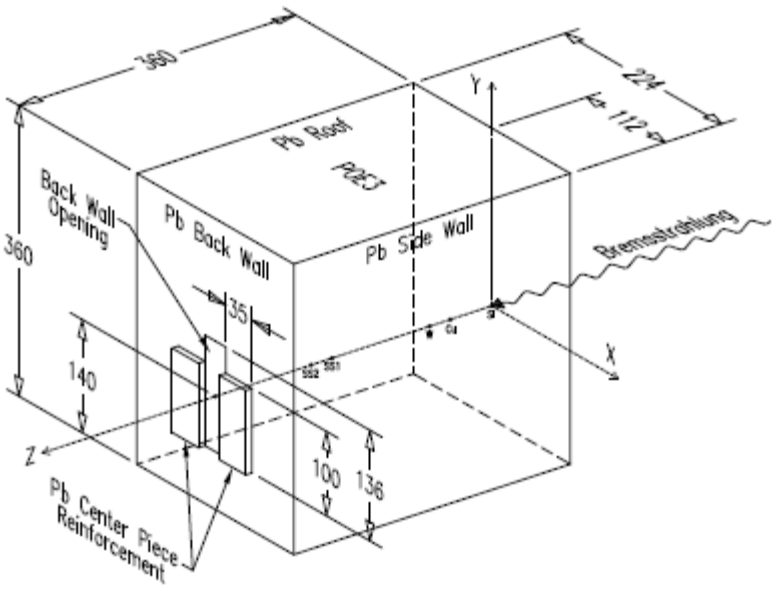

Fig.2 - Schematic view of POE3 and its elements considered in simulations. The movable lead wall placed inside the back wall is not shown for clarity. All units are in cm but not to scale.

The bremsstrahlung produced in the ID straight section propagates with the synchrotron radiation and strikes the thin silicon crystal and the copper absorber-tungsten beam stop, which are 1 cm, 3 cm and 18 cm in thickness, respectively. In the following, the dimensions (X, Y, Z) of all elements and the upstream position (in Z) of each element are summarized. We are only interested in the case where the lead safety shutters (SS1 and SS2) are open. Hence, the closest distances from the beam axis to the safety shutter (in Y) are also given. The negative sign indicates the Y position is below the beam axis. Units are in cm:

- Silicon crystal: (16.0, 2.0, 1.0) located at Z=0.0
- Copper absorber: (21.4,1.60, 3.0) located at Z=37.0
- Tungsten beam stop: (21.4, 1.80, 18.0) located at Z=40.0
- Lead upper safety shutter 1: (21.4, 15.0, 13.0) located at Z=321 and Y=2.50
- Lead lower safety shutter 1: (21.4, 4.7, 13.0) located at Z=321 and Y=-7.80
- Lead safety shutter 2: same as the safety shutter 1 but located at Z=334.0
- Lead Movable wall: (40.0, 204.0, 13.0) located at Z=347.0
- Lead back wall: (224.0, 360.0, 5.0) located at Z=360.0
- Lead centre piece for the reinforcement: (100.0, 35.0, 8.0) located at Z=365.0 for each side on the X axis.

A schematic view of the movable wall and back wall seen from upstream is given in Fig. 3. A square cornered by *5, 6, 7*and *8* is the outer edge of the movable wall (M) and the area inside the square delineated by *1, 2, 3* and *4* is a hole in the movable wall. Similarly, a square cornered by *13, 14, 15* and *16* is the outer edge of the back wall (B) and a square formed by *9, 10, 11* and *12* is a hole in the back wall. The shaded area indicates the shadow image of the tungsten stop placed near the origin. Scales on the right and the bottom are in units of cm. The beam is 140 cm high from the floor. As shown, the movable wall has a hole (X, Y)=(21.4, 3.0) centred at the beam axis and the back wall has a similar hole of size (X, Y)=(30.0, 136.0). The last element, the lead centre piece is installed for additional shielding, covering from X=15 to 50 cm and -15 to -50 cm. (See also Fig.1). The back wall, side wall and the roof of the POE3 are enclosed by a water phantom in which the energy deposition per unit mass is estimated by the EGS4 code [4]. The thickness of the water phantom is assumed to be 1 cm throughout this article, unless otherwise specified.

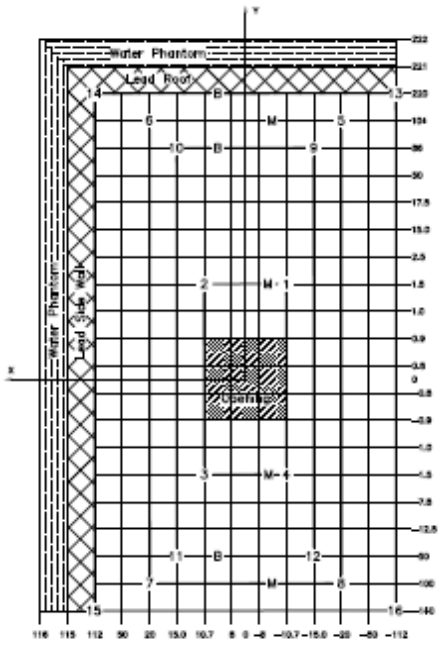

Fig.3 - Schematic view of the movable wall (M) and the back wall (B) seen from upstream. The shaded area indicates the shadow of the tungsten stop placed near the origin. The X and Y coordinates are in units of cm but not to scale.

3. Dose rate distribution immediately behind the back wall

The bremsstrahlung striking the thin silicon crystal (1.0 cm) most likely penetrates through it to hit the copper and tungsten unit causing the cascade showers. The tungsten thickness is 18 cm and the length of the top surface from the beam axis is only 0.9 cm, which is the height necessary for the CT beam clearance.
Looking through the components from upstream, there is an unobstructed area that is open continuously to the experimental area. Hence, it is possible that the radiation higher than the regulatory limit of 5μSv/h will be present behind the back wall of the POE3. Specifically, the area exposed is that which is lined by a top surface of the tungsten stop (Y=0.9) and the movable wall opening upper edge (Y=1.5) over the entire movable wall opening area in the X direction (X=-10.7 to+10.7) as shown in Fig. 4. In Fig.4, the centre of Region ***1*** is the beam axis (through the paper), and after passing through the tungsten beam stop (X, Y, Z)=(21.4, 1.8, 18.0), this area is unshielded. Region ***3*** is also treated in the same way. As mentioned earlier these two Regions are shadowed by the tungsten stop. Regions ***2, 4*** are not covered by any shielding materials. Regions ***5, 6, 7, 8*** and ***9*** are shielded by the 13 cm-thick lead movable wall. Because of the symmetrical geometry with respect to the Z axis, Regions considered above may suffice to map out the dose rates of interest.

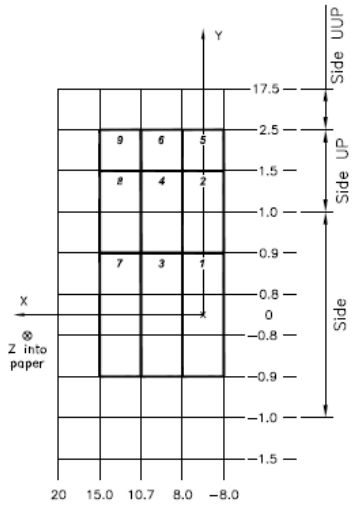

*Fig.4 - Regions of interest in water phantom for dose estimates behind the back wall when looking through the POE3 from upstream. Region**1** and **3** are shadowed by the tungsten stop, which is placed near the origin. Region **2** and **4** are not covered by any shield. Regions **5**, **6**, **7**, **8** and **9** are shielded by the movable wall. Coordinates are in cm but not to scale.*

Our main objective in this section is to assess the dose rate for Regions ***2*** and ***4*** as well as for Regions ***1*** and ***3.*** These Regions are exposed to radiation since no shield is placed to cover these areas. To estimate the dose rate, a 5 cm-thick water phantom is set immediately behind the lead centre reinforcement. The dose rate is calculated in a 1 cm interval in the water phantom to see how it varies with the water depth.

The maximum dose rate is found in Region ***1*** and the results are shown in Fig.5 as a function of the water depth. The maximum takes the value 0.505±0.040 μSv/h between 1 and 2 cm in the water phantom. Hence, the dose rate behind the back wall is well under the regulatory limit of 5 μSv/h.

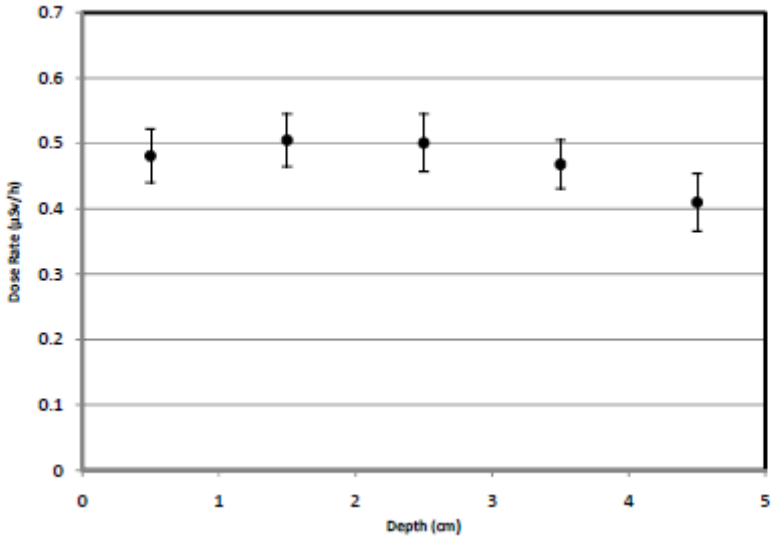

*Fig.5 - Dose rate in Region **1** as a function of depth behind the back wall.*

4. Conclusion

Radiation dose studies are conducted for the POE3 of the BMIT ID beamline. The POE houses three monochromators for CT, DEI and KES studies. Since this multi-purpose beamline is intended for animals and humans, the safety against radiation must be considered thoroughly. In the POE3 various safety features such as a tungsten beam stop, two safety shutters, a lead movable wall and a lead centre reinforcement are incorporated. However, when the CT or DEI are in use, two safety shutters must remain open, prompting concern regarding radiation exposure and a subsequent examination of the dose rate around the POE..

When bremsstrahlung strikes the copper/tungsten unit, the dose rate behind the back wall of the POE3 is found to be well below the regulatory limit of 5 μSv/h. The tungsten beam stop, W(21.4, 1.8, 18.0) is capable of containing the radiation in the POE3 as far as the back wall is concerned.

An expanded version of this manuscript was submitted to *Radiation Physics and Chemistry*.

Acknowledgement

The research described in this paper is supported by NSERC, NRC, CIHR and the University of Saskatchewan.

References

[1] Dean Chapman, BioMedical Imaging and Therapy Beamline Preliminary Design Report, CLS Design Note 26.2.1.2, 2006
[2] J. Asai, H. Hirayama, Nucl. Instr. and Meth. A**539** (2005) 654.
[3] J. Asai, Nucl. Instr. and Meth. A**580** (2007) 173.
[4] W.R. Nelson, H. Hirayama, D.W.O. Rogers, The EGS4 code system, SLAC-265, 1985.

The SYRMA project for clinical mammography @ Elettra Safety, Control and Supervision Systems

A.Abrami[1], K.Casarin[1], V.Chenda[1], D.Dreossi[1], E.Quai[1], G. Tromba[1], A.Vascotto[1]

[1]*Sincrotrone Trieste SCpA, Strada Statale S.S.14 km 163.5, 34012 Basovizza, Trieste, Italy*

Abstract

The Elettra beamline for mammography with Synchrotron Radiation (SR) has been operating since March 2006. The clinical aim is to apply the PHase Contrast (PHC) imaging technique to a selected number of patients, recruited by radiologists according to a protocol approved by the Hospital Ethic Committee. Due to the laminar nature of SR beam, PHC images are obtained scanning the patient and the detector simultaneously through the beam.
Technical issues, national radiation protection and safety guidelines, both for patients and for operators, have been faced with during the design and implementation phases of this project. A description of equipments and systems is presented.

1. Introduction

The aim of the SYnchrotron Radiation for MAmmography (SYRMA) project [1] is to perform "in vivo" synchrotron radiation mammography on a selected number of patients recruited by the radiologist of the Trieste Public Hospital on the basis of BI-RADS classification [2]. The target cases are dense breasts with uncertain diagnosis after conventional mammography and ultrasonography.
The use of PHC imaging technique in mammography contributes to increase the image contrast and to improve the visibility of different details. Edge enhancement produced in PHC images results in a better visualization and characterization of lesions as well as in an improved differentiation of the glandular structures, leading to an higher sensibility and specificity of mammographic exam [3].
The use of a monochromatic beam permits to optimize the X-ray energy, as a function of the breast characteristics, reducing the delivered dose.

The project foresees three phases: the 1st phase, which started on March 13th, 2006 and is now next to conclusion, foresees to perform PHC mammography on 70-100 patients utilizing conventional screen-film systems; the 2nd phase provides the implementation of digital detectors (commercial and in-house developed) and the 3rd one the introduction of new imaging techniques.
During the 1st phase of the project, a collaboration with Fuji Italia has permitted to study the application of PHC imaging technique using Fuji Imaging Plate (IP) as detector [4]; two mammographic examinations have then been carried out with this imaging system without changing anything in the Safety, Control and Supervision Systems.

2. Beamline Layout and Equipments

SYRMA project has been developed at SYRMEP (SYnchrotron Radiation for MEdical Physics) bending magnet beamline. To perform clinical studies, the layout of the beamline has been deeply modified (Fig.1), with the addition of the *patient room* and the *control room* downstream the *experimental hutch*.

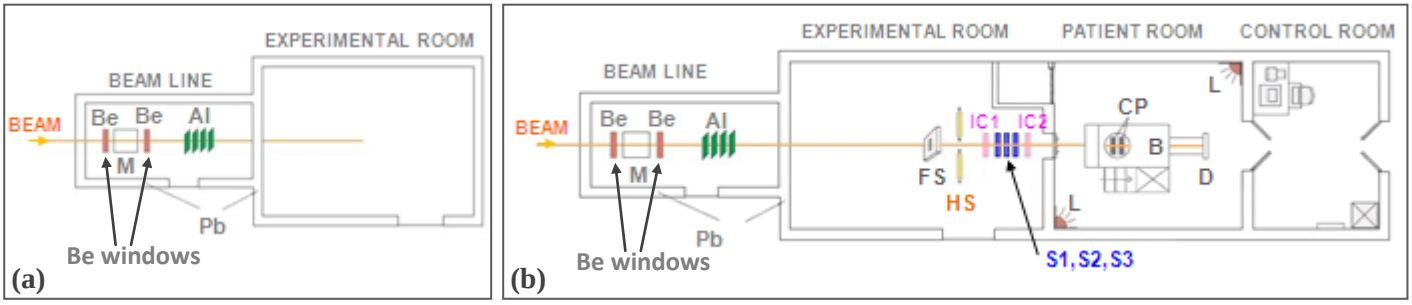

Fig.1 - SYRMEP layout, before (a) and after (b) the clinical mammography project development.

The *monochromator* (M) of the beamline, based on a double Si(111) crystal assembly working in Bragg configuration, is positioned in the *first beamline hutch* and permits to select the working energy in the 8.5-35 keV range; for mammographic studies the useful energy range is restricted to 17-21 keV.
Downstream the monochromator, the beam crosses a *beryllium window* (Be) and is then transmitted in air to a system of *calibrated aluminum filters* (Al), used to modulate the X-ray photons intensity.
A *beam mask* (FS), placed inside the *experimental room*, removes from the beam path the scattered radiation channeled into the beamline and defines with high precision the vertical dimension of the beam. The horizontal dimension is set through a system of *horizontal slits* (HS).
Two transmission *ionization chambers* (IC1, IC2), equipped with custom electronics, are used as beam and dose monitoring system. They have been developed and built in-house, taking into account the beam laminar structure and the high intensity of the synchrotron radiation.
A *fast safety shutter* (S1) is installed to quickly cut off the beam (response time < 20 ms) if dose threshold is exceeded; two further *shutters* (S2, S3) are utilized to define the exposure time of the patient scan (imaging function) and to guarantee safety conditions for the patient room access.
The *patient room* is equipped with a high precision movement *bed* (B), that can be translated vertically and horizontally to optimize the patient's position with respect to the beam, and can be rotated on the horizontal plane to permit different breast projections (Fig.2a). During the examination the patient lies prone on the bed with her breast leaning out of a hole realized on the support itself (Fig.2b).
The bed is equipped with a *breast compressor* (CP) used to equalize tissue thickness, for minimizing dose and optimizing imaging. A conventional *film-screen system* (D) is utilized as image detector and is mounted on a 2 meters long rail to allow distance optimization for PHC imaging purpose.

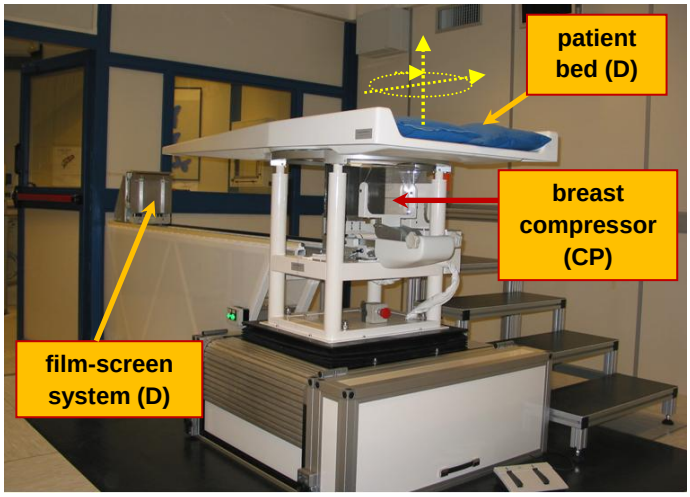

Fig.2a - Patient bed, breast compressor and film-screen system.

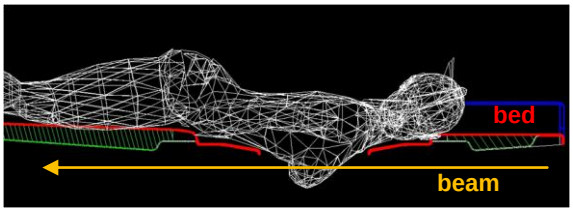

Fig.2b - Patient position during the exam.

All the phases of the mammographic examination are controlled and supervised by the radiologist and the technicians from the *control room*; thanks to the fact that a great part of the wall separating the *control* from the *patient room* is realized in lead glass, they have a direct view of the patient and can shut off the beam (e.g. pushing an emergency button) if necessary.

Taking into account that SYRMEP beamline is utilized also for other studies besides mammographic ones, two alternative working modalities have been developed for the patient room: the *"Patient Mode"* and the *"Experimental Mode"*. The former is specifically developed for clinical mammography, the latter allows to operate the beam, without dose control interlocks, for imaging of biomedical and biological materials, engineering science studies, test of detectors, etc. typically performed in the experimental hutch. A special key called '*Radiologist's Key'* permits to switch from one modality to the other.

3. Safety, Control and Supervision Systems

3.1. Safety Approach and Guidelines

Many *"Technical Directives"* and *"Italian/European legislations"* [5] have been analyzed for a correct approach to the safety aspects of the project. The first question to face was the safety level required for the

overall system. To answer this, the EN1050 Directive concerning the principles for risk assessment was utilized, integrated with the EN954, dealing with the assessment of safety-related parts of control systems.

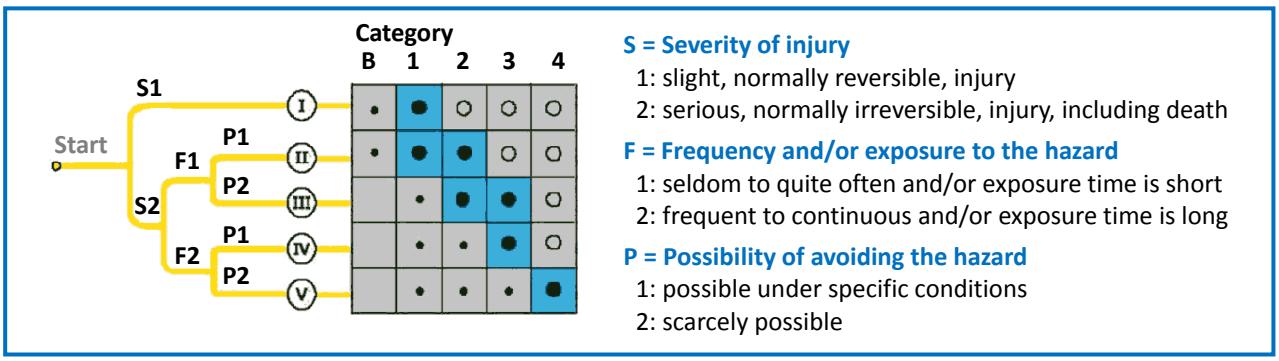

Fig.3 - EN954-1 Safety category decision graph.

The risk assessment with its high demanding requirements (Category 4 for the most critical functions) led to adopt, where possible, the following safety criteria:

- use of decoupled systems with suitable safety grade to monitor critical parameters (e.g. dose);
- redundancy and technological diversification of systems requiring high safety level;
- fail-safe philosophy;
- equipment verification and validation, performed by external and independent specialists.

In the SYRMA project, two main systems deal with radiation safety issues: the *"Dose Control System"* for the control of the dose released to the patient and the *"Patient Access Control System"* for the control of all the procedure of access inside the patient room. The *"Supervision and Human-Machine Interface System"*, provides the interface that permits to set the examination parameters and to carry on the mammographic scan. A further safety related system, called *"Machinery Safety System"*, has been developed to reduce crushing hazards (see Paragraph 3.2.4).

3.2. Systems Overview

The following is a brief analysis of the different systems involved in the clinical trial, and some of the safety related aspects.

3.2.1. Bed-Film System

The *"Bed-Film System"*, controlled by a dedicated PLC, allows to scan simultaneously the patient and the film detector through the beam during mammographic exam.
The bed can be moved horizontally, vertically, and can be rotated on the horizontal plane for different mammographic projections (Fig.2a). A bed controller guarantees all the movements; it provides digital inputs by which other systems can inhibit or stop bed movement if necessary.

3.2.2. Breast Compressor System

The *"Bed-Film System"* is equipped with a "*Breast Compressor System"*, controlled by a dedicated PLC, utilized to equalize tissue thickness for minimizing dose and optimizing imaging. It mainly consists of two paddles, one manual and one motorized, as shown in Fig.4.
The breast compression force must not exceed a maximum of 200 N, which could be harmful for the patient. This condition is fulfilled limiting the compressor motor current; in any case, if the applied force, measured through a Hall sensor, exceeds 200 N threshold, the manual paddle, normally blocked, is automatically released.
Taking into account that the patient support can rotate whereas the breast compressor cannot, a further interlock has been implemented, which prevents rotation during compression.

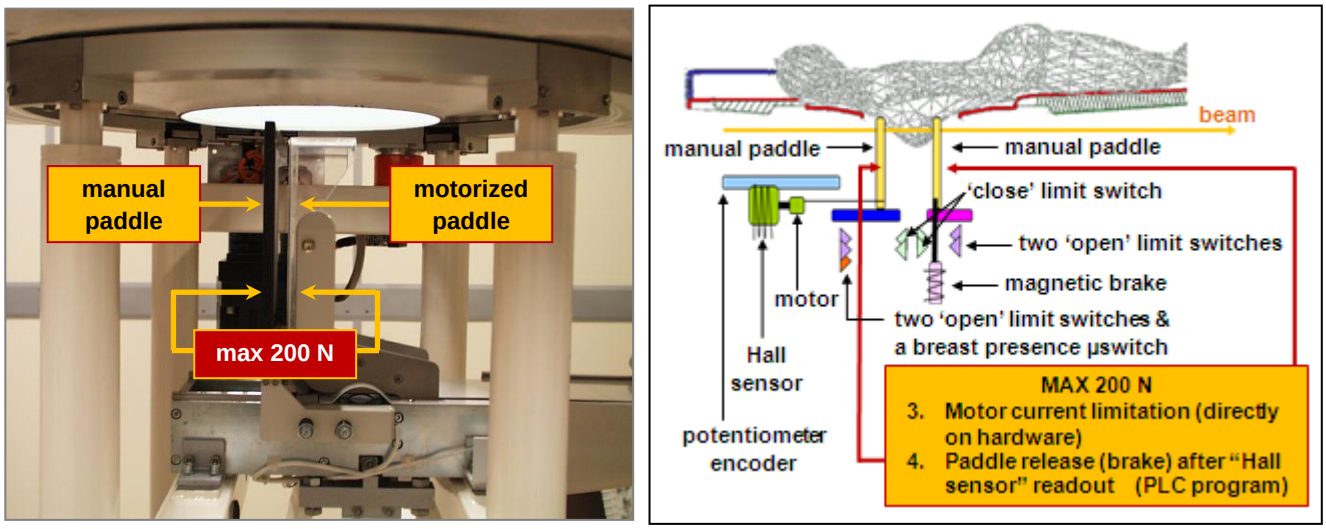

Fig.4 - The Breast Compressor System.

3.2.3. Safety Control Systems: *Patient Access Control* and *Dose Control*

The safety control systems have been realized using a Category 4 PLC. Three processors execute simultaneously the same program and then compare results, blocking the whole system if they differ. The acquired sensors and actuators are duplicated and have been chosen with different technologies to achieve high level of safety.

3.2.3.1. Patient Access Control System

The "*Patient Access Control System (PACS)"* assures safe access procedure to the patient room, avoiding the presence of other persons except the patient inside the hutch during the mammographic examination and assuring that only the breast is scanned through the beam.
It acquires and/or drives acoustic and visual alarms, shutters, door switches, emergency buttons, search panel, presence detectors, etc.
Furthermore, the *Patient Access Control System* interacts with the pre-existing SYRMEP *"Beamline Access Control System (BACS)"*, which assures safety conditions for access inside all the hutches of the beamline. A clear, even if slightly complex, finite state machine diagram fully describes the *"Patient Access Control System"* (Fig.5).

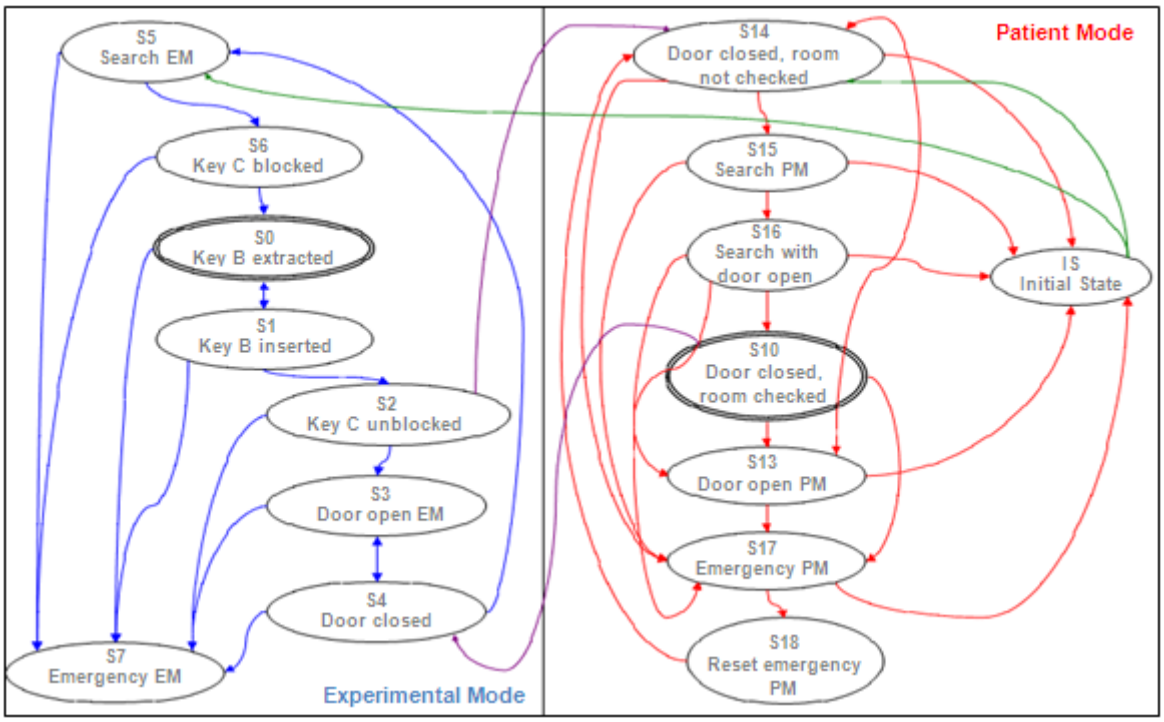

Fig.5 - PACS finite state machine diagram [6].

3.2.3.2. Dose Control System

The "*Dose Control System*" guarantees safety conditions for the patient during the mammographic exam.
The dose delivered to the patient is calculated from the dose rate measured by two calibrated [7] ionization chambers, the bed speed computed through two bed position sensors (Fig.6), and the beam dimensions.
If a pre-fixed threshold of integrated dose is exceeded (20 mGy), the *Dose Control System* forces the closure of the fast safety shutter S1 and of the imaging shutters S2 and S3. Other alarm conditions are emergency button activation, out-of-range monochromator energy, conflict between redundant sensors, out-of-range sensor values, etc.

The "*Dose Control System*" application runs continuously, but the emergency actions are carried out only in *Patient Mode*; in this way scientists can perform experiments without dose interlock in *Experimental Mode*.

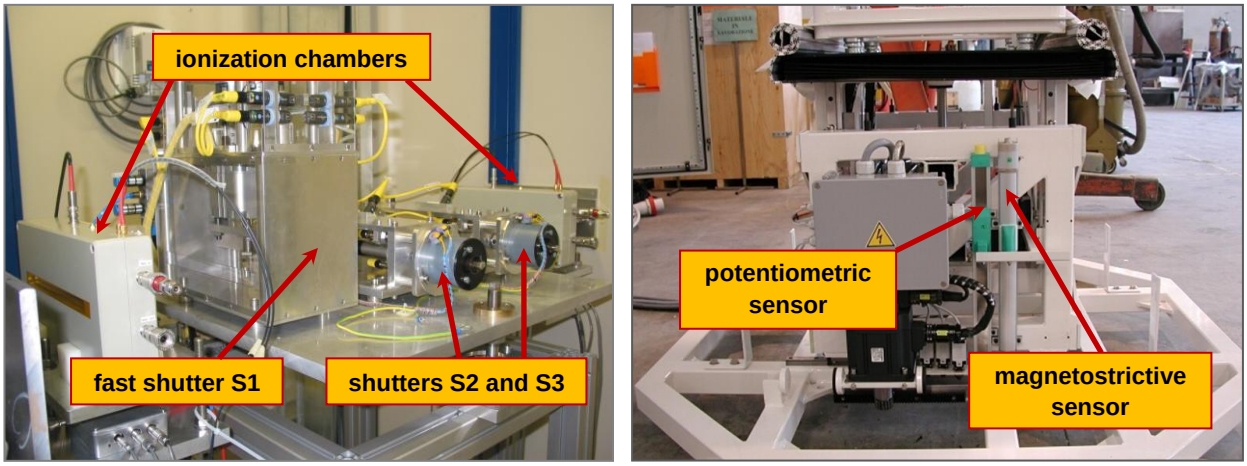

Fig.6 - The ionization chambers with the beamline shutters (on the left) and the bed position sensors (on the right).

3.2.4. Machinery Safety System

The European Standard EN349 defines the minimum gaps to avoid crushing of parts of the human body due to machinery.
Inside the patient room the crushing risk is mainly tied to the bed rotation. The identified risk areas (marked as "A", "B" and "C" zones in Fig.7) have been analyzed according to EN349 and the crushing hazard has resulted unlikely in "A" zone, and not negligible in "B" and "C" zones.
To minimize the risk, two laser scanners performing horizontal plane scans, have been placed inside the patient room, on opposite corners. They have been configured in such a way that, if they detect an obstacle inside the "dangerous area", they inhibit or stop the bed movement.

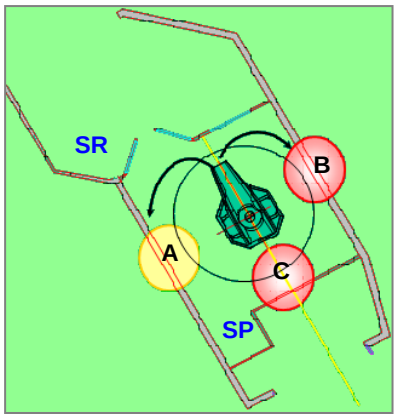

Fig.7 - Risk of crushing against the wall.

3.2.5. Supervision and Human-Machine Interface System

The *"Supervision and Human-Machine Interface" (SHMI)* represents the interface that allows the radiologist to carry out the examination.
High level of reliability has been reached choosing, as hardware, an industrial branded PC equipped with a RAID (Redundant Array of Independent Disks) system, two power supplies and optoisolated serial interfaces, as operating system Linux (Debian distribution) and "C" as programming language.
The *"Supervision and Human-Machine Interface"* permits the beamline staff to optimize the beam for the exam and the radiologist to execute the exam itself, automatically verifying the correct matching of the different parameters, managing the pre-scan phase, carrying out the scan and producing the dose report.

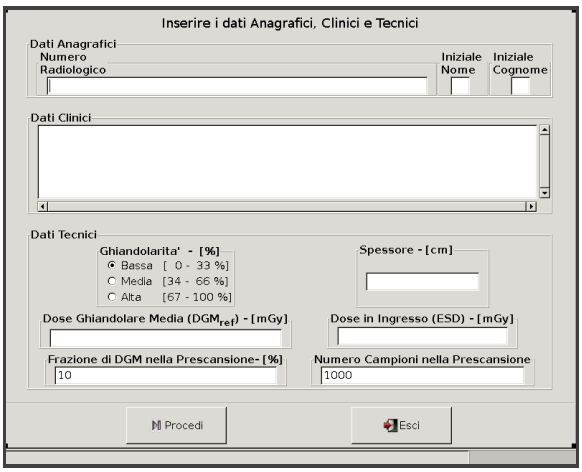

Fig.8 - Screen shot of the form used to insert patient data in the "Supervision and Human-Machine Interface".

4. Conclusions and Perspectives

The 1st phase of the SYRMA project, started on March 13th, 2006, is now next to conclusion: so far 68 patients with an age ranging from 41 to 82 years have submitted to synchrotron mammography at SYRMEP beamline applying PHase Contrast (PHC) Imaging technique. During the three years of operations, the specifically designed and implemented "*Safety, Control and Supervision Systems"* have shown high reliability and efficiency.
The next phases of the project foresee the substitution of the conventional screen-film system, used as image receptor, with digital detectors and the development of new imaging techniques.

References

[1] D. Dreossi *et al.*, "The mammography project at the SYRMEP beamline", European Journal of Radiology (2008), 68, 58-62.
[2] ACR, American College of Radiology, http://www.acr.org
[3] E. Quai *et al.*, "SYRMEP-mammografia con luce di sincrotrone: studio clinico e prospettive future", AIFM09 Proceedings, Reggio Emilia, 2009.
[4] G. Jaconelli *et al.*, "Utilizzo di un sistema CR in mammografia in contrasto di fase con luce di sincrotrone", AIFM09 Proceedings, Reggio Emilia, 2009.
[5] EN 1050 Safety of machinery Principles for risk assessment.
CEI 62-5 Medical electrical equipment.
CEI 64-4 Electrical installations in locations used for medical practice.
EN 418 Emergency Stop Equipment.
EN 964-1 Safety of machinery. Safety related parts of control systems.
EN 349 Safety of machinery. Minimum gaps to avoid crushing of parts of the human body.
[6] V. Chenda and A. Abrami, "Specifiche dei Requisiti del Sistema di Controllo Accessi della linea per pazienti (P.A.C.S.)", Elettra Internal Report, 2005.
[7] M. P. Toni *et al.*, "Absolute air-kerma measurement in a synchrotron light beam by ionization free-air chamber", Workshop on "Absorbed Dose and Air Kerma Primary Standards", Paris, 2007.

Shielding Design for the Imaging and Medical Beamline at the Australian Synchrotron

P. Berkvens[1] and D. Häusermann[2]

[1]*European Synchrotron Radiation Facility – BP 220, Grenoble Cedex 09, France*

[2]*Australian Synchrotron – 800 Blackburn road, Clayton, VIC 3168, Australia*

Abstract

The Imaging and Medical beamline at the Australian Synchrotron will be dedicated to high resolution imaging of cells, tissues, 'objects' (tumours, fine structural details in organs and bones), cell tracking using nano-particles and other contrast markers, research in the interaction of radiation with cells - cancer and healthy - to improve radiotherapy prescriptions and treatments and the extension of the above programs to clinical research with patients.
The present paper gives a short introduction to the beamline and describes in more detail the shielding design for this 136 m long beamline.
Details are given on the shielding design of the optics hutch, both for bremsstrahlung (and photoneutrons) and synchrotron radiation, with special attention to bremsstrahlung ray-tracing.
The shielding of the transfer tunnel between the experimental hall and the satellite building, as well as the shielding of the hutches in the satellite building are described. The design uses a combination of lead, concrete and earth shielding.

1. The Imaging and Medical Therapy beamline at the Australian Synchrotron

The imaging and medical therapy beamline will offer high-resolution, phase-contrast x-ray imaging of small animals and a wide range of engineering materials. It will also enable research into new cancer treatments. The beamline will be 136 metres long, with a satellite building which will later include a patient reception area and an animal holding and preparation facility. All experiment enclosures will eventually have near-beam surgery facilities for fast preparation-to-measurement animal transfers. The first phase of this 'long beamline' program started commissioning in early 2009, allowing for high resolution phase contrast imaging of large objects.

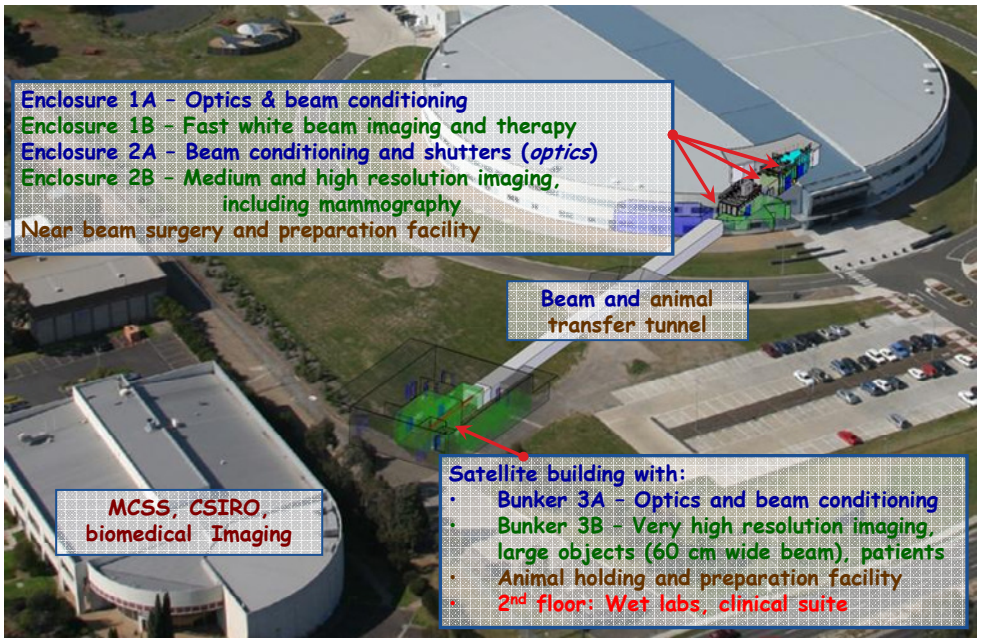

Fig.1 - Layout of the Imaging and Medical Beamline.

Special features of the beamline are:

- phase-contrast and analyser based x-ray imaging, which allows much greater contrast from weakly absorbing materials such as soft tissue than is possible using conventional methods;
- two and three-dimensional imaging at high resolution;
- lower tissue doses than conventional x-ray methods, making longitudinal studies (serial imaging) possible tuneable beam energy, which enables the imaging of specific elements with very high sensitivity, possibly down to submicron scales;
- one of only three beamlines in the world configured for work with a wide range of live animals.

2. Shielding calculations for the optics hutch

The shielding calculations for bremsstrahlung and photo-neutrons were done using the Monte Carlo code *Beamlines* [1]. The following accelerator parameters have been used for the bremsstrahlung calculations.

Electron energy	*3 GeV*
Stored beam current	*400 mA*
Length straight section	*7.6 m*
Average pressure in the straight section	*2. × 10^{-9} mbar*

Table 1 - Accelerator parameters used for the gas-bremsstrahlung shielding calculations.

The shielding calculations were carried out for a value for the stored beam of 400 mA, i.e. twice the nominal current, to be coherent with the general shielding guidance report of S. Costantin [2]. With respect to this report, the value for the pressure has been increased from 1 ntorr to 2 × 10^{-9} mbar. The latter value seems more realistic than the value of 1 ntorr for a current of 400 mA. The residual gas composition shown in table 1 is used, based on RGA measurements in the proximity of crotch-absorbers at the ESRF.

Molecule	*Relative pressure (%)*	*Partial pressure (mbar)*
H_2	71	1.42 × 10^{-9}
CO	20	0.4 × 10^{-9}
CO_2	4	0.8 × 10^{-10}
CH_4	2	0.4 × 10^{-10}
H_2O	3	0.6 × 10^{-10}

Table 2 - Residual gas composition used for the calculations. The partial pressures in the third column correspond to a total pressure of 2 × 10^{-9} mbar.

At the time of the shielding calculations, the details of the optical elements were not yet known. The calculations have been carried out using typical optical elements (detailed 3D simulations of existing ESRF components). The configuration consisted of a pair of slits followed by a double crystal monochromator. This layout is shown schematically in figure 2.

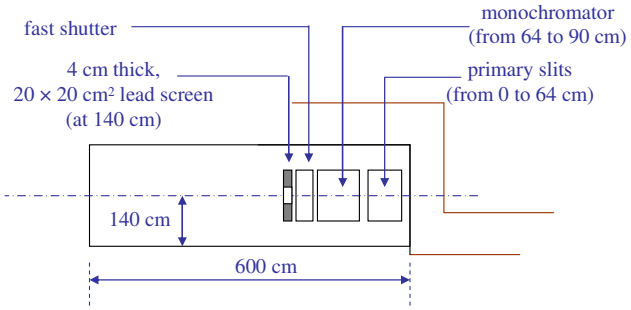

Fig.2 - Schematic layout of the white beam hutch used for the Monte-Carlo calculations for scattered bremsstrahlung and photo-neutron shielding.

Figure 3 shows, as an example, the photon ambient dose equivalent rates behind the optics hutch side wall, as a function of the distance along the hutch, for different lead thicknesses of the hutch side wall and the total ambient dose equivalent rates behind a 25 mm lead wall. The results show that a 25 mm sidewall will keep

dose rates below the 0.5 µSv/h limit for non-exposed workers up to an average pressure in the straight section of 8 10^{-9} mbar (at 400 mA).

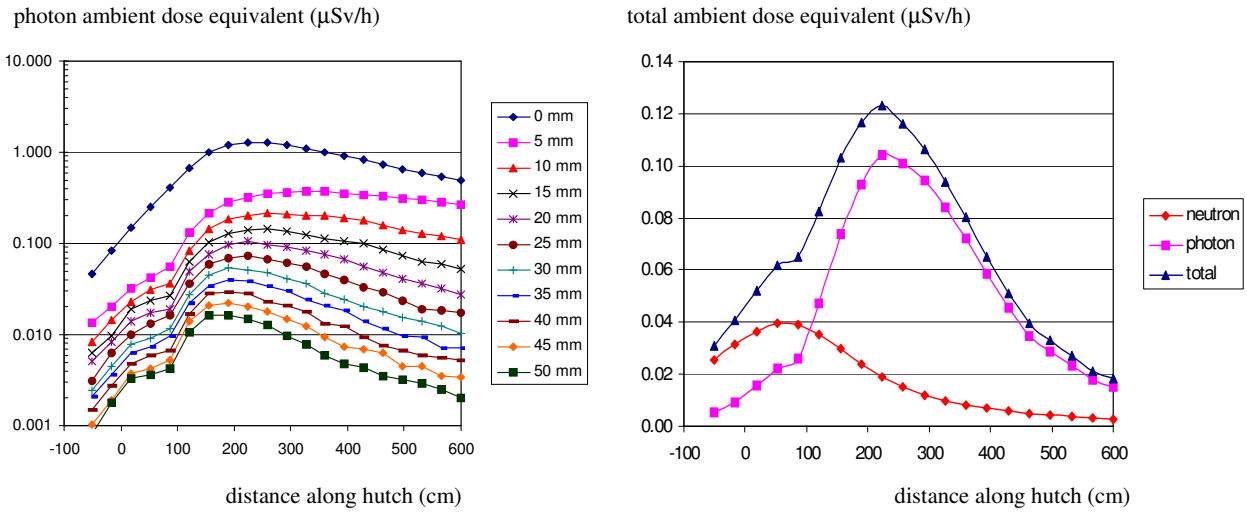

Fig.3 - Photon ambient dose equivalent rates behind the optics hutch side wall, as a function of the distance along the hutch, for different lead thicknesses of the hutch side wall (left); total ambient dose equivalent rates behind a 25 mm lead wall (right).

For the back wall, a lead thickness of 5 cm, with an extra 5 cm of lead in an 80 × 80 cm^2 area around the beam axis was obtained.
The shielding calculations for the synchrotron radiation were carried out using the characteristics of the final wiggler (see table 3). The results for the side wall are shown in figure 4. One sees that the thickness defined for the bremsstrahlung shielding provides adequate shielding also for the synchrotron radiation.

Electron energy	*3 GeV*
Stored beam current	*400 mA*
Insertion device	*Length: 1.5 m* *Period: 48 mm* *Bmax: 4.17 T (E_C = 25 keV*
Front end	*4 mrad full horizontal angle*

Table 3 - Accelerator parameters used for the synchrotron radiation shielding calculations.

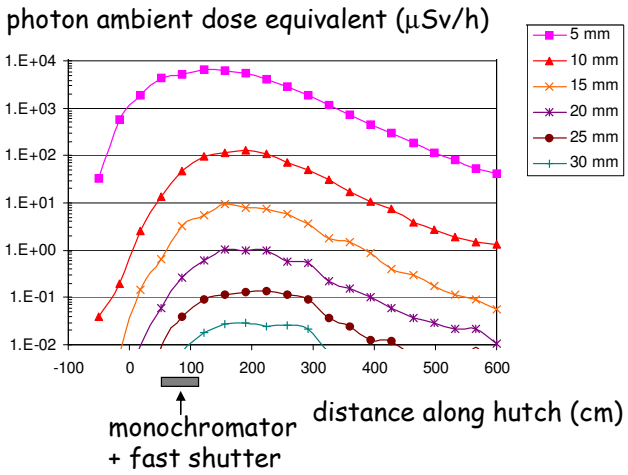

Fig.4 - Photon ambient dose equivalent rates behind the optics hutch side wall, as a function of the distance along the hutch, for different lead thicknesses of the hutch side wall.

3. Bremsstrahlung ray-tracing

Space in the optics hutch is limited. Monte Carlo calculations have been performed to optimise the required bremsstrahlung collimation inside the hutch. Two copper masks are installed in the front end. The first one, placed at 7.4 m from the centre of the straight section, has a full horizontal opening of 3.35 mm and a full vertical opening of 52.7 mm. The second one, placed at 11.9 m from the centre of the straight section, has a full horizontal opening of 6.4 mm and a full vertical opening of 49.5 mm. This defines an effective collimation of ± 0.23 $mrad_V$ and ± 2.08 $mrad_H$. At the end of the hutch a 20 cm thick tungsten beamstop is installed, 15 cm wide and 8 cm high, placed at 18.85 m from the source point. It provides both horizontally and vertically, a 1.5 cm overlap with the 15 cm_H × 5 cm_V rectangular beampipe. The calculations showed that the dimensions of the safety shutter installed at the end of the optics hutch are sufficient to correctly shield under all possible misalignment conditions of the electron beam, without need of further bremsstrahlung collimators. This is illustrated in figure 5 which shows the bremsstrahlung dose rates behind the optics back wall, for three configuration, a perfect aligned electron beam in the straight section, a beam with a 2.63 mrad horizontal misalignment (trajectory from -1 cm to + 1 cm in the 7.6 m long straight section) and a beam with a 3.95 horizontal misalignment respectively. One sees clearly the effect of the copper masks resulting in a net dose decrease for misalignment angles above 3 mrad.

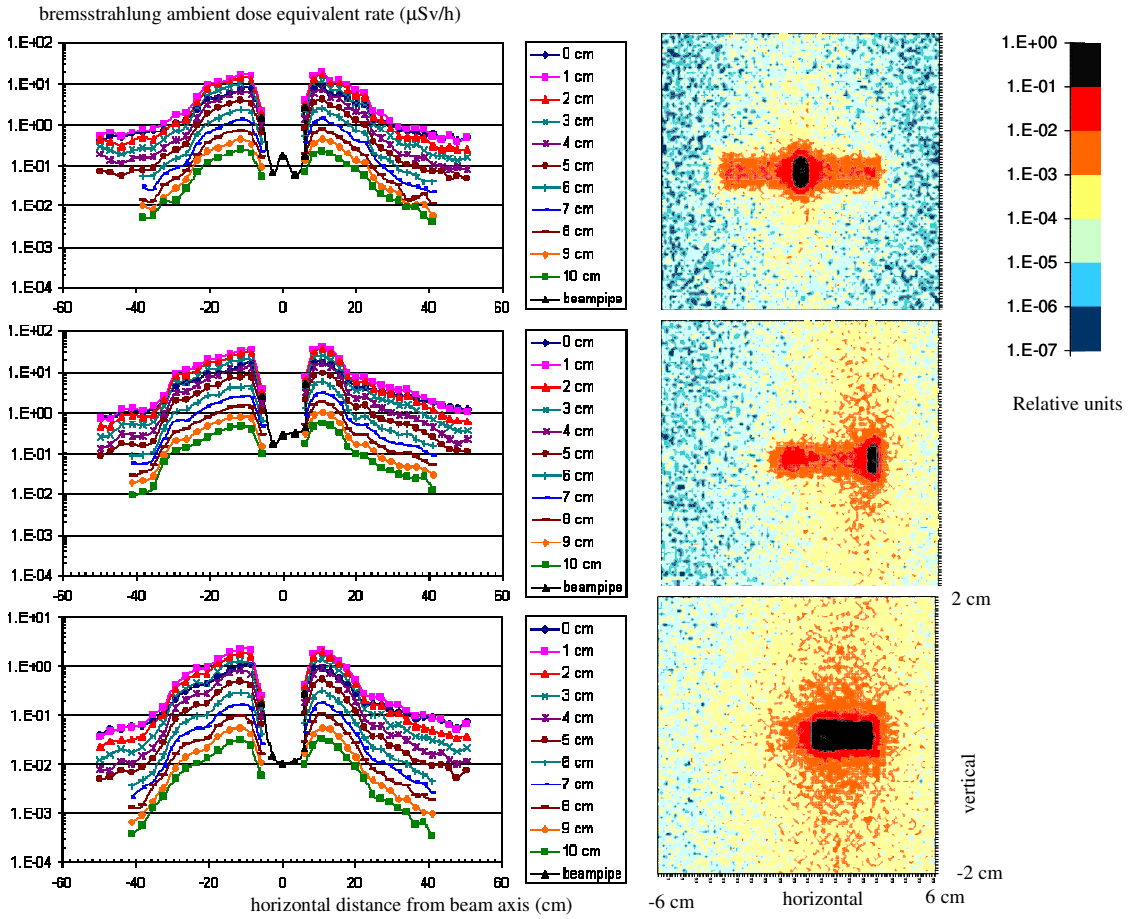

Fig.5 - Left: Bremsstrahlung ambient dose equivalent rate behind the optics hutch back wall, as a function of the horizontal distance from the beam axis (vertical scoring height = ± 2 cm around beam height) - Right: relative dose distribution in a 12 cm_H × 4 cm_V area centred around the beam axis. Top: nominal orbit; middle: orbit horizontally misaligned by 2.631 mrad; bottom: orbit horizontally misaligned by 3.947 mrad.

4. Shielding for the tunnel and the satellite building

A combination of lead, concrete and earth is used for the shielding of the hutches inside the satellite building and for the tunnel between the latter and the experimental hall. A concrete density of 2.4 g/cm^3 is used, while a soil density of 1.8 g/cm^3 is assumed, with the elemental composition shown in table 4.

The results of the optics hutch showed that similar lead thicknesses are required to shield against gas-bremsstrahlung and synchrotron radiation. When using a combination of lead, concrete and earth the thickness requirements will be determined by synchrotron radiation. All calculations are carried out using a low-Z grazing incidence scatterer. Figure 6 illustrates the results of the shielding calculations for the side wall of the 3A optics hutch (distance from beam axis = 200 cm), showing that a 4 mm lead lining on the 44 cm concrete wall is sufficient.

Element	*Relative weight (percentage)*
Oxygen	*47.33*
Sodium	*2.84*
Magnesium	*2.11*
Aluminum	*8.24*
Silicon	*28.1*
Potassium	*2.64*
Calcium	*3.65*
Iron	*5.09*

Table 4 - The elemental composition for soil used in the calculations

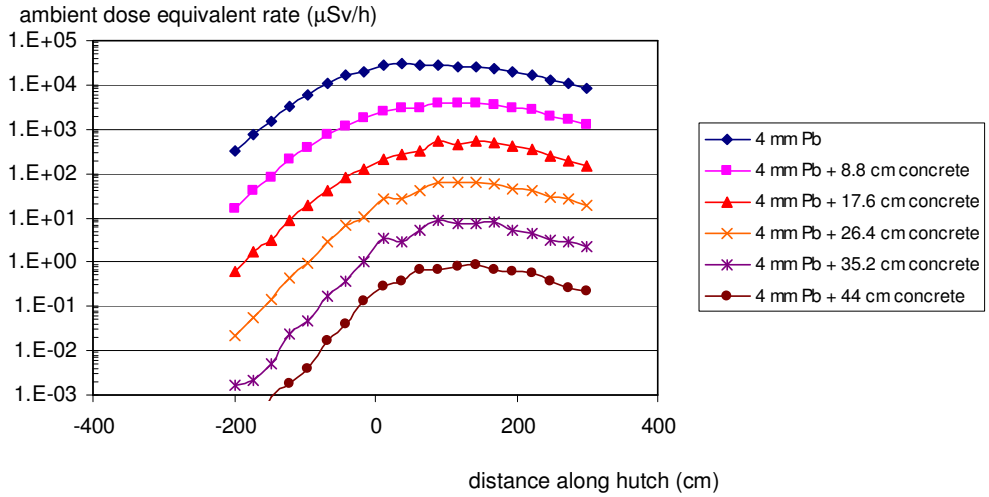

Fig.6 - Ambient dose equivalent rates behind the 3A hutch side wall, as a function of the distance along the hutch (0 cm corresponds to position of scatterer), for different concrete wall thicknesses.

The relative inefficiency of the concrete as shielding material for X-rays is illustrated in figure 7 showing the results for the lead door in the side wall of the 3A optics hutch (distance from beam axis is 244 cm), showing the superior shielding efficiency of the 24 mm thick lead door, compared to the 44 cm thick, lead lined, concrete wall.

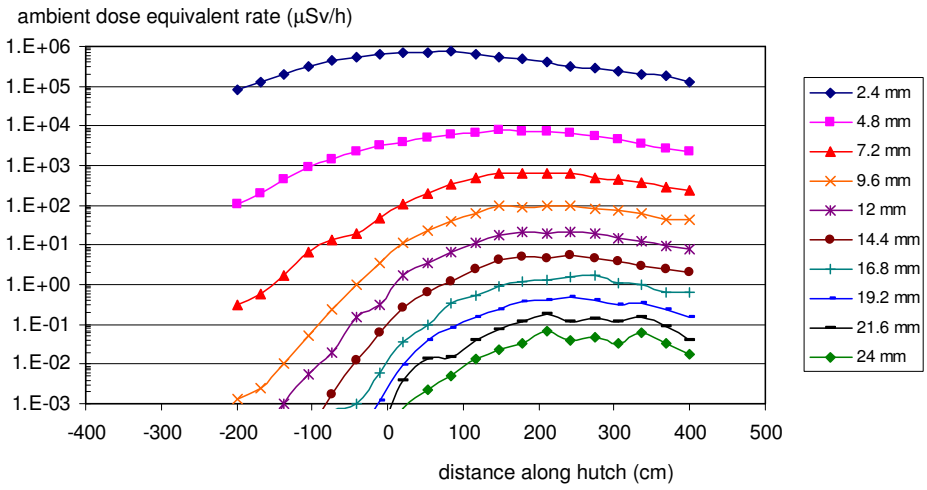

Fig.7 - Ambient dose equivalent rates behind the 3A hutch lead door, as a function of the distance long the hutch (0 cm corresponds to position of scatterer), for different lead thicknesses.

The shielding requirements for the tunnel are determined by backscattered radiation from the 3A optics hutch and from air scatter inside the beam tube. Since backscattering occurs permanently, dose rates from this source must be kept below 0.5 µSv/h. Air scatter will only occur accidentally and from the shielding calculations a maximum closing time of the beam shutter in case of a vacuum problem is obtained (interlocked to the personnel safety system).
Figure 8 shows the ambient dose equivalent rates behind the tunnel outboard side wall (distance from beam axis = 170 cm). No extra earth shielding over the 20 cm thick concrete wall is required for distances more than 40 m from the 3A hutch wall. A 4 mm lead cladding of the tube over the last 20 m upstream of the 3A hutch wall is foreseen.

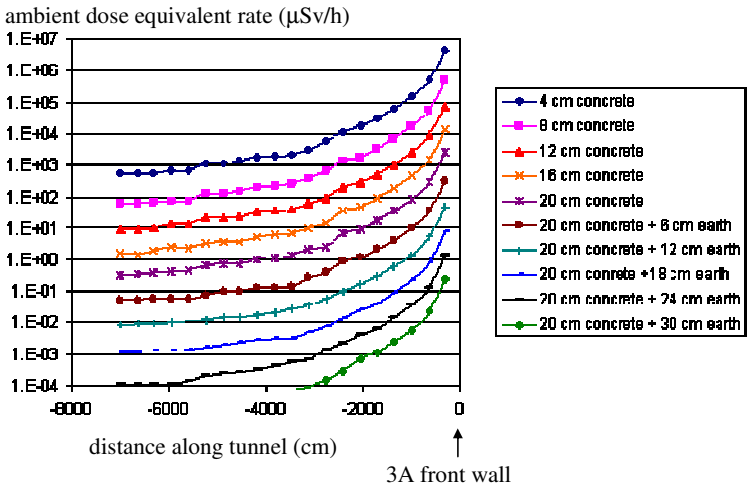

Fig.8 - Ambient dose equivalent rates behind tunnel outboard side wall, as a function of the distance from the 3A hutch outer face of upstream wall.

Finally, figure 9 shows the dose rate behind the outboard tunnel wall, as a function of the concrete thickness and the additional earth thickness. No extra earth shielding is present for the first part of the tunnel, near the experimental hall. The results of figure 8 show that in the case of a sudden vacuum loss an integrated dose of about 20 µSv is obtained for a shutter closure time of 1 s.

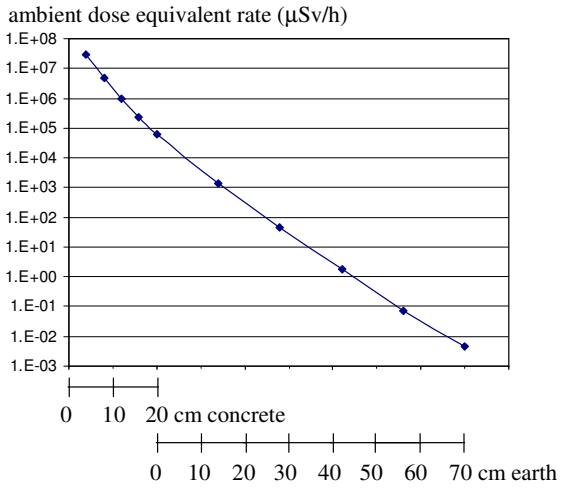

Fig.9 - Ambient dose equivalent rates due to air scatter (atmospheric pressure) behind tunnel outboard side wall, as a function of the concrete + earth thickness.

References

[1] P. Berkvens, R. Kersevan and P. Colomp, Shielding assessment of the optics hutches of the ESRF beamlines, proceedings of Radsynch07 workshop, 2008.

[2] S. Costantin, “Guidance for beamline shielding at the Australian Synchrotron” ASP-RADS-BLS-0001, revision 0 (March 2006).

ALARA Review of NSLS-II Design

W.R. Casey and P.K. Job

National Synchrotron Light Source II, Brookhaven National Laboratory, Upton, N.Y.

Abstract

There has been extensive discussion of appropriate shield design criteria during the early phases of the National Synchrotron Light Source II (NSLS-II) project. The U.S. Department of Energy requires that shielding for occupiable areas (assuming 2000 hrs/yr occupancy) reduce radiation levels to 5 μSv/h, and that levels should be reduced below that to As Low as Reasonably Achievable. This ALARA determination must be documented in a detailed report.

This paper reviews the ALARA analysis for the NSLS-II project and demonstrates that the design criteria of 5 μSv/h for the storage ring enclosure and 0.5 μSv/h for the beam line enclosures is ALARA. Methods and assumptions used in the ALARA analysis are described and the results of the calculations are presented.

1. Introduction

Radiation exposure to staff and users as the result of National Synchrotron Light Source II (NSLS-II) operations must comply with Brookhaven National Laboratory (BNL) and Department of Energy (DOE) radiation requirements and must be maintained as low as reasonably achievable (ALARA). The purpose of this document is to review the basis for the design choices used to limit radiation exposure at NSLS-II and demonstrate that the shielding has been effectively and optimally integrated into the design of NSLS-II facilities.

In particular, this analysis is intended to demonstrate that the following requirements from 10 CFR Part 835 have been adequately addressed:

Part 835 Sec. 835.1002 - Facility design and modifications.

During the design of new facilities or modification of existing facilities, the following objectives shall be adopted:

(a) Optimization methods shall be used to assure that occupational exposure is maintained ALARA in developing and justifying facility design and physical controls.

(b) The design objective for controlling personnel exposure from external sources of radiation in areas of continuous occupational occupancy (2000 hours per year) shall be to maintain exposure levels below an average of 0.5 mrem (5 microsieverts) per hour and as far below this average as is reasonably achievable. The design objectives for exposure rates for potential exposure to a radiological worker where occupancy differs from the above shall be ALARA and shall not exceed 20 percent of the applicable standards in Sec. 835.202.

(c) Regarding the control of airborne radioactive material, the design objective shall be, under normal conditions, to avoid releases to the workplace atmosphere and in any situation, to control the inhalation of such material by workers to levels that are ALARA; confinement and ventilation shall normally be used.

(d) The design or modification of a facility and the selection of materials shall include features that facilitate operations, maintenance, decontamination, and decommissioning.

2. Sources of Radiation Exposure at NSLS-II

NSLS-II will be a synchrotron light source operating at 3 GeV with a maximum stored beam of 500 mA. The storage ring will be supplied by an injection system consisting of a 200 MeV linac and a 3 GeV booster synchrotron. The injection system can deliver 15 nC/s when initially filling the ring, but will normally provide ~ 15 nC/pulse when topping off the storage ring about once/minute.

Electron storage rings are in wide use throughout the world for this purpose and sources of occupational radiation exposure to workers at these facilities are well known. Radiation exposure to workers or the public is almost entirely from external exposure occurring during operation of the storage ring. Because the overall power associated with the NSLS-II accelerators and storage ring is very small compared to that associated with a high intensity accelerator, activation hazards are in general low. As an example, the highest level observed from induced activity at the existing NSLS (operating since 1983) is typically < 0.1 μSv/hr at contact with a few locations at 20 – 40 μSv/h, many of these latter locations decreasing rapidly over time after the electron beam has been turned off.

Activation hazards have been evaluated and confirmed to be low in reference 1. Activation hazards evaluated include:

- Exposure to residual radiation induced in machine components and beam dumps
- Inadvertent release of activated cooling water to the environment
- Inadvertent release of radioactive contamination to groundwater by allowing rainwater to leach through activated soil
- Exposure to activated air.

This paper will evaluate the potential for exposure from direct radiation penetrating the shielding and the design criteria used in determining the shield thickness for the accelerator and photon beam lines.

Sources of external radiation which must be shielded are generated at electron loss points within the accelerator and at photon scatter points in beam lines. In preparing the design, the locations of loss points were identified and estimates of electron losses were developed in conjunction with the accelerator physicists responsible for the design (see reference 2).

3. Dose Assessment and Optimization Analysis

Part 835.1002 requires that the shield design objective for controlling personnel exposure from external sources of radiation in areas of continuous occupational occupancy (2000 hours per year) shall be to maintain exposure levels below an average of 5 microsieverts per hour and as far below this average as is reasonably achievable. The design objectives for a radiological worker where occupancy is snot continuous shall be ALARA and shall not exceed 20 percent of the applicable standards in Sec. 835.202.

NSLS-II operation will produce external radiation levels above background in the following locations: (a.) Ring Building, (b.) RF Building, (c.) Injection Building, (d.) Bermed areas above linac and booster. Only the Ring Building will have a continuous occupancy throughout the year and is the focus of this analysis (see attachment A for occupancy assumptions). The other locations will have intermittent occupancy. The bermed areas will have minimal occupancy during operations and will be restricted as necessary to limit the potential for exposure.

The design objective used to shield all of these loss locations is 5 μSv/h during normal operations in contact with the exterior surface of the closest shield wall, thereby satisfying the first part of the section 835.1002 requirement for continuously occupied locations. It is worth noting that the calculations determining the required shield thicknesses were performed using a conservative set of assumptions for the following factors:

- Beam losses are assumed to occur at a single point (rather than scattered and distributed over a more lengthy surface)
- The most conservative attenuation lengths in shield material are used
- Doses are calculated using thick target dose equivalent factors
- Electron loss estimates are conservatively picked and are based on a 2 hour life time (rather than the expected 3 hour life time)
- No credit is taken for self-shielding associated with internal accelerator components.

Measurements made at the European Synchrotron Radiation Facility comparing actual radiation levels to calculated levels based on a similar set of assumptions determined that predicted levels were conservative by a factor of 10 – 20 for their facility.

4. ALARA Evaluation

It should be noted again that only the Ring Building has a continuous occupancy. In order to satisfy the ALARA criterion, we need to evaluate the total dose that would be saved if a lower design criterion was used and compare that to the additional costs that are incurred in increasing the shield thickness. If the value of the dose saved is less than the cost of increased shielding, then the additional costs can be viewed as not warranted and the shield considered to be optimized. The dose savings for 5000 hours of user program and 800 hours of accelerator physics studies are included. The details of the ALARA optimization calculation are given in attachment A.

4.1. Accelerator Enclosures

Using the occupancy and operating assumptions described in attachment A, the 30 year integrated dose equivalent resulting from NSLS-II normal operations and machine studies is estimated in attachment B to be ~ 1.75 Sv for a shield designed to 5 μSv/h. The saved dose for designing to 2.5 μSv/h is ~8.9 Sv . The value of the saved dose is $946,000 and the cost of increasing the shield thickness to reduce radiation levels to 2.5 μSv/h is ~$1,800,000[†]. It is concluded that the dose saved by shielding to 2.5 μSv/h does not warrant the additional costs; and the shield design can be considered optimized.

There is one small portion of the Ring Building affected by the higher losses in the injection region. A separate analysis was performed which indicates that supplemental shields are cost effective for the injection region and should be provided to reduce radiation levels to 5 μSv/h in this area during 1 Hz injection periods.

4.2. Hutch Shields

Using the occupancy and operating assumptions described in attachment A, the 30 year collective dose equivalent for 58 beam lines resulting from a 5000 hours per year operating schedule is ~ 108 person-Sv for experimental end stations (typically called mono stations) and the First Optical Enclosure (FOE) hutches designed to 5 μSv/h. The 30 year collective dose for hutches designed to 0.5 μSv/h is ~ 11 person-Sv. The saved dose for designing to 0.5 μSv/h is ~97 person-Sv. The value of the saved dose is $106,000,000 and the cost of increasing the shield thickness in both FOE and the mono-hutch to reduce radiation levels to 0.5 μSv/h is ~$1,450,000. It is concluded that the dose saved by shielding the hutches to 0.5 μSv/h is quite substantial and worth the increased costs. The hutches will be shielded to 0.5 μSv/h.

5. Administrative Controls to Maintain Exposure ALARA During Operations

There are a number of programs that will be in place when NSLS-II operates to ensure the effectiveness of shielding and control of radiation exposure.

Accelerators and beam lines will be subject to an initial commissioning period under highly controlled conditions to confirm that adequate shielding consistent with the shielding policy is provided. Set-points for interlocked radiation monitors and beam loss monitors will also be established during commissioning to ensure that fault conditions are detected and interlocked in a manner consistent with the shielding policy.

The on-going effectiveness of shielding will be actively monitored by radiation instruments located on the experimental floor and other locations, and by frequent area-surveys performed by the health physics personnel. Additional local shielding will be provided to reduce the radiation field as needed. Passive area monitors will also be used to integrate doses in various areas. The results will be analyzed for trends, and shielding will be improved in the form of supplementary shielding as appropriate.

The work areas adjacent to the accelerator enclosures (Linac, Booster, and Storage Ring) and beam lines, including the Service Buildings, will be posted as radiologically Controlled Areas. The tunnel providing access to the inner area of the site and the berms adjacent to the Linac and Booster may also be posted. Posting requirements will be determined during machine commissioning. Proper radiation and facility

[†] Total cost of concrete based on increasing the thickness of concrete shielding in walls and roof by 15 cm. This cost is based on estimates provided by the NSLS-II Conventional Facilities Division.

specific training will be required for access to all posted areas. During the initial years of commissioning and operation, a radiation dosimetry badge will be issued for all personnel working in the Controlled Areas. It is expected that following verification of shielding effectiveness that short-term users and visitors will not be required to wear a dosimeter while on the experimental floor. This verification process is expected to take 2 – 3 years. Access into the Controlled Areas will be controlled through the use of card readers (or other similar controlling device) at access points to the building. Areas within the Controlled Areas may have additional postings such a Radioactive Material Areas and Radiation Areas, as required. Direct access to either the electron or synchrotron beams will be prevented by the use of radiation safety interlocks described in the Preliminary Safety Assessment Document (PSAD). Although not frequently needed at the NSLS, Radiological Work Permits (RWP) will be issued by Radiological Control Division personnel as required in accordance with the criteria in the BNL Radiological Control Manual.

A radiation monitoring program will be established in the Controlled Areas to protect workers and to assure that their doses are kept ALARA. Radiation surveys will be performed to assure that proper shielding is in place, to monitor machine operations and to assure the containment of sealed sources or experiment samples. Different types of radiation monitoring will occur at NSLS-II, e.g. personal dosimetry (e.g. Thermoluminescent Devices or TLDs), passive area dosimetry (e.g. TLDs), active area monitors with local and remote read-out to the Control Room, and hand-held survey instruments used by trained personnel.

6. Conclusion

Based on the analysis summarized above, we conclude:

A. The concrete bulk shield for the storage ring designed 5 μSv/h complies with the requirements defined in Part 835.1002 and is ALARA.

B. Supplemental lead shields provided in the injection region which reduce radiation levels to μSv/h complies with requirements defined in Part 835.1002 and is ALARA.

C. The lead shielding in the beam line hutches designed to 0.5 μSv/h complies with the requirements defined in Part 835.1002 and is ALARA.

D. The estimated total annual dose for the facility designed to these criteria is ~ 0.4 person-Sv with an average dose per worker/user assuming 3500 workers of ~ 110 μSv.

It is worth noting that there have been two design reviews of the proposed NSLS-II shields by a knowledgeable group from other synchrotron radiation sources to assure that the shielding methodology and assumptions are reasonable and consistent with international practices. The Review Committee concluded that the proposed shields are reasonable and consistent with designs at other facilities.

References

[1] P.K. Job and W.R. Casey, “Preliminary Activation Analysis of Soil, Air and Water near the NSLS-II Accelerator Enclosures”, NSLS-II Technical Note 50, August 15, 2008.
[2] P.K. Job and W.R. Casey, “Shielding Requirements for NSLS-II”, BNL-79774-2008-CP, January 2008.

Attachment A

Operating and Occupancy Assumptions for ALARA Design Review

1. Operating Conditions

We assume the NSLS-II will be operated with the following parameters.

- Energy – 3 GeV
- Stored Current – 500 mA
- Life-time – 2 hours

We assume 5000 hours per year for user program with the following machine fills:

- Top-off every 72 secs to keep current at or near 500 mA
- 200 complete fills per year

We assume 1000 hours per year of accelerator studies with the following parameters:

- 200 hours per year at 1 Hz injection rate and maximum injection current (15 nC/s)
- 800 hours per year for other studies at conditions similar to normal operation (i.e. 500 mA stored beam, top-off operation 1 pulse per minute top off.

2. Anticipated Occupancies Around Storage Ring

2.1. During User program

The highest occupancies on the floor will occur during the operating periods in which the user program is on-going. In order to estimate the potential radiation exposure that will take place during the user program, estimates of occupancies must be assumed as described below. For analysis purposes we assume the occupancies described below. These estimates are conservative and maximize the potential occupancies and radiation exposure. It should be noted that the occupancies for the users and NSLS-II beam line staff is much higher than that of the NSLS-II operating staff. NSLS-II operating staff (e.g. members of the RF Group, power supply group, and interlock group) are not routinely on the floor, but rather enter the building to adjust or trouble shoot components during studies or normal operations to seek to improve performance. Higher occupancies are assumed for members of the ESH Group and floor coordinators who have a greater routine presence on the floor.

2.1.1. Group 1 - Beam line staff & users at mono-chromatic end-station

We assume 3 personnel per beam line located at an average distance of 30 cm from an end station wall. We assume 58 beam lines in operation located at an average distance of 10 meters from the storage ring wall. We assume 5000 hrs/y occupancy with storage ring operating.

2.1.2. Group 2 - Beam line personnel performing maintenance in FOE while storage ring operating

Periodically beam line personnel must enter the FOE to perform install, adjust or maintain equipment within the enclosure. Such entry requires that the beam line be secured by shutting the safety shutter. Therefore such work will normally be done during scheduled accelerator maintenance periods in order to maximize beam line productivity, therefore we assume only a 10% occupancy during the standard 5000 hour operating year. We assume 2 personnel at each of 58 beam lines working 30 cm from the storage ring wall for 500 hrs/y with accelerator operating and beam line off.

2.1.3. Group 3 - Infrared beam lines

We assume 3 Infra-Red scientists per beam line, 6 beam lines with occupancy at 1 m from wall and 4 beam lines at 10 meters from the storage ring wall. We assume 5000 hrs/y occupancy with storage ring operating

2.1.4. Group 4 - Beam line personnel working on top of FOE while beam line is in operations

Provisions are made for use of the top of the FOE for storage. We assume that there will be need intermittently during beam line operations for personnel to place or retrieve equipment from the hutch top. We assume a total of 5% of the operating cycle as the occupancy on the top and that the person is kneeling down rather than standing. We also assume that the person accesses the hutch by walking on the mezzanine. Therefore, we have 1 person per beam line, 58 beam lines, 30 cm from the hutch top. 250 hours per year on hutch-top; 25 hours per year on mezzanine traveling to hutch top – 1 m from mezzanine floor

2.1.5. Group 5 - Members of the Power Supply Group

We assume a maximum of 2000 person hours per 5000 hour operating year on the mezzanine working at an average distance of 1 meter from the floor.

2.1.6. Group 6 - Members of the Vacuum Group

We assume a maximum of 2000 person hours per 5000 hour operating year on the mezzanine working at an average distance of 1 meter from the floor.

2.1.7. Group 7 - Members of the Insertion Device Group

We assume a maximum of 100 person hours per 5000 hour operating year on the mezzanine working at an average distance of 1 meter from the floor.

2.1.8. Group 8 - Members of the Interlock Group

We assume a maximum of 100 person hours per 5000 hour operating year on the mezzanine working at an average distance of 1 meter from the floor.

2.1.9. Group 9 - Floor Coordinators, health physics staff and ESH personnel

We assume a maximum of 2500 person hours (5 people at 500 hours each) per 5000 hour operating year working at a distance of 1 m from the SR wall and mezzanine floor. We also assume a maximum of 500 person hours per 5000 hour operating year (5 people at 100 hours each) working at a distance of 30 cm from end station and also from FOE.

2.2. During Accelerator Physics studies

Occupancies on the experimental floor during accelerator studies will be much lower than occupancies during the normal user program since beam lines are not available for research use. However, it is assumed that some personnel will be present to set up for future work and to make adjustments to beam line and research equipment. These estimates are based on current experience at NSLS and other light sources and are judged to be conservative estimates.

2.2.1. High current, fast injection studies assumed for 200 hours/per year

2.2.1.1. Group 1 - Beam line staff & users at mono-chromatic end-station

We assume 1 person for every other beam line working at a distance of 10 meters from the storage ring wall for a total of 29 people working during the 200 hours.

2.2.1.2. Group 2-Beam line personnel performing maintenance in FOE while storage ring operating

We assume 1 beam person per every other beam line for a total of 29 people working in FOEs at a distance of 30 cm from the storage ring wall. We assume FOEs are occupied for 100 hours during accelerator studies.

2.2.1.3. Group 3 - Infrared beam lines

We assume 1 infrared beam line scientist for every other beam line, a total of 3 people working at 1 meter from the storage ring wall and 2 people working at 10 meters from the storage ring wall. We assume 200 hrs/y occupancy.

2.2.1.4. Group 4 - Beam line personnel working on top of hutch during studies

We assume 1 person for every other beam line, a total of 29 people exposed for 10 hours on the hutch top during high injection studies. We also assume 1 hour on mezzanine traveling to hutch top at 1 m from mezzanine floor.

2.2.1.5. Group 5 - Members of the Power Supply Group

We assume a maximum of 80 person hours on the mezzanine working at an average distance of 1 meter from the floor.

2.2.1.6. Group 6 - Members of the Vacuum Group

We assume a maximum of 80 person hours on the mezzanine working at an average distance of 1 meter from the floor.

2.2.1.7. Group 7 - Members of the Insertion Device personnel

We assume a maximum of 4 person hours on the mezzanine working at an average distance of 1 meter from the floor

2.2.1.8. Group 8 - Members of the Interlock Group

We assume a maximum of 4 person hours on the mezzanine working at an average distance of 1 meter from the floor

2.2.1.9. Group 9 - Members of the Floor Coordinators, health physics staff and ESH personnel

We assume a maximum of 100 person hours working at a distance of 1 m from the SR wall and mezzanine floor.

2.2.2. 1 pulse/min injection assumed for 800 hours/per year

2.2.2.1. Group 1 - Beam line staff & users at mono-chromatic end-station

We assume 1 person for every other beam line working located at a distance of 10 meters from the storage ring wall for a total of 29 people working for 800 hours during accelerator studies

2.2.2.2. Group 2-Beam line personnel performing maintenance in FOE while storage ring operating

We assume 1 beam person per every other beam line for a total of 29 people working in FOEs at a distance of 30 cm from the storage ring wall. FOEs are occupied for 400 hours during accelerator studies.

2.2.2.3. Group 3 - Infrared beam lines

We assume 1 infrared beam line scientist for every other beam line, a total of 3 people working at 1 meter from the storage ring wall and 2 people working at 10 meters from the storage ring wall. We assume 800 hrs/y occupancy during accelerator physics studies.

2.2.2.4. Group 4 - Beam line personnel working on top of hutch during studies

We assume 1 person at every other beam line, a total of 29 people exposed for 50 hours per year on the hutch top and 5 hours per year on mezzanine traveling to hutch top at 1 m from mezzanine floor.

2.2.2.5. Group 5 - Members of the Power Supply Group

We assume a maximum of 320 person hours on the mezzanine working at an average distance of 1 meter from the floor.

2.2.2.6. Group 6 - Members of the Vacuum Group

We assume a maximum of 320 person hours per year on the mezzanine working at an average distance of 1 meter from the floor

2.2.2.7. Group 7 - Members of the Insertion Device personnel

We assume a maximum of 16 person hours per year on the mezzanine working at an average distance of 1 meter from the floor.

2.2.2.8. Group 8 - Members of the Interlock Group

We assume a maximum of 16 person hours per year on the mezzanine working at an average distance of 1 meter from the floor

2.2.2.9. Group 9 - Members of the Floor Coordinators, health physics staff and ESH personnel

We assume a maximum of 400 person hours working at a distance of 1 m from the SR wall and mezzanine floor.

3. Comparison Of Accelerator Physics Studies On Shielding Requirements

Based on these assumptions identified above, we can calculate the total number of electrons/year accelerated and lost in ring. This parameter is a key factor in determining the adequacy of the shield.

3.1. Electrons lost during User Program

200 fills per year → 200 x 1.3 μC / fill = 2.6 x 10^2 μC/y → 2.6 x 10^2 x 6.24 x 10^{12} e/μC = 1.62 x 10^{15} electrons per year injected and lost per year.

With 2 hour life and 500 mA beam we will lose ~ 11 nC/min

If injection efficiency is 80%, we must inject 13.2 nC/min

Total number of electrons injected and lost over 5000 hours of stored beam operation is:

5000 hours/y x 60 min/h x 13.2 nC/min = 3.96 x 10^6 nC/year lost during stored beam =

3.96 x 10^6 nC/year x 6.24 x 10^9 e/nC = 2.47 x 10^{16} electrons per year lost

Total number of electrons lost during user program is 1.62 x 10^{15} + 2.47 x 10^{16} =

2.63 x 10^{16} per year

3.2. Accelerator Physics Studies

We assume 200 hours of 1 Hz injection studies at 15 nC/pulse.

200 hours/y x 3.6 x 10^3 s/h x 15 nC/s injected x 6.24 x 10^9 e/nC = 6.74 x 10^{16} electrons per year lost

We assume that the other 800 hours are at 1 injection /min rate at 15 nC/pulse.

800 hours/y x 60min/h x 15 nC/min injected x 6.24 x 10^9 e/nC = 4.49 x 10^{15} electrons per year lost

Total electron/yr lost during accelerator physics studies = 6.74 x 10^{16} + 4.49 x 10^{15} = 7.19 x 10^{16}

4. Conclusion

Over the course of the year, electrons lost during accelerator physics studies have the potential to be higher than the total losses that occur during the user program. The potential for radiation exposure during accelerator studies will depend on the nature of the studies and the occupancies on the experimental floor during the accelerator studies. Accelerator studies are normally scheduled well in advance and many participants in the normal user program will not be present since beam lines are not available during studies. Occupancy assumptions used in our calculations during accelerator study periods are therefore much lower than normal operating periods.

However, as indicated in the analysis above for electrons accelerated per year, it is clear that high intensity injection studies have the potential to produce higher radiation levels in occupied areas. During the early years of commissioning and operations, 1 Hz injection periods will likely be needed to establish operating parameters that permit achievement of design goals for accelerator performance. Because of the potential for higher radiation levels during prolonged 1 Hz injection studies, all accelerator studies will require work planning and administrative control of occupancy, particularly in areas located near the storage ring wall (including work conducted inside the FOE) and on the mezzanine floor. Such restrictions will be most probable when initial commissioning of the ring is conducted, and periodically, but not frequently during the remainder of the operating life-time of the facility (such as recovery of vacuum after bleed-up periods). Because of the special controls that will be applied and the unpredictable forecasting of prolonged 1 Hz injection over the 30 year history of the facility, the potential radiation exposure of 1 Hz operation is not included in the estimates of total integrated dose for the facility. The total integrated dose does include the estimates of dose received during 800 hours of accelerator studies conducted at normal operating parameters.

The FERMI project @ Elettra: radiation protection and safety issues

G.Tromba[1], K.Casarin[1] , E. La Torre[1], F.Longo[1,2], E.Quai[1], and A.Vascotto[1]

[1]*Sincrotrone Trieste SCpA, Strada Statale S.S.14 km 163.5, 34012 Basovizza, Trieste, Italy*

[2]*INFN sezione di Trieste, Via A. Valerio 2, 34127 Trieste, Italy*

Abstract

FERMI is a fourth generation light source under construction at the Sincrotrone Trieste laboratory, close to the Elettra synchrotron light source. It will be a single-pass seeded FEL, based upon the conversion of the 1.2 GeV linac used in the past as injector of the Elettra storage ring and recently replaced with a full energy booster synchrotron.
The FEL will operate in the wavelength ranges 120 nm ÷ 40 nm in the first phase, 25 nm ÷ 5 nm in the second one.
The original layout of the linac has been deeply modified with the addition of seven new accelerating sections received from CERN, the substitution of the conventional termoionic gun with a new photoinjector and the installation of two bunch compressors systems. In order to fulfill the stringent requirements of the project, the machine will be equipped with an energy feedback system and a high accuracy low level RF system, capable of reaching very accurate stabilities in terms of RF phase and amplitude. The machine will operate in a single bunch at 50 Hz.
The linac is housed in an underground tunnel 180 m long. The earth provides for the lateral shielding. The undulator and experimental halls under development downstream of the accelerator tunnel are at the same underground level. At the end of the undulator hall, 100 m long, a set of bending and focusing magnets transport the beam to the beamdump, while the produced FEL light continues in the forward direction and is extracted through the front-end. In the experimental hall, the first part of the beamlines, including the first two optics components, are enclosed inside a shielded hutch.
The yearly dose limits we enforced for *free*, *supervised* and *controlled* areas are 0.5 mSv, 2 mSv and 5 mSv respectively, compared to the corresponding limits of 1 mSv, 6 mSv and 20 mSv established by Italian regulations in compliance with the European/Euratom directives. The classification of different areas around the accelerator will be presented.
Similarly to the Elettra facility, the personnel safety system will be based on low level computers, Programmable Logic Controllers (PLCs), chosen with high safety level programmed with *fail safe* logic and redundancy in controls using, where possible, diverse criteria in the choice of the actuators. The logic of the safety system will be discussed.
Environmental monitoring outside the tunnels will be based on a network of gamma and neutron detectors located at some reference points in the experimental hall and in the undulator Service Area. In addition, some gamma monitors located in the vicinities of the beamlines exits will be interlocked with the personnel safety system to prevent unwanted exposures to personnel.

1. Introduction

The original layout of Elettra was based on a 1.2 GeV, 10 Hz, electron Linac operating as an injector for the Elettra storage ring. Injection operation was carried out with all the beamlines beam stoppers closed and all the front-end hutches searched: the energy of the injected beam was then ramped inside the storage ring up to 2.0 GeV (with a stored current of 320 mA) or up to 2.4 GeV (with a stored current of 140 mA), according to the users'shifts calendar.
To permit full energy injection and top-up operation the project of a new injector, consisting of a 100 MeV 3Hz linac pre-injector and a 2.5 GeV booster, started in March 2005 [1].
The design and construction of the new injector lasted about 3 years: the "old" linac was shut off in October 2007 and from March 3rd 2008, after the connection of the booster with the storage ring, Elettra storage ring was again operating for the users with the new injector. From The October 2007 a phase of revision and upgrading of the "old" linac started, to permit its re-utilization for the FERMI project.

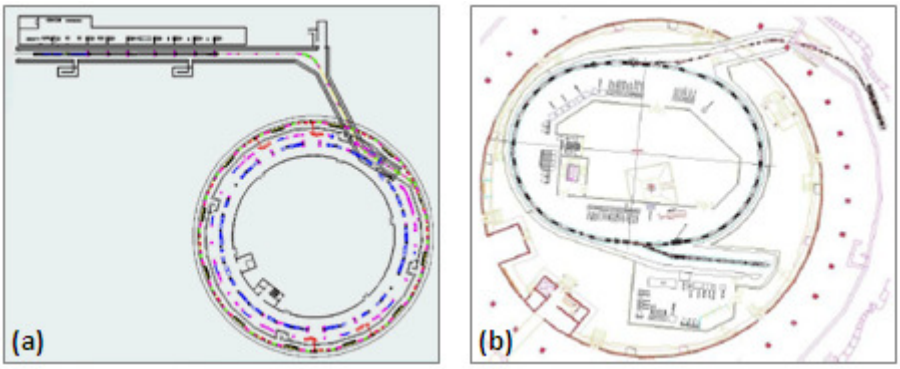

Fig.1 - The original Elettra layout with the old linac (a) and the new booster injector layout (b).

2. The main features of the FERMI project

The FERMI@Elettra light source is a high brilliance 4th generation, single-pass seeded FEL, based upon the re-utilization of the "old" 1.2 GeV Elettra linac. It has been designed to accelerate electrons up to 2.0 GeV at 0.1 μA maximum average current and optimized to produce FEL beams in two fundamental wavelength ranges: 100÷20 nm (FEL1) and 20÷3 nm (FEL2). The whole accelerator is housed in an underground tunnel.

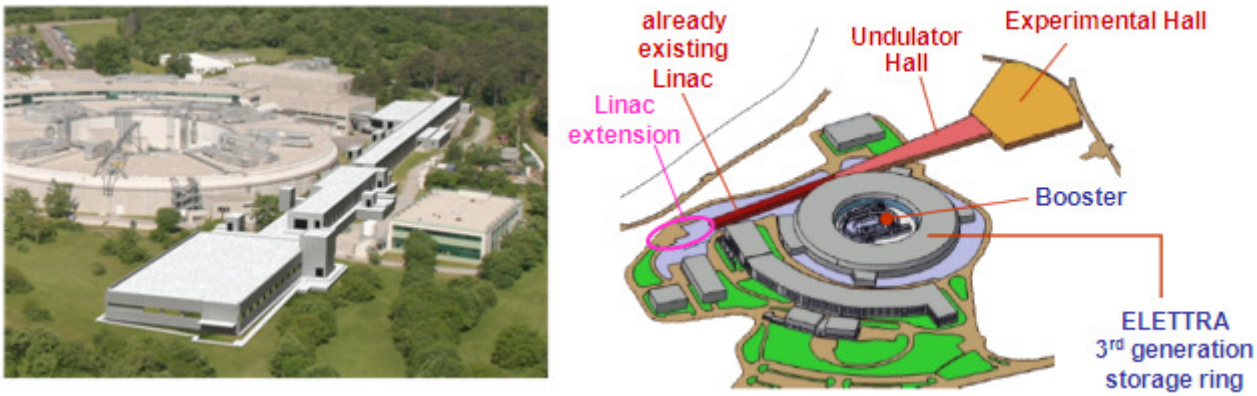

Fig.2 - The FERMI building project.

As far as the logic of the safety system is concerned, the FERMI accelerator will be divided into three main areas: the *Linac*, where the electron beam is produced and accelerated up to the maximum energy, the *Undulator Hall* where the electrons interact with the magnetic field of the undulators producing the FEL beams, and the *Experimental Hall* where the FEL beams are extracted and utilized by researchers.
A Personnel Safety System will assure safety conditions for personnel entering the accelerator tunnels and for the Experimental Hall users. It will be based on a Siemens SIMATIC S7 Programmable Logic Controller (PLC) of high safety level (Category 4). The main safety criteria that will be applied are redundancy (e.g. double door switches), diversification of actuators/controls (e.g. double and different technology switches for all the beam stoppers), and fail-safe logic.

2.1. The Linac

With the development of the FERMI project, the layout of the pre-existing linac will be deeply modified: the original gallery will be extended (upstream the already existing tunnel, as shown in Fig.2), to permit the installation of seven new accelerating sections donated by CERN and of all the new machine components. The termoionic gun will be substituted with a high brightness photoinjector developed in collaboration with MAX-lab and the Particle Beam Physics Laboratory at UCLA [2].
To operate the new accelerator at 50 Hz, instead of the original 10 Hz, eight new TH2132 klystron modulators will add to the previous seven and new RF plants will be installed. Two diagnostic lines at 100 MeV and at 300 MeV will be constructed in the first part of the tunnel to characterize the beam.

At the end of the linac sections, the beam, accelerated up to the maximum energy, will be transported to the the Undulator Hall or will be bended along a further diagnostic line (i.e. the original linac-to-ring transfer line) ending with a beam dump (see Fig.3).
A beam stopper (BST_{Linac}) placed at the end of the linac sections will permit to stop the electrons within the linac area and will be utilized in the definition of the personnel safety condition for entering inside the Experimental Hal front-end hutch (see Paragraph 2.3).
The linac gallery will have an entrance door, which will work also as emergency exit, and four emergency exits, all controlled by the Personnel Safety System. A door that can be opened only from the tunnel inside, positioned at the beginning of the tunnel, will permit to move inside the gallery the most bulky machine components.
Access inside the tunnel will be inhibited by the Personnel Safety System if radiofrequency is applied to the photo-injector RF cavity or to the accelerating sections. Once the radiofrequency is shut off, the person who wants to enter the accelerator gallery will have to pass an authorized badge in the badge reader next to the door, extract the safety key unlocked by the Personnel Safety System, wait for the final assent given by the control room operator who unlocks the door after recognizing the person through a camera, open the door, enter, close the door and deposit the key in the internal key panel.
As long as a safety key is present in the internal key panel or extracted from the external one and as long as a name results in the PLC presence list, the Personnel Safety System will prevent the control room operator from applying radiofrequency to the photo-injector RF cavity or to the accelerating sections.
A search procedure will guarantee that nobody remains inside the machine tunnel after the shutdown periods.

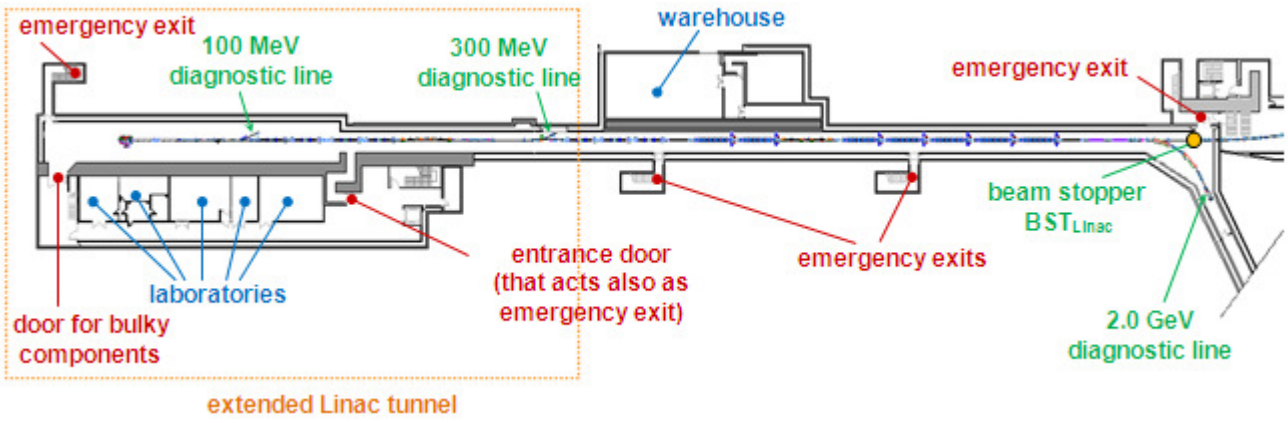

Fig.3 - The FERMI Linac project.

The part of the machine tunnel already constructed is shielded laterally by earth and on the roof with 2 m ordinary concrete ($\rho = 2.3 g/cm^3$) in the first part (where electron energy reaches 0 ÷ 600MeV) and with 0.65 m ordinary concrete plus 1.35 heavy concrete ($\rho = 3.6\ g/cm^3$) in the second part (where the beam can be accelerated up to 2.0 GeV). As far as shielding calculation is concerned, the parameters taken in consideration for the original linac design (1992) are listed in the following table.

maximum acceleration energy	2 GeV
maximum average current:	0.1 μA
acceleration efficiency along the sections	20%
beam loss scenario	continuous total beam loss at the end of the linac if the beam was not correctly bended along the linac-to-ring transfer-line
occupancy factor for the free areas outside the tunnel	1
dose limit for the free areas	0.1 mSv/year

Table 1 - FERMI parameters for shielding calculation.

On the right side of the linac extended tunnel, beyond the shielding wall, some laboratories (photo-injector laser beam, timing, vacuum, etc.) will be located, to be classified as free areas with full occupancy factor (see Fig.2). On the roof an extension of the already built klystron gallery will be constructed, to be classified as free area (exception done for the fenced areas next to the klystron modulators when switched on).

As a result, the extended tunnel shielding design provides for a 2 m ordinary concrete wall on the right side and 2 m ordinary concrete roof.

2.2. The Undulator Hall

As far as the Undulator Hall is concerned, the parameters taken in account for the shielding calculation are the same as for the Linac in terms of maximum energy and current. The laboratories to be constructed over the first part of the Undulator Hall roof (Laser laboratory and Service Area) will be free areas with full occupancy factor. The roof will be shielded with 2.55 m ordinary concrete, the tunnel will be laterally shielded by earth, and a wall of 3 m will separate the Undulator Hall from the Experimental Hall (see Fig.4).

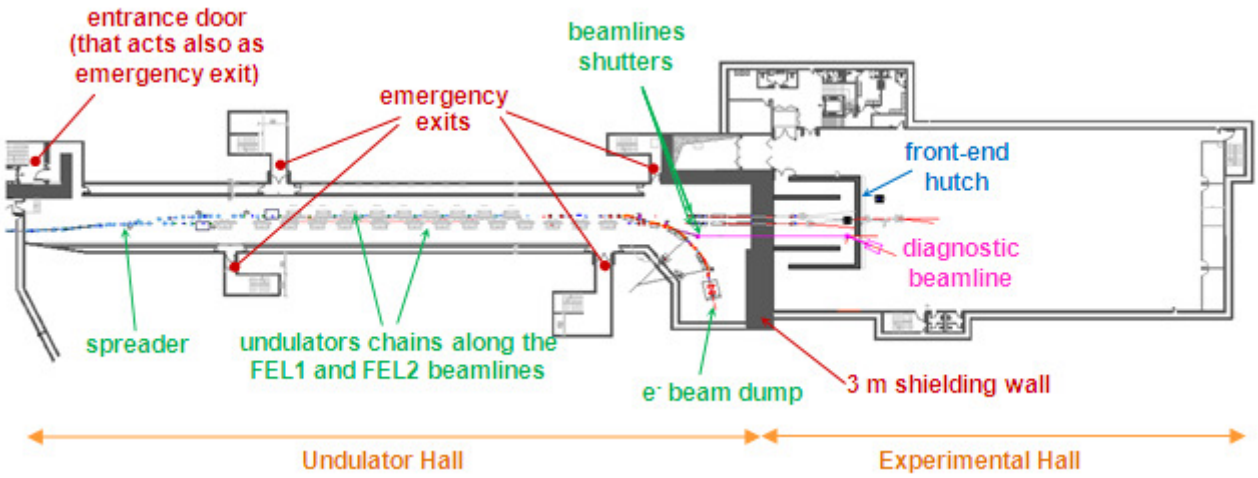

Fig.4 - The Undulator Hall and the Experimental Hall.

The electron beam, channelled alternatively along the FEL1 or FEL2 beamline through a set of bending and focusing magnets (*spreader*), will interact with the magnetic field of the undulator chains to produce the FEL radiation. At the exit of the undulators, the electrons will be transported towards the beam dump whereas the FEL beams will be extracted through the front-end wall.
The Personnel Safety System will check the correct bending of the electron beam towards the beam dump, by continuously monitoring the current of the bending magnets (to stop the beam in case of failure) and by continuously comparing the current measured by a toroid placed at the end of each undulator chain with the current detected by a toroid placed at the end of the final beam dump transfer-line. Two permanent magnets, positioned along the FEL1 and the FEL2 beamline, after the bending of the electron beam towards the beam dump, will prevent accidental electrons channeling into the beamlines.
Each beamline will have two tungsten shutters placed upstream the 3 m shielding wall.
A specific diagnostic beamline, named “High energy streak camera optical transport line” and indicated in pink in Fig.4, will utilize the visible radiation produced by the electrons bended towards the beam dump at the exit of the undulator chains, to monitor the longitudinal stability of the electron beam and, as a consequence, the FEL photon pulse stability.

The Undulator Hall tunnel will have one entrance door and five emergency exits. The enter the tunnel the same safety conditions provided for the Linac access will have to be fulfilled. A search procedure will guarantee that nobody remains inside the machine gallery after the shutdown periods.

2.3. The Experimental Hall

Besides the diagnostic beamline described before, the Experimental Hall will host 3 beamlines: DIPROI (DIffraction and PROjection Imaging), EIS (Elastic and Inelastic Scattering) and LDM (Low Density Matter).

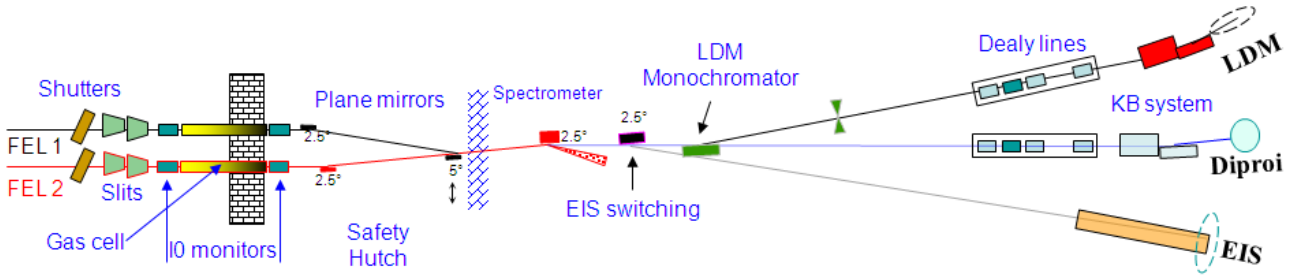

Fig.5 - FERMI beamlines.

The first part of the beamlines, including the first two optics components, will be enclosed inside a front-end hutch shielded laterally with 0.60 m ordinary concrete and in the forward direction with 0.80 m ordinary concrete.
Access inside the hutch will be inhibited by the Personnel Safety System if the linac beam stopper BST_{Linac} is open or if one of the the beamline radiation monitors, placed just outside the front-end hutch, will detect a level of radiation exceeding a fixed threshold. To enter the hutch, the operator will have to insert a safety key in a panel to unlock a second key to open the door. A search procedure is provided to be sure that nobody remains inside the hutch before starting operations with the beam.
The Personnel Safety System will permit to extract FEL radiation inside the front-end hutch only if a set of satety conditions will be fulfilled: the hutch must be searched, the beamline monitors must work correctly and detect no alarm radiation dose rate, the electron beam must be correctly bended towards the beam dump at the end of the Undulator Hall.

3. Radiation protection criteria and dose limits

The areas classification and the provided dose limits are listed in the following table.

Area classification	Areas description	Target limit	Dose limit provided by Italian law
Controlled areas	Machine tunnel with linac in stand-by (access controlled by safety system), delimited areas close to activated components and beam dumps, delimited zones around klystron modulators	5 mSv	20 mSv
Free (not classified)	Experimental hall - low permanence areas	0.5 mSv	1 mSv
Free (not classified)	Experimental hall - user stations Laser hall and Service area during normal operation	0.1 mSv	1 mSv

Table 2 - Areas classification and dose limits.

4. Radiation monitoring

Environmental radiation monitoring will be based on El.Se. S.r.l. gamma/neutron monitors (16 atm pressurized argon-nitrogen ionization chambers plus BF3 rem counters) and on passive thermoluminescence dosimeters (GR200A TLDs).
A gamma monitor will be placed outside the Experimental Hall front-end hutch along each beamline and will be connected to the Personnel Safety System. If a pre-fixed threshold limit dose will be exceeded, the Personnel Safety System will close the BST_{Linac}, the beamlines beamstoppers and will inhibit the photo-injector cavity radiofrequency.
The response of these ionization chambers to pulsed gamma radiation field has been tested inside the “old” Elettra linac tunnel before its shutting off [3].

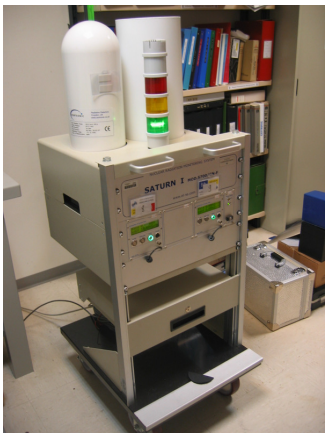

Characteristics of the gamma ionization chambers

- model: Centronic Mod. IG5
- response as a function of energy:
  80keV÷120keV: ±20%
  120keV÷2MeV: ±5%
- equivalent doserate range: 0.01μSv/h÷0.1Sv/h
- environmental conditions: 0÷50°C
- precision on environmental doserate measurements: ±5%
- automatic change of scale based on microprocessor

Characteristics of the neutron rem counters

- model: FAG Biorem

Fig.6 - The gamma/neutron monitors that will be utilized for FERMI environmental dosimetry.

5. First benchmark of Geant 4 simulation code

To face some of the future tasks (e.g. the calculation of the shielding around the first mirror in the Experimental Hall front-end hutch), a Monte Carlo code based on Geant 4 will be developped.
To calculate the shielding thickness needed for the FERMI accelerator, semi-empirical formulas were utilized [4-6], validated in the past by experimental measurements carried out inside the Elettra storage ring service area. The details of the experiments are described in reference [7].
The gamma radiation field produced by the 900 MeV electron beam impinging on a ring beamstopper was measured at different angles through a PTW Freiburg (model 32003 - volume 10000 cm^3) ionization chamber placed beyond the Service Area shielding wall (see Fig.7).

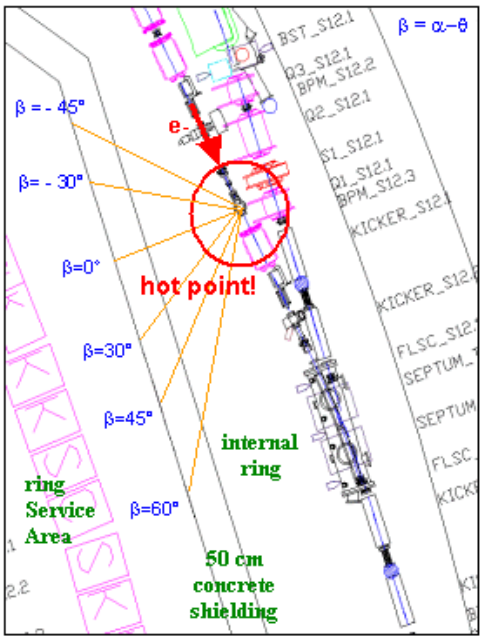

target material (beam stopper)	copper
target shape	cylinder
target radius r	4 cm
target thickness t	8 cm
target attenuation coefficient μ_1	0.271 cm^{-1}
radiation length in target X_0	1.45 cm
shielding material	ordinary concrete (ρ = 2.35 g/cm^3)
α	98°
distance target-shielding a at 90°	183.6 cm
shielding attenuation coefficient μ_2	0.053 cm^{-1}
shielding thickness d at 90°	50 cm

Fig.7 - Layout of the experimental measurements described in reference [7].

The same geometry was simulated with Geant 4 toolkit to construct a benchmark with semi-empirical formulas and experimental measurements.
An appropriate Geant 4 physics list including electromagnetic, low energy neutron and hadronic processes was selected. The detector was simulated as a water sphere of 30 cm diameter. The dose was calculated from the energy deposited by secondary charged particles produced by primary gammas and neutrons. Results at β=0° (Fig.7) are shown in the following figures.

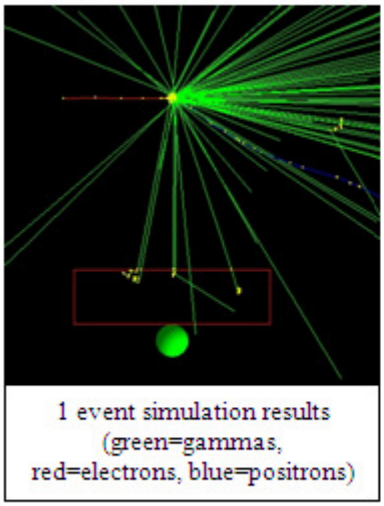

1 event simulation results
(green=gammas,
red=electrons, blue=positrons)

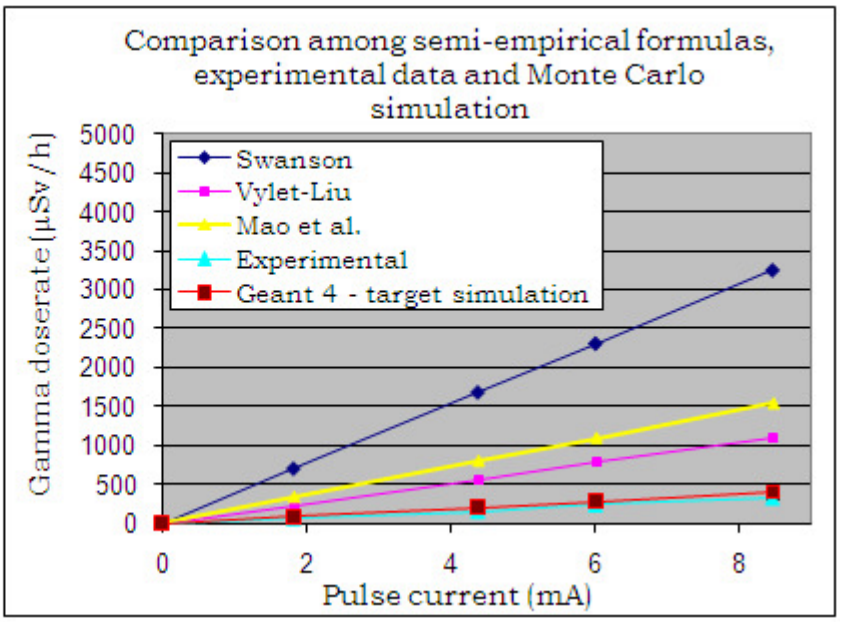

Fig.8 - Preliminary benchmark of semi-empirical formulas and experimental measurements with Geant 4 simulation.

6. Summary and perspectives

The FERMI@Elettra light source is now under construction at Elettra and will accelerate an electron beam up to 2.0 GeV at a maximum current of 0.1 µA to produce high brilliance FEL beams: main shielding design, Personnel Safety System interlocks and gamma radiation monitors for environmental radiation dosimetry have been described and discussed. To face the future tasks (e.g. the calculation of the shielding around the first mirror in the Experimental Hall front-end hutch) we have started to develop a Monte Carlo code able to simulate complex geometries. Preliminary results obtained with Geant 4 toolkit have been described and the study is now in progress.

References

[1] M. Svandrlik, "Overview of the status of the Elettra booster project", Proceedings of EPAC08, Genoa, Italy, 2201-2203.

[2] M.Trovò *et al.*, "Status of the FERMI@Elettra photoinjector", Proceedings of EPAC08, Genoa, Italy, 247-249.

[3] A. Vascotto *et al.*, "Development and Experimental Performance Evaluation of a Dose-Rate meter for Pulsed Beam", these proceedings

[4] W. P. Swanson, "Radiological safety aspects of the operation of electron linear accelerators", Technical Reports Series n.188, IAEA, 1979

[5] X. S. Mao *et al.*, "90 degrees Bremsstrahlung Source Term Produced in Thick Targets by 50 MeV to 10 GeV Electrons", SLAC-PUB-7722, 2000

[6] V. Vylet and J. C. Liu, "Radiation Protection at high energy electron accelerators", Rad. Prot. Dos., Vol.96, n.4, 2001

[7] K. Casarin *et al.*, "The new full-energy injector for the Elettra light source", 2nd RADSYNCH International Workshop, Grenoble, 2002.

Development and Experimental Performance Evaluation of a Dose-Rate meter for Pulsed Beam

A. Vascotto[1], M. Ballerini[2], G. Merlino[2], K. Casarin[1], S. Sbarra[1]

[1]*Sincrotrone Trieste S.C.p.A., Strada Statale S.S.14 km 163.5, 34012 Basovizza, Trieste, Italy*

[2]*El.Se. S.r.l., Via Pier della Francesca 26, 20090 Trezzano sul Naviglio, Milano, Italy*

Abstract

The detection of pulsed gamma radiation fields requires measurement devices characterized by high precision and fast response capabilities. El.Se. S.r.l., in collaboration with Sincrotrone Trieste, developed the front-end electronics for ionization chamber detector and the associated dose-rate digital meter.
The response of the new electrometer was tested inside the linac tunnel at different beam current intensities and repetition rates. The long-term stability was evaluated through environmental radiation measurements.
The design of the electronics, the performed measurements and the obtained results are presented and discussed here.

1. Introduction

During the construction of the new full energy booster injector at ELETTRA, preliminary studies have been performed to evaluate the response of the existing environmental Silena gamma radiation monitor, in the presence of short-time, high intensity pulsed radiation field.
Based on the experimental results obtained, a research project was defined with the aim of improving the performance of the front-end electronics and designing a new monitoring system able to satisfy the requirements of current legislation on radiation protection.
The first prototype of the new gamma radiation monitor was exposed to a high energy pulsed radiation fields by taking a PTW ionization chamber, connected to a Keithley electrometer, as a reference system.
The obtained results demonstrated that the new gamma monitor complies with the requirements for radiological surveillance monitoring system and is suitable for measurements of ambient dose equivalent and dose rates, taking into account the effects of the response functions of Centronic High-Pressure Ionization Chambers, especially those due to recombination and mixed field composition [1],[2],[3].

2. Electronics Design

The environmental Silena Gamma radiation monitor is composed by a Centronic Ion Chamber Detector mod. IGC5/A6.4 N9.6 and the associated modular electronics: high voltage power supply, 6 decades linear amplifier, auto-ranging & A/D converter, ratemeter and I/O relay board.
Basically the read-out electronic of the ionization chamber consists of a switched integrator connected to a programmable gain amplifier, an Analog to Digital converter (ADC) with a Sample & Hold input circuitry and a u-controller unit (see Fig.1).

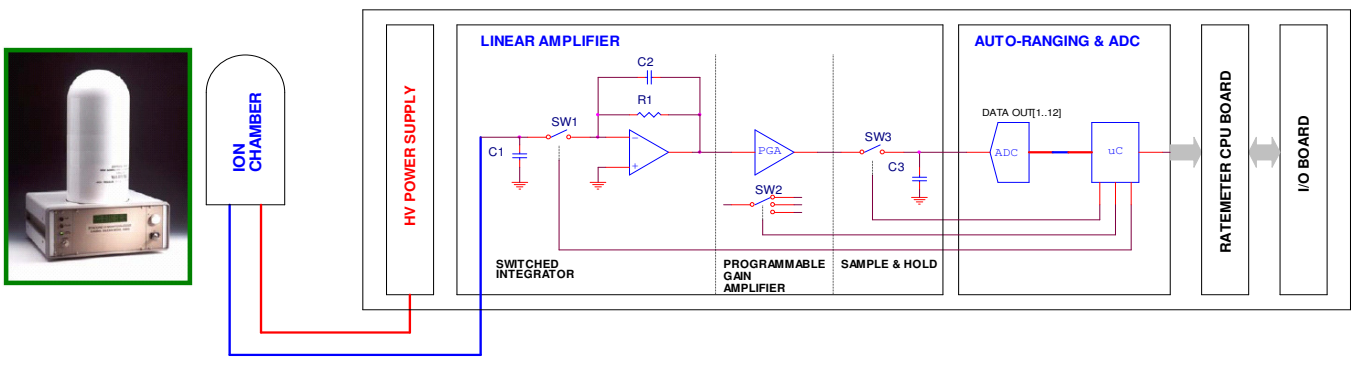

Fig.1 - Silena gamma radiation monitor (in the green box) and block diagram of its functioning.

Cyclically the u-controller unit acquires the data coming from the ADC and manages the different phases of measurement. Every second the charge stored in the input capacitor is transferred to the switched integrator while the gain of the programmable gain amplifier is properly selected, according to the previous processed data. The timing signals are also generated to convert the analog signal in numerical format.
This measurement technique assures high levels of linearity and accuracy, in the presence of stable radiation field, but could be inadequate for measuring the dose value of pulsed fields, because the long integration time required could result in saturation of the first stage and wrong selection of the amplifier programmable gain. Based upon these considerations an experimental acquisition system was designed, capable of overcoming the inadequacy (see Fig.2).

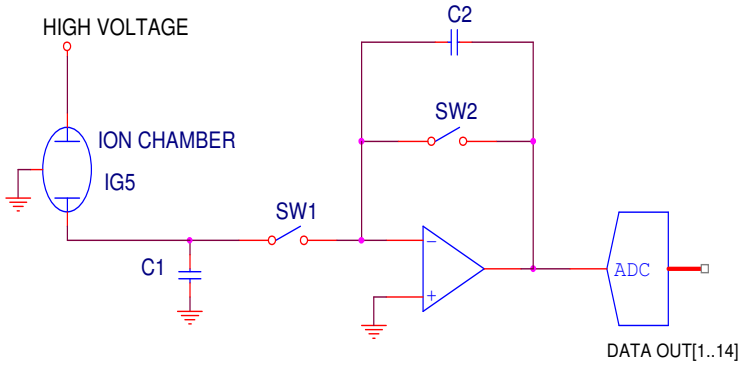

Fig.2 - Schematic of the experimental front-end electronics.

During the normal operation the capacitor C1 is charged by the ion chamber and the analog switches SW1 and SW2 are open. When the integration time is elapsed, the switch SW1 is closed and the charge is transferred to the capacitor C2. The switch SW1 is opened and the ADC starts the conversion. The output voltage signal of the operational amplifier is proportional to the charge accumulated during the integration time interval.

Assuming a constant input current (I_{INPUT}), during the integration time ($T_{INTEGRATION}$), the output voltage (V_{OPAMP_OUT}) of the ideal operation amplifier, when the switch SW1 is closed, is given by:

$$V_{OPAMP\_OUT} = -\frac{I_{INPUT} \cdot T_{INTEGRATION}}{C_2} \quad (1)$$

When the data acquisition is completed the switch SW2 is closed and the capacitor C2 is completely discharged. This operation mode allows no charge produced by the detector to be lost and the input signal to be continuously integrated.
The integration time is remotely selectable by software and different values are provided: 100 µsec, 1 ms, 10 ms, 100 ms and 1s.

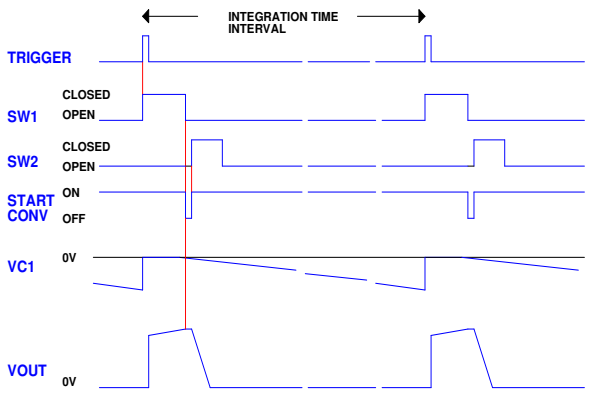

Fig.3 - Signals and timing of the experimental front-end electronics.

After the first tests inside the Elettra Linac tunnel, the experimental circuit was improved by adding two amplification stages and the fine gain in order to cover the desirable dynamic range (see Fig.4).

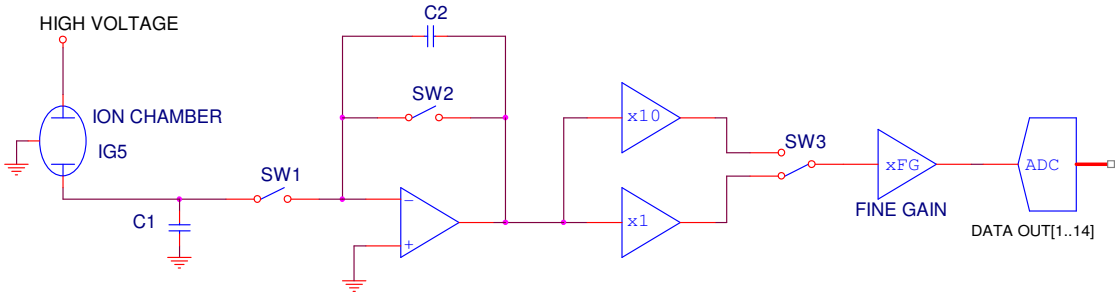

Fig.4 - Schematic of the new prototype front-end electronics.

To prevent saturation of the input stage, due to fast input pulses, the integration time is dynamically adjusted according to the previous acquired value. This method is applicable if the maximum expected input signal, corresponding to the maximum dose rate, within the selected integration period, generates an output signal lower than 50% of the total dynamic range. To satisfy this constraint the u-controller unit collects the data every 1 ms and the charge transferred to the capacitor C2 can be hold or reset, depending on the value acquired.
During the reset period, when the capacitor C2 is completed discharged, the output offset voltage is also measured and digitally subtracted to eliminate the offset errors.
Undesired charge injections are produced during SW1 and SW2 aperture and closure; a precise charge injection circuitry was implemented to compensate this effect, by adding equal and opposite charges.
The temperature compensation technique was also adopted to reduce the thermal drift effects and to guarantee an adequate performance when very low current are measured.
Every second all the acquired data are elaborated by the u-controller unit and the dose-rate value is periodically sent to the digital rate meter. A remote computer control of the Fine Gain stage allows a fine-tune of the calibration factor (A/(uSv/h)) during the calibration procedure.

4. Measurements and results

4.1. Linearity of the read-out electronics

The linearity of the read-out electronics was preliminary tested with an input current range between $3 \cdot 10^{-13}$A up to 10^{-7}A, using a current generator to simulate the equivalent dose rate values. At lower currents the linearity was not verified because the specifications of the current generator, used for these measurements, was not compliant with the required electronic noise level and impedance value.

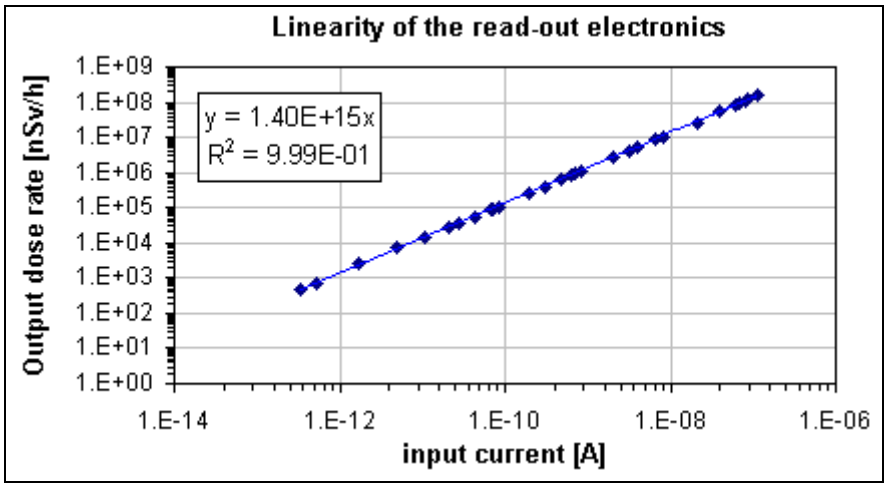

Fig 5 - Linearity of the read-out electronics.

4.2. Radiation measurements inside Elettra Linac tunnel

The upgraded El.Se. prototype, the old-type Silena gamma ionization chamber and a PTW ion chamber model 32003 connected with a Keithley electrometer model 6517 were exposed to gamma pulsed radiation fields inside Elettra Linac tunnel, using the experimental layout shown in Fig.6.
The pulsed radiation fields were produced by the electron beam accelerated up to 900 MeV, impinging on a cylindrical beam stopper with a diameter of 8 cm. The electron beam was operated at 10 Hz producing single and multi-bunch trains of electron pulses (1, 5 and 10 bunches) at different pulse amplitude (1, 2, 5, 10 and 15 mA). The difference in the expected gamma dose rate reaching the three instruments was calculated to be within 15%.

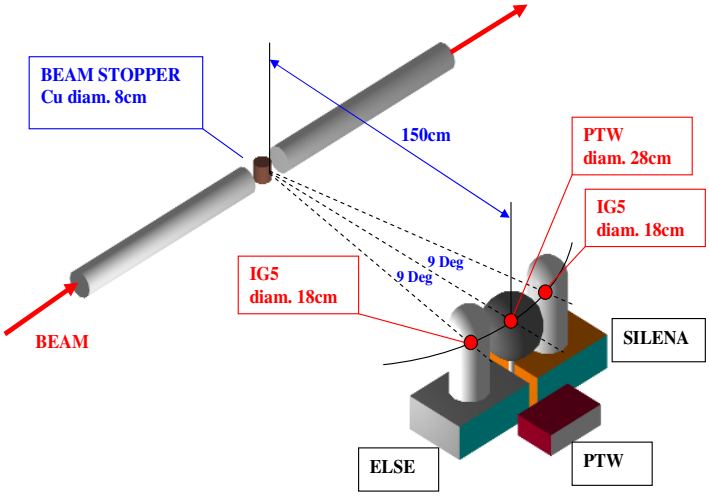

Fig.6 - Experimental layout with the position of the radiation monitors and the PTW ion chamber.

The only data valid for the old-type Silena gamma ionization chamber were the ones with train of single electron bunches of 1 mA amplitude. When the number of bunches or the pulse amplitude was increased, the detector showed overflow values due to the electronics input stage saturation.

The response of the El.Se. prototype to single and multi-bunch trains of electron pulses with 5 mA amplitude are shown in Fig.7. Measurements were taken second by second.
What is interesting to observe is that when a single bunch was extracted from the linac and impinged on the beam stopper, the charges produced inside the chamber were collected and the related signal was elaborated by the electronics within 1 second, producing single peaks with the same amplitude (about 1.2 nC, as shown in Fig.7a). When the number of bunches per train increased up to 5, in some cases the total charge produced inside the chamber was splitted in two ouput peaks (see Fig.7b): the total charge of the two peaks (indicated in red in Fig.7b) was comparable with the charge integrated in the same set of measurements producing single peak outputs, which means that no charge was lost. As the number of pulses or the pulse amplitude was increased up to 10 bunches/train, the probability of splitting the signal in two peaks grew (see Fig.7c), but the total charge/train remained the same (about 11.3 nC). The results obtained at 1, 2, 10 and 15 mA are similar.

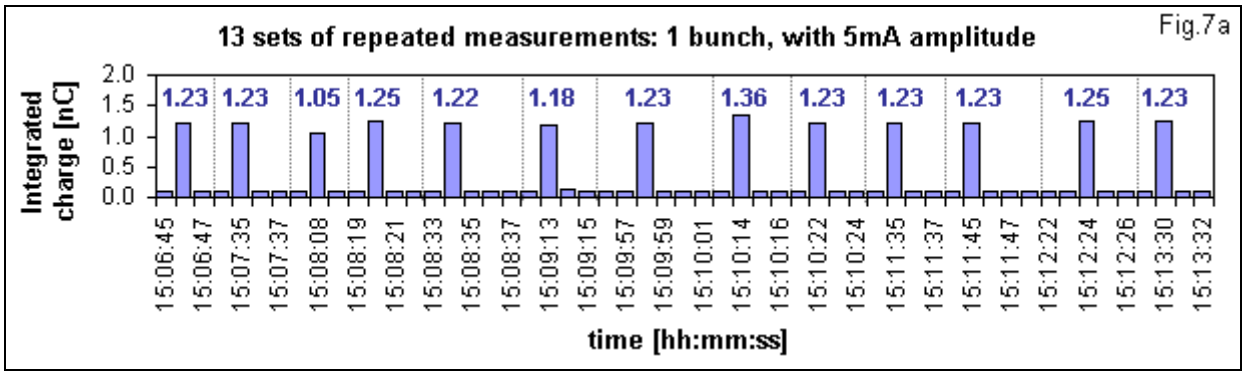

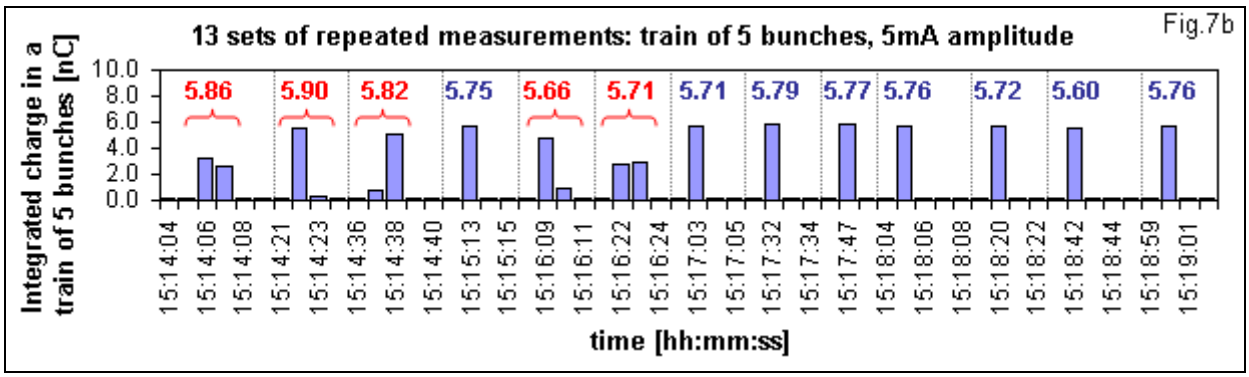

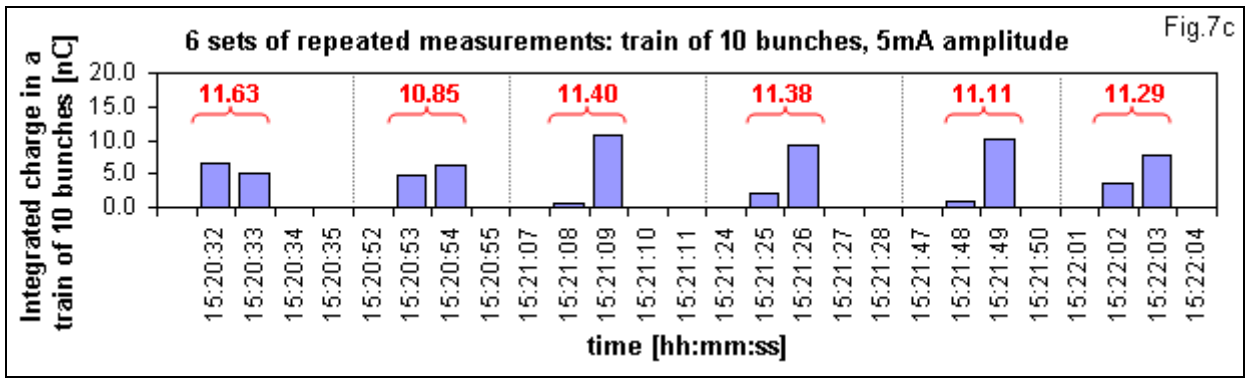

Fig.7 - Response of the EL.SE. prototype to single and multi-bunch trains of electron pulses with 5 mA amplitude.

The response of the El.Se. prototype gamma ionization chamber was also plotted versus the dose per train of pulses integrated by PTW ionization chamber, chosen as reference and already tested in a previous experiment [4].
The obtained trends are shown in Fig.8 and appear linear.

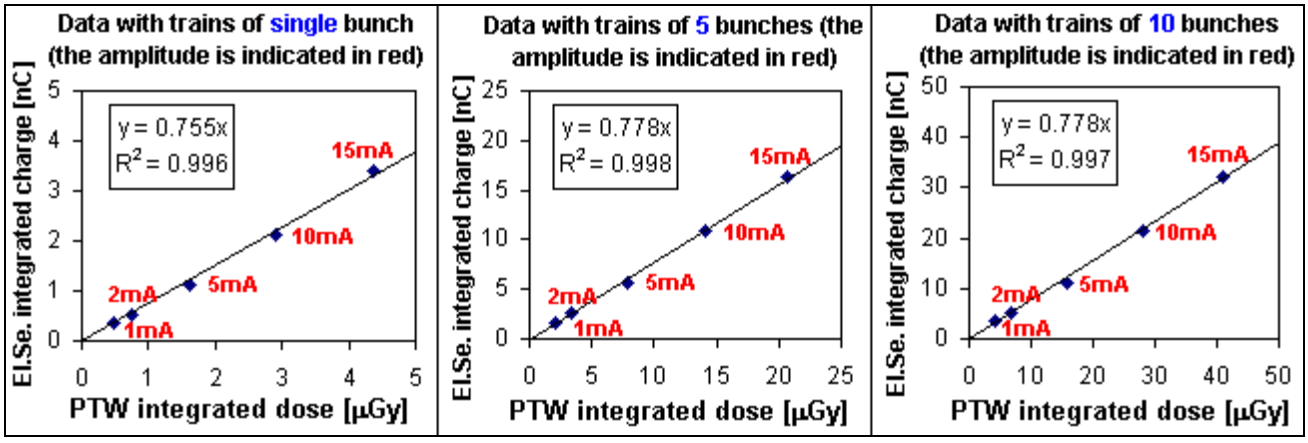

Fig.8 - Response of the EL.SE. prototype gamma ionization chamber plotted vs. the PTW integrated dose.

4.3. Environmental radiation background measurements

The long-term stability of the two El.Se prototypes were evaluated through environmental radiation measurements in comparison with an old-type Silena gamma ionization chamber.
Results are shown in Fig.9: all the detectors proved to be very stable (within 1.5% for all the monitors).
The difference in the mean values of the radiation background is due to the fact that the two El.Se. prototypes readings were plotted before final adjustment of the offset correction factor.

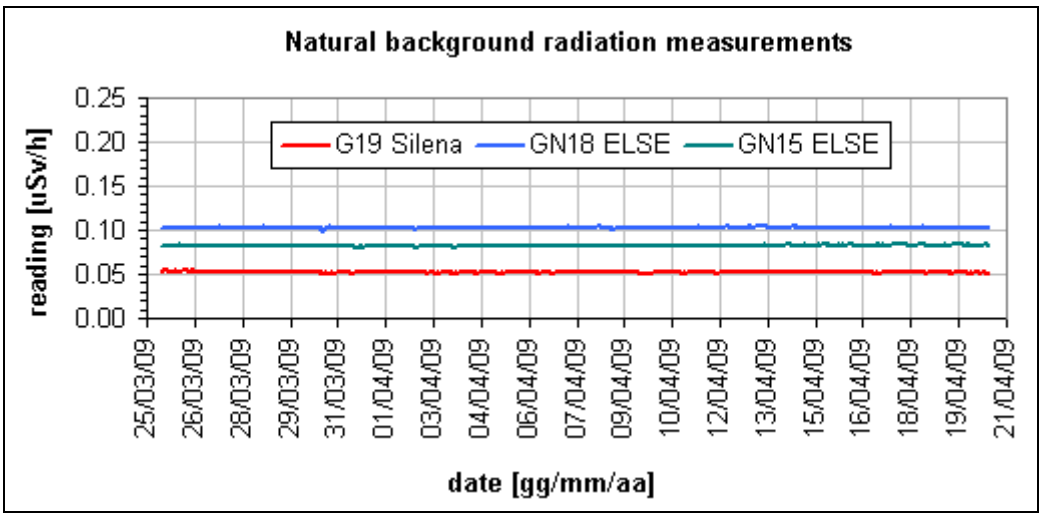

Fig.9 - Stability test of two El.Se. prototypes in comparison with an old-type Silena gamma ionization chamber.

5. Summary

The evaluation of the performances demonstrates that the new El.Se. gamma monitor meets all the expected requirements in terms of accuracy, linearity within 7 decades dynamic range (up to 10^{-7}A - high radiation dose rate), fast time response (<2ms) and long-term stability. The new monitor is able to process high number of charges within a very short time interval and a single shot radiation (e.g. storage ring beam dump). The response to single shot pulse was tested up to 3.5 nC/pulse (corresponding to ~ 4.3 uGy/pulse) and showed a linear trend.
At natural background radiation level, corresponding to a low input current (10^{-14}A), the new monitor proves to be very stable.
The system is completely remotely controlled and the calibration of the electrometer is performed by setting digital offset and gain parameters.

6. References

[1] D. Forkel-Wirth, S. Mayer, H.G. Menzel, A. Muller, T. Otto, M. Pangallo, D. Perrin, M. Rettig, S. Roesler, L. Scibile, H. Vincke, CERN, Geneva, Switzerland - C. Theis, TU Graz, Graz, Austria; M. Latu, Saphymo-Genitron-Novelec, Grenoble, France, "Performance requirements for monitoring pulsed, mixed radiation fields around high-energy accelerators", Proceedings of EPAC 2004, Lucerne, Switzerland.

[2] Christian Theis, Stefan Roesler and Helmut Vincke, "Comparison of the simulation and measurements of the response of Centronic high-pressure ionization chambers to the mixed radiation field of the CERF facility", CERN, Geneva, Switzerland - 06.05.2004 - Technical Note CERN-SC-2004-24-RP-TN.

[3] Christian Theis, Markus Rettig, Stefan Roesler and Helmut Vincke, "Simulation and experimental verification of the response functions of Centronic high-pressure ioniztion chambers", CERN, Geneva, Switzerland - 30.06.2004 - Technical Note CERN-SC-2004-23-RP-TN.

[4] K. Casarin, G. De Ninno, F. Iazzourene, E. Karantzoulis, G. Tromba, L. Tosi, A. Vascotto - Elettra, Trieste, Italy "Injection and FEL lasing with front end open at ELETTRA", Proceedings of the 2003 Particle Accelerator Conference, Portland, Oregon U.S.A., May 12-16, 2003.

Radiation Safety issues for the PF-AR in KEK

H. Nakamura, S. Ban, K. Iijima ,Y. Namito and K. Takahashi

High Energy Accelerator Research Organization(KEK), 1-1 Oho, Tsukuba-shi, Ibaraki-ken, 305-0801, Japan

Abstract

The ambient dose rates in the experimental halls of the Photon Factory Advanced Ring (PF-AR) are measured with the area monitors. The dose rates are usually background level. However, when the beam lifetime decreased suddenly, the dose rates increase. This phenomenon is considered bremsstrahlung due to dust trapping near the duct. We measured the dose rate during the phenomenon and made radiation protection.

1. Introduction

1.1. Present status of the electron accelerators in KEK

There are three electron rings, a positron ring and an electron-positron linac in High Energy Accelerator Research Organization (KEK). Figure 1 shows the location of these accelerators. Two of the electron rings are the Photon Factory (PF) and the Photon Factory advanced ring (PF-AR) used for synchrotron radiation experiments. One of the electron rings (HER) and the positron ring (LER) are used for electron-positron collision experiments (KEKB). The electron-positron linac injects four different beams into the four rings.
The recent improvement in KEK is a simultaneous Top-UP injection for the 3 rings (HER, LER, PF). The simultaneous injection has started since 24th April 2009. The linac provides simultaneously 8 GeV electrons to HER, 3.5 GeV positrons LER, and 2.5 GeV electrons to PF by using the pulse to pulse switching injection system [1]. Figure 2 shows the 3 rings keep the constant current except during PF-AR injection.

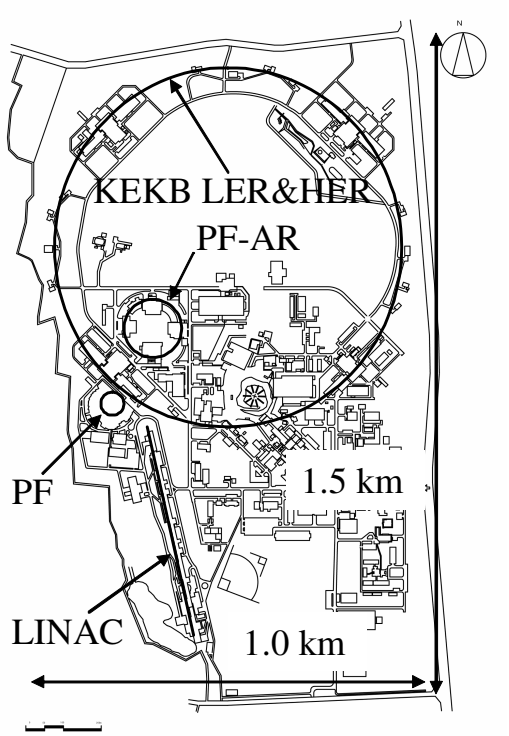

Fig.1 - Plan of electron accelerators in KEK. LINAC locates southwest part in KEK. PF ring locates west of LINAC end. PF-AR ring locates north of LINAC. KEKB 2 rings locate north part of KEK.

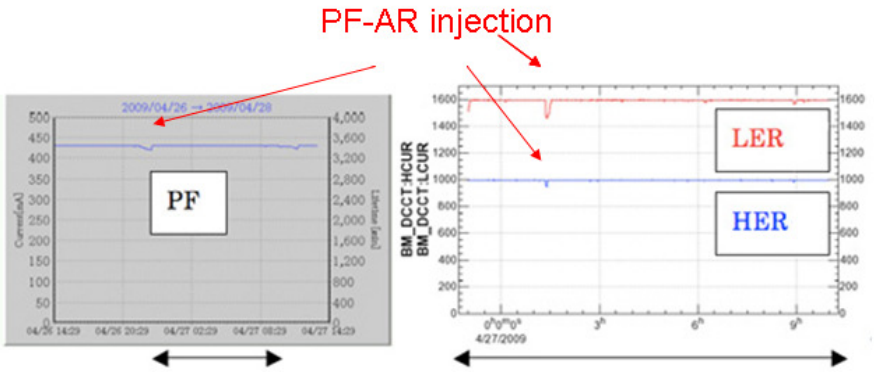

Fig.2 - PF, LER and HER keep each constant current except during PF-AR injection.

1.2. Outline of the PF-AR

The PF-AR is a 6.5 GeV synchrotron radiation source, which operated with single bunch for pulsed hard X-rays. The ring is injected at 3.0 GeV, after that the beam is accelerated to 6.5 GeV and stored initially at 60 mA. The ring has 8 beam lines and 6 insertion devices. Table 1 shows main parameters of the PF-AR[2].

Beam energy	6.5 GeV
Circumference	377 m
Injection energy	3.0 GeV
Typical num. of bunches	1
Initial stored current	60 mA
Beam lifetime (at init.cur.)	20 hours
Num. of insertion devices	6

Table 1 - Main parameters of the PF-AR.

2. Management of radiation safety in the PF-AR

The experimental halls of the PF-AR are radiation controlled areas. The ambient dose rate in the halls should be controlled less than 20 μSv/h. The dose rate is measured by the area monitors named ORG monitors. Figure 3 shows the appearance of an ORG monitor. The monitor consists of a 10-liter ionization chamber for gamma detection and a 1-inch BF3 proportional counter for neutron detection. The monitors give an alarm when the dose rate is over 20 μSv/h. Figure 4 shows the locations of the monitors in the experimental halls of the PF-AR.
The users of the PF-AR should be the radiation workers of KEK. The limit of annual personal effective dose is 20 mSv for the male radiation workers and 6 mSv for the female radiation workers. Target of the personal effective dose is less than 7 mSv for the male workers and less than 2 mSv for the female workers. In Fact, most of the workers are not exposed significantly.

Fig.3 - An ORG monitor consists of a 10-liter ionization chamber for gamma detection and a 1-inch BF3 proportional counter for neutron detection.

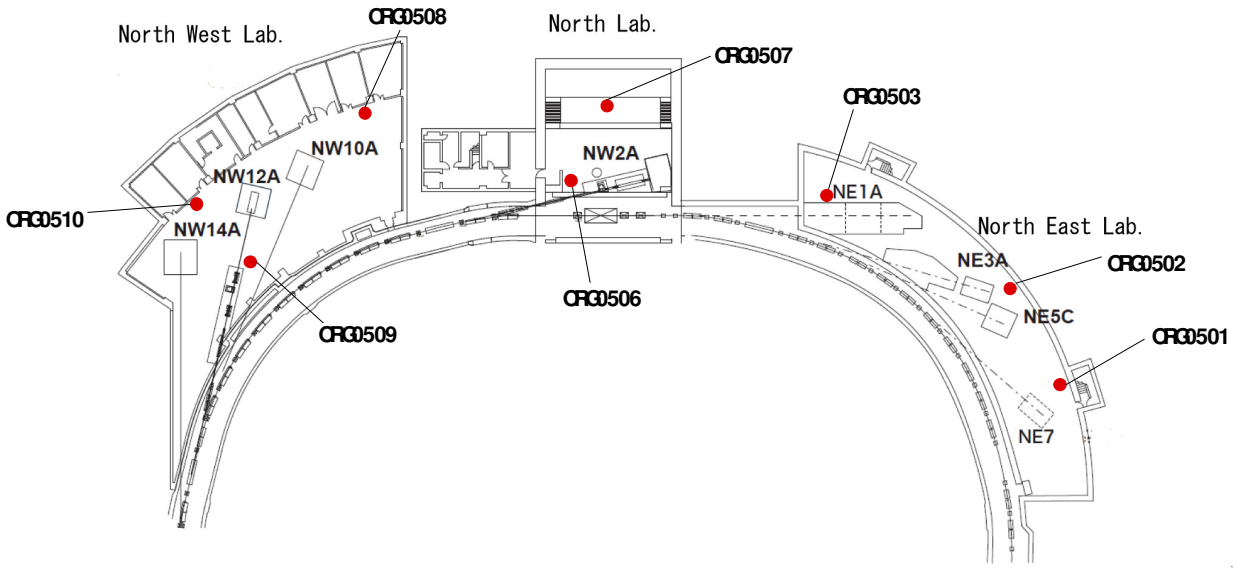

Fig.4 - The locations of the ORG monitors in the experimental halls of the PF-AR.

3. Measurements and studies

Usual ambient dose rate in the experimental halls is background level. However, the dose rate increases when the beam lifetime of the PF-AR decreases suddenly. Figure 5 shows a typical example of the incident occurred at the NW12 beam line in the North West experimental hall. When the beam lifetime decreased from 500 minutes to 100 minutes, the gamma dose rate at ORG0509 monitor increased from 0.1 μSv/h to 1.6 μSv/h and the neutron dose rate increased from 0 μSv/h to 0.2 μSv/h. At that time, ORG0509 monitor was located at the wall of the experimental hall, therefore, there was little information about the dose rate around the beam line.

When another similar incident happened, we measured the dose rate around the NW12 with survey meters. Figure 6 shows the dose rate around the NW12. The maximum dose rate at the surface of the NW12 hutch was 230 μSv/h.

The measurements showed the following conditions for the incident. Changing narrowly the gap of NW14 insertion device which located upper stream of NW12 often triggered the incident. The vacuum level was worse. The beam lifetime decreased. The dose rate around the NW12 increased, however not increased around other beam lines. The dose rate returned to background level when the main beam shutter (MBS) in the beam line was closed.
Since the beam orbit of the ring was newly arranged for installing new beam line NW14, it was suspected for the cause of the incidents. The operation with the old beam orbit was tested. However it did not change the situation.
Measurement of residual radiation from the beam duct of the ring showed the duct near the steering magnet of NW12 was activated. This phenomenon is considered bremsstrahlung due to dust trapping near the duct[3].
Checking the log of the monitors showed similar incidents were occurred before.

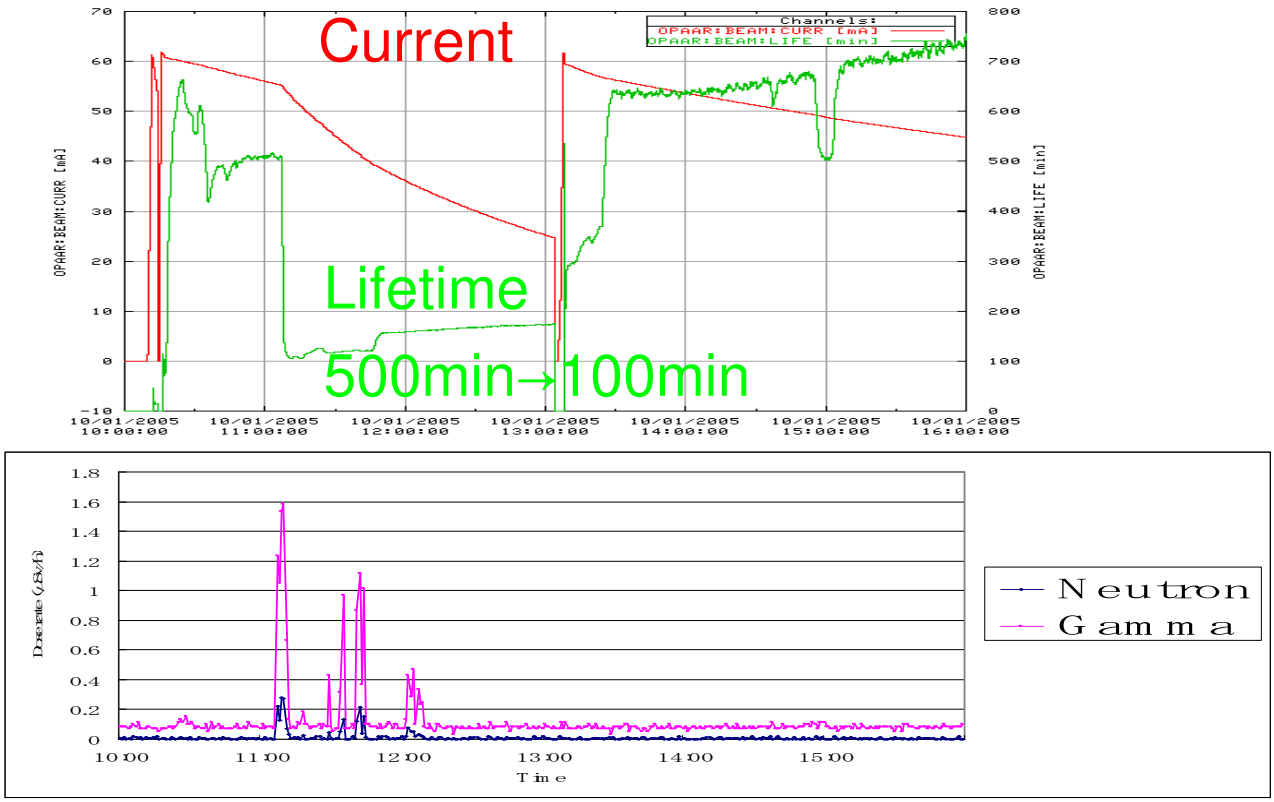

Fig.5 - An example of the sudden beam lifetime decreasing and increase of the dose rate at the ORG0509 monitor in the experimental hall.

4. Measures for safety

The followings were first things what we did for the safety in the experimental hall. We set up the area where people were not allowed to enter because of high dose rate. We changed temporarily the alarm level of the ORG monitors in the experimental halls from 20 µSv/h to 1 µSv/h for detecting the incidents occurred far from the monitors.
Next, lead blocks were installed in the optic hutch of the NW12.
An ionization chamber for interlock was installed out of the optic hutch. It closes the MBS when the dose rate exceeds 5µSv/h and continues for 3 minutes.
Finally, ORG0509 monitor was moved to near the optic hutch of the NW12 for detecting radiation effectively.

5. Results

Nobody in the PF-AR was exposed to significant radiation. The frequency of the incident around NW12 decreased. Other beam line (ex. NE3) also had the incident, but not so often. One of sources of the dust is

considered distributed ion pump (DIP)[4].The frequency of the incident has decreased since DIP-OFF operation started.

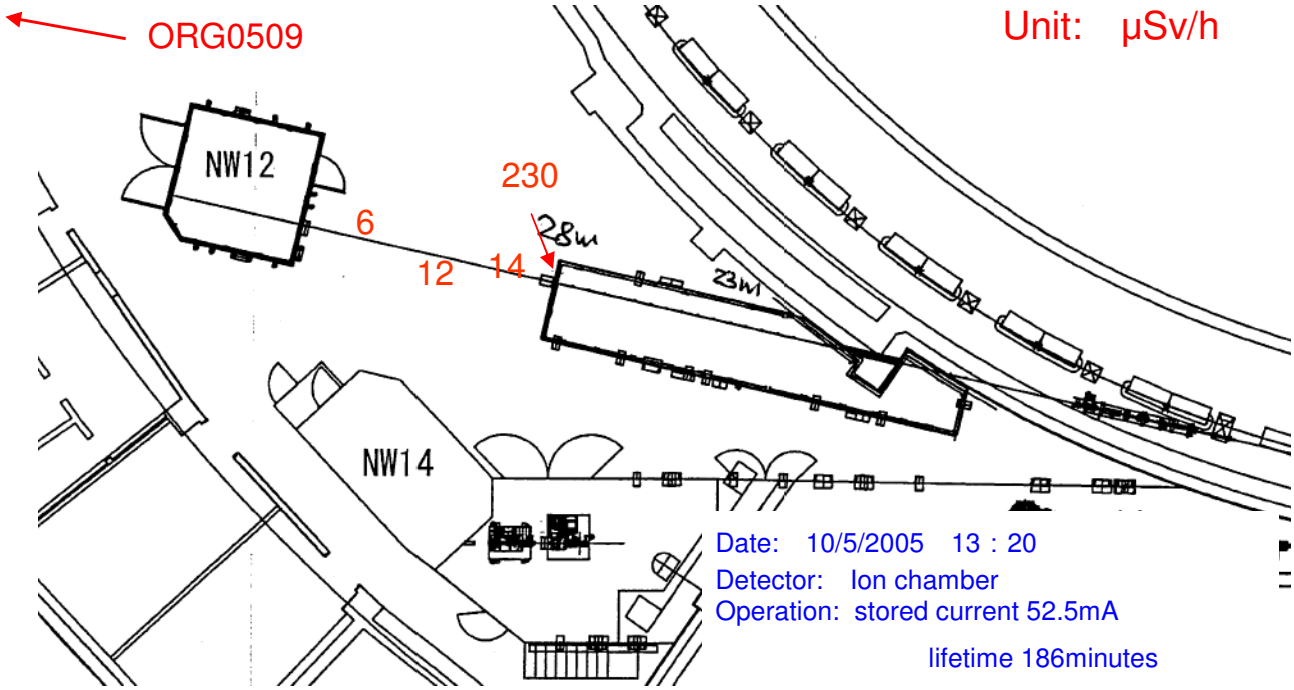

Fig.6 - The dose rate around the beam line NW12 during the beam lifetime decreasing.

References

[1] N. Iida, et al., "Pulse-to-Pulse Switching Injection to Three Rings of Different Energies from a Single Electron LINAC at KEK", PAC09, Vancouver, Canada, May 2009, WE6PFP110.

[2] Y. Kobayashi, et al, "Present Status of PF-Ring and PF-AR in KEK", EPAC08,Genova, Italy, June 2008, 2064-2066(2008)

[3] H. Saeki, T. Momose, H. Ishimaru, "Observations of dust trapping phenomena in the TRISTAN accumulation ring and a study of dust removal in beam chamber", Rev. Sci. Instrum., 62, 874-885 (1991).

[4] Y. Tanimoto, et al., "Improvement of beam lifetime and vacuum system of the PF-AR", Vacuum (2009), doi:10.1016/j.vacuum.2009.06.044

Activation Analysis of Soil, Air and Water near the NSLS-II Accelerator Enclosures

P. K. Job and W.R. Casey

National Synchrotron Light Source-II Project
Brookhaven National Laboratory, Upton NY 11973, USA

Abstract

The radiation environment in the accelerator enclosures is sufficiently high energy to permit the activation of air inside the accelerator enclosures, soil surrounding the concrete shielding of the enclosures and the coolawent water used for cooling various components of the accelerator system like magnets etc. Bremsstrahlung is generated inside the accelerator enclosures by the radiative interaction of the electron beam with the accelerator components. This bremsstrahlung further interacts with the surrounding air, soil and cooling water to produce radioactive isotopes by the emission of neutrons. These interactions could be direct photo-spallation reactions as in the case of air and water activation or could be secondary interactions of high energy neutrons produced by the photoneutron production. The high energy neutrons produced by the photonuclear interactions will penetrate the concrete shield and produce radioisotopes in the surrounding soil by (n,n), (n,2n) etc. interactions. It should be noted that the past experience at the NSLS and other light sources has demonstrated that the potential for air, water or soil irradiation is quite limited and does not warrant significant radiological considerations.

1. Radioactivation due to Beam Losses at NSLS-II

The activation analysis for the NSLS-II accelerator enclosures has been carried out at four distinct locations where the probability for beam loss is a maximum. These are at the linac momentum slit, at the booster injection septum, at the booster extraction septum and at the storage ring injection region. In each case most conservative point beamloss assumptions are employed. In the linac enclosure, a 50% loss of the accelerated beam at 200 MeV is assumed at the momentum slit. The assumed pulse rate is 10 pulses of 15 nC a minute. At the booster injection septum also a 50% loss of the beam at 200 MeV is assumed. The assumed pulse rate is 5 pulses of 15 nC a minute. At the booster extraction septum a 20% beam loss at 3 GeV is assumed at the rate of 5 pulses of 15 nC a minute. The assumed beam dissipation at the storage ring injection region is 18 nC a minute, with 2 hour beam life time, taking into account for the injection losses at the septum. A continuous operation of 5000 hours at the top-off mode is assumed for the facility.

These estimates of beam losses are conservatively derived and will provide an over-estimate of the actual losses that will take place during normal operation. There will be beam stops in the booster and linac enclosures that will also receive beam during commissioning and tuning periods. Losses at these beam stops have not been included in this analysis, since they will be locally shielded with photon (lead) and neutron (polyethylene) shields.

2. Soil Activation

The potential for soil activation is limited at the electron accelerators, since the main radiation component, bremsstrahlung, is in the forward direction [1] of the electron beam and gets absorbed by the machine components like magnets, absorbers etc. The soil berm is generally at very large angles (almost at right angles) to the forward direction of the electron beam. However there exists a potential for the high energy neutron component to penetrate through the transverse concrete shield and produce radioisotopes in the soil [2]. Some of these isotopes can be leached from the soil by rain water and migrate to the ground water systems. It is important to assess this risk for NSLS-II and determine the potential consequences to the environment.

2.1. Methodology to Estimate Soil Activation

The mechanism of formation of radionuclides in the soil is due to the interaction of high energy neutrons with the elements in the soil. In the present analysis only the high energy neutron component needs to be

considered, because only these neutrons have the penetrating power to escape the concrete shielding. As required by the BNL subject area Accelerator Safety, analysis has been done to estimate the rate of formation of two radioactive isotopes ^{3}H and ^{22}Na in the soil during the routine operation of NSLS-II. Table 1 gives the summary parameters used for this analysis. The cross section values are obtained from the literature [3,4] and the soil composition for the Long Island soil has been provided by the BNL Environmental and Waste Management Services Division [5]. The soil density at the Long Island is taken as 1.6 gm/cm^3.

Parent Nucleus	Weight (%) In soil	^{3}H Production Threshold (MeV)	^{3}H Production Cross section (mb)	^{22}NaProduction Threshold (MeV)	^{22}NaProduction Cross section (mb)
^{16}O	51.3	15.0	3.07		
^{23}Na	0.0196	20.0	6.81	15.0	36.6
^{24}Mg	0.21	25.0	6.48	25.0	28.2
^{27}Al	1.65	25.0	8.23	50.0	14.5
^{28}Si	45.1	50.0	3.54	50.0	14.5
^{39}K	0.063	50.0	3.56		
^{40}Ca	0.058	50.0	3.0		
^{55}Mn	0.012	50.0	2.0		
^{56}Fe	1.44	50.0	1.65		

Table 1 - Soil Composition and Cross Sections used for Activation Analysis Cross Sections for High Energy (>50 MeV) Neutrons.

From Table 1 the following average parameters can be derived.

Weighted average cross section for ^{3}H production	3.35 mbarns
Weighted average cross section for ^{22}Na production	14.56 mbarns
Weighted average of soil atomic mass number	22.17
Atomic Number density of soil	4.35 x 10^{22} atoms/cm^3
Number density of ^{3}H producers (100%)	4.35x 10^{22} atoms/cm^3
Number density of ^{22}Na producers (47%)	2.04 x 10^{22} atoms/cm^3

When the electron beam interacts with the storage ring components or beam stops an electromagnetic shower will be generated within the material due to successive bremsstrahlung and pair production interactions. The ultimate product of these interactions is a large number of low energy gammas, electrons, positrons and a few neutrons. Almost 80% of the neutrons emitted are with a median energy of 2.1 MeV and are effectively attenuated by the concrete shielding. However, the high energy component of the neutrons can penetrate the concrete shielding and cause interactions in the surrounding soil.
The high energy neutron (HEN) component in the transverse direction of the beam loss location on a thick target is provided by Fasso [6] et al. as:

$$1.3 \times 10^{-3} \text{ HEN/ GeV/ electron/ steradian}$$

The neutron flux at the external surface of the concrete shield wall of thickness 'r' cm at a distance of 'R' cm from the source in the transverse direction, without assuming any self shielding for the neutrons in the target can be estimated as:

$$\Phi(0) = \frac{1.3\times10^{-3}}{R^2} N_e \times E \times e^{-r/\lambda} \text{ neutrons/cm}^2\text{.s} \quad (1)$$

where N_e = Number of electrons interacting with the target material / sec
E = Energy of the electron in GeV
R = Distance of the flux point from the source in cm
r = Thickness of the concrete shield in g/cm^2
λ = Attenuation length of HEN in concrete in g/cm^2 (115 g/cm^2)

Table 2 summarizes the electron energy dissipation at various locations under consideration and the resulting neutron fluxes, Φ(0), on the exterior surface of the concrete shield . The concrete shield thickness and the distances to the activation locations from the loss points are taken from the 80% architectural design drawings of the NSLS-II.

As high energy neutrons traverse through the soil a large fraction of neutrons are removed from the soil by the elastic and non-radiative capture reactions. These neutrons do not take part in the activation reactions. The neutron removal cross section for the soil is given in the literature [7] as 0.016 cm^{-1} for the soil density of 1.6 gm/cm^3. The high energy neutron flux in the soil as a function of soil thickness (x) can be written as:

$$\Phi(x) = \Phi(0)\, e^{-\Sigma x} \tag{2}$$

Where Σ is the neutron removal cross section of the soil and Φ(0) and Φ(x) are neutron flux values at a soil thickness of 0 and x cm correspondingly. The neutron flux declines in an exponential manner with the mean path (1/Σ) of neutrons in the soil. In approximately 4.8 mean free paths (300 cm) 99% of the neutrons will be removed from the soil by the removal reactions. The average flux of neutrons for activation reactions in the soil can be written as:

$$\Phi_{av} = \frac{\int \Phi(x)dx}{\int dx} = \frac{\int \Phi(0)e^{-\Sigma x}dx}{\int dx} \tag{3}$$

Where Φ(0) is the flux at the external surface of the concrete shield and the integration is carried out for 300 cm of the soil thickness. Integrating equation (3) for 300 cm of soil and substituting for Σ of the soil, it can be shown that:

$$\Phi_{av}\,(\text{soil}) = 0.2066\, \Phi(0)$$

Beam Loss Locations	Number of electrons lost /sec	Distance of dose point R (cm)	Concrete thickness r (cm)	Neutron Flux Φ(0) ($n/cm^2.s$)	Average Neutron Flux Φ_{av} ($n/cm^2.s$)
Linac momentum slit Floor	7.8×10^9	170	50	2.53×10^1	5.23
Linac momentum slit Lateral wall	7.8×10^9	150	50	3.25×10^1	6.72
Booster injection septum Floor	3.9×10^9	170	50	1.26×10^1	2.61
Booster injection septum Lateral wall	3.9×10^9	150	50	1.63×10^1	3.36
Booster extraction septum Floor	1.56×10^9	170	50	7.59×10^1	1.57×10^1
Booster extraction septum Lateral wall	1.56×10^9	150	50	9.75×10^1	2.01×10^1
Storage Ring Floor	1.87×10^9	188	68	5.14×10^1	1.06×10^1

Table 2 - High Energy Neutron Flux at the Exterior of the Concrete Shield and Average Flux in the Soil.

$$\text{Rate of radioactive atom production in soil} = \Phi_{av}\, N\, \sigma \tag{4}$$

where Φ_{av} = Average high energy neutron flux in the soil ($n/cm^2.s$)
N = Number density of element in the soil producing the radioactive isotope
σ = Neutron cross section of the element for activation (cm^2)

The number of atoms of the radionuclide of interest (n) per unit volume is governed by the following differential equation during the period of irradiation:

$$\frac{dn}{dt} = -\lambda_R n + \Phi_{av} N \sigma$$

The equation has the following solution applying the boundary condition when n = 0, t=0:

$$n(t) = \frac{\Phi_{av} N \sigma}{\lambda_R} (1 - e^{-\lambda_R t}) \quad (5)$$

where λ_R = Decay constant of the radioactive isotope
t = Irradiation time (for NSLS-II operations, a conservative annual irradiation time of 5000 hours is considered).

Thus the specific activity (Bq/cm^3) induced in the soil as a function of time by this nuclide of interest:

$$A(t) = \Phi_{av} N \sigma (1 - e^{-\lambda_R t}) \quad Bq/cm^3 \quad (6)$$

The activity of the radioactive nuclide of interest in the soil is calculated using equation (6) and available cross sections from Table 1.

2.2. Results of Soil Activation Calculations for NSLS-II

Table 3 gives the activity in the soil at various beam loss locations created due to ^{3}H and ^{22}Na by 5000 hours of NSLS II operation.
Using the methodology established in the Accelerator Safety Subject Area, the leachable concentration created in the soil has also been given. Leachability of 100% and 7.5% are assumed for ^{3}H and ^{22}Na correspondingly. A water concentration factor of 1.1 is taken due to the annual rain fall of 55 cm at Long Island, according to reference [8]. It can be mentioned that the soil underneath the concrete floor is not exposed to rain fall and the potential leachability of radioactive isotopes from the soil to the water table at these locations will be minimal.

Beam loss Location	Average HEN Flux in soil Φ_{av} (n/cm^2.s)	^{3}H Soil Activity (Ci/cm^3)	^{3}H Leachable to water (pCi/liter)	^{22}Na Soil Activity (Ci/cm^3)	^{22}Na Leachable to water (pCi/liter)
Linac momentum slit Floor	5.23	0.31×10^{-15}	0.34	0.30×10^{-14}	0.25
Linac momentum slit Lateral wall	6.72	0.40×10^{-15}	0.44	0.38×10^{-14}	0.31
Booster injection septum Floor	2.61	0.62×10^{-15}	0.68	0.56×10^{-14}	0.46
Booster injection septum Lateral wall	3.36	0.80×10^{-15}	0.88	0.77×10^{-14}	0.64
Booster extraction septum Floor	15.7	1.87×10^{-15}	2.06	1.81×10^{-14}	1.49
Booster extraction septum Lateral wall	20.1	2.40×10^{-15}	2.64	2.32×10^{-14}	1.91
Storage ring Floor	10.6	1.27×10^{-15}	1.39	1.23×10^{-14}	1.01

Table 3 - Activity in the soil at various beam loss locations created by ^{3}H and ^{22}Na.

As specified in the Accelerator Safety Subject Areas; we assumed 100% leachability for tritium and 7.5% leachability for sodium. A soil water concentration factor of 1.1 is also provided in the Subject Area. These calculated values are well within the BNL Action Levels of 1000 pCi/l and 20 pCi/l for ^{3}H and ^{22}Na. Therefore no additional engineered safeguards are required.

3. Activation of air in the Accelerator Enclosures

Routine accelerator operations at NSLS-II would generate small amounts of air activation at high beam loss locations due to photoneutron reactions of bremsstrahlung in air. The isotopes produced due to air activation are ^{13}N (half life =10 min), ^{11}C (half life = 20 min) and ^{15}O (half life = 2.1 min). These would be produced

within the accelerator enclosure and attain saturation activity within hours of accelerator operation, but would decay quickly because of the short half lives and remain primarily within the confines of the enclosure. The air activation analysis for the NSLS-II has been carried out at four distinct locations of the accelerator enclosures, as given in section 2, where the probability for beam loss is a maximum. These rates of assumed point beam loss, are also given in section 2.

3.1. Methodology of Air Activation Calculations

The mechanism for formation of radionuclides in the air is the photoneutron interaction of bremsstrahlung with air nuclei. The threshold for (g,n) reactions in air is 10.55 MeV for ^{13}N and 15.67 MeV for ^{15}O. In addition ^{11}C is formed of photospallation of both nitrogen and oxygen. Using the neutron yield expression from reference [9] and taking the effective Z for air as 7.26, the neutron yield in air is given by the expression:

$$Y = 1.21 \times 10^8 Z^{0.66} \text{ neutrons/Joule} = 4.5 \times 10^8 \text{ n/J} \quad (7)$$

Implicit in the release of neutrons, is the formation of an unstable nucleus in air, which may be radioactive. Equation (7) gives only the Giant Resonance Neutron (GRN) yield. The yield of High Energy Neutrons (HEN) increases the total neutron yield by about 6%. But since most of the GRN neutrons are well below the threshold energies mentioned above, using the yield of GRN neutrons alone will give a conservative estimate of the radionuclide formation.

The change in number (n) of radioactive atoms in air per unit time if no ventilation flow is present is:

$$\frac{dn}{dt} = YFW\,(1- e^{-x/\lambda}) - \lambda_R n \quad (8)$$

where W = Beam energy dissipated at the location (watts)
x = Effective air path of bremsstrahlung in the accelerator enclosures (4 meters)
λ = Effective bremsstrahlung attenuation length in air [6] (385 meters)
λ_R = Decay constant of the radioactive nuclide (s^{-1})
F = Fraction of beam energy that converts into bremsstrahlung and escapes into air.

In the case of beam loss at the linac momentum slit and septa, a conservative radiation yield of 50% is assumed (F=0.5) [2]. Attenuation due to the local shielding that will be provided around the high loss points is not taken into account in these calculations. In reality a fraction of this bremsstrahlung will get absorbed in the accelerator components without ever traversing through air.

Solving equation (8) for initial conditions n=0 for t=0

$$n = \frac{WFY}{\lambda_R}\,(1 - e^{-x/\lambda})\,(1- e^{-\lambda_R t})$$

The activity due to these radionuclides is equal to $\lambda_R n$

$$A = WFY\,(1 - e^{-x/\lambda})\,(1- e^{-\lambda_R t}) \quad Beq$$

Since the radionuclides formed have short half lives (< 20 min), saturation is achieved quickly during operation and the activation at saturation becomes:

$$A = WFY\,(1 - e^{-x/\lambda}) \quad Beq \quad (9)$$

Of the total saturation activity, 88% is from ^{13}N, 9.5% is from ^{15}O and 1.9% is from ^{11}C, reference [10].

3.2. Results of Air Activation Calculations for NSLS-II Accelerator Enclosures

Table 4 gives the activity in air at the four specified beam loss locations inside the accelerator enclosures of NSLS-II. The volume of air in each enclosure is also given in Table 3. The air changes in the enclosures cause mixing of the activity in the entire volume of the enclosure. The air in the storage ring is supplemented by 5000 cfm of air to maintain the positive pressure inside the storage ring. An equivalent rate of air volume seeps out from the storage ring. The air is re-circulated in the linac and booster tunnels.

Beam loss location	Beam loss (watts)	Charge loss (nC/s)	Enclosure volume (m^3)	^{13}N (μCi)	^{15}O (μCi)	^{11}C (μCi)	Concentration (μCi/cm^3)
Linac momentum slit	0.25	1.25	473	13.20	1.43	0.28	3×10^{-8}
Booster injection septum	0.125	0.625	1304	6.60	0.71	0.14	5.7×10^{-9}
Booster extraction septum	0.75	0.25	1304	39.60	4.28	0.84	3.4×10^{-8}
Storage Ring injection region	0.90	0.30	7594	47.52	5.13	1.03	7×10^{-9}

Table 4 - Saturation Activity in Air at Various Beam Loss Locations.

The computed concentration of radionuclides in air at various beam loss locations inside the accelerator enclosures for the conservative set of beam loss assumptions is lower than the derived air concentration for occupational computed from DOE order 5400.5. Once the operation is shut down, this concentration will rapidly decrease due to radioactive decay and air ventilation. As has been the case at NSLS and other light sources, it is clear that there will be no problems associated with air activation within the enclosures of NSLS-II accelerators.

We have also used these calculations to estimate the potential dose at the site boundary from air releases to the atmosphere. These calculations have been performed by B. Hooda of the BNL Environmental and Waste Management Services Division using the CAP88 program. He has concluded that the annual dose to a person living at the site boundary from air releases from the NSLS-II operations will be << 0.001 mrem/year and can therefore be considered negligible.

4. Radioactivation of the Cooling Water

Activation of water for cooling the magnets and the other accelerator components may be estimated by the similar method as the estimation of air activation inside the accelerator enclosures. The primary reactions leading to the activation of cooling water are the bremsstrahlung interactions with ^{16}O in water. The most abundant of the radionuclides produced by this process is ^{15}O. Other activation products that are formed include ^{11}C (4.4% of ^{15}O), ^{3}H (at saturation, 2.2% of ^{15}O) and ^{13}N (about 1% of of ^{15}O). ^{15}O has a radioactive half life of 2.05 minutes and attain saturation during a short period of operation. Because of the long half life of ^{3}H (12.3 years), this radionuclide will not attain a substantial fraction of its saturation activity in 5000 hours.

4.1. Methodology to Estimate Cooling Water Activation

The main mechanism for formation of radionuclides in the cooling water is the photoneutron interaction of bremsstrahlung with oxygen nuclei. The threshold for this reaction is 15.67 MeV. In addition some ^{11}C, ^{13}N and ^{3}H are also created due to bremsstrahlung interactions with water. Using the neutron yield expression from reference [9] and taking the effective Z for water as 3.34, the neutron yield in water is given by the expression,

$$Y = 1.21 \times 10^{8}\, Z^{0.66} \text{ neutrons/Joule} = 2.68 \times 10^{8} \text{ n/J} \qquad (10)$$

Implicit in the release of neutrons, is the formation of an unstable nucleus in water, which may be radioactive. Equation (10) gives only the Giant Resonance Neutron (GRN) yield. The yield of High Energy Neutrons (HEN) increases the total neutron yield by about 6%. But since most of the GRN neutrons are below the threshold energies for photoneutron reactions, using the yield of GRN neutrons alone will give a conservative estimate of the radionuclide formation. Assuming the abundance of ^{15}O as 100% for each neutron created, the change in number (n) of radioactive atoms per unit time if the cooling water is in a closed loop is given by:

$$\frac{dn}{dt} = YFW\,(1- e^{-x/\lambda}) - \lambda_R n \qquad (11)$$

where W = Beam energy dissipated at the location (watts)
x = Average path of bremsstrahlung in water (assumed to be 2 cm for the cooling water hoses)
λ = Effective bremsstrahlung attenuation length in water [11] (50 cm)
λ_R = Decay constant of the radioactive nuclide ^{15}O (s^{-1})
F = Fraction of beam energy that converts into bremsstrahlung (assumed to be 50%)

Solving equation (11) for initial conditions n=0 for t=0

$$n = \frac{WFY}{\lambda_R}\,(1 - e^{-x/\lambda})\,(1- e^{-\lambda_R t})$$

The activity due to ^{15}O is equal to $\lambda_R n$

$$\text{Activity} = WFY\,(1 - e^{-x/\lambda})\,(1- e^{-\lambda_R t}) \quad \text{Beq} \qquad (12)$$

Because the half life of ^{15}O is only 2.05 min, it will reach saturation rapidly.
The saturation activity under static conditions will be given by:

$$\text{Saturation Activity} = WFY\,(1 - e^{-x/\lambda}) \quad \text{Beq} \qquad (13)$$

The saturation activity of ^{15}O can be calculated from equation(13). The saturation activity of other nuclides can be calculated from the saturation activity of ^{15}O. It can be noted that ^{3}H will take a long time to attain saturation. In this case equation (12) can be used to calculate the build up of activity of ^{3}H for known period of operation. In the present calculations it is assumed that the cooling water is in a closed system and the total water inventory in the closed loop is ~100,000 gallons (3.78×10^8 cm^3).

4.2 Results of Cooling Water Activation Estimates

Among the accelerator components which require cooling, the storage ring septum is a highest beam loss location. The saturation activity of radionuclides in the storage ring cooling water is estimated using equation (13) for 18 nC of charge dissipation per minute. Table 5 provides the saturation activity of the radio nuclides in the cooling water of the NSLS-II storage ring. As mentioned earlier, ^{3}H will attain saturation only after decades of operation. After 5000 hours of continuous operation, the concentration of ^{3}H will be only 3% of the saturation value.

Beam loss (watts)	Charge dissipation (nC/min)	^{15}O (μCi)	^{11}C (μCi)	^{13}N (μCi)	^{3}H (μCi)
0.90	18	134	5.6	1.2	2.8

Table 5 - Saturation Activities of Radionuclides in the Cooling Water of the Storage Ring (per 100,000 gallons of water).

The computed concentration of radionuclides in the cooling water of 100,000 gallons ($3.78x10^5$ litres) is orders of magnitude smaller than the derived concentration for environmental discharge limits in the DOE

order 5400.5. Once the operation is shut down, concentration of all nuclides, except that of ^{3}H, will rapidly decrease due to radioactive decay of the short lived isotopes.

References

[1] Bathow, G., et.al., "Measurements on 6.3 GeV Electromagnetic Cascades and Cascade Produced Neutrons" , Nucl. Phys., B2 (1967).
[2] Radiation Protection for Particle Accelerator Facilities, NCRP Report 144 (2003).
[3] Alexandrov, A.A., et.al., "Induced Activity in Soil", Atomaya Energia, 34-3 (1973).
[4] Gabriel, T.A., "Calculation of Long Lived Induced Activity in Soil", ORNL-TM-2848 (1970).
[5] Private communication with D. Paquette, BNL hydrogeologist.
[6] Fasso, A.,et.al., "Radiation Problems in the Design of LEP Collider", CERN-84-02 (1984).
[7] Borak, T.B.,et.al., "The Underground Migration of Radionuclides Produced in Soil", Health Physics, 23 (1972).
[8] Bleser, E.J., "Shielding for AGS J10 Scraper", AGS/AD/Tech.Note 444(1996).
[9] Schaffer, N.M., "Reactor Shielding for Nuclear Engineers", NTIS, Springfield, VA (1973).
[10] Swanson, W.P., "Radiological Safety Aspects of Electron Linear Accelerators", IAEA 188 (1979).
[11] Attix, F.H., "Introduction to Radiological Physics", John Wiley, New York (1986).

Simulation of Gas Bremsstrahlung Radiation from APS Undulator Straight Sections using MARS[‡]

J. Dooling and L. Emery

Accelerator Systems Division, Advanced Photon Source, Argonne National Laboratory, 9700 S. Cass Ave. Argonne, IL 60439, USA

Abstract

We analyze the production of gas bremsstrahlung (GB) with regard to power, dose rate, and distributions. The contact dose behind a beam stop is simulated for stops fabricated from lead and tungsten. We compare the production of photoneutrons (PNs) from measurements and simulations. The beam stop dimensions necessary to shield a GB extremal ray are examined.

1. Introduction

A number of studies have been undertaken to quantify and measure the radiation produced at the APS and to specify the means necessary to mitigate its hazards. Specifically, APS Technical Bulletins (TB) and Light Source (LS) Notes [1,2,3,4] provide physical and engineering guidance regarding radiation source strength, material properties, and shielding requirements. Neutron fluences, measured in two undulator insertion device (ID) beamlines [5,6], 6ID and 11ID, are compared here with MARS simulations. MARS [7,8] is a group of freely available but closed source Monte Carlo programs used for the description of high-energy particle transport though matter. MARS is used to model the interaction of 7-GeV electrons in the APS storage ring (SR) with various forms of matter that may be encountered and the radiation resulting from those interactions. After a brief introduction in section one, the second section focuses on analysis of the gas bremsstrahlung (GB) source. Analytical, numerical, and empirical bremsstrahlung source descriptions are compared. In section three, earlier EGS4 results are given alongside recent MARS simulations estimating the dose in a tissue phantom in contact with a heavy-metal beam stop. MARS estimates of GB-induced, photoneutron production are compared with earlier measurements in section four. In section five, the first optics enclosure (FOE) geometry is modeled, and a method for calculating the extremal ray shielding requirement is described. MARS simulation results are summarized in section six. Throughout this document, error bars represent the standard deviation about the mean value.

2. Analysis

In the first part of this section we will compare the power and dose rate from gas bremsstrahlung (GB) photons calculated with an analytical formula, a MARS simulation, and a semi-empirical analysis [9] used in APS documents TB-20 [2] and LS-260 [10]. Some discrepancies are revealed. Next, we will check how well the MARS spatial photon distribution corresponds to analytical estimates.

The production of GB photons [11,12,13] can be determined from the radiative mass stopping power:

$$\left.\frac{dT}{dx}\right|_{rad} = -\frac{\rho T}{X_0}, \tag{1}$$

where T is the electron kinetic energy in MeV, and ρ is the mass density of the medium; in this regime, $T \approx E_o$, the total electron energy ($E_o = T + mc^2$). The radiation length is defined as

[‡] Work supported by U.S. Department of Energy, Office of Science, Office of Basic Energy Sciences, under Contract No. DE-AC02-06CH11357.

$$X_0^{-1} = 4\alpha r_e^2 \frac{N_A}{A^*} Z_{eff} \left(Z_{eff} + 1\right) \left[\ln\left(\frac{183}{Z_{eff}^{1/3}}\right) + \frac{1}{18} \right], \quad (2)$$

where X_0 is expressed in units of g/cm^2, N_A is Avagadro's number, the fine structure constant α=1/137, the classical electron radius r_e=2.83x10^{-13}cm, A* is the effective atomic mass described below, and Z is the atomic number [14,15]. Tsai [16] and Yao et al. [17] express the radiation length slightly differently but with virtually the same numerical results. The effective atomic mass of a gas mixture such as air is defined as a sum of the weighted molar fraction of the atomic mass of each component in the mixture,

$$A^* = \sum_i f_i A_i \ . \quad (3)$$

For the main constituents of air (N, O, and Ar) A*=14.66 g/mole. In a manner similar to that given by Eq. (3), the effective atomic number for air is determined as Z_{eff}=7.31. Given A* and Z_{eff}, the radiation length for air is found to be 37.06 g/cm^2. High-energy electrons will interact with the electrons and nucleus of individual atoms, not collectively with the molecules. Equation (1) expresses the photon energy loss per electron per cm and provides a convenient way to calculate the GB power. The total GB power is written as

$$P_\gamma \left\{ \frac{MeV}{s} \right\} = 1.7x10^{18} \frac{p\{nTorr\} I\{mA\}}{T_K\{K\}} \frac{\rho\left\{g/cm^3\right\}}{X_o\left\{g/cm^2\right\}} L_{ss}\{cm\} T\{MeV\}, \quad (4)$$

where I is the stored beam current, p is the residual gas pressure, T_K is the residual gas temperature, and L_{ss} is the total length of the straight section. The total GB power per mA from 7 GeV electrons in a residual background gas pressure of 1 nTorr air at 293K (20°C) is 4.28x10^{-7} W for a 1538-cm-long straight section. For all temperature-dependent calculations made here, it is assumed T_K=293K. Residual gas analysis (RGA) studies of gas composition in APS insertion device (ID) beamlines 6 and 11 indicated Z_{eff} values vary significantly [5,6]. A comparison of GB power levels, normalized to 1 nT and 1 mA, are given in Table 1. The MARS result is approximately 20 percent less than the analytical value; however, the measured GB power levels are low by factors of 3.8-24.

	Z_{eff}	*$P_{\gamma,meas}$ [5,10,18,19] (W/Torr/mA)*	*Analytic, Eq. (4) (W/nTorr/mA)*	*MARS (W/nTorr/mA)*
Air	7.3	(1.0x10^{-7})	4.28x10^{-7}	3.4x10-7
6-ID e$^-$	4.08	0.6±0.03x10^{-8}	1.46x10^{-7}	*1.16x10-7
10-ID e$^+$	4.6	1.0x10^{-8}	1.82x10^{-7}	*1.45x10-7
11-ID e$^-$	3.18	1.9±0.14x10^{-8}†	0.94x10^{-7}	*0.75x10-7

* MARS Air result scaled with Z_{eff}.

† Given as 2.9x10^{-8} W/nTorr/mA (118 GeV/s/nTorr/mA) in Ref. 5

Table 1 - Comparison of measured, predicted, and simulated normalized GB power.

No analytical estimates are given for GB power in Refs. 10 or 19. A semi-empirical dose prediction based on a flux-to-dose conversion factor is provided where the background gas is assumed to be air (see the discussion associated with Eq. (7)). The GB power used in LS-260 [10] comes from Rindi [14], but its quantity is only partially provided. An estimated level of 1.2x10^5 photons per second is mentioned for the beamlines in Refs. 10 and 19; however, the average photon energy is not given, nor are the conditions for

which the estimate is made (current or pressure). As discussed below, the average photon energy determined from the analytical GB spectral distribution is found to be 531 MeV. Assuming the estimated photon rate is made for 100-mA operation in an air background of 1 nTorr, the normalized GB power is $1.0\text{x}10^{-7}$ W/nTorr/mA. The estimated level is roughly a factor of 4 times lower than the analytical result presented in Table 1; this discrepancy has been noted elsewhere [20]. Now that the GB power is calculated, let us estimate the dose. Normally, one would continue to use a simulation program for this calculation. However, for the simple geometry described here, we can compare analytical and numerical results, as well as examine what people did in the past.

Using flux-to-dose conversion factors provided by Rogers [21], an estimate of maximum GB dose can be obtained once the photon flux and average photon energy are known. The GB photon spectral fluence was predicted by MARS for 300-mA, 7-GeV electrons striking a 24-cm length, 1-atmosphere (760 Torr, ρ_{air}=0.001205g/cm^3) air target. The total photon fluence is determined by integrating gamma spectral fluence over the energy range and multiplying this result with the cross-sectional area of the volume in which the photon spectrum is tallied. In MARS, the dose from photons in a given region is determined by integrating the spectral fluence with the energy-dependent flux-to-dose conversion factor [21,22]. For the dose calculation, a cross-sectional area of 1 cm^2 is used. We must scale for gas pressure (p_{ss}=1 nTorr) as well as for the straight-section length (L_{ss}=1538 cm). The average GB photon energy determined from the MARS spectrum over the energy range of 0.2 MeV to 7000 MeV, $\langle k_m \rangle$=356 MeV. In MARS output, the dose from photons in a given region is determined by integrating the spectral fluence with the energy-dependent flux-to-dose conversion factor [21,22]:

$$\dot{D}_{\gamma,\text{MARS}} = \int_{k_{min}}^{k_{max}} dk\, SPG(k) \cdot f_\phi(k); \tag{5}$$

however, here we want to follow the steps used in the analytical approach. Using the normalized power found in Table 1, the photon flux in 1 cm^2 per mA is just the GB power divided by the average energy per photon. The dose rate can be expressed as

$$\dot{D}_{GBm} = \frac{P_{GBm}}{\langle k_m \rangle} \frac{f_\phi(\langle k_m \rangle)}{A_{min}} I p, \tag{6}$$

where A_{min}=1cm^2. The value of $f_\phi(\langle k_m \rangle)$ was found by linear interpolation of Rogers' simulation data [21] (=$2.74\text{x}10^{-10}$ Sv cm^2). The analytical spectrum varies as 1/E, differing from that of the simulation at low energy. MARS indicates a modest enhancement of the low-energy photon spectrum. Integrating over the same energy range, the average analytic photon energy $\langle k_a \rangle$ = 531 MeV. Using the power level defined in Eq. (4), the analytic dose rate is determined using the same form as Eq. (6), replacing $\langle k_m \rangle$ with $\langle k_a \rangle$. The value of $f_\phi(\langle k_a \rangle)$ is again interpolated from Rogers' data (=$3.22\text{x}10^{-10}$ Sv cm^2). Finally, a semi-empirical, total beam-integrated GB dose rate was used to determine the source term for the EGS4 simulations and is expressed as [9]

$$\dot{D}_{se} = \frac{f_\Gamma \Gamma L_{ss}}{\pi \theta_{gb}^2 X_o L (L + L_{ss})}, \tag{7}$$

where f_Γ is another effective flux-to-dose conversion factor for bremsstrahlung photons [10,19] (f_Γ=3×10^{-6} Gy/hr/Γ), Γ is the number of electrons per second (300 mA=1.873×10^{18}e/s), L_{ss} is the length of the ID straight section, $\theta_{gb}=1/\gamma$ is the characteristic opening angle of the radiation cone ($1/1.37\times10^4$=73 μrad), X_o is the radiation length in air for 1 nTorr (37.1 g/cm^2/ρ_{1nTorr}=2.35×10^{16}cm), and L is the length from the end of the straight section to the observation point (2440 cm). Comparison of initial dose rates are given in Table 2. The MARS GB power is 20 percent lower than that from the analytic model; however, the two dose results differ by less than 1 percent owing to the difference in average energy.

The dose rate given by Eq. (6) relies on the integration of the MARS photon spectal fluence to determine the total power and average photon energy. With these quantities, the dose rate is calculated manually using the flux-to-dose conversion factor just described; this is referred to as the MARS spectral fluence result in Table

2. The dose rates for this and the analytical case are determined assuming that all the GB power is intercepted by a 1-cc target volume defined by $r=1/\sqrt{\pi}$ cm and that the dose is uniform throughout this volume. In reality, neither of these assumptions are true. The dose will spread out beyond the boundaries of the target volume, especially at the downstream (DS) end of the phantom where the maximum dose is obtained. The GB transverse beam distribution, however, is still relatively narrow. The dose within the FWHM radius r_{FWHM} is much higher than that of the 1-cc cylinder. Assuming the radius of the GB beam at the output of the straight section is $\theta_{gb}L_{ss}$ yields 0.112 cm; this increases to 0.293 cm at the DS end of the phantom. The MARS simulation yields r_{FWHM}=0.267 cm at the DS end of the phantom. Using the simple model given by Eq. (6) (all GB power contained within the angular cone), the dose calculated at the source will be the same as that at the DS end of the phantom, since in both cases the radii of the GB is less than $1/\sqrt{\pi}$. We are ignoring any showering or absorption in the phantom. When considering the dose from GB radiation, a 1-cc volume can be employed but should more accurately reflect the transverse beam size. Rather than arbitrarily using a cylinder where $2r\approx1$ cm or a 1-cm cube, a more pertinent geometry would be a cylinder where the radius is defined by the width of the beam, such as r_{FWHM}. In the present case where the simulation predicts r_{FWHM}=0.267 cm, the length of the cylinder becomes $1\ cm^3/(\pi[0.267\ cm]^2)$=4.47 cm. The 1-cc volume now takes on the dimensions of a short drinking straw. Employing this criterion, the analytical and MARS fluence calculations via Eq. (6) both yield dose rates of approximately 6.5 Sv/hr; the full MARS simulation, which accounts for beam spreading and absorption, indicates 3.1 Sv/hr. The semi-empirical formula takes spreading into account via distance from the source [23].

Method	Analytic source $r=1/\sqrt{\pi}$ (r=0.293 cm)	MARS spectral fluence $r=1/\sqrt{\pi}$ (r=0.293 cm)	Semi-empirical	MARS direct $r=1/\sqrt{\pi}$ (r=0.267 cm)
$\dot{D}_r$ (Sv/hr)	1.75 (6.48)	1.76 (6.52)	2.23	0.70 (3.13)

Table 2 - Maximum GB dose rate estimates in a 1-cc cylindrical volume where the cross sectional area is 1 cm^2. The first two values in parentheses assume full power within the FWHM volume; whereas the MARS direct value refers to the peak dose within the simulation FWHM volume and thus accounts for beam spreading and absorption. The maximum dose rates are estimates at the DS end of the FOE phantom without any shielding present. No geometrical effect is evident for the semi-empirical estimate.

The GB transverse spatial distribution is examined at the location of a beam stop, 31 m downstream of the center of the undulator straight section. A linear y-profile of the bremsstrahlung photon flux obtained from a 10^{th} order polynomial fit to the integrated data is shown in Figure 1. The beam width is in reasonable agreement with the opening angle approximation $2L\theta_{gb}$=4.52mm (L=31 m). One would like to know if the 1-atm, 24-cm-long air target used to generate the GB radiation leads to an accurate description of the GB photon beam or does multiple scattering broaden the distribution. GB generated by scattered electrons will possess a portion of the angular deviation of the electron. The angular width of the GB radiation cone may be expressed as a quadrature sum of the intrinsic thin-target GB opening angle with a function of the electron scattering angle expressed as $\Theta^2_{GB}=\theta^2_{gb}+f^2(\Theta_{rms})$, where for high-energy electrons [7] $\Theta_{rms}= E_s/T\sqrt{(2x/X_o)}$ (projected distribution), x is the distance in radiation lengths these particles travel through the target medium, and $E_s=\sqrt{(4\pi/\alpha)}m_ec^2$ =21.2 MeV. The projected rms electron angle is Θ_{rms}=59.7 μrad for 7 GeV. Our hypothesis is that electrons scatter once through the gas, and thus the rms electron angle may not be given accurately by the above thin-target formula. A simple model is chosen for $f(\Theta_{GB})$, namely $f(\Theta_{rms})=k_{gb}\Theta_{rms}$, where k_{gb} is a constant to be determined from MARS simulations. From Fig. 1, the total opening angle [24] is $\Theta_{GB}=5.07x10^{-3}m/2L$=81.8 μrad; the value of k_{gb} is calculated to be k_{gb}=0.62. This suggests that scattered electrons in the air target are contributing to the angular width of the GB beam. If k_{gb} was zero, then this would be an indication that there was at most one scattering of the electrons. If k_{bg} was 1, multiple scatterings of electrons would be taking place in the air target. The effect is modest, but clearly limits the degree to which the air target pressure or length could be increased to improve simulation statistics. Thus we keep the air target model of 1 atm, 24 cm for the rest of the analyses.

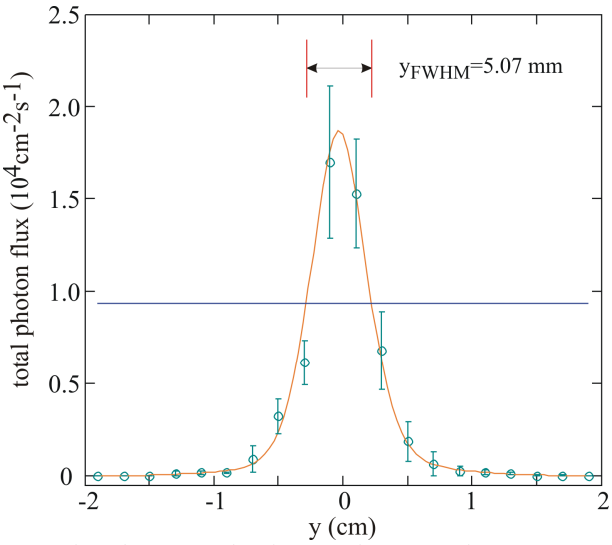

Fig.1 - MARS GB y-distribution and polynomial fit 31 m downstream of the air target.

3. Contact Dose

MARS is used to compare the dose levels reported in TB-20 [2] from simulations using EGS4. The EGS4 calculation did not account for the production of photoneutrons (PNs) in the target, and an arbitrary factor of 2 was used to include the neutron contribution to total dose. In all cases presented here, the production of PNs is included in MARS results. In the MARS simulation 300 mA of electrons at an energy of 7.0 GeV is used to generate the GB beam. In the simulation, the thickness of the target shield block was varied from 1 to 30 cm. The simulation dose was recorded in a tissue phantom, 20 cm by 20 cm in transverse dimensions and 30 cm in depth, in contact with the beam stop. The minimum volume employed in the analysis is 1 cm^3. MARS is set up to provide histograms in Cartesian coordinates; however, we expect the radiation dose, 3-D profile to have cylindrical symmetry. We need to generate an r-z distribution from MARS data to find the maximum dose. This is done by Abel inversion (AI) of x-z or y-z histogram average dose data [25]. The radial density (dose) can expressed as

$$f(r,z) = -\frac{L_y}{\pi}\int_r^a \frac{dF(x,z)}{dx}\frac{dx}{\left(x^2 - r^2\right)^{1/2}}, \tag{8}$$

where a is the radial boundary of the dose rate profile; and F(x,z), given in units of mSv/hr, is the y-averaged, x-z dose rate obtained from MARS across the y-thickness of the phantom L_y=20 cm. The AI technique requires the line density, which is obtained by taking the product of the average dose F(x,z) and L_y. Note that because of symmetry, the radial profile can equally be expressed in terms of the x-integrated dose rates by swapping x with y in Eq. (8). Equation (8) has to be evaluated at $z=z_{max}$, i.e., the z position where the dose is maximum. When a stop is present, even for the minimum thickness simulated (1cm), z_{max} is located at the upstream end of the phantom in the z-section adjacent to the beam stop. We make the assumption that the peak dose occurs at x=0, the center of the phantom.

TB-20 and the MARS AI method are compared in Figure 2. At 10 cm, the maximum dose predicted with the EGS4 analysis is approximately twice that from MARS for peak dose in 1 cc. This result is puzzling since both simulations use similar physics in this region where the electromagnetic shower dominates the dose rate. Comparing MARS and EGS4 output for stop thicknesses up to 30 cm, the attenuation of dose rate in the photon-dominated regions are approximately the same, as shown Figure 3. For thicker targets however, the dose rate no longer follows photon attenuation, as PNs begins to dominate. At the time the EGS4 simulations were conducted for TB-20, neutron contributions were not included in the dose. To account for the missing neutrons, the authors of TB-20 assumed that neutrons were responsible for half the dose and thereby lowered the dose rate limits by a factor of 2. For comparative purposes, the lowered dose rate limit of 1.25 μSv/hr is indicated in both Figs. 2 and 3.

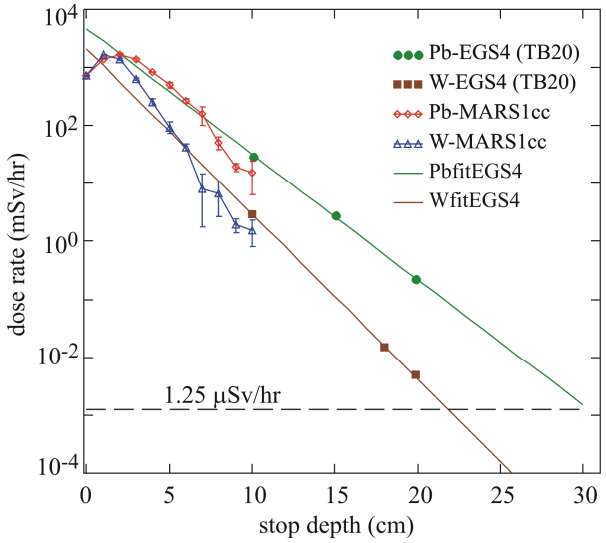

Fig.2 - Maximum dose from MARS in 1 cc and EGS4 from TB-20 for Pb and W stop thicknesses.

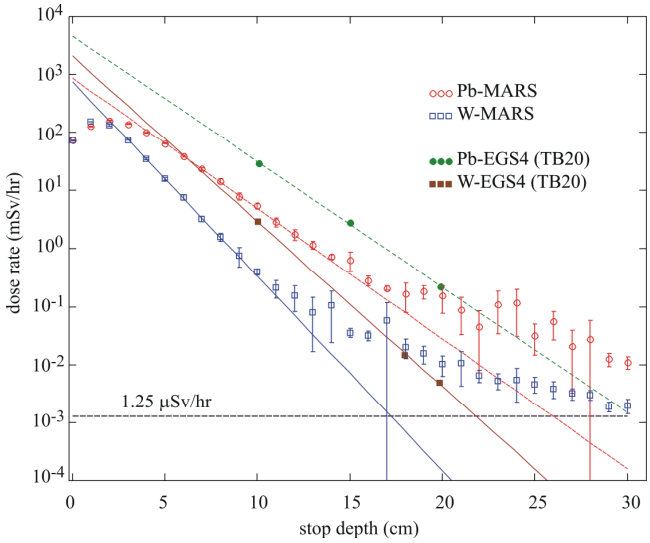

Fig.3 - Maximum MARS phantom dose (4x4x5 cm^3 element) and EGS4 dose for Pb and W stop thicknesses. Exponential fits for EGS and MARS data are given in the photon-dominated dose regions. Dashed lines compare results in Pb and the solid, in W.

The mass attenuation coefficients for Pb and W are given in Table 3. The coefficient of the exponent should approximately represent the minimum mass attenuation coefficient for each metal. These coefficients are compared with minimum mass attenuation values given by Hubbell [26] which occur near 4 MeV for both Pb and W.

	μ/ρ (4 MeV) (cm^2/g)	μ/ρ EGS4 (cm^2/g)	μ/ρ MARS (cm^2/g)
Pb	0.0420	0.0439	0.0456
W	0.0404	0.0341	0.0401

Table 3 - Mass attenuation coefficients for Pb and W comparing EGS4 and MARS with min. attenuation near 4 MeV.

4. Photoneutron (PN) Production

A study of PN dose resulting from GB [10,19] striking thick targets of various materials was conducted by Pisharody et al. [5,6]; specifically, the materials examined were Cu, Fe, W, and Pb. A comparison of these data with MARS simulations is presented here to evaluate its ability to simulate PN dose. In Refs. 5 and 6, an Andersson-Braun (AB) remmeter was used to measure the PN dose. The plan geometry of the MARS simulation is presented in Figure 4; in this case, an iron target receives the GB beam. The simulation dose is again recorded in a tissue phantom, 20 cm by 20 cm in transverse dimensions (y and z) and 30 cm in depth (x), relative to the incident beam.

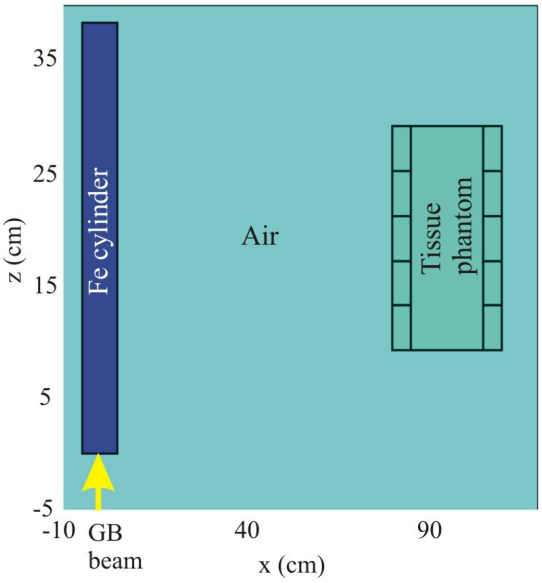

Fig.4 - Plan geometry of the MARS PN measurement simulation.

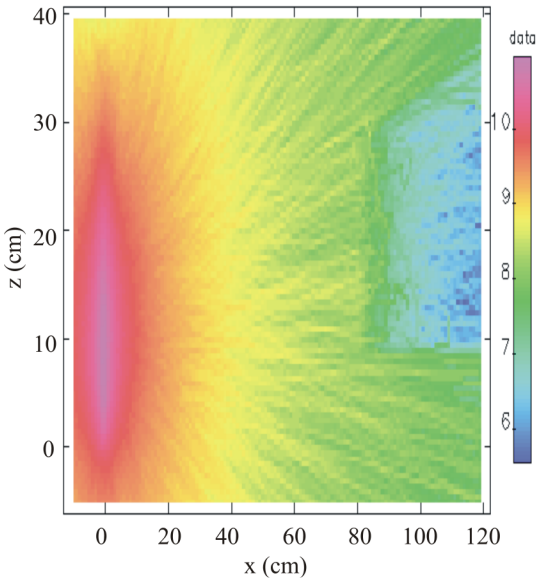

Fig.5 - Contour plot of uncorrected MARS PN dose from an APS GB beam striking the Fe target shown in Fig. 4. Dose is presented on a log scale.

In Fig. 5, a contour plot of the PN dose predicted by MARS is shown for the geometry given in Fig. 4. The simulation results presented in Fig. 5 must be normalized for the actual pressure and current as mentioned above. PN dose results from measurements given in Refs. 5 and 6, and scaled MARS simulation output are presented for comparison in Table 4. The PN measurements presented in Table 4 are obtained from beamlines 6-ID and 11-ID. For 6-ID, the measured PN dose rate for Fe is the average for the two highest current levels (93.4 and 92.7 mA) in Table 6 of Refs. 5 and 6, likewise for Cu and W, and from the highest current for Pb. For 11-ID, the measured PN dose rate for Fe is the average of the three highest current levels (96.6, 93.3, and 90.2 mA) in Table 5 of Refs. 5 and 6, likewise for Cu, but the lowest three for W and Pb. Target dimensions are varied to maintain lengths of $20X_o$ and widths of $6X_o$. The dose rates given in Table 4 for beamline 6-ID are approximately 3-5 times larger than the measured values; whereas those given for beamline 11-ID are much closer. Several possibilities exist that may explain the differences in the two sets of results: 1) Residual gas Z_{eff}. The actual Z_{eff} values in undulator beamlines are difficult to definitively ascertain. 2) Residual gas pressure. Pressure is another parameter that can vary from beamline to beamline. The Z_{eff} quoted for 11-ID is 3.18, yet the GB power from this line is 3-4 times higher than that of 6-ID. This suggests that the pressure or other factors may be considerably different for these two lines. 3) Beam pipe misalignment. Prior to the installation of an ID in the 6-ID undulator straight section, but after the GB measurements had been made, a 1-mrad bend in beam central orbit trajectory was noted through this region. The misalignment may have reduced the GB power by a factor of 3 in 6-ID.

Beamline	6-ID				11-ID			
Target Material	Fe	Cu	W	Pb	Fe	Cu	W	Pb
I (mA)	93.1	90.1	88.5	76.1	93.4	92.2	78.4	76.2
P (nT)	9.69	9.41	9.29	8.22	8.97	8.88	7.78	7.54
AB Remmeter (μSv/hr)	0.150	0.130	0.186	0.177	0.371	0.462	0.393	0.425
MARS (μSv/hr)	0.674	0.665	0.526	0.525	0.406	0.417	0.254	0.313

Table 4 - Comparison of PN dose measurements made in Refs. 5 and 6 for beamline 6-ID and 11-ID with MARS simulations correcting for Z_{eff} between air (7.3) used in MARS and a measured values of 4.08 (6-ID) and 3.18 (11-ID).

5. First Optics Enclosure (FOE) Study

Simulation studies have been conducted with MARS to assess shielding requirements. In the first study, dose levels in contact with the outside wall of the FOE are examined when GB radiation strikes a Pb beam-stop within the FOE. In the second study, the thickness of lead required to shield against the GB extremal ray is determined. For brevity, only the results of the second study are mentioned here. The FOE Pb shielding thicknesses used are 19 mm for the outside wall, 50 mm plus an additional 50 mm by 1-m^2 sheet centered on the beamline for the back wall, and 12 mm for the roof.

In the second task, dose from GB radiation striking a thick target scatterer within a beam pipe is simulated to compare with a similar analysis given in TB-20 to determine the extremal ray requirement. The geometry used for the new study described here is simple and obtained by replacing the square cross-section beamstop with a cylinder of the same length, 30 cm. The radius of the Pb target is varied while dose is recorded using the back-wall tissue phantom. Each data point is the average of ten MARS runs with 5×10^8 events per run representing the 7-GeV, 300-mA electron beam. The GB beam size was provided in Fig. 1. For the smallest target radii, a fraction of the primary GB beam passes by the target altogether (or perhaps experiences one scattering within the Moliere radius) and directly strikes the Pb shielding on the back wall. A fraction of this radiation then showers through the shielding to the back-wall phantom. Dose in the back wall phantom as a function of target radii is shown in Figure 6. For radii of 3 cm and above, primary bremsstrahlung is essentially blocked. Dose in the phantom varies weakly with target radius for r>3 cm.

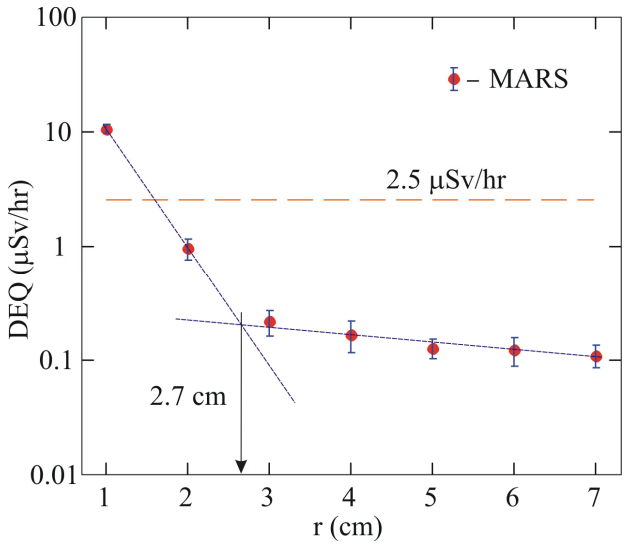

Fig.6 - Back-wall phantom dose versus beam target radius. The intersection of the fast and slow response curves represents the minimum radius of the Pb stop required to fully shield the back-wall phantom from direct GB radiation.

The dose in the phantom appears to be characterized by two behaviors: 1) a large variation with radius for small target dimensions and 2) a much smaller change for larger radii. The small radius dose appears to be the result of direct primary GB on the FOE back wall, as well as scattering up to the Moliere radius. The Moliere radius, the characteristic transverse dimension of the shower, may be written as [17] $X_m=X_oE_s/E_c$, where E_s was defined in Section 2, and the critical energy may be expressed as $E_c(\text{MeV})=800/(Z+1.2)$. The critical energy in Pb is 9.6 MeV, the radiation length is 5.8 g/cm^2, and the Moliere radius is 12.8 g/cm^2. In terms of physical length, the Moliere radius=X_m/ρ_{Pb}=1.1 cm. Assuming the beam edge radius r_e to be twice the FWHM value given in Fig. 1, then r_e=2(0.507 cm)=1.14 cm. The extremal distance r_{ed} is taken to be the difference between the back-wall phantom dose breakpoint radius r_{bp} and the beam-edge radius $r_{ed} = r_{bp} - r_e$. As shown in Fig. 6, r_{bp} = 2.7 cm; thus, r_{ed} = 1.56 cm ≈ 1.6 cm. Relative to the Moliere radius, the separation thickness is 1.6 cm/1.1 cm=1.45≈1.5; therefore, the separation between the extremal ray and the edge of the shielding is 1.5 X_m. In the context of TB-20 therefore, an extremal ray should come no closer than 1.6 cm to the lateral edge in Pb. For W with a Moliere radius of 0.65 cm, a similar argument sets the extremal ray shield edge separation at 0.98 cm≈1.0 cm. TB-20 [2] recommended that the extremal ray in the case of bremsstrahlung ray-tracing should not be closer than 4.5 cm from the lateral beamstop edge in Pb and 3.0 cm in W. The extra thickness in TB-20 provides additional protection, but specifications may need revisiting.

6. Discussion and Summary

GB power predicted by MARS in terms of the initial dose rate agrees to within 20 percent of the analytical model, see Table 1. Given the two independent methods employed, one should conclude that MARS does reasonably well simulating GB power. However, analysis and simulation both are significantly higher than the measured GB power. Possible explanations for the discrepancy were presented in Section 4 and include uncertainty in beamline Z_{eff}, pressure, and undulator straight section alignment. MARS does a good job reproducing the GB spatial distribution (see Fig. 1) in agreement with thin-target GB theory. Care must be taken, however not to make the air target too thick. An air-target pressure of 1 atmosphere and length of 24 cm appears to be an upper limit. Comparison of initial maximum dose rates predicted by MARS and the analytical model show good agreement; in addition, similar results are obtained with EGS4 in TB-20; however, an important difference is noted. The maximum dose from TB-20 appears conservative in the photon-dominated shower regions of the stops; however, this is not the case for thick stops. In the latter circumstance, dose comes primarily from photoneutrons. The Abel inversion method provides an accurate estimate of dose provided that statistics in the average dose profiles are good and the profiles are well behaved.

As for comparisons with PN measurements, MARS simulation results presented in Table 4 are approximately 4-5 times the measured values in beamline 6-ID and very close to that measured in 11-ID. Given the variability in the measured GB power due to fluctuations in Z_{eff} and pressure, MARS performs well. In addition, the MARS simulation work shows that, in order to properly model the PN dose, an accurate measure of undulator beamline Z_{eff} and pressure are necessary. As with the GB power mentioned above, the simulated PN dose levels generally exceed measured results.

An alternative method for determining the extremal ray thickness was used with MARS relative the approach taken in TB-20. By varying the radius of a cylindrical Pb target and calculating the dose in the back-wall phantom, one could observe the thickness where the direct and Moliere-scattered GB radiation was effectively turned off. The beam-edge radius of 1.1 cm and a dose break point radius of 2.7 cm indicates that 1.6 cm of Pb as an extremal ray thickness should be sufficient. The simulations indicate an additional thickness of 1.5 X_m should be sufficient to shield the extremal ray determined from ray-tracing.

References

[1] N. Ipe, D.R. Haeffner, E.E. Alp, S.C. Davey, R.J. Dejus, U. Hahn, B. Lai, K.J. Randall, and D. Shu, "Guide to Radiation Beamline Shielding Design at the APS," ANL/APS/TB-7 (1993).

[2] P. K. Job, D. R. Haeffner, and D. Shu, "Bremsstrahlung Scattering Calculations for the Beam Stops and Collimators in the APS Insertion-Device Beamlines," ANL/APS/TB-20 (1994).

[3] W. Yun et al., "Radiation Shielding of Insertion Device Beamlines Using a Mirror as the First Optical Element," ANL/APS/TB-21, February 1995.

[4] P. K. Job et al. "Guidelines for Beamline and Front-End Radiation Shielding Design at the Advanced Photon Source," ANL/APS/TB-44, Rev. 3, September 2008.

[5] M. Pisharody, E. Semones, and P. K. Job, "Dose Measurements of Bremsstrahlung-Produced Neutrons at the Advance Photon Source," ANL/APS/LS-269 (1998).

[6] M. Pisharody, E. Semones, and P.K. Job, Nucl. Instrum. Methods A, 430, 542 (1999).

[7] N. V. Mokhov and S. I. Striganov, "MARS15 overview," Technical Report Fermilab-Conf-07/008-AD, 2007.

[8] N. V. Mokhov et al., "Physics models in the MARS15 code for accelerator and space applications," in Int. Conf. on Nuclear Data for Science and Technology, AIP Conf. Proc. 769, 1618-1623 (2004).

[9] J. C. Franck, "Bremsstrahlung du Faisceau Stocke sur les molecules Residuelles de la Chambre Avide de Suder ACO," LURE EP 88–01 (1988).

[10] M. Pisharody, P. K. Job, S. Magill, J. Proudfoot, and R. Stanek, "Measurement of Gas Bremsstrahlung from the Insertion Device Beamlines of the Advanced Photon Source," ANL/APS/LS-260, March 1997.

[11] H. W. Koch and J. W. Motz, Rev. Mod. Phys. 31(4), 920 (1959).

[12] W. R. Nelson, "Properties of the EM Cascade," SLAC-PUB-4203, February 1987.

[13] J. C. Liu, W. R. Nelson, and K. R. Kase, Health Physics 68(2), 205 (1995).

[14] Rindi, Health Physics 42, 187 (1982).

[15] G. Tromba and A. Rindi, Nucl. Instrum. Methods A 292, 700 (1990).

[16] Y.-S. Tsai, Rev. Mod. Phys. 46(4), 815 (1974)
[17] W.-M. Yao et al., Journal of Physics G 33, 1 (2006).
[18] P. K. Job, M. Pisharody, E. Semones, Nucl. Instrum. Methods A 438, 540 (1999).
[19] M. Pisharody et al., Nucl. Instrum. Methods A 401, 442 (1997).
[20] Y. Asano et al., Nucl. Instrum. Methods A 451, 685 (2000).
[21] D. W. O. Rogers, Health Physics 46(2), 891(1984).
[22] ICRP Pub. 51, "Data for Use in Protection Against External Radiation," Annals of the IRCP, 17(2/3), Pergamon, New York, 26 (1987).
[23] Y. Asano and N. Sasamoto, Radiation Protection Dosimetry 82(3), 167 (1999).
[24] H. J. Moe, "Radiological Considerations for the Operation of the Advanced Photon Source Storage Ring – Revised," ANL/APS/LS-295 (1997).
[25] H. Hutchinson, Principles of plasma diagnostics, Cambridge, New York, 1987, p. 124.
[26] J.H. Hubbell, NSRDS-NBS 29, August 1969.

The Effectiveness of Thin Low-Z Scrapers in Electron Storage Rings

P. K. Job, S. Kramer and W.R. Casey

National Synchrotron Light Source-II Project
Brookhaven National Laboratory, Upton NY 11973, USA

Abstract

Brookhaven National Laboratory is in the process of constructing a new Electron Synchrotron for scientific research using synchrotron radiation. This facility, called National Synchrotron Light Source II (NSLS-II) [1], will provide x-ray radiation of ultra high brightness and exceptional spatial and energy resolution. It will also provide advanced insertion devices, optics and detectors designed to maximize the scientific output of the facility. The project scope includes the design, construction, installation, and commissioning of the following accelerators: a 200 MeV linac, a booster accelerator operating from 200 MeV to 3.0 GeV, the storage ring which stores 500 mA current of electrons at an energy of 3.0 GeV and 56 beamlines for experiments. It is planned to operate the facility primarily in a top-off mode, thereby maintaining the maximum variation in stored beam current to < 1%.

The NSLS-II with high stored beam energy operation and top-off injection, makes the radiation protection a critical issue.The radiation shield wall of the tunnel is designed to for a loss of 1.1 nC/min of charge, at any one location around the ring. The injection region is shielded for an injection and stored beam loss of 13 nC/min. This thinner shielding around the ring is a concern should the beam develop high current instabilities at locations other than the heavily shielded injection region, that would cause the beam to dump or develop a very short life time. A method has been proposed to control the location of losses by the installation of thin low-Z scrapers in the better shielded injection region. This is to control beam loss without significant deterioration in the stored beam life time and shield effectiveness. This paper presents the results of FLUKA [2] simulation and test measurements to study the effect of thin low-Z scrapers in the storage ring of NSLS-II. Test measurements are conducted at NSLS-I storage ring to study this effect.

1. Use of Scrapers in the Electron Storage Rings

Scrapers in the electron storage rings of third generation synchrotron radiation sources serve two important purposes. They are utilized to provide protection for insertion devices and other storage ring components, minimizing the beam hallow of the injected beam. They define the momentum aperture for the beam for optimum Touschek life time. Scarpers also provide a location for the controlled beam dumps in self shielded diploes for intentional or un-intentional RF and interlock dumps. NSLS-II has planned vertical and horizontal beam scrapers within the heavily shielded injection region with possible additional supplementary shielding if necessary. Comparison study has been made between a low-Z element like copper with a high-Z element like tungsten for the effectiveness of the scraper. The radiological dose impact on the experimental floor as a function of the thickness of the scraper is also evaluated by simulation and measurements.

2. FLUKA Simulations for Scraper Effectiveness

Two scraper configurations are simulated with FLUKA Monte Carlo simulation program. Fig.1 gives the geometry used for FLUKA simulations.

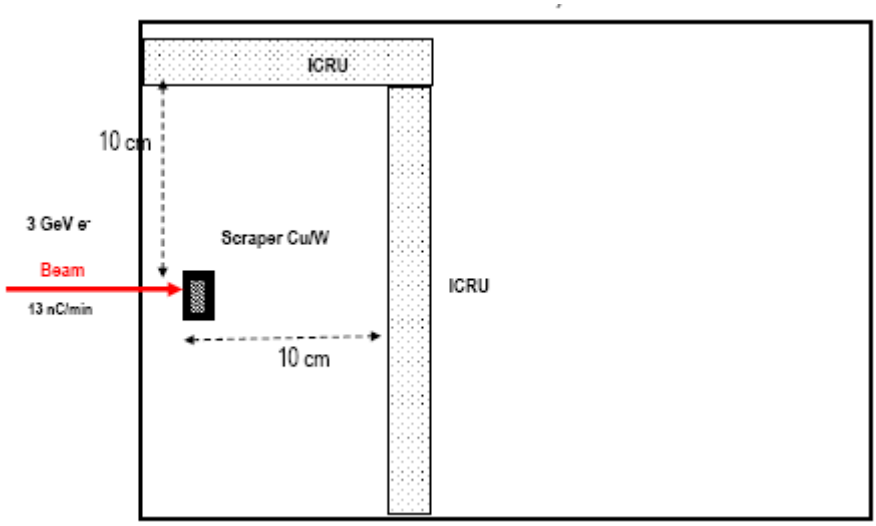

Fig.1 - Geometry used for FLUKA Simulation.

Copper, with good thermal properties, is chosen as the low-Z element and Tungsten as the high-Z element. The copper scraper simulated was 14 mm thick and 20 mm in diameter. The thickness of copper configuration is approximately 1 radiation length (X_0). This is considered to be thin in terms of radiation lengths. The thickness of tungsten is 20 mm, which is approximately 5 radiation lengths of tungsten, a relatively thick scraper. In both cases the transverse and forward scattered dose rates are scored in the ICRU tissue. In addition to, the angular and energy profiles of the scattered electrons emerging after interacting with the scraper are scored by FLUKA.

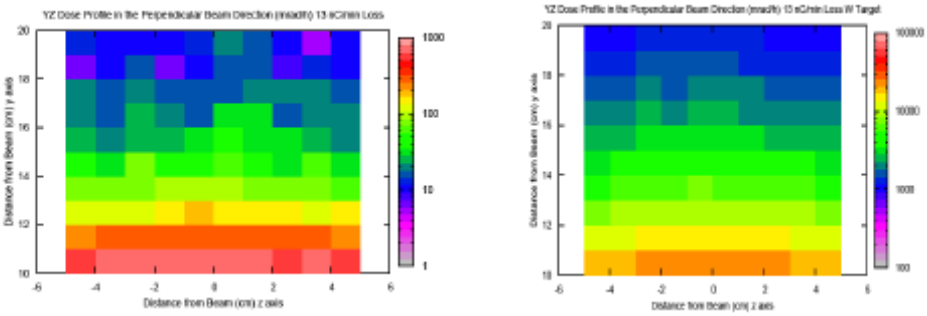

Fig.2a - with Cu Scraper *Fig.2b - with W Scraper*

Transverse Dose Rate at 10 cm from the Cu and W Scrapers.

Fig.2 a and b gives the transverse directed dose at a distance of 10 cm from the scraper for 14 mm thick copper and 20 mm thick tungsten. The dose rate is scored in terms of mrad/h for a beam interaction rate of 13 nC/min. It can be seen that the dose rate due to transverse scattered electrons and photons from the thin copper scraper is two orders of magnitude lesser than that of the thick tungsten scraper. This is clearly an advantage from the point of radiation safety on the experimental floor. No additional supplementary shielding is necessary for a thin copper scraper in the beam.

The emerging electron energy distribution from a thin copper and a thick tungsten scraper are also investigated. Fig.3a and b provide the electron spectra emerging from the scraper in both cases after interaction.

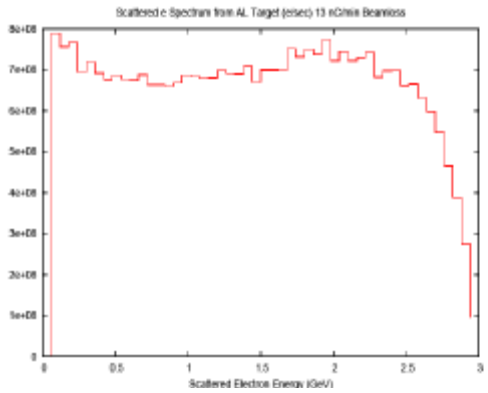

Fig.3a - Cu Scraper

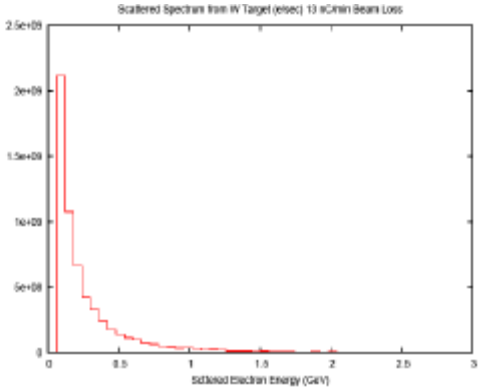

Fig.3b - W Scraper

The Emerging Electron Energy Distribution from Cu and W Scrapers.

It can be seen that in the case of the copper scraper, the emerging electrons have a wide energy distribution from 0-3.0 GeV. The $1X_0$ copper scraper is not slowing down the electrons as much as the $5X_0$ tungsten scarper. Large number of electrons lost only a small fraction of their initial energy, after interacting with $1X_0$ thick copper, where as almost all of the electrons interacted with $5X_0$ tungsten lost the entire energy. The hope is that the electrons which lost only the fraction of the energy can follow the orbit and dump at the next dipole, which is self shielded. More simulations are required to prove this effect. The tungsten scraper slows down most of the electrons locally creating transverse scattering and higher radiation fields around the scraper, which is illustrated in Fig. 4a and b.

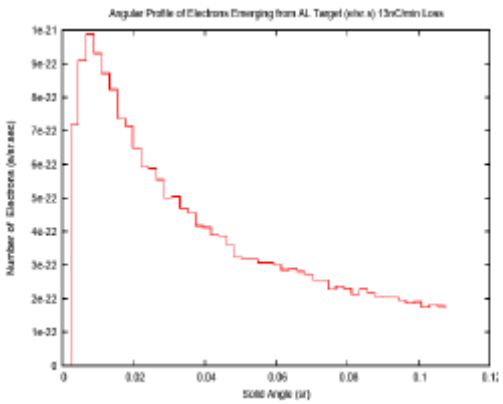

Fig.4a - Cu Scraper

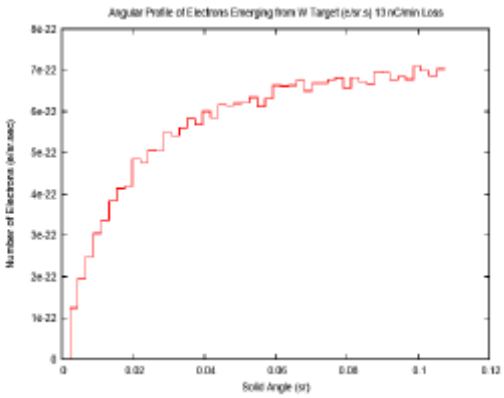

Fig.4b - W Scraper

Angular Scattering Profile of Emerging Electrons.

Fig.4a and b gives the angular scattering profiles of the emerging electrons from the copper and tungsten scrapers as the function of solid angle, per steradian. The beam direction (0 steradian) is the origin. After interacting with $1X_0$ copper scraper, the electrons have considerable forward momentum, whereas interaction with $5X_0$ tungsten scatterer create wide angle scattering of electrons. This causes high transverse radiation dose rates locally around the scraper.

3. Test Measurements at NSLS Storage Ring

The results of the FLUKA simulation are verified with test measurements at the NSLS storage ring. The National Synchrotron Light Source (NSLS) has two electron storage rings that have been in operation since 1983. The VUV ring is a low energy ring with a critical energy of ε_c ~0.6 KeV, which as a result of the low energy synchrotron radiation was built without a radiation shield tunnel, requiring careful understanding and reduction of the radiation losses. The X-ray ring is higher in energy with a radiation tunnel and less radiation loss issues. The free standing radiation shield walls and local shielding of the VUV ring protect user from the bremsstrahlung radiation during injection and low lifetime operations. As a consequence of this limited

shielding, Beam Loss Monitors (BLM) have been an important part of the beam diagnostics for this ring and have been online since about 1988. These BLMs include ionization chambers (IC), scintillation detectors (SD) and more recently diode detectors (DD).

A copper horizontal scraper of 7.5 mm thick was installed in the VUV ring of the NSLS for the purpose of testing the results of FLUKA simulations. Several radiation monitors were employed to detect the beam scraping by the scraper as a function of scraper location. The goal for these radiation monitors is to measure the local charge lost from the ring either during injection or stored beam operation and hopefully point out the cause of the lost beam and how to minimize the loss. Most monitors will measure both the electron and γ-ray component of the shower when electrons hit the vacuum chamber or the scraper. The beam life time was also monitored as a function of scraper position with respect to the beam orbit.

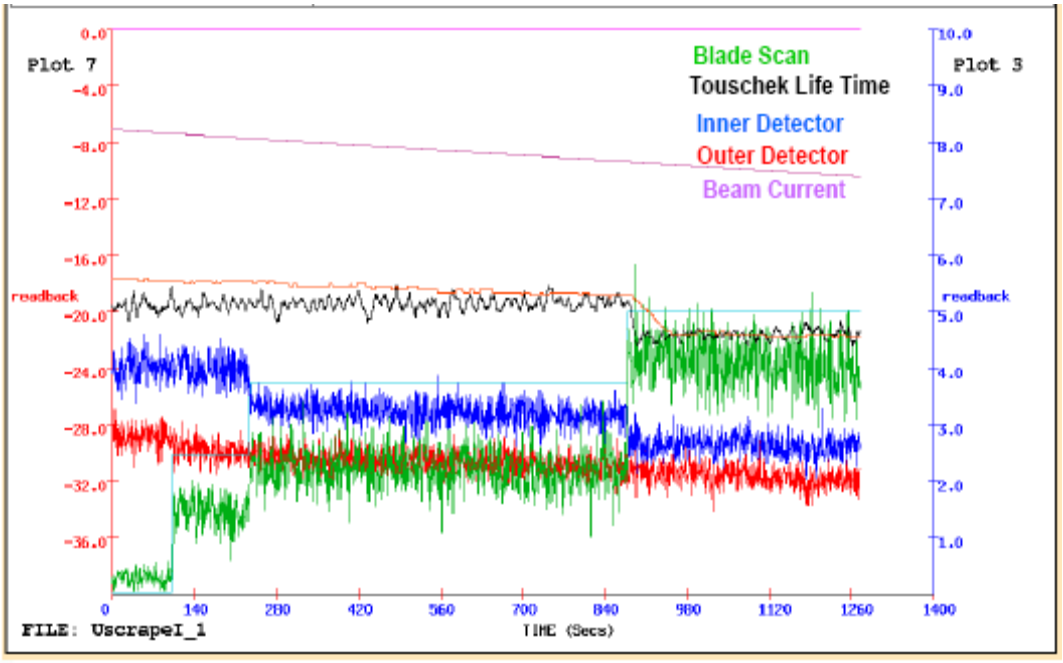

Fig.5 - Results of the Scraper Test Measurements at NSLS.

Fig.5 gives the results of the scraper test measurements at NSLS VUV ring. The installed horizontal scraper was of 7.5 mm thick copper. Its horizontal position with respect to the beam orbit can be controlled and read by an encoder. The plot shows the relative position of scraper with respect to the beam orbit. The plot also shows the corresponding Touschek life time of the beam. Two radiation detectors, one at the inboard and one at the outboard side of the beam orbit, were continuously monitoring the scattered electrons and photons as the scraper blade scan proceeded. The beam current was also monitored.

It was observed that as the scraper position was scanned, inserting it towards the beam orbit, the Touschek life time remained constant until a threshold position was reached. Beyond this threshold location, the scraper was cutting into the core of the beam, causing a decrease in the touschek life time. Both inner and outer orbit radiation detectors showed slight decrease in scattered radiation as the scraper was inserted towards the beam orbit, signaling a reduction in the scattered radiation due to beam interactions with the scraper. We conclude that this effect is due to electrons, which loose a fraction of their forward momentum due to interactions with scraper, tend to bend towards inward of the orbit to be stopped by the self shielded dipoles in the ring. The dipole yoke act as an effective beam dump absorbing the radiation. This causes a reduction in the radiation environment detected by the inner and outer Beam Loss Monitors.

4. Summary and Conclusions

Low-Z thin scrapers of less than one radiation length of thickness have several advantages over the high-Z thick scrapers. Most importantly they do not require additional local supplementary shielding inside or outside the storage ring. The small energy loss of the electrons due to interactions with the thin copper

scraper render them mostly in the forward direction and eventually get them dumped in the next dipole magnet in the ring. This causes low photon radiation exposure outside the storage ring shield wall with reduced transverse scattering of electrons and photons. Low-Z elements like copper, silicon etc. have low photoneutron production per primary electron resulting low neutron dose outside the storage ring shield wall. This effect must be verified by additional investigations.

Additional measurements are planned at the NSLS storage ring to further verify some of the observations of this paper

References

[1] National Synchrotron Light Source II Project, Preliminary Design Report, November 2007.
[2] FLUKA, A Multi-particle Transport Code, CERN Report 2005-010 (2005).
[3] National Synchrotron Light Source, Safety Assessment Document, BNL 49214-Rev002, March 1996.

Experiences from First Top-Off Injection At The Stanford Synchrotron Radiation Lightsource

J.M. Bauer, J.C. Liu, A.A. Prinz, and S.H. Rokni

Radiation Protection Department, SLAC National Accelerator Laboratory, Menlo Park, CA 94025, U.S.A.

Abstract

As the Stanford Synchrotron Radiation Lightsource (SSRL) of the SLAC National Accelerator Laboratory (SLAC) is moving toward Top-Off injection mode, SLAC's Radiation Protection Department is working with SSRL on minimizing the radiological hazards of this mode. One such hazard is radiation that is created inside the accelerator concrete enclosure by injected beam. Since during Top-Off injection the stoppers that would otherwise isolate the storage ring from the experimental area stay open, the stoppers no longer prevent such radiation from reaching the experimental area.

The level of this stray radiation was measured in April 2008 during the first Top-Off injection tests. They revealed radiation dose rates of up to 18 microSv/h (1.8 millirem/h) outside the experimental hutches, significantly higher than our goal of 1 microSv/h (0.1 millirem/h). Non-optimal injection increased the measured dose rates by a factor two. Further tests in 2008 indicated that subsequent improvements by SSRL to the injection system have reduced the dose rates to acceptable levels.

This presentation describes the studies performed before the Top-Off tests, the tests themselves and their major results (both under initial conditions and after improvements were implemented), and presents the controls being implemented for full and routine Top-Off injection.

1. Overview

1.1. Introduction to SSRL

The "Stanford Synchrotron Radiation Lightsource" (SSRL) evolved from the high-energy physics synchrotron "SPEAR" of the early 1970s and has by now been twice upgraded. The current storage ring, SPEAR3, is fed by a 10 Hz 150 MeV Linac and a Booster, which accelerates the electrons to 3 GeV before injecting them through the BTS line (Booster-To-SPEAR) into the SPEAR3 ring. The ring carries a current of 100 mA, and is typically refilled three times a day, each time from about 85 mA back up to 100 mA. Later this year SPEAR3 will run with a current of 500 mA, and injection will also soon be upgraded from currently 1.5 to 5 W maximal injection power. SPEAR3 is currently providing synchrotron radiation to 13 photon beamlines with about 30 experiment stations.

1.2. Motivation for and Modes of Top-Off Injection

Up to now, the Injection Stoppers (IS), which isolate the storage ring from the experimental area, are being closed for the time the storage ring is being filled. While this closing ensures that neither electrons nor Bremsstrahlung can reach the beamline hutches during injection, it also causes temperature changes at optical components, which results in alignment changes. At 100 mA these shifts are still small enough, but at higher currents they become disruptive. Fig.1 illustrates modes of operation for future 500 mA operation. If injection would be performed three times a day (top left of Fig.1), the changes in alignment throughout the day would be large. Raising the frequency of injection keeps the alignment more stable, because the intensity of the SR beam would stay more constant. The ultimate goal is trickle injection: Injection once a minute (bottom right of Fig.1). Such high injection frequency requires Injection Stoppers to stay open and requires good injector performance. It also leads to higher beam losses over time, since the stored beam current remains high, where the beam lifetimes are shortest. Note that other facilities adopted the term "top-up" for the same mode of operation.

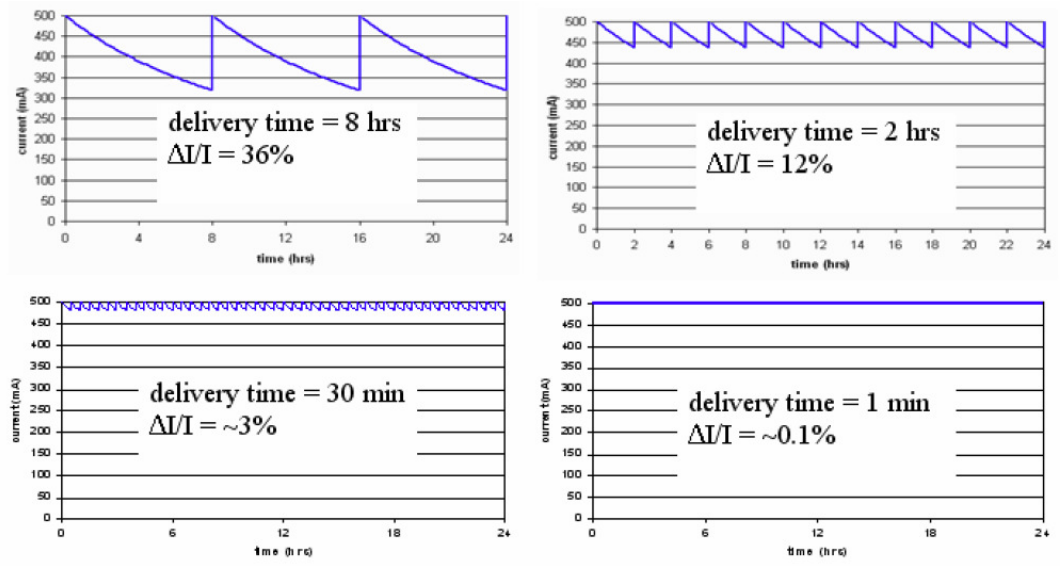

Fig.1 - Illustration of possible modes of operation throughout one day at 500 mA.

2. Preparing for Top-Off

2.1. SSRL/LBNL Ray Trace Studies

Since the beam chamber apertures and magnets constrain where beam can go and whether beam can be stored, SSRL, in collaboration with Lawrence Berkeley National Laboratory, performed a ray trace study to determine the limits on the magnet settings that ensure that injected beam will never make it past certain apertures ("safety endpoints") and hence never enter the experimental area [1]. These settings now serve as the basis for the envelope that the Top-Off Safety System is enforcing.

2.2. Radiological Considerations

During normal Top-Off operation, additional radiation can be expected from forward-angle Bremsstrahlung created when electrons from the injected beam hit apertures. This dose must be small enough that the experimental area sees not more than 1 mSv (100 mrem) in 1000 hours from all sources.
Additional radiation may be created by mis-steered beam, which is defined as beam that is not following its intended trajectory but is still within the bounds of the safety system, i.e., within the safety endpoints. Simulations estimate dose rates of up to 22 mSv/h (2.2 rem/h) at 5 W injection, but such serious mis-steering is expected to happen only very rarely, and radiation monitors will be in place to terminate injection if any radiation dose rate above 0.02 mSv/h (2 mrem/h) is detected.
The worst radiological consequences would be due to beam entering a beamline hutch, but such an event is very unlikely, as it requires several serious system failures and mis-steering at the same time. According to simulations, the dose rate could reach up to 3.3 Sv/h (330 rem/h) at 5 W injection, but with radiation monitors quickly shutting off injection on such high radiation (within ~1 second), the per-event dose is limited to 0.74 mSv (74 mrem) maximum.

2.3. Dose Components

The radiation detected at the outside of the hutch can be split into a total of four components, depending on (1) whether the radiation passes through the accelerator enclosure walls or enters the hutch through the beam pipe, followed by a scatter on the first optical element, and on (2) whether the radiation is created by stored beam or by injected beam. The components are accordingly labeled in the following way:

- D_{sw} – radiation from stored beam, passing through wall
- D_{sb} – radiation from stored beam, passing through beam pipe & scattering at 1st optical element
- D_{iw} – radiation from injected beam, passing through wall
- D_{ib} – radiation from injected beam, passing through beam pipe & scattering at 1st optical element

Only the last component, D_{ib}, is added when moving to Top-Off injection. All other components are already present in current operation.

2.4. Top-Off Safety Systems

Several of the safety systems being added at SPEAR3 for Top-Off are part of the so-called "Beam Containment System" (BCS):

- The Stored Current Interlock ensures that photon beamlines can open for Top-Off injection only with stored current above 50 mA. (This is important because the lattice necessary for successfully storing beam is unlikely to result in mis-steered injected beam.)
- The ring and BTS line apertures, which were part of the above-mentioned ray trace analysis, may not be modified without prior approval.
- Magnet Power Supply Interlocks prohibit Top-Off injection if the voltage or current at specific magnets are beyond specified limits.
- Clearing Magnets along dipole photon beamlines bend away any electron that would make it into the beamline.
- Radiation monitors stop Top-Off injection if they detect a dose rate above 0.02 mSv/h (2 mrem/h) outside the photon beamline (Dose Rate Interlock).

The other Top-Off safety systems are not part of the BCS:

- A Daily Dose Interlock is implemented through the radiation monitors, restricting the dose to maximal 0.01 mSv (1 mrem) per day.
- A Charge Loss Interlock similarly blocks Top-Off injection if more than a certain number of electrons are lost each day.

Present, but not counted as safety systems, are also Machine Protection System interlocks and tight software warnings. Note that the Top-Off safety system only inhibits Top-Off injection. Non-Top-Off injection, i.e., injection with Injection Stoppers closed, is not affected.

3. Beam Test Phase

3.1. Beam Conditions

Two major types of injection were studied during the tests: (1) High-Efficiency Injection, consisting of normal 1 W injection with about 60 to 80% injection efficiency. (2) Low-Efficiency Injection, during which the 1 W injection beam was intentionally mis-steered inside the BTS by modifying specific parameters. This created losses inside the SPEAR3 ring at apertures and lowered the injection efficiency to about 30 to 50%.

3.2. First Tests

The first set of Top-Off tests took place April to July 2008. Two types of detectors with remote readouts monitored radiation close to the hutches: The interlocked, SLAC-built Beam Shut-Off Ion Chambers (BSOIC); and the Beamline Radiation Monitors, HPI 6030 ion chambers with HPI 6012 readout modules. Since the Top-Off BCS did not yet exist at that time, access to the experimental area was restricted. Surveys were taken with handheld dose meters to determine the location of the highest radiation at the hutches.

Fig.2 illustrates a typical period of such tests for two photon beamlines, BL 5 (top) and BL 11 (bottom). The left half of each plot shows three high injection efficiency fillings to 100 mA (light blue lines with triangle shape). The measured radiation outside BL 5 (red) rose whenever the Injection Stoppers of that beamline were opened (indicated by green box-lines). Such behavior was not seen at BL 11 (pink line indicating the measured radiation, orange the stopper open/closed state). The data from low-efficiency injection are displayed in the right part of the plot. As expected, the time to reach 100 mA increased. The radiation reached higher levels at BL 5, and BL 11 also showed measureable radiation.

At other times during the tests, even higher radiation was seen than displayed in Fig.2: Up to 18 microSv/h (1.8 mrem/h) during high-efficiency injection, and up to 30 microSv/h (3 mrem/h) during low-efficiency injection, both at BL 5. The levels of radiation measured by the remotely read instruments were confirmed in field surveys.

The results fall into three major categories: Beamlines like BL5 with significant radiation during both high- and low-efficiency injection; beamlines like BL11 at which excess radiation was only measured during low-efficiency injection; and beamlines that did not display excess radiation in either situation.

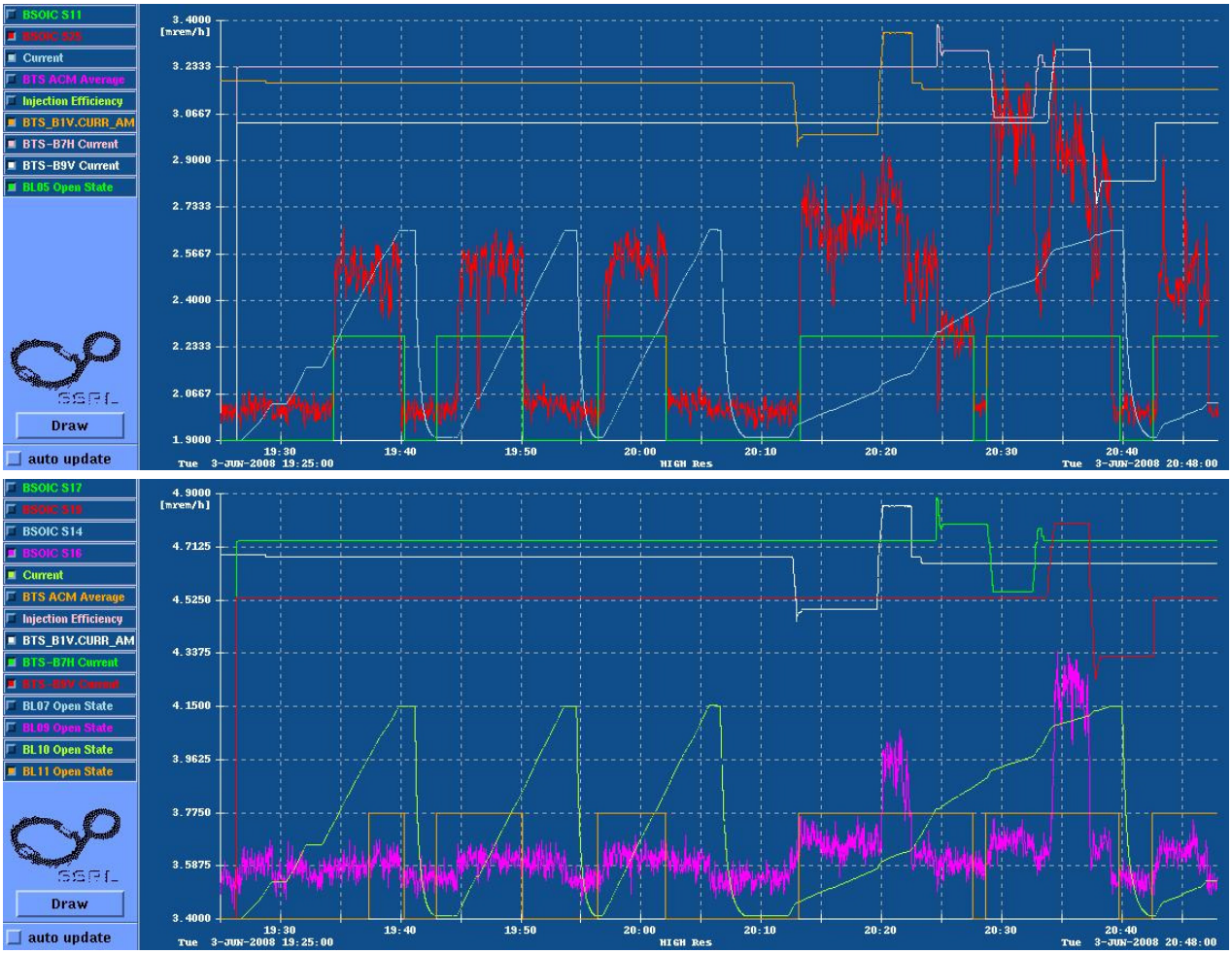

Fig.2 - Typical results from first Top-Off tests for BL 5 (top) and BL 11 (bottom). Three high-efficiency injections (left) were followed by one low-efficiency injection. The units on the vertical axis correspond to the radiation measurements of the BSOIC (red on top, pink on bottom).

Extrapolating the measured radiation to long-term operation at 100 mA, 200 mA and 500 mA trickle injection reveals that even for the worst beamline, BL 5, the total dose during 100 mA operation would lead to a dose on the order of only 190 microSv (19 mrem) in 1000 hours. At 500 mA trickle injection, however, the additional dose from component D_{ib} (the component special to Top-Off) can be up to 2.34 mSv (234 mrem) in 1000 hours. This clearly indicated a need to improve injection.
Of the other dose components, only D_{sb}, the dose from the stored beam's Gas Bremsstrahlung traveling through the beam pipe into the beamline hutch, was high with a maximum of 1.66 mSv (166 mrem) in 1000 hours of future 500 mA trickle injection operation. This dose is solely due to stored beam and does not increase during Top-Off injection. Additional shielding will be required for the beamlines with the highest values of D_{sb}.

3.3. SSRL Improvements to Injection

While the injection system was adequate up to now, Top-Off injection raised the bar, and SSRL responded. The effect of changes to the horizontal and vertical position and angle of the injected beam, to its energy and to its timing were studied. With new diagnostic devices, SSRL gained better control of the beam optics and lattice. During the Summer 2008 down-time, the last vacuum windows were removed from the BTS line, creating one single vacuum volume from the Linac all the way to SPEAR3. The simulations promised sufficient improvements (Fig.3).

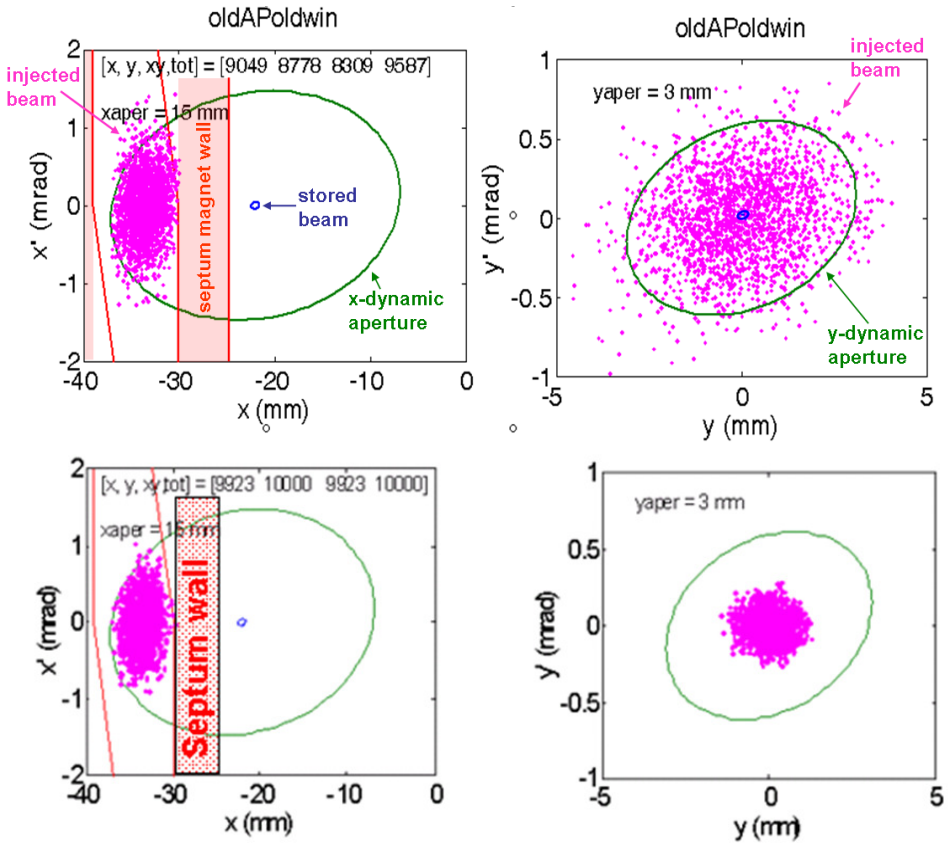

Fig.3 - Results of SSRL simulations studying the effect of the vacuum windows (top with windows, bottom without windows) on the x and x' (left) and the y and y' distributions of the injected beam. The plots indicated that removal of the windows leads to tighter focused beam.

3.4. Measurements with New Injection

In Fall 2008, the measurements of radiation during Top-Off were repeated with the improved injection beam. The dose rates were indeed found to be lower, about 10 times lower than before, with 1.6 microSv/h (0.16 mrem/h) now being the worst reading measured during high-efficiency injection. Extrapolating this worst dose rate to 1000 hours leads to an estimation of just 92 microSv (9.2 mrem) during 500 mA trickle injection operation.

Low-efficiency injection also showed much lower dose rates than before, only up to a maximum of 4.8 microSv/h (0.48 mrem/h). The 1000 hour dose comes still to 2.8 mSv (280 mrem), but prolonged operation in this mode would be untenable, since it would take 50 minutes to just add 100 mA to the stored current. The measurements with the new injection therefore cleared the way to Top-Off injection operation.

4. Summary of Test and Path Forward

The initial tests revealed that the long-term dose rate was of no concern for 100 mA Top-Off operation, but that improvements to the injection system were needed for higher currents. Once these improvements were in place, the system performed with radiation levels low enough that radiation can be expected to be within the limits even for 500 mA trickle injection.

Top-Off is scheduled to start in July 2009, first only for a few photon beamlines, others to be added in the coming months. Warning systems for injection beam lattice and optics, as well as Daily Dose Interlock and Charge Loss Interlock are expected to be in place for operation at higher currents. 500 mA operation is scheduled to start in Fall 2009. Additional shielding will be needed for some beamlines, not for Top-Off operation, but for radiation from Gas Bremsstrahlung created in stored beam operation, and a new safety system will lower the risk from thermal damage caused by the beam. And on the horizon, beyond 2009, are upgrades to trickle charge injection and to injection above 1.5 W in power.

5. Conclusion

After the first Top-Off tests measured higher dose rates than expected, SSRL improved the injection system such that the radiation during Top-Off injection is now projected to be low enough even for 500 mA trickle injection. Still, stored-current dose issues will need to be addressed for operation at more than 200 mA. Normal user runs will soon include Top-Off injection, and operation at higher currents will follow shortly thereafter, leading to a major improvement in the performance of SSRL.

References

[1] J. Safranek *et al.,* "SPEAR3 Accelerator physics update," PAC07-TUPMS055, SLAC-PUB-12949, Proceedings of Particle Accelerator Conference (PAC 07), Albuquerque, New Mexico, U.S.A., June 2007.

Top-Up at Diamond Light Source: preparation and initial practical experience

F. Burge and P. Bonner

Diamond Light Source Ltd., Harwell Science and Innovation Campus, Chilton, Didcot, UK, OX11 0DE

Abstract

Diamond Light Source is a 3 GeV electron storage ring, which has been successfully operating in top-up mode since October 2008, having previously operated in decay mode only. Although in the UK there is no legal requirement to submit a safety case to the relevant authority (the Health and Safety Executive) when implementing top-up operation for the first time, it is required to keep doses ALARP and within the 1 mSv annual dose limit which Diamond has set for all staff, users and visitors. Prior to operating Diamond in top-up mode, a study of the radiological safety implications was carried out to ensure that these requirements could be met. The study involved calculation using FLUKA of dose rates arising from accidental beam losses. These losses took the form of either continuous losses in a front end arising from poor injection, or loss of a single injected electron pulse into a beamline optics hutch. In addition to the calculations, dose rate measurements were made outside beamline hutches under conditions of deliberately engineered beam losses in front ends, intended to compare as closely as possible with those modelled. As a result of this study, a number of changes to Diamond's radiation monitoring regime were proposed and implemented before top-up operation was permitted. The study also helped to define the limits within which top-up would be permitted to operate.

1. Radiological hazards of Top-Up operation

Top-up operation introduces additional radiation hazards which are not present when injection takes place with shutters closed, as it exposes the beamlines to the injected electron beam and to the gamma and neutron radiation generated inside the storage ring during injection. Beam losses from top-up were not considered when the shielding for DLS was designed, so it was especially important to verify that the existing shielding was adequate to cope with the increased injection losses. The side wall of a typical optics hutch is constructed from 30 mm lead, which has been specified to protect against scattered gas bremsstrahlung and synchrotron radiation, not the high energy products of the initial scattering of an electron beam.

2. Modelling and Measurements

2.1. Beam loss scenarios

The results of electron tracking studies for top-up beam losses [1] led to three generic scenarios being considered for dose calculations using Fluka [2], [3].

- Electrons could be injected directly through the open shutters into the optics hutch of a beamline, scattering from the tungsten gas bremsstrahlung collimator and giving rise to elevated gamma and photoneutron doses outside the hutch.
- Injected electrons could reach and scatter from components in the Front End of a beamline. The cascade products would enter the optics hutch, and scatter from the gas bremsstrahlung collimator.
- Injected electrons could be lost in the storage ring (the expected location is the insertion device, as the aperture here is smallest) and the cascade products enter the optics hutch, where they scatter from the gas bremsstrahlung collimator.

For electrons to be injected directly into a beamline due to a single fault, the dipole immediately before the beamline must be at less than 20 % of nominal field. All 48 dipoles in the DLS storage ring are wired in series so this fault has a very low probability of occurring. There are more complex faults which could cause this type of loss, involving errors in multiple magnets combined with energy offsets between stored and injected beams. It has been shown that, although interlocks can be set to prevent such losses occurring continuously, they may not act quickly enough to prevent a single pulse from being injected into the storage ring and through an open beamline shutter.

Losses in the front end may occur under certain fault conditions which cannot be excluded by the stored beam and energy interlocks. The particle tracking studies showed that, depending on the design of the front end, electrons would either strike the first fixed aperture or pass through it and strike the vacuum vessel wall. No electrons reached the second limiting aperture. A combination of magnet and trajectory errors were required for electrons to be lost in this manner.

The third category of electron losses – those which occur continuously in the storage ring – will occur under normal operation in both decay and top-up modes. The difference in top-up mode is that it is injected electrons rather than stored beam which are lost.

2.2. FLUKA modelling

The FLUKA geometry model consisted of a section of ratchet wall and a generic optics hutch. Tracking studies [1] showed that beamline I20 has a front end acceptance closest to the beam centre line, and that if top-up is demonstrated to be 'safe' (in terms of injection directly into the hutch being impossible) for this beamline, all other beamlines will also be safe. I20 also has canted undulators. Since this reduces the amount of gas bremsstrahlung entering the optics hutch, the side walls are shielded with 22 mm lead rather than the 30 mm which is used on most of the existing DLS beamlines. It is therefore also a good beamline to use for radiation shielding calculations. The front end limiting apertures, which are copper absorbers, were modelled in a simplified form.

FLUKA was run for each beam loss scenario using 5 x 10^6 primary electrons per calculation cycle. Biasing techniques were used to reduce the run times and to increase the probability of photonuclear interactions. The results of 10 such cycles were used to determine the average dose and the statistical error. Doses were scored outside the side walls of the hutch, using rectangular 'bins' of size 10 cm x 10 cm x 10 cm. The scoring regions were set to cover the areas of interest and a range of ± 50 cm from beam height in the vertical direction. The scoring area was not extended outside the ratchet side walls of the storage ring, as the electron losses were not expected to significantly challenge the bulk storage ring shielding. For continuous losses in the storage ring, electron transport thresholds were set so that the primary electrons did not enter the hutch. In practice, this is achieved by the dipole magnet.

FLUKA scores particle fluence in the region of interest, and a user routine [4] containing fluence-to-dose conversion coefficients for the appropriate energy and particle type was used to convert to ambient dose equivalent, H*(10). In order to make a comparison with the measurements described in the following section, an electron loss rate of 5 mA min^{-1} was assumed in the calculation of dose rates. This is equivalent to a power loss of 0.47 W at 3 GeV, and is at least 100 times greater than the loss which would be expected in normal operation.

The loss of a single injected pulse of electrons on the gas bremsstrahlung collimator in the optics hutch resulted in maximum doses of 1.4 µSv nC^{-1} ± 8 % gamma, and 24 µSv nC^{-1} ± 0.6 % neutron outside the shielding, as shown in Figure 1. Typically, top-up will be operated with 0.1 nC per pulse. As discussed above, interlocks on stored beam and injected beam energy will prevent losses of more than one pulse of electrons in this manner.

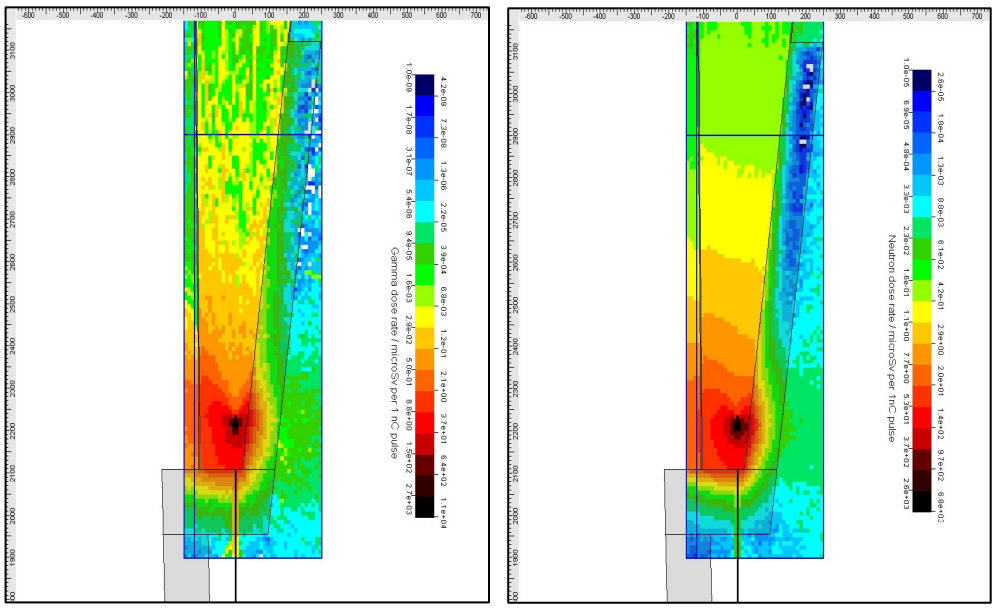

Fig.1 - Gamma and neutron dose rates from injection of single 1 nC electron pulse into beamline hutch.

Various possibilities exist for losses in the front end. Considering a loss at a grazing angle of 0.1° on the vacuum vessel between the first and second fixed apertures, maximum dose rates outside the hutch for a loss rate of 5 mA min^{-1} were 44 µSv h^{-1} ± 33 % gamma and 133 µSv h^{-1} ± 7 % neutron, as shown in Figure 2.

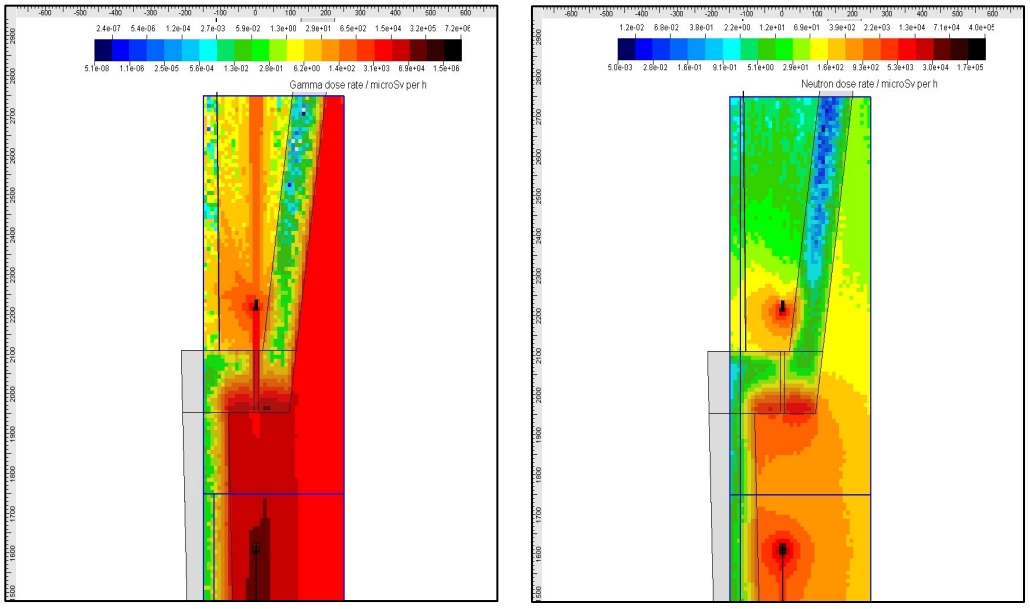

Fig.2 - Gamma and neutron dose rates from grazing incidence beam loss in front end.

Losses in the storage ring ID straight were modelled by considering a mis-steered electron beam striking the vacuum vessel at the location of the insertion device, 20 m upstream of the ratchet end wall. At a grazing angle of 0.1°, maximum dose rates outside the hutch for a loss rate of 5 mA min^{-1} were 45 µSv h^{-1} ± 50 % gamma and 56 µSv h^{-1} ± 8 % neutron, as shown in Figure 3.

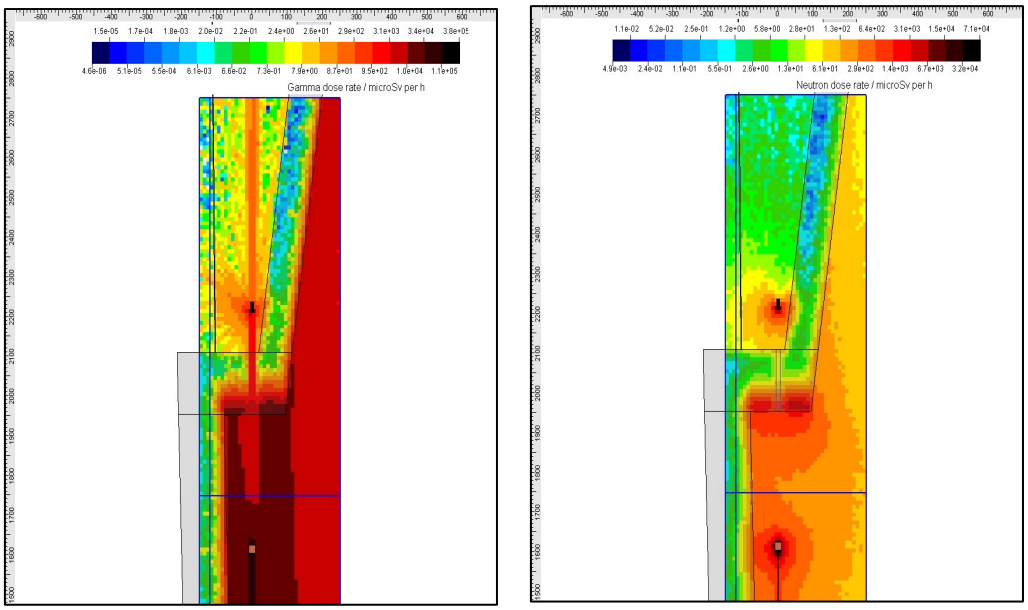

Fig.3 - Gamma and neutron dose rates from grazing incidence beam loss at insertion device.

Whilst there is nothing to prevent losses in the ID straight occurring at a shallow grazing angle, the tracking studies suggested that losses in the front end would actually be at grazing angles greater than 1°. Dose rates when the grazing angle is increased are significantly lower, as under these conditions most of the cascade is stopped by the ratchet end wall rather than entering the hutch through the beam port.

2.3. Measurements

As noted above, the continuous loss of injected electrons in the storage ring does not require fault conditions to occur. It was therefore possible to carry out a series of measurements in which these losses were arranged to take place preferentially at a nominated location in the ring. This was achieved by putting bumps on the injected beam as it passed through the machine cell of interest, which caused it to scrape somewhere upstream of the front end. With an injection rate of 10 mA to 20 mA per minute, it was assumed that up to 5 mA min^{-1} would be lost in the cell of interest. This was found to be the minimum loss which allowed dose rates above background to be detected outside the beamline. Gamma and neutron dose rate measurements were taken outside the hutches of all operational beamlines, using hand-held radiation monitors and also the neutron-sensitive Centronics IG5 ion chamber. Measurements were made with insertion devices fully out and at minimum gap. For all beamlines except I02, which is immediately downstream of the injection region, it was necessary to inject with no stored beam and lose the charge locally. For I02, it was possible to set up poor injection on top of a stored beam.

Typical measured dose rates on insertion device (ID) beamlines were less than 1 µSv h^{-1} gamma and less than 10 µSv h^{-1} neutron. No significant difference was found between different ID beamlines, and it did not appear to matter whether the ID gap was open or closed. A ‘hot spot’ on the hutch wall opposite the gas bremsstrahlung collimator was identified as scattered solid target bremsstrahlung, as gas bremsstrahlung will pass through the collimator and scatter from the first optical element. Later tests without beam bumps confirmed this. Slightly elevated dose rates were also measured along the storage ring ratchet wall, next to the insertion device. At the time of the measurements, only one dipole beamline, B16, was operational. On this beamline, radiation measurements detected no evidence of the beam losses taking place near the dipole.

3. Conclusions

3.1. Analysis of measurement and model results

It was not possible to quantify precisely the beam loss location and angle used for the measurements, which meant that a direct comparison with the results of the Fluka calculations was of limited value. The dose rates predicted by the model tend to be higher than those which are observed. This is possibly because the local

electron losses during the measurements were not as great as had been assumed, or because the simple geometry of the model does not include many large machine components between the scattering point and the ratchet wall aperture which can intercept the shower of scattered radiation prior to it reaching the beamline.

On this basis, it was concluded that the model represented the worst case dose rates which would be observed during poor top-up injection. It was apparent from both measurements and modelling that neutrons would be the dominant factor in dose rates outside the beamline. Consequently, the IG1 gamma ion chambers which had been initially installed on beamlines were replaced with IG5 neutron-sensitive chambers. These chambers were tested inside the linac vault to ensure that they responded in a pulsed radiation field. The identification of 'hot spots' led to some installed monitors being re-located, and an increased number of moderated TLDs have been included in the existing environmental dosimetry programme around the beamlines.

Given that the loss rates assumed for the measurements and the modelling are artificially high, it can be concluded that none of the beam loss scenarios considered above will result in dose rates which are a cause for concern outside the beamline hutches.

3.2. Changes to hardware interlocks and software limits

In order to prevent the accident scenarios discussed in this paper, a number of additional hardware interlocks were implemented in the Personnel Safety System (PSS):

- A 'top-up key' must be turned in the machine control panel before top-up injection can commence.
- A stored beam in excess of 50 mA is required before top-up injection can start, as an inability to store beam is indicative of dipole failure. This interlock was over-ridden for the top-up measurements, where injection took place without stored beam.
- The storage ring dipole current must be within ± 1 % of its nominal value before top-up injection can start.
- The current in dipoles 2 and 3 of the booster-to-storage ring (BTS) transfer line must be within ± 1 % of nominal. This sets limits on injected beam energy within ± 5 %, and ensures that injected electrons cannot be transmitted directly into a beamline optics hutch.

To support the hardware interlocks, and act as an early warning of potential fault conditions, a set of software limits have also been implemented in the top-up control program. These are designed to inhibit injection if stored beam does not exist or if its lifetime is too low, if the storage ring injection efficiency is too low, or if the storage ring or BTS dipole currents are out of range. These limits should prevent excessive loss of injected beam in the storage ring or front ends.

3.3. Installed radiation monitors

The installed radiation monitors are part of the PSS and will close shutters or dump the beam if they detect elevated levels of radiation. Until top-up operation was implemented, the monitors had been set to alarm based on dose rate, with a threshold of 4 $\mu Sv\ h^{-1}$. For top-up, an alarm on integrated dose was introduced (whilst maintaining the dose rate alarm), which sets a limit of 2 μSv per 4 hour period. In the event that this limit is exceeded, injection is inhibited for the remainder of the 4 hour period, and the machine goes into decay mode operation. The machine operator receives a warning when the monitors are approaching their integrated dose threshold, which allows them to take preventative measures.

Practical experience to date has revealed instantaneous dose rates up to 15 $\mu Sv\ h^{-1}$, but only during the brief injection periods. The integrated dose threshold has never been reached during user beam shifts, and has only been approached closely during certain periods of machine development work when there may be unusual injection patterns.

4. Current operation and future work

As of June 2009, DLS has been operating in top-up mode with a maximum stored beam of 250 mA. Injection takes place every 10 minutes, maintaining a stored beam current between 248 mA and 250 mA.

A separate top-up related issue regards increased losses in the storage ring itself and in particular concerns about possible radiation damage to insertion devices. Efforts are therefore being made to understand and reduce beam losses at the insertion devices. Some experiments have also been carried out with TLDs to help in quantifying the doses delivered, although with the majority of insertion devices being in-vacuum, this makes it difficult to relate the measured dose to that received by the magnetic arrays.

Developments in other areas at DLS will see the commissioning of four more beamlines and the completion of an RF cavity test facility by the end of 2009. The stored beam will also be increased to reach the design current of 300 mA once both RF cavities are fully conditioned.

References

[1] I.P.S. Martin, C.P. Bailey, R. Bartolini, E.C. Longhi and R.P. Walker, "Top-Up Safety Simulations for the Diamond Storage Ring ", Proceedings of EPAC08, Genoa, WEPC044, 2085-2087 (2008).

[2] A. Fassò, A. Ferrrari, J. Ranft and P.R. Sala, "FLUKA: a multi-particle transport code", CERN-2005-10, INFN/TC_05/11, SLAC-R-773 (2005)

[3] G. Battistoni, S. Muraro, P.R. Sala, F. Cerutti, A. Ferrari, S. Roesler, A. Fassò and J. Ranft, "The FLUKA code: Description and benchmarking", Proceedings of the Hadronic Shower Simulation Workshop (2006)

[4] S. Roesler and G.R. Stevenson. "Deq99.f – A FLUKA user-routing converting fluence into effective dose and ambient dose equivalent", CERN-SC-2006-070-RP-TN (2006)

Radiation Safety Considerations for the TPS Accelerators

R.J. Sheu, J. Liu, and J.P. Wang

National Synchrotron Radiation Research Center, 101 Hsin-Ann Road, Hsinchu Science Park, Hsinchu 30076, TAIWAN

Abstract

This study investigates the characteristics of prompt radiation field and some issues of induced activities due to the operation of the Taiwan Photon Source (TPS). Starting from assumed beam loss scenarios and using the FLUKA Monte Carlo simulations, energy spectra and dose distributions of the prompt radiation field for its shielding design were studied. Radiation environment around the penetrations on shielding walls were also taken into account. As to the impact of induced radioactivity, we also used the FLUKA to evaluate the residual activities, remanent dose rates, and their time behaviors for various target materials and cooling times based on conservative irradiation conditions. The paper summarizes the present status of the radiation safety evaluation for the TPS accelerators.

1. Introduction

The Taiwan Photon Source (TPS) in National Synchrotron Radiation Research Center (NSRRC) will be a 3 GeV light source with a circumference of 518.4 m and operating fully at 400 mA in top-up mode, aiming to provide synchrotron light with extremely high brilliance and low emittance of less than 2 nm-rad [1]. It is now approaching its final design and will start civil construction by the end of this year. In addition to its main body of a 3-GeV electron storage ring, the accelerator complex includes a 150-MeV LINAC and a large 3-GeV concentric booster. Significant amount of radiation will be produced due to the loss of such high-energy electrons and result in radiation safety concerns. Generally, four kinds of radiation sources originating from the operation of a synchrotron accelerator should be considered – bremsstrahlung, neutrons, induced activation and synchrotron light. The former three forms of radiation sources result from interactions between lost electrons and accelerator components or walls. Electrons of greater energies interact with matter and cause an electromagnetic cascade [2]. The resultant copious bremsstrahlung photons with a broad energy spectrum tend to be forward-peaked and are the primary target for shielding design. Neutrons are produced by photonuclear interactions from high-energy gamma rays; although neutrons are much fewer and lack a strong directional dependence. Shielding against them is also an important part of the shielding design due to their strong penetration of matter. Induced activation can be found in accelerator components when exposed to highly intense radiation. The susceptibility to activation is dependent on the energy and power of the incoming radiation as well as target material. As to the radiation protection against synchrotron radiation, due to the complex combination of synchrotron source, beamline configuration and optical design, shielding design will be conducted separately according to the distinct characteristic of each beamline and will not included in this paper.

The design objective of radiation safety system is to minimize the hazards arising from these sources. Fig.1 is a portion of the TPS layout showing the main accelerator components and its bulk shielding configuration [1]. Its basic structure consists of a ratchet style shielding for the outer wall of the storage ring and shielded labyrinths in the inner shielding wall for mainly personnel access. The 150-MeV LINAC will be housed in an independent room with 1 m thick concrete shielding. Both the storage ring and concentric booster will be installed in a shared tunnel made of 1 m thick concrete walls and removable roof. The shielding in the injection area and ratchet end walls will be at least 1.2 m thick concrete. This study aims to evaluate the general characteristics of prompt radiation field outside the bulk shielding and radiation streaming through some penetrations, as well as possible impact from induced radioactivities due to the TPS operation.

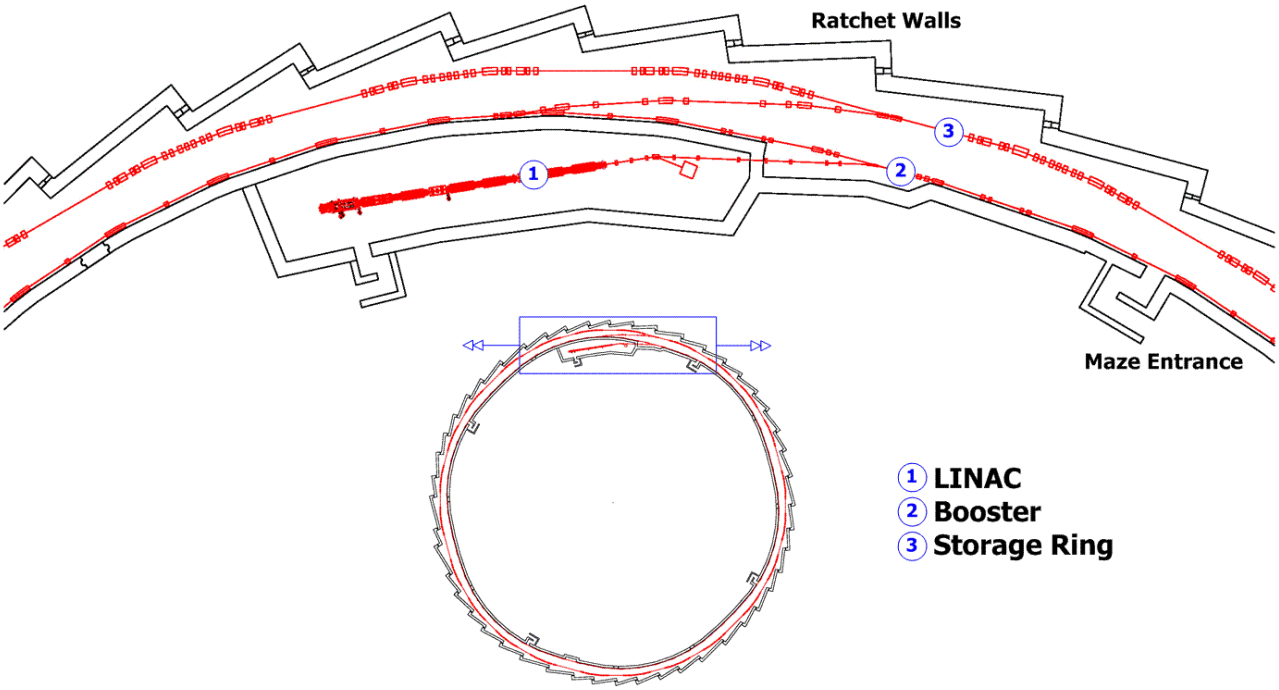

Fig.1 - A schematic layout of the main accelerator components and shielding design of the TPS.

2. Materials and Methods

2.1. Design Dose Limits and Beam Loss Analysis

In Taiwan, the Atomic Energy Council has established dose limits as basic guidelines for radiation protection. For radiation workers, the annual effective dose should not exceed 50 mSv and the accumulated dose should not exceed 100 mSv for five consecutive years. In addition, the dose limit for both non-radiation workers and the general public off site is 1 mSv per year. To comply with ALARA principle and recommendations from similar facilities, we have decided to accept a more challenging dose limits for the TPS of 1 mSv/y for all staff and users who are working 2000 hours a year and an environmental dose of 0.5 mSv/y at site boundaries for operating 6000 hours a year. These design limits guide shielding requirements and the design of radiation safety program and systems.

Beam loss analysis is crucial for the shielding design of an accelerator facility. All electrons generated from the gun filament, accelerated by the LINAC and booster, transferred by transport lines, and finally injected into the storage ring are eventually lost somewhere along the orbit. To facilitate the evaluation of possible beam losses, we have logically divided the electron trajectory into the following accelerator sections: GUN → LINAC → LTB → Booster → BTS → Storage Ring, where LTB is the transport section from LINAC to booster, and BTS is referring to that from booster to storage ring. Based on the design specifications of TPS and through operation experience with the existing Taiwan Light Source (TLS), our accelerator physicists have determined a relatively conservative assumption about the beam transfer efficiencies between these accelerator sections as shown in Fig. 2. The overall beam transfer efficiency from LINAC to storage ring is about 48% and 73% from booster to storage ring. Our assumed numbers are slightly more conservative than those of the SLS [3], which is the first light source featuring a concentric booster design and full-time top-up operation. This comparison is reasonable and instructive since we have adopted the same concept of accelerator design. The max LINAC output is about 2.25 W and the minimum lifetime for 400 mA stored beam is 7 hours. It is clear that this is not a worse-case beam loss; this is an assumed beam loss scenario under normal operating conditions. Based on this reference beam loss, we also have defined a more conservative operation envelope to ensure the safety envelope, i.e. the design limits, will not be exceeded.

Under normal operating conditions, total electron loss rates occurring in the shared tunnel were estimated to be about 2.43×10^{10} and 1.71×10^{8} electrons per second during beam injection and storage periods, respectively. To estimate the total number of electron losses per year, we have conservatively assumed 6000 hours of operation in 300 days. For each daily operation of the TPS, the storage ring is started by a fresh

injection to its maximum current, immediately followed by 20 hours of top-up operation, and finally terminated by dumping the beam. Then, annual summation of electron losses due to the operation of TPS has been estimated to be 7.71×10^{15} electrons per year. To specify the operational boundary conditions, we have defined envelope conditions for abnormal operation by increasing the maximal electron loss rate at each stage to five times the quota under normal condition [1].

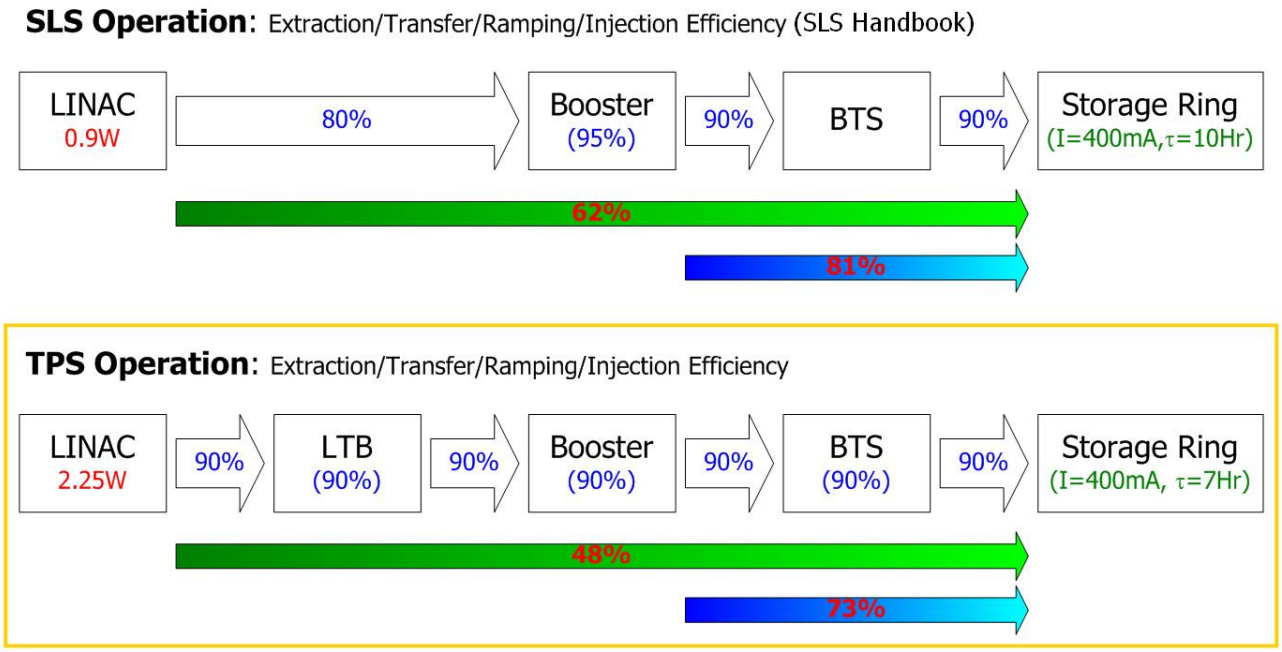

Fig.2 - Comparison of beam transfer efficiencies between main accelerator components of the SLS and TPS.

2.2. Calculation Methods

In this study, two extreme beam loss cases are assumed to bound the possible beam loss scenarios occurring in the shared tunnel, i.e. all electrons are lost at one point or they are lost uniformly along the electron orbit [4]. A high-energy electron accelerator is a very complex device containing many components. For point and uniform beam loss models, the geometries of the TPS accelerators and shared tunnel have been greatly simplified to facilitate the simulation. The point beam loss model is the worst case of beam loss for radiation protection in accelerators. Comparing with the worst case of point beam loss, we consider uniform beam loss around the booster or storage ring should be more realistic for long-term dose evaluation since most of the hot spots could be easily compensated by local shielding arrangement. When the TPS LINAC operates in stand-alone mode, all accelerated electrons from the output of the last section have to be absorbed by a dedicated beam dump. Our beam dump is the same design as that in the NSLS-II [5] which is a three-layer cylinder with an iron target inside and wrapped with 15 cm thick lead and 20 cm thick polyethylene in both lateral and forward direction. We have used the FLUKA Monte Carlo code [6] to simulate the high-energy electron induced electromagnetic cascade and the subsequent photonuclear reactions to calculate the energy spectra and dose distributions of those secondary particles, including gamma rays, neutrons and muons. FLUKA is not only a particle transport and interaction Monte Carlo code but also, with recent development, an integrated code for the buildup and decay of produced radioisotopes. Calculations of induced radioactivities and their time evolution as well as tracking of emitted radiation from unstable residual nuclei can be performed together and on-line with radiation transport.

3. Results and Discussion

3.1. Prompt Radiation

Energy spectra and dose distributions of the prompt radiation field outside the bulk shielding of the TPS have been investigated using the FLUKA Monte Carlo simulations. First of all, for a 2.25 W LINAC beam power during stand-alone operation, dose rates outside the independent LINAC room should be within the range between 0.1 and 83 μSv/h in forward directions and between 1.1 and 14 μSv/h in lateral directions. The

minimal and maximal bounds of the dose ranges are estimated by considering the scenarios of how and where the beam is lost during LINAC operation: electrons impinge on our well-shielded beam dump or electrons unexpectedly hit a target without any local shielding. Regarding the possible dose rates outside the shared tunnel due to the operation of booster and/or storage ring, proper modeling of the beam loss in the TPS tunnel is the first step and of most importance to dose estimation. Energy spectra of secondary particles outside the bulk shielding reveal that, because of thick concrete shielding, the dose contributions from photon and neutron components outside the lateral wall of the TPS tunnel are roughly comparable. Muon contribution is negligible. For an event of full beam loss, the estimated doses outside the lateral shielding wall are about 12 and 0.2 μSv per event for point and uniform loss scenarios, respectively. During the beam injection period, the maximal dose rates in the experimental hall have been estimated to be about 128 and 3.4 μSv/h corresponding to point and uniform beam losses. On the other hand, during the beam storage period, the maximal dose rates of decay loss will be about 1.7 and 0.02 μSv/h corresponding to point and uniform beam losses. As stated in Section 2.2, those dose rates corresponding to the uniform beam loss model or with local shielding are considered to be more realistic in the long term. Taking into account reasonable use and occupancy factors, these estimated dose rates enhance our confidence in achieving the design dose limit of 1 mSv/y for staff and users working 2000 hours in the TPS.

According to the conservative estimates of annual beam loss and calculated dose distribution, annual dose assessment as a function of distance can be derived and the results are shown in Fig. 3. Two distances shown in Fig. 3 are of particular interest, i.e. 2 m and 43.8 m, corresponding to the locations near the surface of outer shielding wall and at the nearest site boundary of the TPS, respectively. Under normal operation conditions, the maximal annual dose in the experimental hall of TPS is estimated to be 0.44 mSv/y and the total dose at the nearest site boundary is only about 14 μSv/y. For the worst operation case before interlock system to intervene, i.e. our operation envelope, the maximal annual dose in the experimental hall may increase to 2.2 mSv/y and the total dose at the nearest site boundary will then be roughly 70 μSv/y. The possible doses at the nearest site boundary due to the TPS operation are apparently far below the environmental dose limit of 0.5 mSv/y, i.e. 500 μSv/y. On the other hand, the maximal dose of 2.2 mSv/y in the experimental hall is obtained based on the condition of 6000-h operation; therefore the expected personnel dose for 2000-h working time should be less than 0.73 mSv/y and that is also within our design limit of 1 mSv/y. The dose assessment confirms that the present shielding and interlock design should be able to provide enough protection for ensuring the safety envelope of TPS operation including normal and abnormal conditions.

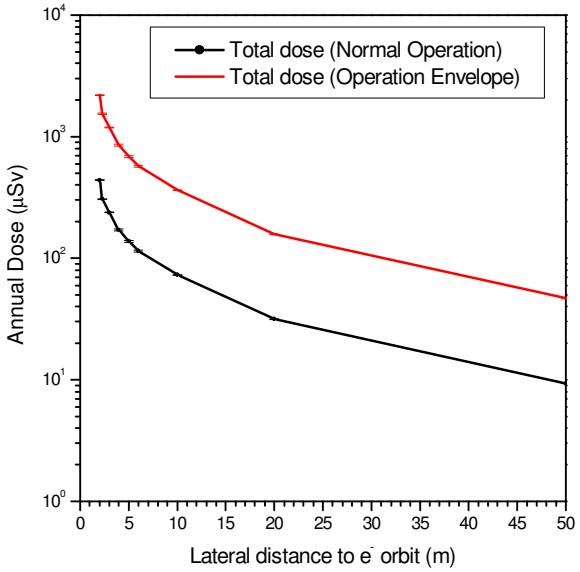

Fig.3 - Annual dose assessment for the TPS operation.

3.2. Radiation through Penetrations

Based on the assumed beam loss scenarios, the above results indicate that our bulk shielding arrangement for the TPS accelerators should be highly practicable to achieve its annual dose limit. However, in reality, no practical accelerator shielding can be constructed perfectly intact without penetrations for the access of personnel and supporting utilities. Compared to the relatively thick shielding walls, radiation streaming through those penetrations should be more carefully evaluated because they undermine the integrity of bulk shielding. In this section, we consider three kinds of penetrations around the inner shielding walls of the TPS including labyrinths for personnel entrance, air-conditioning ducts and underground trenches. For more detailed layout and dimensions please refer to our design handbook [1]. We carried out the FLUKA Monte Carlo simulations to investigate the design in detail and to understand the radiation field around those penetrations. To justify the maze design, we need to compare the doses outside those penetrations with a reference value, which has been reasonably chosen to be the dose outside an intact shielding wall.

First, according to the layout of the TPS shielding as shown in Fig. 1, a total of five maze entrances have been allocated along the inner shielding walls of the TPS mainly for personnel access, four standard-sized mazes for the long shared tunnel and a small one for the independent LINAC room. They are all typical four-legged maze design. Figs. 4(a) and 4(b) show the calculated dose distributions around the maze, the total dose at the maze exit is about 90% of the reference value for a storage ring beam loss scenario and meets our design goal without question. When considering a booster beam loss occurred near the maze mouth, the total dose at the maze exit increases to about 40% higher than that of the reference. This modest increase does not pose serious concern for radiation safety in practical situations and should be acceptable since our machine physicists do not expect significant full-energy beam losses in those regions during booster operation. Energy spectrum scoring also indicates that thermal neutrons resulting from multiple scatterings and streaming through the maze are the most evident portion of dose contribution at the maze exit.

In addition to the maze entrances, there are also 24 ducts on the upper part of inner shielding walls for air-conditioning piping and 96 underground trenches for the connection between accelerators and supporting utilities. Figs. 4(c) and 4(d) show the predicted radiation environment around the TPS tunnel with respect to the beam losses occurred in the storage ring and booster, respectively. The shielding design for the air duct appears to be acceptable since, in both cases, the doses at the duct outlet and its neighborhood are all comparable to or well below the reference dose outside the shielding. The calculated dose at the duct outlet for a storage ring beam loss is about 80% of the reference value and further drops to only 10% of the reference value for a booster beam loss. In contrast, the trench arrangement is not ideal in terms of radiation safety. The dose at the exit of the trench for a storage ring beam loss is then 70% higher than the reference dose and, more severely, the dose at trench exit for a booster beam loss is much higher than the reference by an order of magnitude. As to the dose contribution, no matter the air ducts or underground trenches, the neutron component is always the dominant one to the total dose at the exits similar to that of the above personnel mazes. To further reduce the dose, radiation protection in the neighborhood of the trench exits will be enhanced by local shielding after all necessary cable and piping are settled down. In fact, all the exits of the air ducts and trenches of the TPS tunnel will be located inside 24 nearby rooms called the Control Interface Area (CIA). All the CIA rooms locating along the inner shielding walls of the TPS tunnel will be radiation control area with limited access to authorized staff. Taking into account the shielding enhancement and limited occupancy factor, we are confident to make sure our design dose limit in these CIAs will be met even with all these penetrations on the TPS bulk shielding.

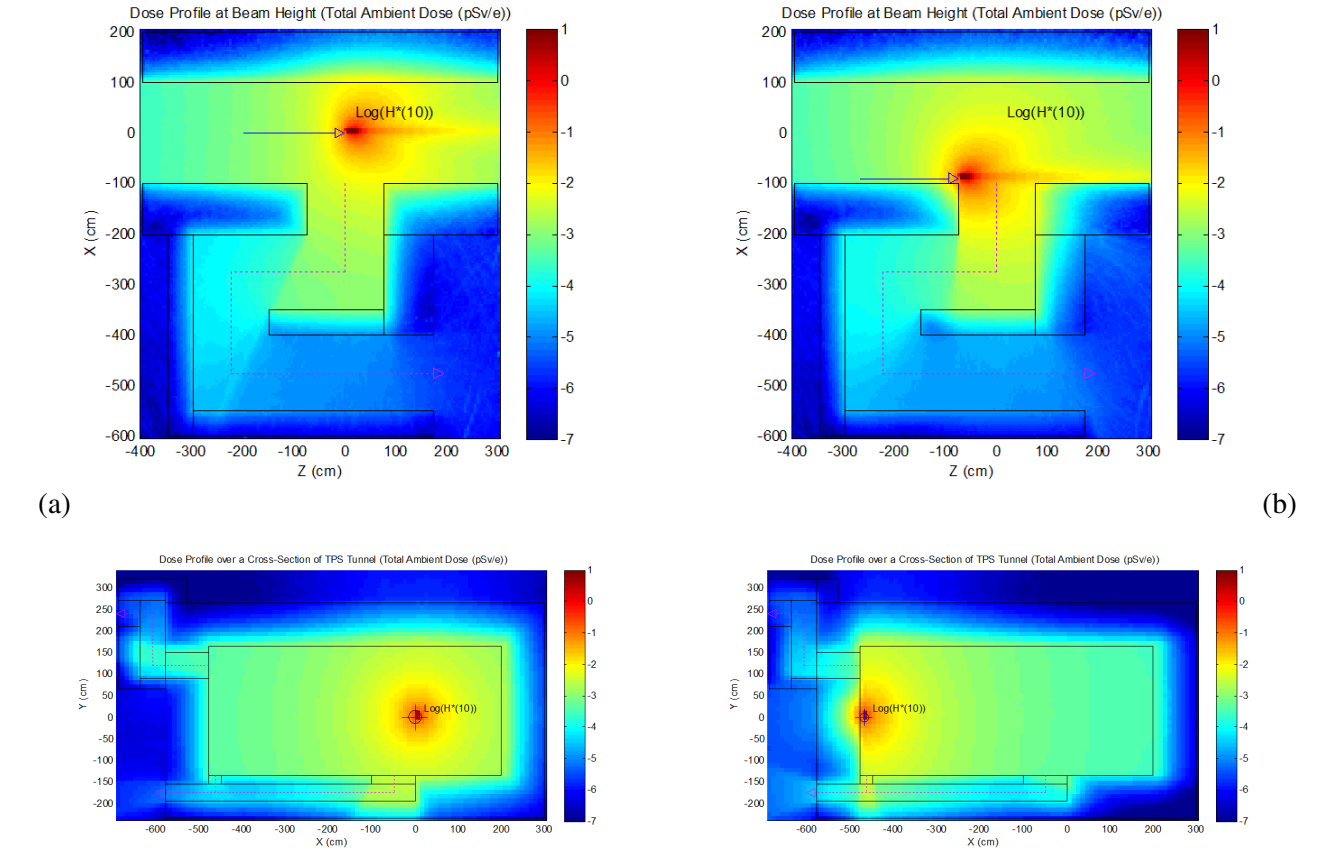

Fig.4 - Dose distributions around TPS penetrations including personnel maze, air-conditioning ducts and underground trenches for the storage ring and booster beam losses.

3.3. Induced Radioactivity

Radioactivity may be induced in various accelerator components and its surroundings when irradiated by a high-energy electron beam directly or exposed to the secondary radiation fields. At the TPS facility, the potential materials to be activated are aluminum, iron, copper, tungsten, and lead. In addition, the concrete shielding housing the accelerator, the air and cooling water inside the tunnel may also become activated due to high-energy bremsstrahlung and its subsequent neutron interactions. They present an additional hazard that needs to be carefully analyzed and managed. Our estimations of induced radioactivity and remanent dose rates in these materials are based on the direct FLUKA calculations. When it is available, the FLUKA-calculated results are compared with those listed in the well-known IAEA-188 report [2] for verification and validation. Two extreme irradiation conditions for the TPS operation are assumed to investigate the possible impact. One case (case 1) is a long-term continuous irradiation by an average low-power beam loss of 7.71×10^{15} electrons per year (~0.12W) and the other case (case 2) is a short irradiation period by an intense full injection power of 4.48×10^{10} electrons per second (~21.5W). The first condition corresponds to the irradiation situation of a 20-year operation during TPS lifetime and the second condition intends to simulate a possible irradiation event of a 1-hour beam loss during injection difficulty. This section briefly presents the results of our activation analyses; the TPS design handbook can be consulted for details [1].

Using the FLUKA Monte Carlo calculation, we can obtain the production rates of all radionuclides in an irradiated material. Depending on many factors, the production rates are quite different from isotope to isotope. Having the production rate and half-life of each isotope, FLUKA can further predict the time behaviour of each isotope during beam irradiation and after shutdown. Radioactivity builds up during the accelerator operation. When operations stop, there is a rapid decay of short-lived isotopes. After that, only median- and long-lived isotopes remain. The time evolution of residual radionuclides strongly depends on the irradiation profile. Figs. 5(a) and 5(b) show the time evolution of the maximal specific activities inside various targets for the case (1) and (2) irradiation conditions respectively. For case (1) 20-year operation, some long-lived radionuclides have the opportunity to build up and play an important role after the shutdown

of machine. For case (2) 1-hour high-power irradiation, the maximal residual activities in targets are obviously higher than those in case (1), but they decay quickly after shutdown since only short-lived radionuclides are dominantly produced and accumulated. It is evident that, among these materials, aluminum is the most preferred and tungsten is more susceptible to activation. Lead and copper are roughly the same degree of susceptibility to be activated.

Electrons, positrons, X-rays or gamma rays emitted from the decay of radionuclides result in remnant dose around an activated component. They may pose a possible radiation hazard to the workers nearby during a maintenance period after machine shutdown. Figs. 5(c) and 5(d) show the decay of the residual dose rates at 1m away from various targets for the same case (1) and (2) irradiations respectively. As expected, the initial residual doses for the case (2) irradiation are much higher than those for the case (1), but concurrently they undergo a much faster decay due to the dominance of short half-lived isotopes in this case. Since most radionuclides are produced in a certain depth below the surface of the target. Due to the self-shielding effect of target material, the remnant dose rates in either case is not very high and should only have moderate impact on the staff working nearby during a maintenance period.

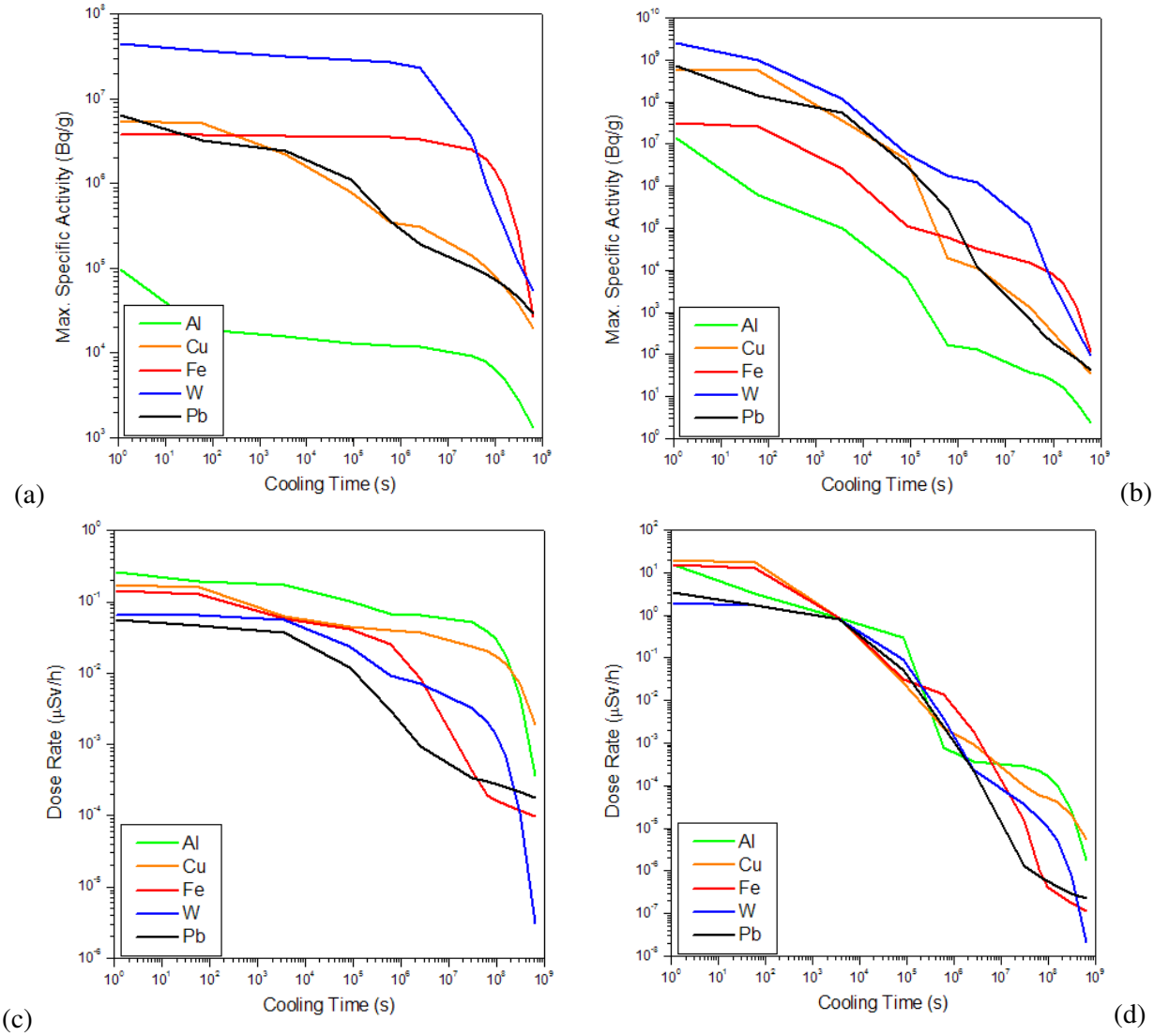

Fig.5 - Time evolution of the maximal specific activities inside various targets and the remanent dose rates at 1m away from targets for Case (1) and (2) irradiations respectively.

Although the potential for activation in bulk shielding should be limited at an electron accelerator, since most of the beam energy is absorbed by components such as magnets, absorbers or local shielding. It is deemed desirable to evaluate the degree of activation of the concrete shielding wall and to determine whether it is a radioactive waste or not. Following the same methodology, we have performed a residual activity zoning study for a concrete silo where an iron target is located inside and bombarded by 3-GeV electron beam. Our

results indicate that the massive concrete block used in bulk shielding can be treated as a general waste without further storage for cooling [1]. Considering the impact of possible environmental release, the activation of air and cooling water in the accelerator tunnel should be evaluated cautiously. Taking into account the material compositions, reaction cross sections, and the half-lives of the radionuclides produced, it is seen that ^{13}N and ^{15}O produced by the $^{14}N(\gamma,n)^{13}N$ and $^{16}O(\gamma,n)^{15}O$ reactions in air and water are the radioisotopes of most importance [2]. Based on the current estimates, even considering the maximal injection power loss (~21.5W) in the tunnel, the possible concentrations of ^{13}N and ^{15}O in the air and cooling water inside the tunnel are well below the AEC exemption limit of 100 Bq/g for these two radionuclides.

4. Concluding Remarks

Prompt radiation fields and induced radioactivity due to the operations of TPS accelerators have been investigated using the FLUKA Monte Carlo simulations. Based on conservative and representative beam loss scenarios, radiation levels outside the bulk shielding and radiation streaming through penetrations on shielding walls were evaluated. The results demonstrate that the basic shielding design of the TPS is highly feasible and the 1 mSv/y design dose limit for staff and users should be practicably achievable. Meanwhile, the environmental dose at the nearest site boundary is also far below the regulatory requirement with comfortable margin. In addition to prompt radiation hazards, the design and operation of the TPS accelerators also requires a careful assessment and planning for the radioactivity induced around the facility. Our calculated results lead to the conclusion that the TPS is a fairly low electron consumption synchrotron light source; therefore radioactivities induced in accelerator components and surrounding concrete walls are rather moderate and manageable; and possible activation of air and cooling water and their environmental releases should be negligible.

References

[1] NSRRC, “Taiwan Photon Source (TPS) Design Handbook”, National Synchrotron Radiation Research Center, January 2009.

[2] W.P. Swanson, “Radiological Safety Aspects of the Operation of Electron Linear Accelerators”, Technical Report Series No. 188, International Atomic Energy Agency (1979).

[3] SLS, “Safety Report about the Swiss Light Source”, SLS Handbook, Chapter 9, Paul Scherrer Institute (1997).

[4] R.J. Sheu, J. Liu, J.P. Wang, K.K. Lin, G.H. Luo, “Characteristic of prompt radiation field and shielding design for Taiwan Photon Source”, ICRS-11/RPSD-2008, Pine Mountain, GA, USA, Apr. 13-18, 2008.

[5] BNL, “Preliminary Design Report of National Synchrotron Light Source II”, Brookhaven National Laboratory (2007).

[6] A. Ferrari, P.R. Sala, A. Fassò, J. Ranft, “FLUKA: a Multi-particle Transport Code”, CERN 2005-10, INFN/TC_05/11, SLAC-R-773 (2005).

Shielding Design of the SPring-8 XFEL Facility

Yoshihiro Asano[1]

[1]*XFEL Project Riken/SPring-8 1-1 Koto Sayo Hyogo 679-5148, Japan*

Abstract

Shielding design of the 8 GeV class X-ray Free Electron Laser facility at SPring-8 (XFEL/SPring-8) has been performed by using the semi-empirical code,SHIELD11, and the Monte Carlo code, FLUKA for the bulk shield. These results were compared with each other. The Beamline hutches of the XFEL/SPring-8 have been also designed and estimated the leakage doses including the incident conditions of the abnormal electron aberrance.

1. Introduction

The 8 GeV class X-ray Free Electron Laser facility at SPring-8 (XFEL/SPring-8) is now under construction to obtain the X-ray laser with the shortest wavelength of less than 0.1 nm based on the practical experience of the SCSS prototype facility (250MeV, 30nC/s) [1]. XFEL/SPring-8 is based on three new technologies. One is the low emittance thermionic gun, one is the C-band accelerators of up to 8GeV and 60 nC/s, the other is the in–vacuum type undulators. The length of this system is about 415m, 235m, and 66m for the accelerator section, the undulator section, and the experimental hall, respectively. Based on the ALARA principles, the design criteria at the SPring-8 site are 8μSv/h, 2.5μSv/h, and 100μSv/y, for the radiation controlled area, the boundary of the controlled area, and the site boundary, respectively. For the shielding design of the facility, we employed the SHIELD11 code [2], analytical methods and the Monte Carlo code FLUKA [3], and the results were compared with each other..

2. XFEL/SPring-8

The XFEL/SPring-8 facility has been constructed at just close to the 1km long beamline of SPring-8. The accelerated 8 GeV electrons passing through the undulator with about 120m length go down into beam dump with the inclined angle of 20 degrees, and then the laser lights go straight into the experimental area through the shield wall in the direction of the SPring-8 storage ring. Fig.1 shows the illustration of the XFEL/SPring-8 comfigurations including the electron beam loss assumptions. The facility will have 5 beamlines by using the switing magnet to swing the accelerated electron beam, and two beamlines are now under construction in the first stage. This machine has three bunch compressors and two chicaines, and these components can remove the dark current. Therefore, the maximum energy of dark current at the each sections can be shown in this figure. Based on the beam dynamics simulations, we dicided the beam loss assumptions as follows,

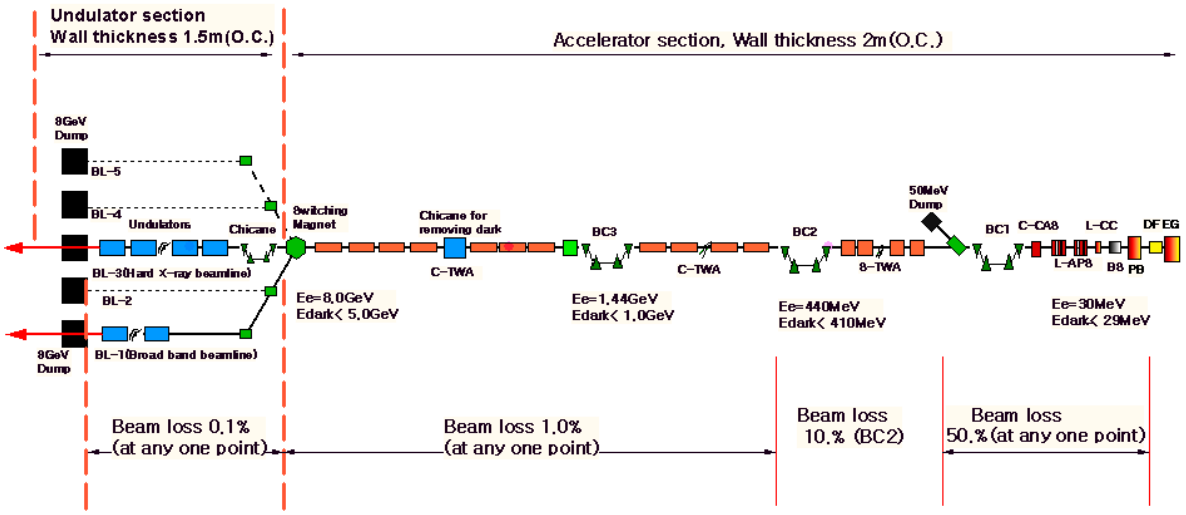

Fig.1 - Illustration of the XFEL/SPring-8 comfiguretions including the electron beam loss assumptions.

50% from the electron beam deflector to 50 MeV dump (electron energy is up to 50 MeV), 10% from 50 MeV dump to the beam compressor No. 2(BC2, electron energy is up to 440 MeV), and 1 % at any points from BC2 to the out of switching magnets in the accelerator section. In the undulator section, 0.1 % beam loss were assumed at any one point except the 8 GeV dump because the beam must be high quality to oscillate the X-ray laser. Besides, the beam loss must be avoided as low as possible to protect the radiation damage of the permanent magnet of the undulators so that the beam halo monitor [4] and the beam loss monitor [5] will be installed in this section.

3. Comparison between Jenkins' formula, SHIELD 11 and FLUKA calculations

For the bulk shielding calculations of SPring-8, we employed the Jenkins' formula [6] and modified Swanson's formula [7]. Recently, SLAC released the convenient code for the bulk shield calculation, SHIELD 11, based on the Jenkins' formula that has some distinct features such as the capability of wide application, especially without restriction of the scattering angle, with considering the self shielding of the target, and local shield, automatically. In order to apply the shielding design of the XFEL/SPring-8, the calculation results between Jenkins' formula, SHIELD11, and FLUKA were compared each other for the calculation models as shown in Fig.2. In this model, we employed the cylindrical target made of iron with 20cm in thickness and 20cm in radius. For the shield wall, we employed the ordinary concrete with the density of 2.2 g/cm^3 and from 1 m to 2.5 m in thickness. In the SHIELD 11 calculations, we performed with

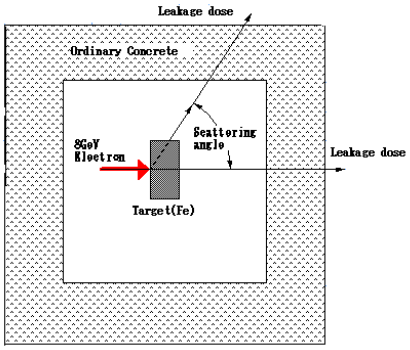

Fig.2 - Calculation models for the intercomparison of the semi-empirical methods and Monte Carlo code.

and without considering the self shield of the target. For the Jenkins' calculations, we considered two cases, one is only considering the shield wall, the other is considering the shield wall and 20 cm iron target as a local shield. In the FLUKA simulations, effective dose with worst geometry and ambient dose were estimated. The attenuation lengths which were employed in SPring-8 shielding design and in SHIELD 11 are summarized in Table 1 for ordinary concrete with the density of 2.2 g/cm^3, iron, and lead. In this table, the upper stands indicate the attenuation lengths which used in the SPring-8, and the lower stands indicate the attenuation lengths of the SHIELD 11 for each radiation source. For photons, the attenuation lengths are almost same. On the other hand, the attenuation lengths of the iron and lead are different for neutrons and the attenuation lengths for high energy and intermediate neutrons are the same in the SHIELD 11 code.

(cm)

Material		Neutron			Photon
		High Energy (λ_1)	Intermediate (λ_3)	Giant resonance (λ_2)	(λ)
Ord. Concrete	SPring-8	54.6	25.0	13.7	18.9
	SHIELD11	54.55	25.0	13.64	19.1
Iron	SPring-8	21.3	12.4	6.8	4.3
	SHIELD11	18.6	18.6	6.0	4.3
Lead	SPring-8	22.7	18.3	10.0	2.1
	SHIELD11	17.6	17.6	8.54	2.1

Table 1 - Attenuation lengths which we employed in SPring-8 shielding design and SHIELD11.

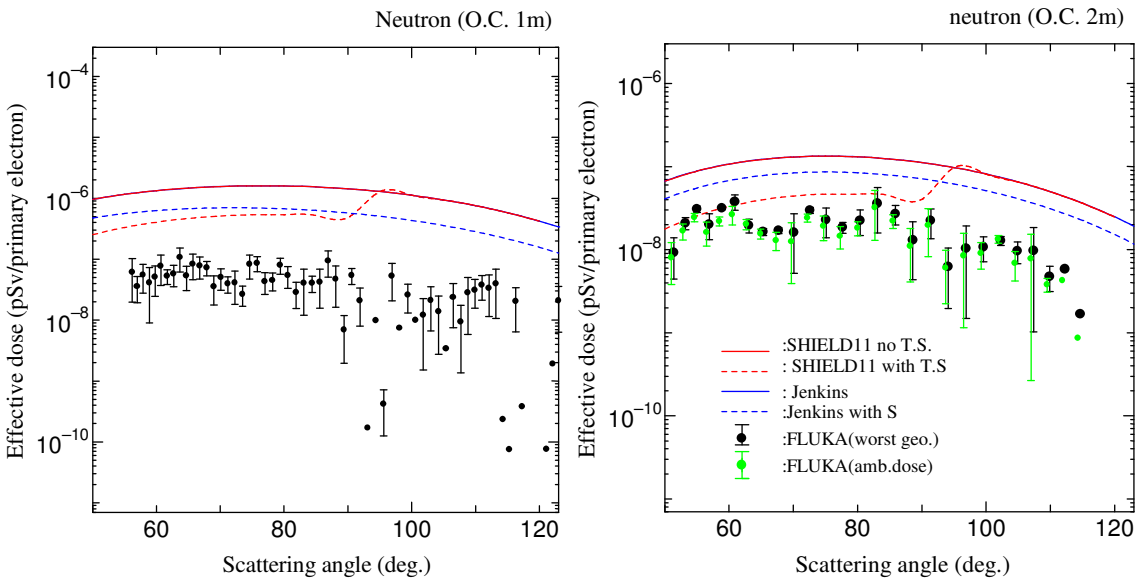

Fig.3 - Neutron leakage dose distributions in the lateral direction for the case of ordinary concrete shield wall with 1m (left side) and 2m(right side) thick. Red dotted and solid lines indicate the calculation results by using SHIELD 11 with and without considering the self shielding of the target, respectively. Blue dotted and solid lines are the results using Jenkins' formula with and without considering the local shield of iron. Black and green dots are the results by using FLUKA for the effective dose (worst geometry) and the ambient dose.

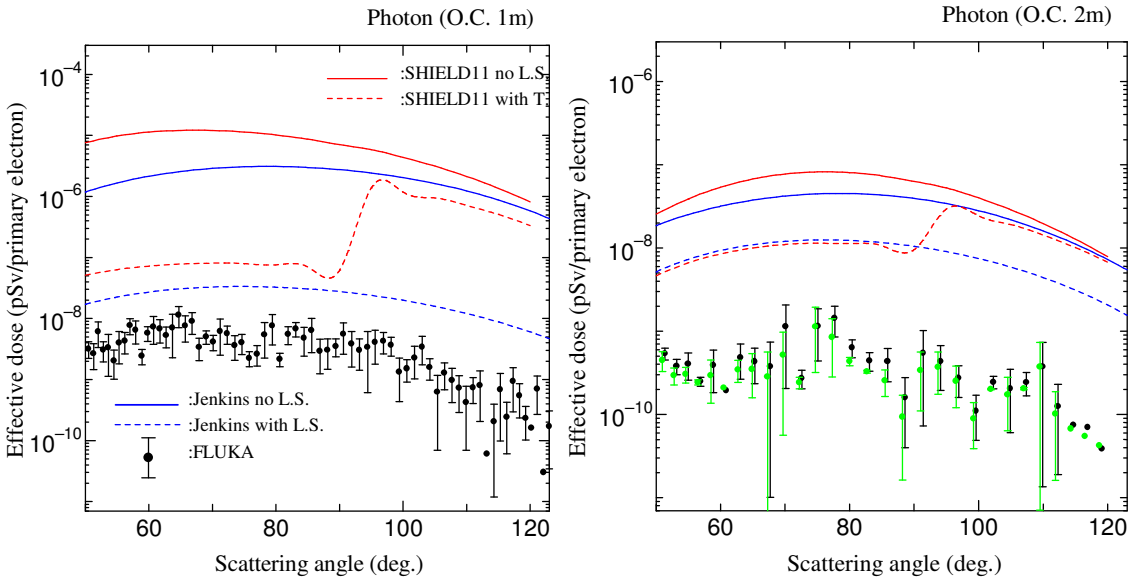

Fig.4 - Photon leakage dose distribution in the lateral direction for the case of 1m and 2 m shield wall of ordinary concrete. Each line and dots indicate the same meaning as Fig.3.

The calculation results of the neutron leakage dose distributions in the lateral direction are shown in Fig.3 for the shield wall of 1 m and 2 m ordinary concrete, and photon dose distributions are in Fig.4.for 1m and 2m shield wall. In these calculations, the SHIELD 11 calculations indicate more conservative leakage dose than that of the FLUKA calculations, and nearly equal of the Jenkins' calculations. The leakage dose calculations in the forward direction are shown in Figs.5 and 6 as functions of scattering angle and the thickness of shield wall. As shown in these figures, the results of the Swanson's are most conservative for photon dose in the case of less than 2 m thickness of the shield wall. On the other hand, the FLUKA simulations show the highest values for neutrons.

4. Shielding calculations around the beam dump and the beamline of XFEL/SPring-8

The beam dump of 8 GeV is installed with inclination angle of 20 degrees and Fig.7 shows the illustration of the beam dump area. The 8 GeV beam dump has a double cylindrical structure, and the core (inner cylinder)

is made of graphite, and outer is the iron with 40 cm thick. The iron plate with 65 cm thick is placed at the upper side of the dump for the shield. The thicknesses of the bulk shield in lateral direction and the roof are 1.5 m, and 2.5 m in the forward direction. Two collimators and one sweep magnet are installed for the safety in front-end of the XFEL beamline. The leakage dose distributions outside the roof are shown in Fig.8 by using SHIELD 11during the electron beam injection into the dump. In the calculation, the electron beam intensity is 1nC with the repetition rate of 60 Hz. As shown in the figure, the neutron dose is dominant outside the roof.

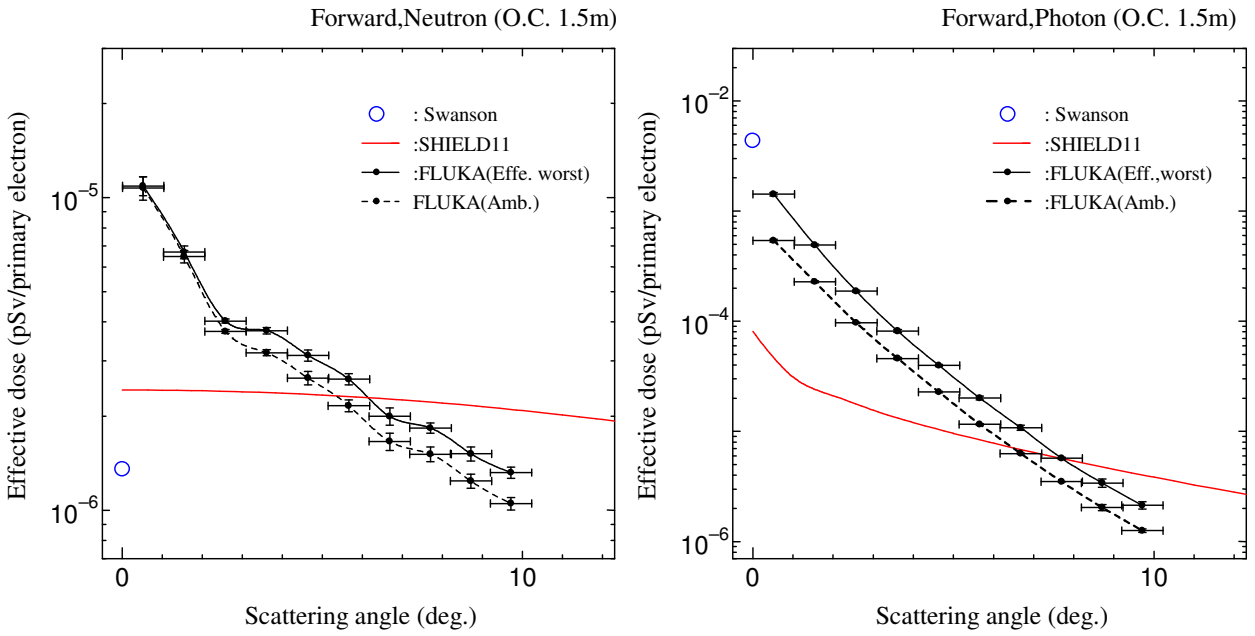

Fig.5 - Leakage dose distribution in the forward direction with the ordinary concrete shield wall of 1.5m thick as a function of the scattering angle as shown in Fig.2. The left side figure is for neutron dose, and right side is for photon dose. Blue circle indicates the calculation results of the modified Swanson's, red line is the SHIELD 11 calculation. Black solid line and dotted line show the FLUKA simulation of effective dose with worst geometry and the ambient dose, respectively.

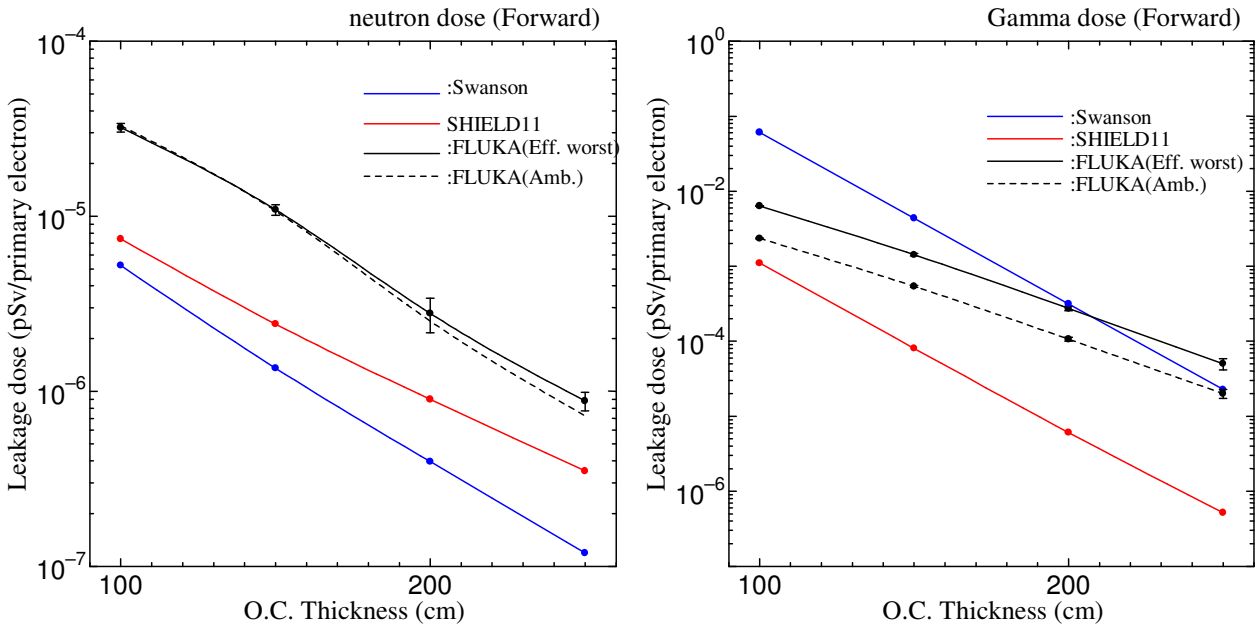

Fig.6 - Leakage dose distribution as a function of the ordinary concrete thickness at the 0 degrees scattering angle. The left side figure is for neutron dose, and right side is for photon dose. Blue line shows the results of the Swanson's, and others are the same as Fig.5.

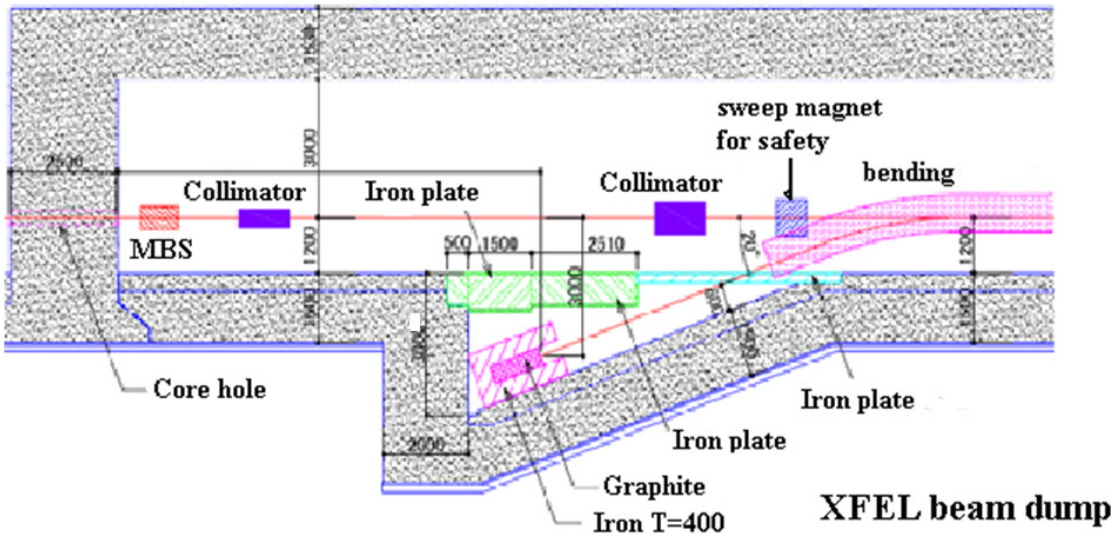

Fig.7 - Cut a way view of beam dump area.

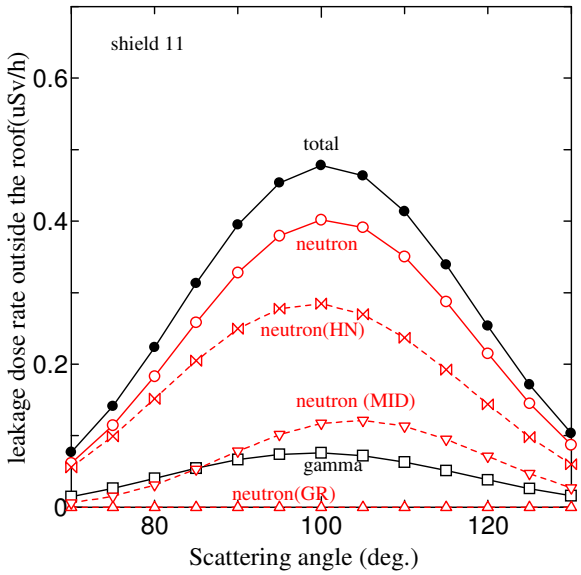

Fig.8 - Leakage dose distribution outside the roof.(neutron(HN) means the dose due to high energy neutrons, neutron (MD) means the dose due to intermediate energy neutrons, and neutron(GR) means the dose due to giant resonance neutrons).

The 8 GeV electrons are always injected into beam dump by the bending magnet. However, we must take care of the accidental conditions such as the power loss of the bending magnet by some blunder. In this case, the 8 GeV electrons can invade into optics hutch even though the safety interlock system is tripped immediately, and this is very dangerous. To avoid this situation, the sweep magnet for the safety must be installed in the downstream of the bending magnet. Fig.9 shows simulation result of the dose distribution by using FLUKA during this dangerous case. In this case, the sweep magnet is designed as 0.9Tesla and 57 cm in length, and the aperture size of the first collimator is 13mm ϕ at 5 m distance from the magnet. This figure shows that the trajectory of the 8GeV electron is inclined by the sweep magnet and the electrons hit the collimator. Some bremsstrahlung photons invade into the optics hutch through the hole of the shield wall to lead XFEL into the experimental area. However, 8GeV electrons never inject into the optics hutch.
In the shielding design of the XFEL/SPring-8, we assumed the beam loss of 0.1% will be occurred within the undulator section. When the electron beam loss is occurred in the undulator section, the power of the bremsstrahlung which invades into the optics hutch depends strongly on the collision angle of the electron beam and the aperture size of the collimator. Figure 10 shows the simulation results of the injection angle dependence of the invaded power into the optics hutch with the same calculation configuration as shown in Fig.9 by using EGS4[8]. In the simulation, we found that the invaded power is saturated when the injection

angle is less than about 0.5 mradian so that we set the 0.1mradian for the safety calculation of the XFEL beamline. The simulation results of the photon dose and the neutron dose distribution around the optics hutch are shown in Fig.11by using FLUKA. In the case, 0.1% of the 8GeV electrons is lost at the upstream of the bending magnet of the beam dump. The simulation configuration is the same as shown in Fig.9 and the shield wall of the optics hutch side wall is 80 cm ordinary concrete, and 1m for the back wall. In the simulation, the copper with 5 cm thickness is assumed for the first scatterer and the local shield made of lead with 10cm in thickness. As shown in the figure, the doses due to neutrons caused by photo-nuclear reactions of the bremsstrahlung are notable in the optics hutch.

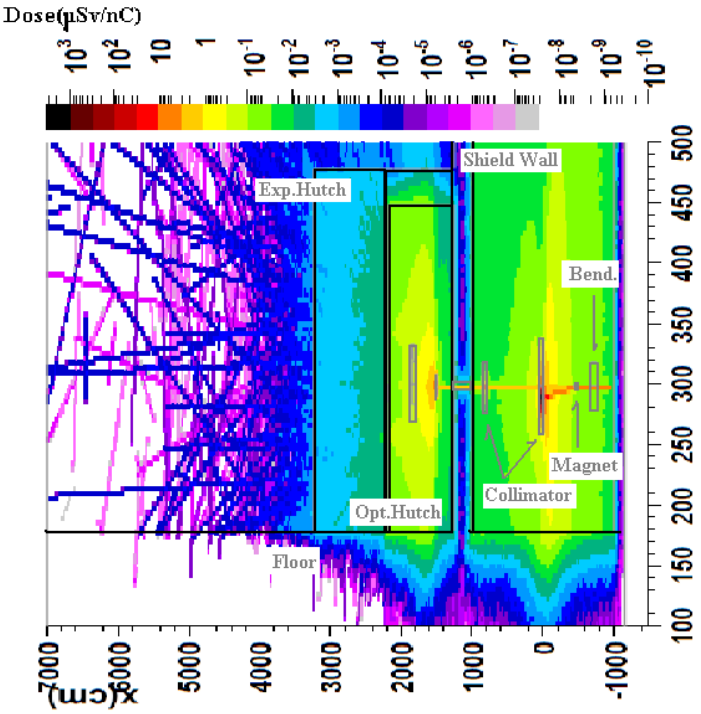

Fig.9 - The dose distribution when the power of bending magnet is lost and the electron beam hits the collimator.

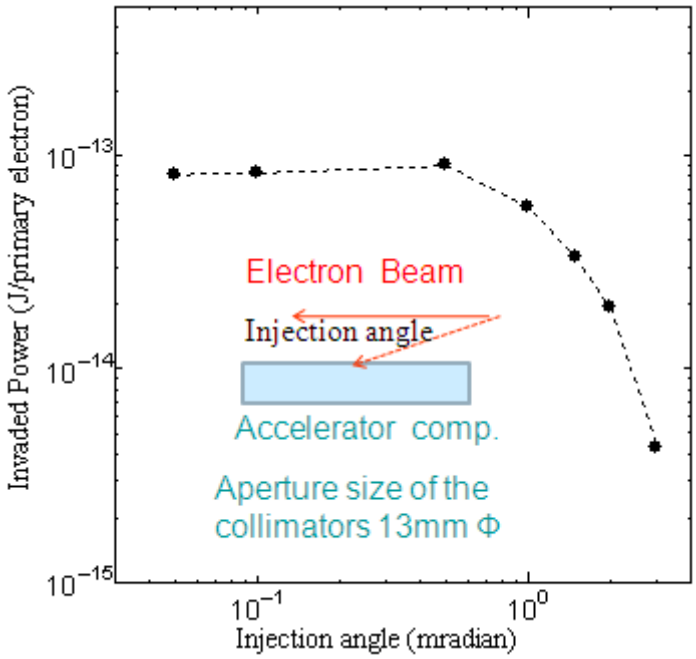

Fig.10 - Injection angle dependence of the invaded bremsstrahlung photon power.

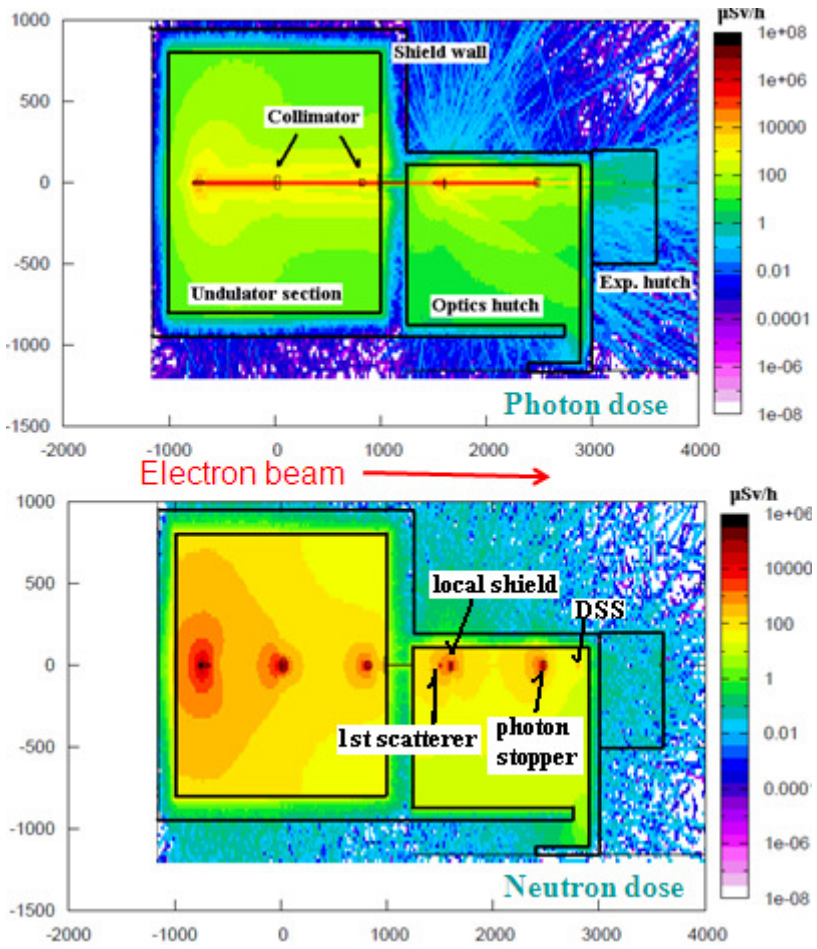

Fig.11 - Photon and neutron dose distributions due to 0.1% electron beam loss at the upstream of the bending magnet. (The upper and lower stands are photon and neutron dose distributions, respectively. The size of the local shield for 1st scatterer is 60cmWx60cmHx10cm lead, photon stopper is 50cmWx50cmHx40cm lead).

5. Summary

For the design of the bulk shield of XFEL/SPring-8, we employed the SHIELD11 code, the Jenkins' formula, the modified Swanson's method, and the Monte Carlo code FLUKA, and compared each other. As the results of the leakage dose at the lateral direction, we found the calculation results by using the Jenkins' underestimate in comparison with the SHIELD 11 for gamma dose, and neutron doses are almost the same. Both gamma and neutron doses calculated by SHIELD11 show the conservative values in comparison with that of FLUKA (effective dose with worst geometry). For the doses at the forward direction, SHIELD 11 underestimates both the gamma and neutron doses in comparison with that of FLUKA so that we must take care of the calculations in the forward direction. For the XFEL beamline shielding, we must consider three radiation sources, one is the synchrotron radiation including XFEL, one is the gas bremsstrahlung, and the other is the high energy radiations due to the accelerated electron beam loss including photoneutrons. In the XFEL/SPring-8 case, however, the two former sources make not so much severe conditions in comparison with that of the electron beam loss. And these conditions strongly depend on the injection angle of the electron beam loss. For the estimation of the radiations due to the electron beam loss, we employed the FLUKA code in the shield design of the XFEL/SPring-8 beamline. The shield tunnel and the building of the XFEL/SPring-8 have been constructed, and the accelerators are now under construction. The commissioning will be started in next year.

References

[1] T. Shintake et al., "A Compact free-electron laser for generating coherent radiation in the extreme ultraviolet region", Nature Photonics Vol.2 p555-559 (2008).
[2] W. R. Nelson & T. M. Jenkins, "The SHIELD 11 Computer code", SLAC-Report 737 (2005).

[3] A. Fasso, A. Ferrari, J. Ranft and P. R. Sala, FLUKA Proc. Monte Carlo 2000 Conf. Lisbon 955-960 (2001) http://www.fluka.org
[4] H. Aoyagi, T. Bizen, K. Fukami, N. Nariyama, Y. Asano, T. Itoga, H. Kitamura, T, Tanaka, “Beam halo monitor using diamond detector for interlock sensor at XFEL/Spring-8”, DIPAC 2009 TUPB24, Basel, Switzerland.
[5] X.-M. Maréchal, Y. Asano, T. Itoga, “Beam based development of the a fiber beam loss monitor for the Spring-8/XFEL”, DIPAC 2009, Basel, Switzerland.
[6] T. M. Jenkins, “Neutron and photon measurements through concrete from a 15 GeV electron beam on a target-Comparison with models and calculations “, Nucl. Instrum. Methods V159 265 (1979).
[7] H. Dinter et al.,” Calculation of Electron-photon doses behind beam absorbers at high energy electron accelerators”, Radiation protection dosimetry 28 207 (1989).
[8] W. R. Nelson, H. Hirayama, D. W. O. Rogers,” The EGS4 code system” SLAC-265 (1985).

Bulk shielding design for the MAX IV facility

Magnus Lundin[1], Lennart Isaksson[1], Bent Schröder[1]

[1] *Lund University, MAX-lab, P.O. Box 118, SE-221 00 Lund, Sweden*

Abstract

This paper reports on the design of the bulk shields of the linac tunnel, the ring and the short pulse facility of the new MAX IV facility. MAX IV is funded and construction is planned to start in 2010.

1. Overview

MAX IV will be situated in the outskirts of Lund, Sweden and replaces the current MAX-lab facility which houses three rings with energies of 500, 700 and 1500 MeV. The MAX IV facility has a 3 GeV full energy linac injector for its 530 m circumference ring. The linac will also be used for the Short Pulse Facility (SPF) at which the electrons pass through one or several undulator devices to generate very short light pulses in the keV range. Figure 1 shows an overview of the site.

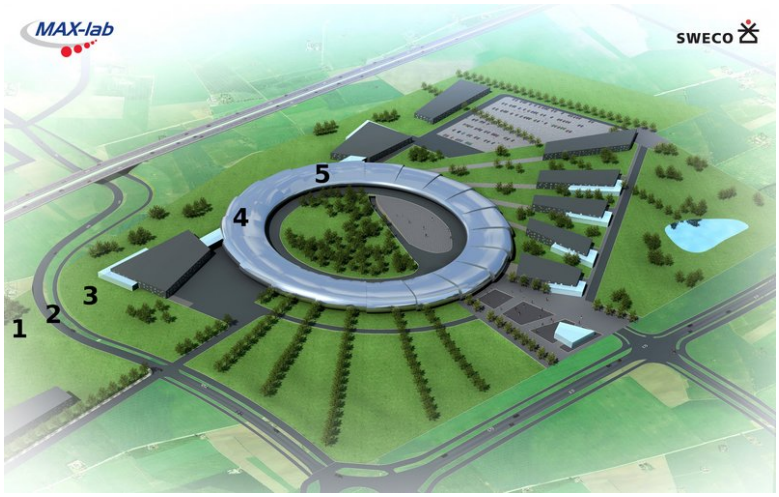

Fig. 1 – Overview of the MAX IV site.

The source model used in the shielding calculations for the dose equivalent rate due to bremsstrahlung, low, medium and high energy neutrons was adopted from [1] but normalized to the 90° data in [2]. The shielding material attenuation lengths were mainly obtained from [3].

2. The linac

The linac will be operated in two different modes. One is where it is used to fill or top-up the ring and this mode will always be active, i.e. its "duty" is 1. The linac can also be operated for the SPF and will then run at full power. This mode will only be active 1/3 of the time. The different operating modes of the linac are summarized in table 1.

The projected electron losses in the linac tunnel and transport beam lines during normal operation will determine its required shielding. At this stage, no data concerning these losses exist for the MAX IV facility. Values from similar facilities found in literature range between 0.1% and 12%. The values adopted for MAX IV are provided in table 2

Mode	Rate (Hz)	Energy (GeV)	Charge (nC)	Power (W)	Duty
Fill/top-up	0.1	3.0	1	0.3	1.0
SPF	100	3.0	1	300	0.33

Table 1 – Operating modes of the linac.

Location	Energy (GeV)	Loss (%)	Beam power @100Hz(W)	Loss power @100Hz(W)
linac	0-0.2	20	0-20	0-4
linac	0.2-3	1	20-300	0.2-3
transport/SPF	3	1	300	3

Table 2 – Projected maximum losses at a single point during normal operation of the linac. The beam power and loss power is for the linac SPF mode

Referring to figure 1, the linac runs in an underground tunnel which starts at location 1 and continues to location 4 where the electrons can be directed upwards to the ring. The electrons can also continue in the linac tunnel to the SPF located at 5. The area above the tunnel at locations 1, 2 and 3 does not belong to the MAX IV facility and is freely accessable to the public. The length of the linac between locations 1 and 4 is approximately 300 m.

The bulk shielding calculation was carried out for the linac tunnel at locations 1-4. The electron energy and the projected losses at a single point at these locations are provided in table 3 (refer also to table 2).

Location	Energy (GeV)	Loss (%)	Loss @ 100 Hz (W)
1	0.2	20	4
2	1.0	1	1
3	1.5	1	1.5
4	3.0	1	3

Table 3 – The electron energy and the projected losses at a single point for locations 1-4. The last column is the loss in Watts when the linac operates in SPF mode.

Table 4 shows the linac tunnels at location 1. The klystron tunnel is to the left and the linac tunnel to the right. The electrons travel into the figure. The linac is located 100 cm off the floor and the height of the linac tunnel is 250 cm. The vertical shield thickness above the linac is 50 cm of concrete, 20 cm of insulation and 380 cm of earth. The dose rates for bremsstrahlung, low, medium and high energy neutrons were calculated on the grids g0-g4 which are offset 10 cm from the ground. The result of this calculation is also shown in table 4.

At a maximum dose rate of 0.1 μSv/h, the public can spend 1000 h at location 1 until the dose limit adopted for MAX IV of 100 μSv is reached. Taking the duty of 0.33 into account, this increases to 3000 h. The procedure above was carried out for locations 2, 3 and 4 and table 5 summarizes these results.

From table 5 it follows that the public can spend 2000 h per year above the linac tunnel. At location 4 iron had to be added in order to obtain an occupancy of 2000 h per year. The weight of the iron shield at location 4 is approximately 1260 kg/m .

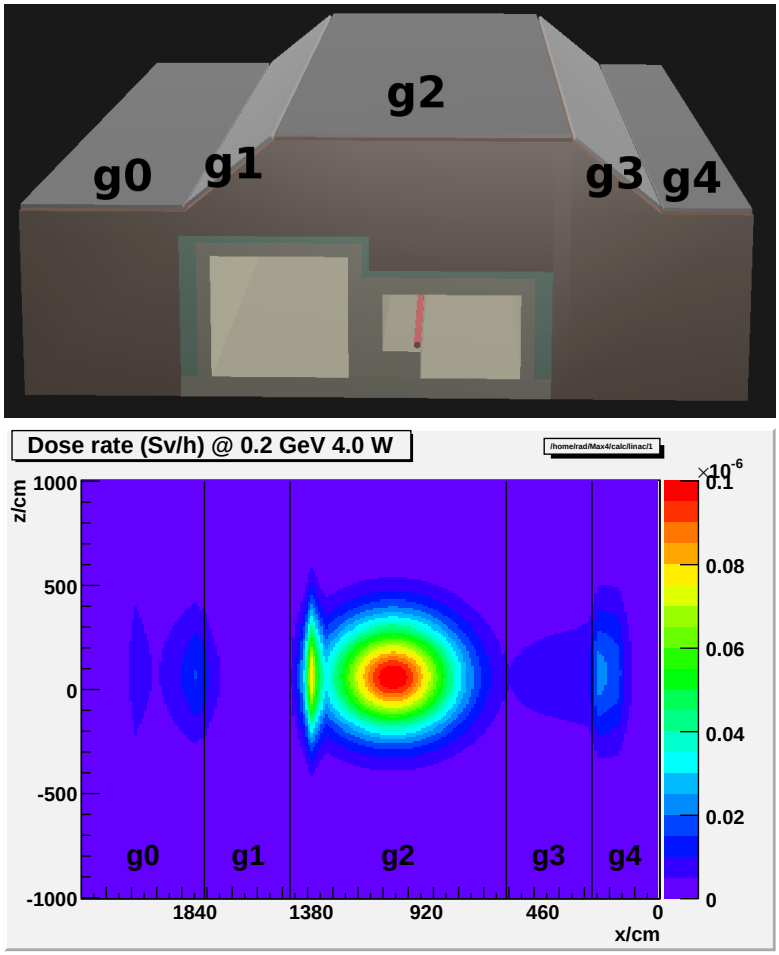

Table 4 – Top: the linac and klystron tunnels at location 1 and the grids g0-g4 on which the dose rate was calculated. Bottom: the corresponding dose rate on grids g0-g4 for a loss at z=0.

Location	Vertical shield	Dose rate (μSv/h)	Dose limit (mSv)	Hours
1	50 cm concrete, 380 cm earth	0.10	0.1	3000
2	230 cm concrete	0.15	0.1	2000
3	150 cm concrete, 200 cm earth	0.05	0.1	6000
4	30 cm iron, 150 cm concrete	1.50	1.0	2000

Table 5 – The results for locations 1-4. The number of hours was calculated taking the duty factor into account.

3. The Short Pulse Facility

If the electrons are not directed upwards to the MAX IV ring, they can continue in the extension of the linac tunnel to the SPF. The electrons will pass through an undulator device, generating photons with energies in the region of 10 keV. These photons travel parallel to the electron beam up to the point at which the electron beam is deflected by a dipole magnet towards another undulator, the test beam facility or the beam dump.

It is assumed that 1% of the electrons can be lost at a single point but since losses at different points can add up in the forward direction, a loss of 2% was assumed at the dipole bend.

Table 6 shows the result of this calculation. The upper panel of table 6 shows the experimental area (upstream view). The electrons are deflected 20° by the dipole (not shown) and the undulator photons continue at 0° through the wall to the experimental area. The grids g0 and g1 on which the dose rates were determined are located on the walls of the experimental area. x is the distance to the photon beamline along grid g0, y is the height above the photon beamline and w is the distance to the photon beamline along grid g1. The loss points were at the dipole bend (2%) for grid g0 and outside the side wall (1%) for grid g1.

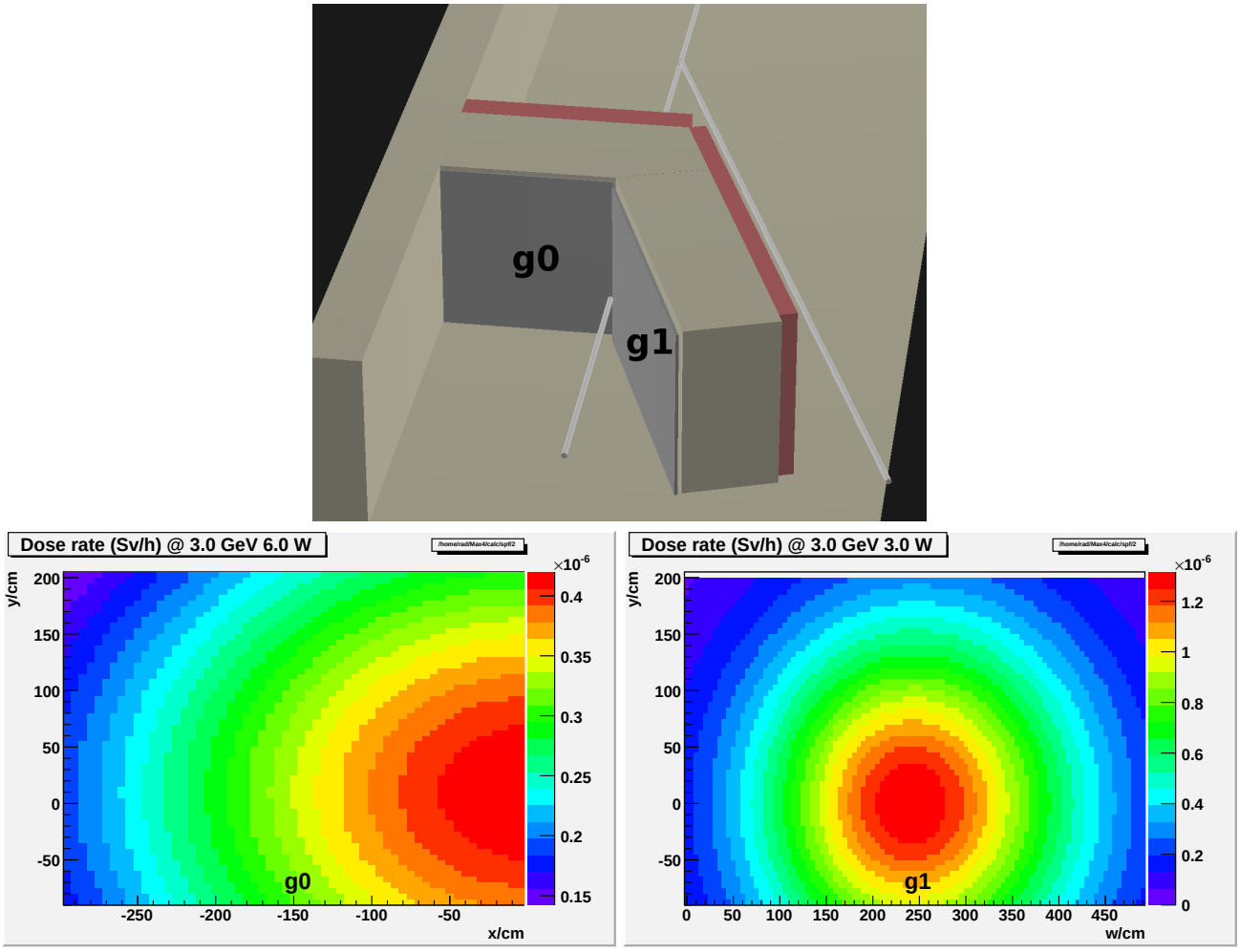

Table 6 – The calculated dose rates for the SPF. Top: the SPF layout showing the two grids on which the dose rates were calculated. Bottom: the dose rate on the the forward (g0) and side (g1) grid.

The results for the SPF are given in table 7. The corresponding number of hours have been determined for the two grids taking the duty factor into account.

Grid	Shield	Dose rate (μSv/h)	Dose limit (mSv)	Hours
g0	50 cm iron, 200 cm concrete	0.4	1.0	7500
g1	30 cm iron, 160 cm concrete	1.3	1.0	2300

Table 7 – The results for grids 0 and 1. The number of hours was calculated taking the duty factor into account.

4. The ring

The circumference of the MAX IV 3 GeV ring is 530 m and it contains 20 straight sections, one for injection and 19 for insertion devices (the length of one straight section is 5 m). The stored current will be 500 mA. For 4 injections per 24 h, the assumed electron loss scheme is given in figure 2

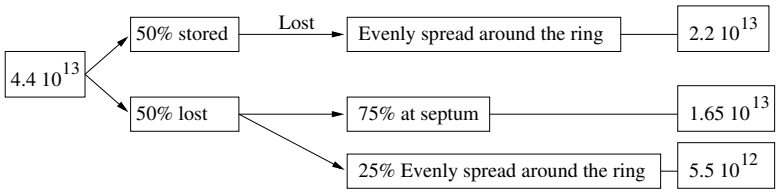

Fig. 2 – 24 h electron loss scheme. 50% of the electrons are lost during injection, mostly at the septum.

The losses that are spread evenly around the ring are assumed to occur with equal probability at a single point in each of the 20 cells. In table 8 one sector of the ring is shown between the positions of the centers of two adjacent long straight sections. The distance between the centers is 26.5 m. The assumed point of loss is in the center of the straight section as indicated by the solid circle. The shielding wall is 1 m concrete and the distance from the loss point to the ratchet wall is about 20 m. The ratchet wall is reinforced with 10 cm of lead covering 2^o or 70 cm on both sides of 0^o.

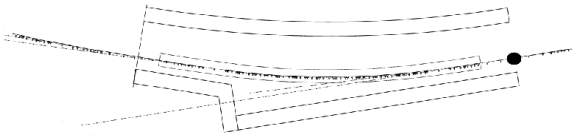

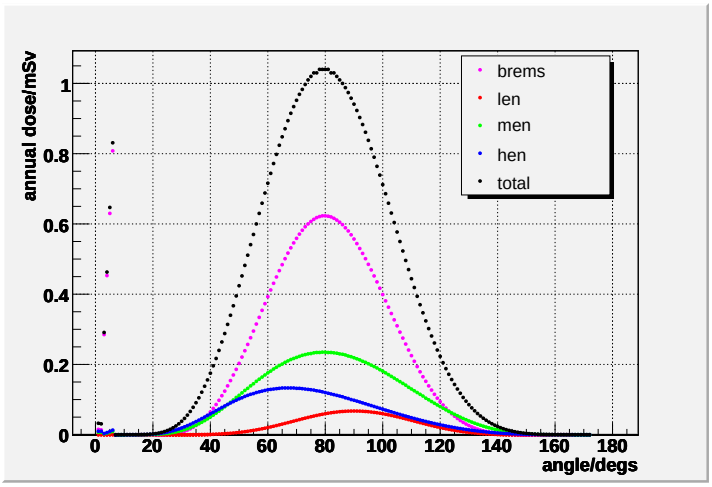

Table 8 – A section of the ring and the calculated dose.

The annual dose (2000 h) 50 cm off the concrete wall is also shown in table 8 as a function of the angle with respect to the direction of the electron beam. The total dose is shown as well as the individual contributions due to bremsstrahlung, low, medium and high energy neutrons. In table 9 an alternative to the normal shielding wall is shown. In order to decrease the distance from the center of the long straight section to the exit of the ratchet wall to about 16 m, two parameters are changed. First, the shielding wall is moved closer to the ring magnetic structure, second the 1 m concrete wall is replaced by 30 cm iron and 10 cm borated polyethylene

over a distance of 6 m.

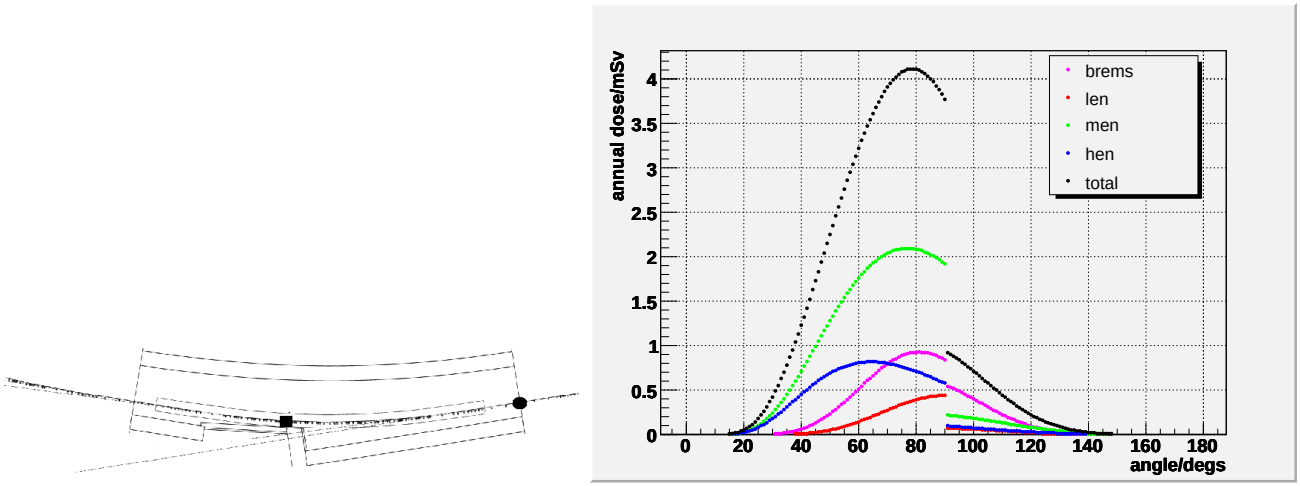

Table 9 – A section of the ring for the alternative configuration and the calculated dose.

The point of loss is assumed to be located at the solid rectangle. The annual dose (2000 h) 50 cm off the wall is also shown in table 9 as a function of the angle with respect to the direction of the electron beam. The location at which the maximum dose of 4 mSv occurs is in the first optical hutch of the beamline. The occupancy time of 2000 h is probably a factor of 10 too much. The hutch will be interlocked when the beamline shutters located just before the ratchet wall are open and access will not be permitted.

5. Conclusions

In this paper the bulk shielding calculations for the upcoming MAX IV facility were presented. The shielding for the linac tunnels is dictated by the requirements imposed by the SPF mode and the fact that parts of the tunnels are below an area accessible to the public. The MAX IV ring, with a circumference of 530 m, will be operated in top-up mode, and the required shielding is similar to other 3 GeV storage rings with a circulating current of 500 mA. Finally, the shielding of the SPF was described in some detail.

References

[1] NCRP Report No. 144
Radiation protection for particle accelerator facilities.
National Council on Radiation Protection and Measurements, 2003

[2] A guide to radiation protection and radioactivity levels near high energy particle accelerators.
A. H. Sullivan, Nuclear Technology Publishing, 1992

[3] NSLS-II Preliminary Design Report (2007)
Brookhaven National Laboratory

In vacuum ID beam line shielding commissioning and direct gas-bremsstrahlung measurements at Synchrotron SOLEIL

J-B. Pruvost[1], P. Berkvens[2], F. Justine[1], C. Mage[1]

1: Synchrotron SOLEIL – BP.48, 91192 Gif sur Yvette Cedex France.

2: European Synchrotron Radiation Facility – BP220 Grenoble Cedex 09 France

Abstract

The Synchrotron SOLEIL is the new French third generation 2.75 GeV synchrotron light source in Saint-Aubin, France. SOLEIL is now operating 17 beam lines at 300 mA and top-up mode, since November 2008. This paper describes the last in-vacuum ID beam line installed on the SOLEIL storage ring and the radiation safety commissioning tests made in order to check and validate the effectiveness of the beam line shielding of the optics hutch. Results obtained at 300 mA and 400 mA are presented. At the occasion of this common radiation safety test, a direct gas-bremsstrahlung measurement assessment was realized with the collaboration of Paul Berkvens (ESRF). The display of the measurement setup is presented and the results obtained discussed.

1. Introduction

The synchrotron SOLEIL is the new French third generation synchrotron light source. It will operate 26 beam lines by the end of 2011, including 18 insertion devices and 6 bending magnet beam lines, plus 2 infra red beam lines. Fifteen beam lines (9 ID, 6 BM) plus two infra red beam lines are now operational, delivering a 300 mA synchrotron beam in top-up mode for user experimentations. Three other ID beam lines are under commissioning at the moment of this paper and one other is under construction. Before the end of 2009, 19 beam lines (including 2 infra red) will be operational at 400 mA in top-up mode.
This paper describes the radiation safety measurements performed during the first openings of the SIXS beam line front end in order to validate the effectiveness of the beam line shielding of the first optics hutch. These measurements were performed in top-up mode, at 300 mA the February 17th and at 400 mA the March 31st.

2. Presentation of the SIXS beam line

The SIXS beam line is dedicated to surface X-ray diffraction and diffusion studies for solid surfaces and interfaces structures in different and multi environment conditions. Its synchrotron light source is an in-vacuum insertion device, U20 type, set on a short straight section, with a minimum gap aperture of 5.5 mm. The beam line display in the experimental hall consist in three lead shielded hutches with one optical hutch and two separate experimental hutches housing two different experimental set-up and detectors for a multi environment diffractometer and a UHV diffractometer.
The figure 1 presents the SIXS beam line display in SOLEIL's experimental hall, showing the three lead shielded hutches.
In this paper we are focusing on the optics hutch shielding and the radiation tests performed to check and validate this shielding.
The SIXS beam line shielding has been designed by Monte Carlo calculations [2] of the scattered gas-bremsstrahlung radiations and analytical calculations of scattered synchrotron radiations produced by the U20 ondulator. For this kind of insertion device beam line, the gas-bremsstrahlung radiations largely dominate the radiation source term in order to determine the hutch shielding.

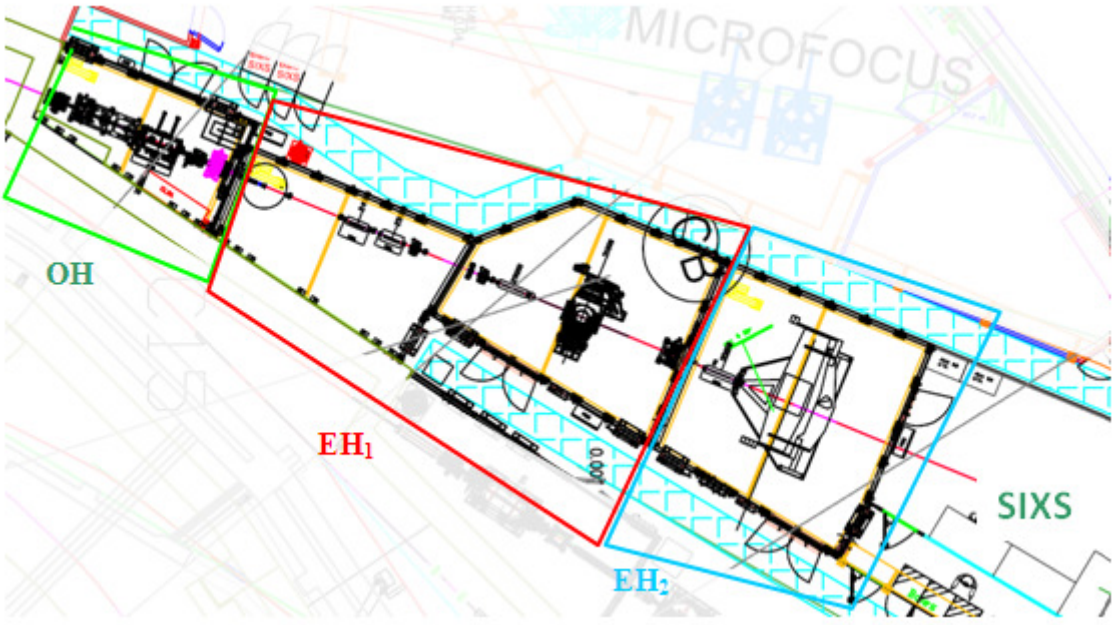

Fig.1 - Layout of the SIXS beam line in the experimental hall of synchrotron SOLEIL.

The table 1 below gives the parameters and residual gas composition in the straight section vacuum pipes and ondulator vessel used for the shielding calculations. We assumed an average vacuum pressure of 2.10^{-9} mbar along the straight section at 500 mA and a residual gas composition based on the typical RGA results at ESRF similar ID section.

Electron beam energy	2.75 GeV
Stored beam current	500 mA
Straight section length	7.74 m
Average vacuum pressure	2. 10^{-9} mbar
Front end aperture	2 x 2 mm^2
U20 type minimum gap	5.5 mm
Maximum vertical magnetic field	1.03 T
Vacuum residual gas composition	
H_2	80 %
CO	10 %
CO_2	5 %
CH_4	3 %
H_2O	2 %

Table 1 - Parameters used for MC calculations to define lead shielding thicknesses of the SIXS optics hutch.

These parameters and MC calculations performed by P. Berkvens with the "Beamlines"[2] code lead to panel lead shielding thicknesses of 15 mm for the side wall, 80 mm for the back wall and 10 mm for the roof[3], assuming that roof access is strictly forbidden during operation.

3. Radiation safety protocol to test beam line shielding efficiency

Before allowing the beam line to take synchrotron beam in the hutch, it is mandatory by French regulation Authority to test and verify the shielding efficiency and the tightness of the shielding panels of the hutch.

3.1. Beam line hutch set up

For this purpose, a radiation safety test is scheduled by the radiation safety group, the beam line team and the vacuum group as soon as the beam line is ready to take the maximum beam load of stored beam current achievable with the ID at its minimum gap. In order to perform such a test, the ID has to be ready in the storage ring, the front end must be complete and operational and the first optics hutch has to be fully equipped with all the utilities and the personal safety system (PSS) already tested and operational.

For such radiation tests, the optics hutch is almost empty with only the end of the front end vacuum system. After the ending valve of the front end, a filters chamber is mounted in order to protect a water cooled beryllium window from the high power of the SR beam. An additional nitrogen circulation is installed behind the beryllium window in order to protect it from the ozone produced by the SR beam in the air of the hutch. The scattering of both gas-bremsstrahlung and SR beam is realized by the use of copper water cooled scatterer that will be set in different positions along the beam axis during the test. Figure 2 presents photography of the mounting with the filters chamber, the beryllium window and the copper scatterer.

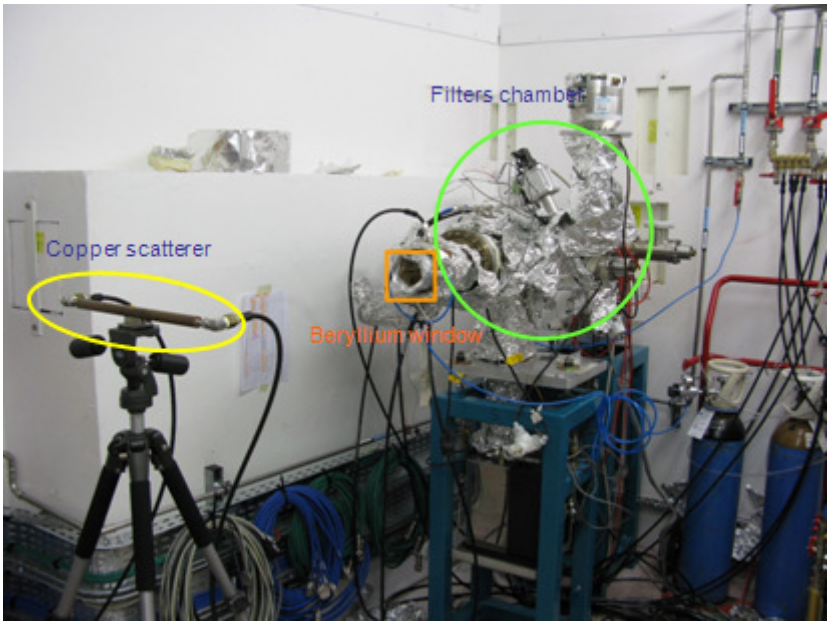

Fig.2 - Mounting for the radiation safety test of the optics hutch.

Radiation measurements are realized with both portable radiation monitors and passive thermo luminescent dosimeters (TLD) displayed all around the hutch on each panel and with specific attention at joints between panels and at doors panels and frame which are weak points of the hutch shielding tightness. An additional fixed radiation monitoring is performed by the ionization chamber installed along the side wall panel and connected to the PSS. This monitor is dedicated in normal operations to interlock the front end during top-up operation if the integrated dose gets higher dose than the accepted dose threshold of 2 µSv within four hours of integration.

3.2. Sequence of the radiation safety test measurements

First of all, the front end is open with low current stored. Then, the ID is slowly closed, step by step, up to the minimum gap value of the ID. This allows the correct alignment of the synchrotron source and the front end to be checked before going further with a beam imaging monitor place a bit downstream of the beryllium window. Then, a first radiation survey is performed around the hutch in order to search any important leakage in the shielding. Usually, the stored beam current is about 30 or 50 mA for this first step.
Then after, the maximum current available is injected into the storage ring and maintain by top-up mode. Few amount of current being regularly injected with opened front end to keep the stored current at a given value. A complete radiation survey is realized for each position of the copper scatterer in the optics hutch.
Figure 3 presents the three positions of the copper scatterer used during the radiation safety test of SIXS first optics hutch.

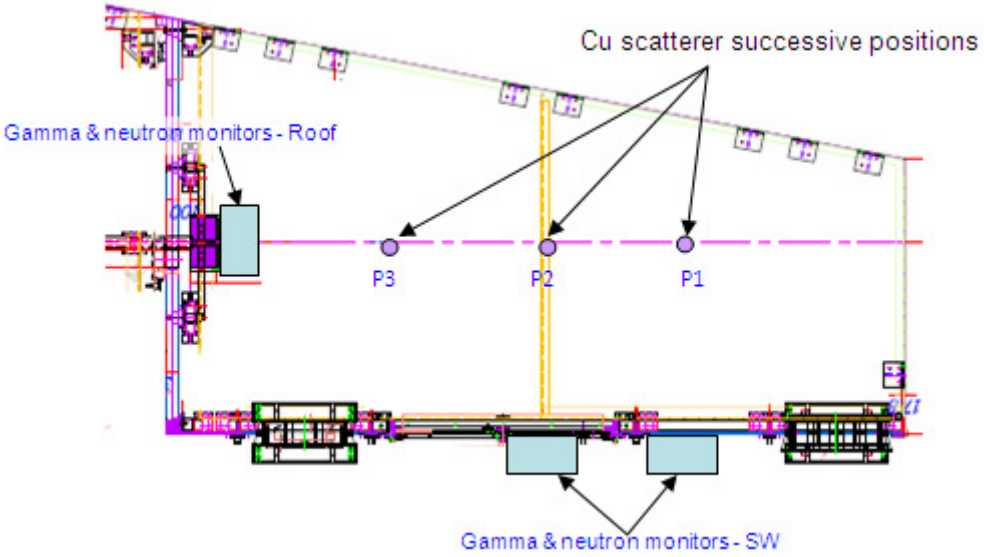

Fig.3 - Successive scatterer positions within the radiation measurements around the SIXS optics hutch.

Figure 4 presents two beam views taken during the radiation tests. The first one showing the synchrotron beam on a X-ray beam imager in order to verify that it is not even partly cut by a misalignment of the different front end absorbers or diaphragms with the ID. The second picture shows the visible synchrotron light beam crossing the beryllium window and hitting the copper scatterer.

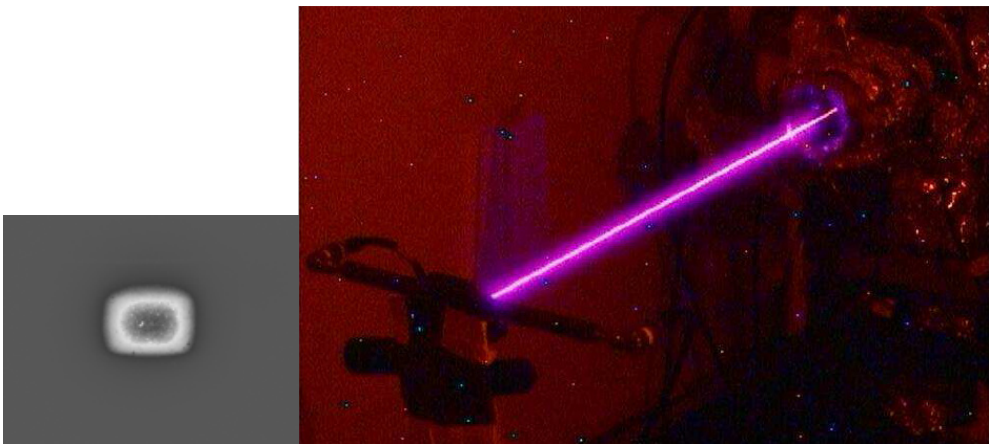

Fig.4 - Synchrotron light beam alignment check with front end aperture (left) and lightning of the synchrotron beam in the air of the optics hutch (right).

4. Radiation measurements

4.1. First attempt by February 17th 2009

The first radiation safety test of the optics hutch of SIXS beam line was performed during the night of Tuesday February 17th.

4.1.1. Direct gas-bremsstrahlung measurements

Prior to the radiation safety measurements, we take the opportunity of this radiation test to have some measurements of direct gas-bremsstrahlung produced in the straight section of this in vacuum ID beam line. This campaign was made possible by the help of Paul Berkvens, head of ESRF safety group, who came at SOLEIL with the specific detectors used for these measurements within the framework of collaboration with SOLEIL safety group. These measurements were performed by exposing a small Farmer type ionization

chamber (PTW 31002) into the direct gas-bremsstrahlung beam. The ionization chamber was connected to a PTW Unidos dosimeter system outside of the optics hutch. The ionization chamber was placed on the copper scatterer support behind 13 mm of lead in order to avoid the synchrotron radiations coming from the upstream and downstream bending magnets of the straight section. The U20 ID was set fully open (30 mm) in order to cut the synchrotron radiation production of the ID. Dose rate measurements were performed for different stored current values from 50 mA to 450 mA witch was the maximum stored beam achievable at that time.
The goal of these measurements was to verify that the gas-bremsstrahlung power produced by the electrons in the straight section is actually proportional to the square electron beam intensity stored in the synchrotron ring of SOLEIL.
As usually admitted, the gas-bremsstrahlung power could be described by equation (1) below:

$$P = C \times \frac{dE}{dx}(E_e) \times p \times I \times L \qquad (1)$$

where p refers to the vacuum pressure in the straight, I to the electron beam intensity, L to the length of the straight section, and

$$\frac{dE}{dx}(E_e): \text{to the electron stopping power } (\propto E_e)$$

Then, p being proportional to the beam intensity and to the energy of electrons, one can describe the gas-bremsstrahlung intensity proportional to the square of the electron beam energy and to the square of the beam intensity stored in the ring as described in formula (2) presented below.

$$P \propto E_e^2 \times I^2 \times L \qquad (2)$$

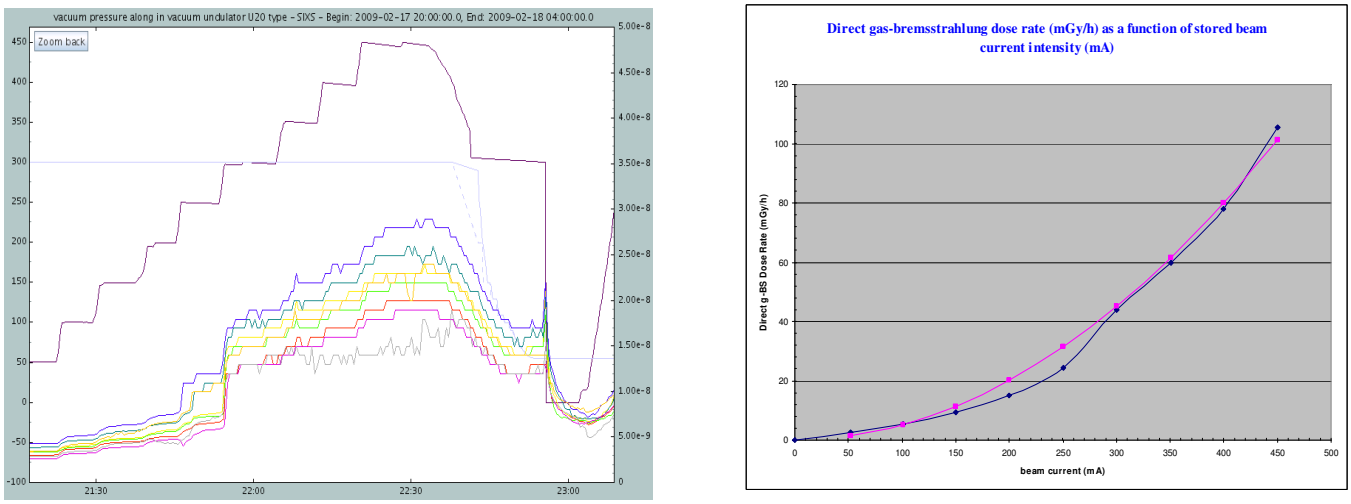

Fig.5 - Left : Electron intensity in the storage ring and different measured vacuum pressures in the straight section of SIXS (I14-C). Highest values of pressure refer to the in vacuum ID vessel gauges. Right: Direct gas-bremsstrahlung dose rates measured for current intensity from 50 mA to 450 mA (blue curve). Quadratic fit of the intensity of the electron stored beam (pink curve)

Taking into account the natural background, one can see that, on the right of Figure 5, we obtain a slightly good agreement with a quadratic current response of the direct gas-bremsstrahlung dose rates measured into the beam axis.

4.1.2. Radiation safety controls

Because of a problem on the RF system of the storage ring that happened just after the end of the gas-bremsstrahlung measurements, the radiation safety test was performed at only 300 mA instead of 400 mA as initially scheduled. In top-up operations at 300 mA and with the U20 ID gap closed at 5.5 mm, the average vacuum pressure in the straight was about 1.5 10^{-8} mbar. Radiation measurements pointed out the fact that in front of the doors of the hutch and on the roof dose rates are a bit higher than expected and with repeated

pics over 1 µSv/h where shielding has been designed to have less than 0.5 µSv/h at 500 mA. We also experienced a few total beam trips during the measurement session which lead to integrated dose of 1.5 µSv and 2.3 µSv per beam loss behind the doors and on the roof respectively. These dose levels were very high and mean that in case of a total beam trip, the beam line will be interlocked by the PSS. It was also established that almost the entire beam was lost in the SDC14 straight section (SIXS beam line one). Because of these beam trips, the passive dose dosimeters spread all around the optics hutch were blinded by these large amounts of equivalent dose.
So, in these conditions and with such radiation measurements results it was not possible to validate the efficiency of the SIXS optics hutch and a second radiation test session was scheduled.

4.2. Second attempt by March 31st 2009

In order to be able to status on the quality of the hutch shielding as far as possible independently of any unforeseen event, this second radiation test was split into two parts. First to minimize the risk, radiation surveys were performed in decay mode of operation at 400 mA. Refills were done with closed front end. No radiation leakage was detected and all the dose rates measured were slightly lower than 0.4 µSv/h all around the hutch. Then, the second part of the test was performed in top-up mode at 400 mA almost in the same conditions than the first time. Dose rates measured were found again higher than the goal limit of 0.5 µSv/h, with particular points like door panels at 0.8 µSv/h with occasional peaks at 1.2 µSv/h. This time we did not encounter total beam trips so it was necessary to force total beam losses by tripping the storage ring RF system. These forced beam trips were mainly concentrated in SDC14 and lead again to high integrated doses of about 0.85 µSv behind the doors and almost 1.5 µSv on the roof. Because the beam trips were forced at demand, dose rates could have been measured by portable ionization chambers and the corresponding results (probably underestimated) were 2.3 mSv/h behind the doors and 38 mSv/h on the roof.

4.3. Discussion

This was the first time that such bad results were obtained at SOLEIL for beam line hutch radiation safety tests because it was not possible to authorize the beam line staff to start the commissioning of the beam line with SR beam just after the tests. So what was wrong with this particular beam line?
First, instead of the three first in vacuum ID beam lines, the SIXS U20 ID was not installed before the starting of the storage ring operations but just a couple of months before the tests. So the vacuum pressure was quite poor during the tests (1.5 10^{-8} mbar instead of 2. 10^{-9} mbar for the value retained for shielding calculations) and probably responsible of the higher amount of gas-bremsstrahlung entering the optics hutch.

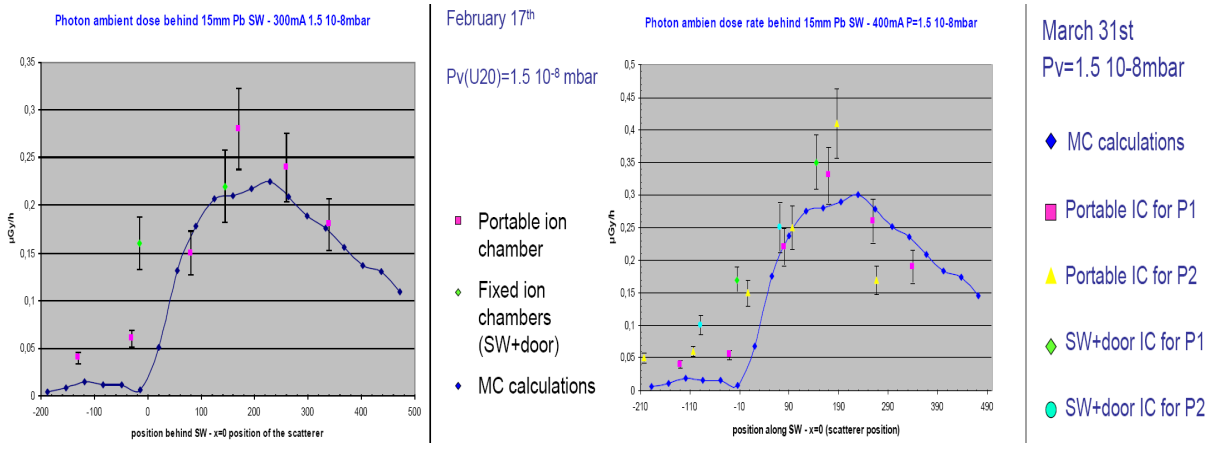

Fig.6 - Comparison of dose rate measurements performed both dates and Monte Carlo calculations done by P. Berkvens with "Beamlines" MC code [2].

Paul Berkvens made some calculations in the same way as the ones performed for the design of the shielding but with the current and the vacuum pressure encountered during the two tests. On Figure 6, one can see that agreement is not so bad between the simulations and the averaged dose rates recorded during both tests but measurements are always higher and this is not enough to explain the pulsed high dose rates observed.

Two additional crucial points have to be presented. First, the effective aperture of the front end is quite smaller than the one used for the shielding calculations (0.6x1.8 mm^2 instead of 2x2 mm^2) but it means that dose rates should be lower than values expected from calculations. Second, the actual residual gas composition is more effective in gas-bremsstrahlung production because of the presence of high Z species as shown in table 2.

Vacuum residual gas composition	
H_2	42 %
CO	30.4 %
CO_2	5.6 %
CH_4	3 %
H_2O	9 %
CF_4	10 %

Table 2 - Residual gas composition in SIXS ID in vacuum vessel given by RGA measurement (to compare with Table 1 composition)

The effects of these two parameters are evaluated in Figure 7 which presents the gas-bremsstrahlung spectrum produced in the different cases. The blue curve refers to the gas-bremsstrahlung produced by a 500 mA electron beam in the straight with a gas composition as described in table 1 and with the front end aperture of 4 mm^2. The red curve is almost the same but with the residual gas composition as presented in table 2. The orange curve is the same than the red one but taking into account the reduced aperture of the front end of 0.6x1.8 mm^2. And the green one, supposed to be more realistic, is almost the same than de orange one but mixing table 1 and table 2 residual gas compositions with respect to in vacuum ID vessel length (2 m with table 2 composition) and complement straight length (~5.7 m with table 1 composition).

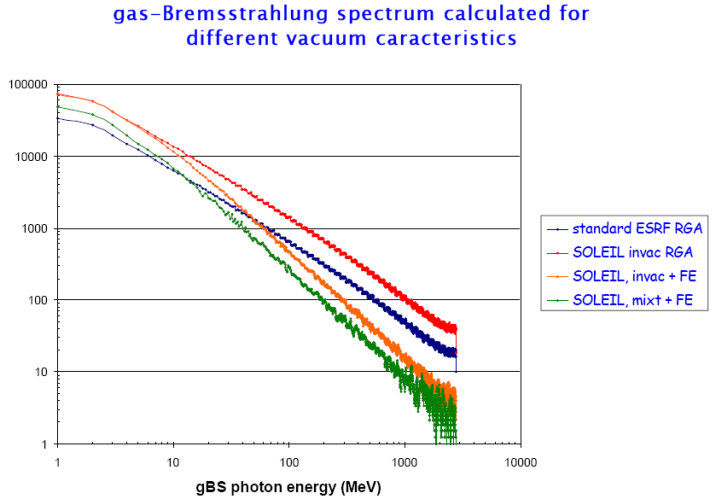

Fig.7 - Comparison of gas-bremsstrahlung spectrum produced by a 500 mA electron beam @ 2. 10^{-9} mbar for different residual gas compositions and front end apertures. Calculations made by P. Berkvens with "Beamlines" MC code [2].

This could explain partly the results of the dose rate measurements performed, particularly if you take into account that the average pressure was 7.5 times higher than the one used to obtain the green curve, but not completely. The last explanation was given at the occasion of the next shutdown when the ID vacuum vessel was opened to be checked. As it is shown on the pictures of Figure 8, the two sides of the copper liner that protects the permanent magnets of the ID present some sort of a wave clearly visible on the left picture, and even a small hole is quite clearly visible on the right view. This last point could explain the reason why the beam losses are concentrated in that particular straight section and probably why the dose rates measured around the optics hutch where so high with the combination of the other facts pointed out above.

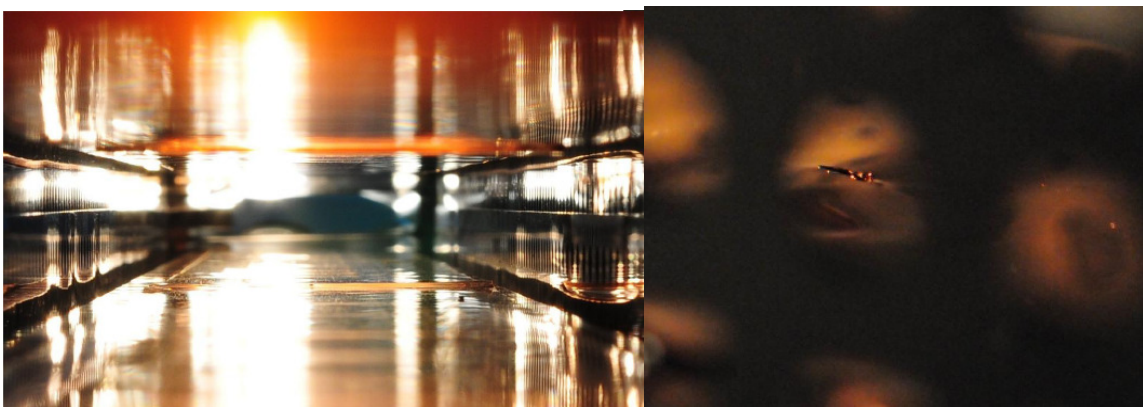

Fig.8 - Damages visible on both side of the protection liner of the magnets of the U20 in vacuum ID of beam line SIXS. On the left view, the bumps up and down sides; on the right view the hole.

5. Conclusion and additional notes

These measurements and results point out the fact of how the vacuum conditions are critical with respect to gas-bremsstrahlung production and radiation protection around the ID beam line in synchrotron facilities. So a great care has to be taken during the shielding design to take into consideration the vacuum issue and its consequence in terms of shielding and operational constraints.
During the weeks that followed the Radsynch Conference, the in vacuum ID of the SIXS beam line was replaced during the next shutdown and it was observed during the following run that the beam losses do not concentrate anymore in the SDC14 straight section. Unfortunately, the beam line was still not ready to take beam for an additional radiation test at the moment of this paper was written.

6. Acknowledgements

The author wants to thank Paul Berkvens, from the ESRF, for his help and his work produced for this paper and Corinne Mage and Fabien Justine, from radiation safety group of SOLEIL, for their precious and effective work during the measurements.

References

[1] J-B. Pruvost, “Radiation safety commissioning of Synchrotron SOLEIL”, Radsynch07 proceedings (2007).
[2] P. Berkvens, “Assessment of beam line shielding at the ESRF”, Radsynch07 proceedings (2007).
[3] J-B. Pruvost, P. Berkvens, “Shielding requirements for the hutches of the SIXS Beam line”, DIR/SEC/RP/NT/1955, SOLEIL internal report (2007).

RADIATION PROTECTION TECHNOLOGY

- SATURN I -
GAMMA / NEUTRON
MOBILE MONITORS
WITH IONIZATION
CHAMBER
AND ^{3}He or Bf^{3}

- NAUSICAA -
GAMMA AREA
MONITOR
WITH IONIZATION
CHAMBER

ELSE

We are able to supply a complete product range, accessories and technical support to optimize the control systems

We work with Energy
In Radiation Technology

- SATURN I -
ALPHA AND BETA
AIR MONITOR

- ALBA -
ALPHA / BETA
COUNTING SYSTEMS
LOW BACKGROUND

AIR SAMPLER

ISO 9001 BUREAU VERITAS Certification

Via Pier della Francesca, 26 – 20090 Trezzano sul Naviglio (MI)
Tel. 02/48409290 - Fax 02/48409294
Web: www.el-se.com e-mail info@el se.com

ELSE